QUANTITATIVE APPROACHES FOR OBJECT BASED IMAGE ANALYSIS OF SATELLITE DATA

Ph.D. THESIS

by

MOHIT SRIVASTAVA

DEPARTMENT OF CIVIL ENGINEERING
INDIAN INSTITUTE OF TECHNOLOGY ROORKEE
ROORKEE – 247 667 (INDIA)

JULY, 2013

QUANTITATIVE APPROACHES FOR OBJECT BASED IMAGE ANALYSIS OF SATELLITE DATA

A THESIS

Submitted in partial fulfilment of the requirements for the award of the degree

of

DOCTOR OF PHILOSOPHY

in

CIVIL ENGINEERING

by

MOHIT SRIVASTAVA

DEPARTMENT OF CIVIL ENGINEERING
INDIAN INSTITUTE OF TECHNOLOGY ROORKEE
ROORKEE – 247 667 (INDIA)

JULY, 2013

INDIAN INSTITUTE OF TECHNOLOGY ROORKEE
ROORKEE

CANDIDATE'S DECLARATION

I hereby certify that the work which is being presented in this thesis entitled "QUANTITATIVE APPROACHES FOR OBJECT BASED IMAGE ANALYSIS OF SATELLITE DATA" in partial fulfilment of the requirements for the award of the Degree of Doctor of Philosophy and submitted in the Department of Civil Engineering of the Indian Institute of Technology Roorkee is an authentic record of my own work carried out during a period from January 2009 to July 2013 under the supervision of Dr. Manoj K. Arora, Professor, Department of Civil Engineering and Dr. R. Balasubramanian, Associate Professor, Department of Mathematics, Indian Institute of Technology Roorkee, Roorkee.

The matter presented in the thesis has not been submitted by me for the award of any other degree of this or any other Institute.

(MOHIT SRIVASTAVA)

This is to certify that the above statement made by the candidate is correct to the best of our knowledge.

(R. Balasubramanian)
Supervisor

(Manoj K. Arora)
Supervisor

Date: July , 2013

The Ph.D. Viva-Voce Examination of **Mr. Mohit Srivastava**, Research Scholar, has been held on _____.

Signature of Supervisors Signature of Chairman, SRC Signature of External Examiner

Head of the Department/Chairman, ODC

List of Abbreviations

A	Analytical
AA	Average Accuracy
AFI	Area Fit Index
ALOS	Advanced Land Observation Satellite
ANN	Artificial Neutral Network
ARF	A Road Finder
ASCII	American Standard Code for Information Interchange
CA	Combined Accuracy
CART	Classification and Regression Tree
CBF	Cloud Basis Function
CBFNN	Cloud Basis Function Neural Network
CBO	City Block Optimization
CT Scan	Computed Tomography Scan
DN	Digital Numbers
DT	Decision Tree
ED	Empirical Discrepancy
EG	Empirical Goodness
ENVI	Environment Imaging
FAR	False Alarm Rate
FCM	Fuzzy C-Means
FN	False Negative
FNEA	Fractal Net Evaluation Approach
FP	False Positive
FRAG	Fragmentation
GEOBIA	Geographic Object Based Image Analysis
GIS	Geographic Information System
GLCM	Gray Level Co-occurrence Matrix
GLDV	Gray Level Difference Vector
GR	Gain Ratio
GUI	Graphical User Interface
H	Heterogeneity Index
HCM	Hard C-Means

HH, HV	Horizontal-Horizontal and Horizontal-Vertical Polarizations
HMTseg	Hidden Markov Tree segmentation
ID	Identity
IFOV	Instantaneous Field of View
HSI	Hue Saturation Intensity
IO	Image Object
IRS	Indian Remote Sensing
J-M	Jeffries-Matusita
JSEG	J-Segmentation
LiDAR	Light Detection and Ranging
LISS	Linear Imaging Self Scanner
LPI	Line-Point-Intercept
LULC	Land-Use Land Cover
MATLAB	Matrix Laboratory
MDC	Minimum Distance Classifier
MHR	Minimum Heterogeneity Rule
MRF	Markov Random Field
MRI	Magnetic Resonance Imaging
MRTS	Mass Rapid Transit System
MS	multispectral
NAN	Not-a-Number
NDVI	Normalized Difference Vegetation Index
NIR	Near Infra Red
NN	Nearest Neighbor
NSR	Number-of-Segments Ratio
OA	Overall Accuracy
OBA	Object Based Analysis
OBIA	Object Based Image Analysis
OBIC	Object Based Image Classification
OBIE	Object Based Image Extraction
OE	Object Extraction
OR	Over-Segmentation Rate
OrbView	Orbital View

PA	Producer's Accuracy
PALSAR	Phased Array L-band Synthetic Aperture Radar
Pan	Panchromatic
PCA	Principal Component Analysis
PCT	Principal Component Transform
PSE	Potential Segmentation Error
QR	Quality Rate
RADAR	Radio Detection And Ranging
RAG	Region Adjacency Graph
RBFNN	Radial Basis Function Neural Network
RGB	Red Green Blue
ROC	Receiver Operating Characteristics
RS	Remote Sensing
SAN	Shape-Adaptive Neighborhood
SAR	Synthetic Aperture Radar
SEaTH	Separability and Threshold
SFI	Segmentation Fit Index
SONAR	Sound Navigation And Ranging
SPOT	Satellite Pour Observation de la Terre
SRG	Seeded-Region Growing
SRM	Statistical Region Merging
SVM	Support Vector Machine
SWIR	Short Wave Infra Red
TDR	True Detection Rate
TIR	Thermal Infra Red
TM	Thematic Map
TN	True Negative
TP	True Positive
UA	User's Accuracy
UR	Under-Segmentation Rate
USA	United States of America
UT	Union Territory

Abstract

Remote sensing has made enormous progress in recent years. In order to extract useful information from remote sensing data, typically digital image classification is applied. The land use-land cover classes on the earth's surface have different physical characteristics. A land use land cover classification can be performed in a pixel-based environment or an object-based based environment. Pixel-based classification techniques are appropriate for producing land use land cover classification from medium and low spatial resolution remote sensing data. In case of high-resolution images, pixels are smaller than the object under consideration, spectral information within an image is spatially heterogeneous. The object under consideration is composed of several pixels thus within class spectral variation increases. The pixel-based image classification is also affected by 'salt and pepper' noise thereby producing relatively low classification accuracy.

Object-based image analysis (OBIA) produces an efficient solution to this problem, which involves three basic steps. In a first step, a segmentation process is performed by forming the homogeneous regions in order to delineate objects under consideration. In the second step, an attribute selection process may be performed to reduce the number of attributes. In the last step, a classification process applies to these segments using the selected attributes representing spectral and spatial (shape, contextual and textural) characteristics of objects. Additionally, the OBIA has been found useful in extraction of individual objects and targets. For example, urban feature extraction, military target detection etc.

In this research, the object based image analysis (OBIA) has been investigated for extraction of objects from high to very high-resolution remote sensing data. In each of three basic steps, novel approaches have been proposed to improve the quality of object extraction.

Two types of remote sensing datasets, a very high-resolution Quick-bird image and the high-resolution LISS-IV image have been considered for the experiments. The very high-resolution belongs to Quick-bird Pan-sharpened image acquired over Chandigarh region due to its well planned structure and separable classes. The high-resolution LISS-IV image of the typical Indian city (Delhi region) has been considered as another experimental dataset, where the classes are not easily

separable. Total eight classes belong to three categories; linear shape, compact regular shape and compact irregular shape features have been considered from Quick-bird image, while twelve classes have been considered for the LISS-IV image.

A number of segmentation parameters are required to be set for segmenting the image via a segmentation algorithm. The selection of improper values of segmentation parameters may result into over and under segmentation. The lower value of segmentation parameters causes 'over segmentation' whereas higher value causes 'under segmentation'. Thus, it is required to select proper segmentation parameters value to find critical segmentation at which meaningful objects can be formed.

In this research work, semi-automatic fitness functions based on the internal properties of the segments have been proposed to fix the variations in the values of three parameters namely; scale, shape-factor/spectral, and the compactness/smoothness of the most widely used multi-segmentation algorithm.

The quality of the segmentation has generally been evaluated through visual interpretation of segmented images. The quantitative evaluation of segmentation quality may therefore be appropriate. There are two ways for quantitative evaluation, the goodness based approach in which reference image is not required and the quality is evaluated using the intra-segment characteristics while the other one is discrepancy based approach, and the quality is measured by calculating the diversity in a segment from the reference object. In this study, quality measures based on the size and shape differences under the domain of discrepancy based approach have been proposed. The proposed quality assessment approach takes into the errors of omission and commission to calculate the discrepancy between the segment and the reference objects. The combined usage of size and shape differences results into a realistic estimate of the quality of segmentation.

The segmented image carries a number of attributes grouped into spectral, shape, contextual and textural categories. Out of these attributes, the values of some attributes may be similar for more than one class segments. While few attributes appear exclusively in a particular segment and represent different characteristics from the segments of other classes. Working with all the generated

attributes is very time consuming and also requires more memory space for storage and sometimes may create confusion, thus it is efficient to work with only important attributes.

In this work, a combined decision tree-ROC curve approach has been proposed for selecting the required attributes. Significant reduction has been observed in the number of attributes. The attribute set reduces between 4 and 20 from 100 for Pan-sharpened image, from 43 to 10 and 24 for Pan image, and from 85 attributes to 14 and 25 in case of LISS-IV image.

The decision tree has further been used for image classification and individual object extraction. In case of image classification, a tree has been generated and pruned using pessimistic error pruning (PEP). The image is classified using both pruned and unpruned trees. Whereas, in case of individual object extraction, one tree per class has been generated and an object has been extracted at the farthest leaf node by considering all other classes as background. The object extraction has also been done using selected attributes and also using all attributes. Further, the classification and extraction accuracies have been assessed using error matrix and ROC curve respectively. A significant improvement has been observed in both classification and extraction quality with reduced number of attributes in comparison to that when using all attributes.

Highest overall classification accuracy and Kappa coefficient obtained with pruned trees are 91.03%, 0.893, 62.5%, 0.572 and 78.91%, 0.76 respectively for Quick-bird Pan-sharpened, Quick-bird Pan and LISS-IV images, respectively. The highest object extraction quality has been obtained for Quick-bird Pan-sharpened image with TPR of 1 and FAR of 0.03. The corresponding values of TPR and FAR for Quick-bird PAN image are 0.65 and 0.04 respectively and for LISS-IV multispectral image are; TPR: 0.94 and FAR: 0.021. Finally, the classified image using classification outputs and the binary image using the outputs of individual object extraction have been produced.

In summary, the work has been done in three parts and compiles to form a thesis. The first part covers the image segmentation and its quality assessment, a new fitness functions have been proposed for fixation of values of segmentation parameters to create properly segmented image. To assess the quality of segmented image a set of quality indices that take into account errors of omission and commission have also been proposed. The second part of the thesis is related to the selection of the attributes, a quantitative method of attribute selection has also been suggested that

reduces the dimensionality of the segments attributes by selecting important attributes. The object-based image classification and individual object extraction using decision tree has comes under third part of the thesis.

Acknowledgements

First and above all, I praise **GOD**, *the Almighty*, to whom I owe my very existence. This work will never be accomplished without **HIS** blessings. I wish to thank the ALMIGHTY GOD for giving me the strength, health and determination to carry out this research. This thesis appears in its current form due to the assistance and guidance of several people. I would therefore like to offer my sincere thanks to all of them.

Foremost, I would like to express my sincere gratitude to my research supervisors **Dr. Manoj K. Arora**, Professor, and **Dr. R. Balasubramanian,** Associate Professor for the continuous support of my Ph. D. study and research, for their patience, motivation, enthusiasm, and immense knowledge.

I am deeply grateful to **Prof. Manoj K. Arora** for his outstanding support, wise guidance and invaluable suggestions both professional and personal. He always encouraged me to pursue my ideas, offered innumerable creative insights and guided me with unmatched wisdom. He helped me to understand this research work through dividing all objectives into small parts and completing them step by step.This research would not have been possible without his active support.

I owe my most sincere gratitude to the members of the student's research committee, **Dr. R. P. Gupta**, Professor, Department of Earth Sciences and **Dr. K. S. Hariprasad**, Professor, Department of Civil Engineering, IIT Roorkee for their detailed review, constructive criticism and excellent advice during the preparation of this thesis. ***I am grateful to faculty and staff members, Geomatics Engineering Group, for providing laboratory facilities during the course of this work.***

The present research was carried out under an Institute scholarship awarded to me under **MHRD,** New Delhi, India. I am very grateful to Institute for providing generous funds for the research work.

During this work, I have collaborated with many colleagues for whom I have great regard, and I wish to extend my warmest thanks to **Dr. Atanu Bhatacharaya,** Associate Professor, Bharti Vidyapeeth, New Delhi and **Dr. Kamal Kumar,** Assistant Professor, Punjab Engineering Collage, Chandigarh.

I would like to thank my friends and research scholars **Mr. Manoj Kuri, Mr. N. Prabhu, Mr. H. S. Gusain, Mr. Reet Kamal Tiwari, Ms. Deepti Yadav, Ms. Varinder Saini** and all those who have helped me directly and indirectly with my work.

I also thank M. Tech. Geomatics Engineering students **Ms. Shweta Bansal, Mr. Saurabh Vijay, Ms. Arti Tiwari** and **Mr. Shreyansh Singh** for their help and support.

I acknowledge the support provided by my friends **Mr. Sachin Mishra, Mr. Nitin Mishra, Dr. Mohit Kumar, Mr. Manish K. Khandelwal, Mr. R.P. Singh, Mr. L.P. Srivastava, Mr. Dinesh Singh, Mr. Sukanta Halder, Dr. Sanoj**, **Mr. Himanshu Agarwal, Dr. Siddharth Jain** and **Mr. Javed Dhillon** for all their help and hospitability during my stay at IIT Roorkee.

I also acknowledge the support provided by all **Research Scholors** and **M.Tech. students** of Geomatics Engineering Group.

My thanks to **Mishra uncle** and his family, especially sweet **Pari**, for a wonderful and memorable hospitality during my stay at IIT Roorkee, which never feels me away from home.

My thanks to **Dr. Pradeep Kumar,** Scientest, CBRI Roorkee, **Mr. Nuruddin** and **Mr. Ajay Kashyap** for their help and support.

My special sincere, heartfelt gratitude and indebtedness is due to **my brother, my brother in law, my sister, my sister in law,** my dearest **Arzoo, Kunal, Sakshi** and **Shraddha** for their sincere prayers, constant encouragement. I also warmly thank and appreciate my relatives, friends and well wishers for their moral support in all aspects of my life.

I want to express my gratitude and deepest appreciation to **my mother** and **father** for their great patience and understandings. Their encouragement and contribution lifted me to reach this place. I dedicate this thesis to my adoring parents.

(Mohit Srivastva)

Appendix I:

Table I.1: Parameter selection

1	2	3	4	5	6	7	8	9	10	11	12	13
Segment ID	**M-4**	**SD-4**	**MDN-4**	**MDNabs-4**	**M-3**	**SD-3**	**MDN-3**	**MDNabs-3**	**M-2**	**SD-2**	**MDN-2**	**MDNabs-2**
6708	101.57	2.42	2.58	0.84	63.76	1.8	3.73	4.8	90.76	2.11	4.81	6.26
6710	102.51	3.14	4.17	7.6	69.7	4.04	8.08	10.38	98.67	5.32	9.84	11.9
7132	101.4	2.65	4.86	9.22	68.35	3.52	9.03	12.24	96.68	3.66	10.79	14.51
7137	100.78	2.56	4.35	2.5	62.44	2.27	5.05	7.69	89.5	2.35	6.53	9.24
7142	95.61	3.1	10.5	13.25	61.31	3.2	9.82	13.49	86.5	3.21	12.65	14.62
7149	97.75	2.98	3.86	3.33	61.58	1.88	1.89	1.82	88.09	2.33	2.46	2.16
7151	97.6	2.73	3.86	3.79	64.23	1.84	5.33	13.12	90.43	2.08	6.2	16.56
7153	88.97	6.72	7.46	7.46	57	3.55	4.57	4.57	82.21	4.81	5.47	5.47
7157	92.65	3.93	7.89	8.9	61.08	3.34	7.19	7.95	86.82	3.96	8.91	11.48
--	--	--	--	--	--	--	--	--	--	--	--	--

14	**15**	**16**	**17**	**18**	**19**	**20**	**21**	**22**	**23**	**24**	**25**	**26**
M-1	**SD-1**	**MDN-1**	**MDNabs-1**	**A (Pxl)**	**Cmpct**	**BL(Pxl)**	**SI**	**X min (m)**	**Y min (m)**	**X max (m)**	**Y max (m)**	**Cmpct (poly)**
61.81	1.48	2.55	3.42	1071	1.74	250	1.91	76.75	30.7	76.75	30.7	0.31
66.08	3.13	5.75	7.36	210	2.21	204	3.52	76.75	30.7	76.75	30.7	0.1
65.01	2.28	6.12	8.81	183	2.07	144	2.66	76.75	30.69	76.75	30.7	0.17
61.49	1.59	3.71	4.82	754	2.17	226	2.06	76.75	30.69	76.75	30.7	0.26
59.53	1.9	7.6	10.5	395	2	152	1.91	76.75	30.69	76.75	30.7	0.3
60.42	1.57	1.55	1.28	871	1.96	204	1.73	76.75	30.7	76.75	30.7	0.41
61.72	1.48	3.66	6.12	331	1.74	100	1.37	76.75	30.7	76.75	30.7	0.56
56.43	3.1	3.7	3.7	424	1.75	126	1.53	76.75	30.69	76.75	30.7	0.49
59.3	2.51	5.38	5.98	654	2.47	200	1.96	76.75	30.69	76.75	30.7	0.33
--	--	--	--	--	--	--	--	--	--	--	--	--

Table I.2: Format of the training data file (attributes are in the same order as given in Table 6.7).

Attri. Sl. No.	1	2	3	4	5	--	--	10	11	12	13	--	--	79	80	81	--	
ID	M-4	Sd-4	R-4	SDN-4	MDN-4	--	--	GLCM-Homo-4	GLCM-Cont-4	GLCM-Dsm-4	GLCM-Ent-4	--	--	A	L/W	Cmpct	--	Class
28	69.21	14.77	0.25	11.51	8.57	--	--	0.19	47.14	4.97	6.94	--	--	5842	1.81	3.77	--	2
75	68.89	6.29	0.24	9.89	-4.5	--	---	0.22	21.29	3.61	6.24	--	--	8457	1.16	1.83	--	4
87	77.98	5.27	0.24	7.33	9.57	--	--	0.27	13.53	2.87	5.65	--	--	5425	1.51	1.93	--	4
104	75.84	8.01	0.24	15.29	-2.46	--	--	0.28	12.67	2.75	5.71	--	--	54922	2.8	2.13	--	8
185	88.71	5.24	0.24	14.71	1.33	--	--	0.34	8.94	2.2	5.3	--	--	3854	2.75	2.04	--	7
286	87.57	7.11	0.24	10.68	4.1	--	--	0.27	22.1	3.29	6.04	--	--	10456	3.61	3.47	--	5
354	111.59	11.31	0.24	9.26	10.34	--	--	0.23	34.42	4.26	6.69	--	--	17642	3.02	2.47	--	1
--	--	--	--	--	--	--	--	--	--	--	--	--	--	--	--	--	--	--
--	--	--	--	--	--	--	--	--	--	--	--	--	--	--	--	--	--	--

Table I.3: Format of the testing data file (attributes are in the same order as given in Table 6.7).

Attri. Sl. No.	1	2	3	4	5	--	--	10	11	12	13	--	--	79	80	81	--	
ID	M-4	Sd-4	R-4	SDN-4	MDN-4	--	--	GLCM-Homo-4	GLCM-Cont-4	GLCM-Dsm-4	GLCM-Ent-4	--	--	A	L/W	Cmpct	--	--
19	79.19	4.99	0.24	9.84	-4.8	--	--	0.32	11.55	2.5	5.45	--	--	8978	2.45	1.51	--	--
47	141.59	13.31	0.24	9.26	10.34	--	---	0.23	34.42	4.26	6.69	--	--	35642	3.02	2.47	--	--
107	74.51	7.15	0.24	8.08	2.61	--	--	0.28	13.73	2.84	5.91	--	--	1578	1.69	1.75	--	--
152	68.89	7.29	0.24	8.89	-4.5	--	--	0.22	21.29	3.61	6.24	--	--	12457	1.16	1.83	--	--
186	84.71	5.24	0.24	12.71	1.33	--	--	0.34	8.94	2.2	5.3	--	--	3214	2.75	2.04	--	--
208	63.97	6.86	0.24	6.95	-10.1	--	--	0.28	12.88	2.77	5.85	--	--	6542	1.44	1.88	--	--
276	95.4	9.28	0.23	15.11	10.06	--	--	0.2	45.76	4.85	6.58	--	--	9654	2.8	2.12	--	--
--	--	--	--	--	--	--	--	--	--	--	--	--	--	--	--	--	--	--
--	--	--	--	--	--	--	--	--	--	--	--	--	--	--	--	--	--	--

Table I.4: Format of the image file (attributes are in the same order as given in Table 6.7).

Attri. Sl. No.	1	2	3	4	5	--	--	10	11	12	13	--	--	79	80	81	--	
ID	M-4	Sd-4	R-4	SDN-4	MDN-4	--	--	GLCM-Homo-4	GLCM-Cont-4	GLCM-Dsm-4	GLCM-Ent-4	--	--	A	L/W	Cmpct	--	--
0	72.72	11.42	0.24	9.8	-3.12	--	--	0.18	38.75	4.74	6.94	--	--	856	1.57	1.62	--	--
1	74.08	11.69	0.24	13.1	2.59	--	---	0.21	30.72	4.12	6.83	--	--	7458	1.93	1.78	--	--
2	79.21	14.77	0.25	11.51	8.57	--	--	0.19	47.14	4.97	6.94	--	--	542	1.81	3.77	--	--
3	74.51	7.15	0.24	8.08	2.61	--	--	0.28	13.73	2.84	5.91	--	--	1578	1.69	1.75	--	--
4	68.89	7.29	0.24	8.89	-4.5	--	--	0.22	21.29	3.61	6.24	--	--	12457	1.16	1.83	--	--
5	77.98	5.27	0.24	7.33	9.57	--	--	0.27	13.53	2.87	5.65	--	--	5425	1.51	1.93	--	--
6	73.84	6.01	0.24	11.29	-2.46	--	--	0.28	12.67	2.75	5.71	--	--	54922	2.8	2.13	--	--
--	--	--	--	--	--	--	--	--	--	--	--	--	--	--	--	--	--	--
--	--	--	--	--	--	--	--	--	--	--	--	--	--	--	--	--	--	--

Appendix II:

Table II.1: Image segmentation of Quick-bird Pan-sharpen image at different levels with variation in scale parameter.

Level	Scale	Shape Factor	Spectral	Compactness	Smoothness	No. of Segments
L-1	10	0.4	0.6	0.2	0.8	3842
L-2	15	0.4	0.6	0.2	0.8	3668
L-3	20	0.4	0.6	0.2	0.8	3478
L-4	25	0.4	0.6	0.2	0.8	3312
L-5	30	0.4	0.6	0.2	0.8	3221
L-6	35	0.4	0.6	0.2	0.8	3042
L-7	40	0.4	0.6	0.2	0.8	2568
L-8	45	0.4	0.6	0.2	0.8	2278
L-9	50	0.4	0.6	0.2	0.8	1850
L-10	55	0.4	0.6	0.2	0.8	1421
L-11	60	0.4	0.6	0.2	0.8	1189
L-12	65	0.4	0.6	0.2	0.8	1062
L-13	70	0.4	0.6	0.2	0.8	941
L-14	75	0.4	0.6	0.2	0.8	853
L-15	80	0.4	0.6	0.2	0.8	784
L-16	85	0.4	0.6	0.2	0.8	715
L-17	90	0.4	0.6	0.2	0.8	665
L-18	95	0.4	0.6	0.2	0.8	621
L-19	100	0.4	0.6	0.2	0.8	587
L-20	110	0.4	0.6	0.2	0.8	546
L-21	120	0.4	0.6	0.2	0.8	514
L-22	130	0.4	0.6	0.2	0.8	502
L-23	140	0.4	0.6	0.2	0.8	479
L-24	150	0.4	0.6	0.2	0.8	466
L-25	175	0.4	0.6	0.2	0.8	444
L-26	200	0.4	0.6	0.2	0.8	415
L-27	225	0.4	0.6	0.2	0.8	411
L-28	250	0.4	0.6	0.2	0.8	404

Table II.2: Image segmentation of Quick-bird Pan-sharpen image at different levels with variation in shape factor.

Level	Scale	Shape Factor	Spectral	Compactness	Smoothness	No. of Segments
L-1	10	0	1	0.2	0.8	3759
L-2	20	0	1	0.2	0.8	2954
L-3	50	0	1	0.2	0.8	2182
L-4	70	0	1	0.2	0.8	1093
L-5	70	0.05	0.95	0.2	0.8	1084
L-6	70	0.1	0.9	0.2	0.8	1071
L-7	70	0.15	0.85	0.2	0.8	1029
L-8	70	0.2	0.8	0.2	0.8	1025
L-9	70	0.25	0.75	0.2	0.8	999
L-10	70	0.3	0.7	0.2	0.8	992
L-11	70	0.35	0.65	0.2	0.8	974
L-12	70	0.4	0.6	0.2	0.8	957
L-13	70	0.45	0.55	0.2	0.8	924
L-14	70	0.5	0.5	0.2	0.8	918
L-15	70	0.55	0.45	0.2	0.8	903
L-16	70	0.6	0.4	0.2	0.8	885
L-17	70	0.65	0.35	0.2	0.8	862
L-18	70	0.7	0.3	0.2	0.8	834
L-19	70	0.75	0.25	0.2	0.8	819
L-20	70	0.8	0.2	0.2	0.8	805
L-21	70	0.85	0.15	0.2	0.8	798
L-22	70	0.9	0.1	0.2	0.8	781

Table II.3: Image segmentation of Quick-bird Pan-sharpen image at different levels with variation in compactness parameter.

Level	Scale	Shape Factor	Spectral	Compactness	Smoothness	No. of Segments
L-1	10	0.4	0.6	0.05	0.95	3894
L-2	20	0.4	0.6	0.05	0.95	2987
L-3	50	0.4	0.6	0.05	0.95	2046
L-4	70	0.4	0.6	0.05	0.95	994
L-5	70	0.4	0.6	0.1	0.9	978
L-6	70	0.4	0.6	0.15	0.85	964
L-7	70	0.4	0.6	0.2	0.8	951
L-8	70	0.4	0.6	0.25	0.75	917
L-9	70	0.4	0.6	0.3	0.7	892
L-10	70	0.4	0.6	0.35	0.65	869

L-11	70	0.4	0.6	0.4	0.6	834
L-12	70	0.4	0.6	0.45	0.55	828
L-13	70	0.4	0.6	0.5	0.5	825
L-14	70	0.4	0.6	0.55	0.45	814
L-15	70	0.4	0.6	0.6	0.4	808
L-16	70	0.4	0.6	0.65	0.35	797
L-17	70	0.4	0.6	0.7	0.3	795
L-18	70	0.4	0.6	0.75	0.25	795
L-19	70	0.4	0.6	0.8	0.2	752
L-20	70	0.4	0.6	0.85	0.15	752
L-21	70	0.4	0.6	0.9	0.1	749
L-22	70	0.4	0.6	0.95	0.05	744
L-23	70	0.4	0.6	1	0	741

Table II.4: Image segmentation of Quick-bird Pan image at different levels with variation in scale parameter.

Level	**Scale**	**Shape Factor**	**Spectral**	**Compactness**	**Smoothness**	**No. of Segments**
L-1	10	0.4	0.6	0.2	0.8	3974
L-2	15	0.4	0.6	0.2	0.8	3712
L-3	20	0.4	0.6	0.2	0.8	3404
L-4	25	0.4	0.6	0.2	0.8	2951
L-5	30	0.4	0.6	0.2	0.8	2576
L-6	35	0.4	0.6	0.2	0.8	2281
L-7	40	0.4	0.6	0.2	0.8	2004
L-8	45	0.4	0.6	0.2	0.8	1762
L-9	50	0.4	0.6	0.2	0.8	1524
L-10	55	0.4	0.6	0.2	0.8	1268
L-11	60	0.4	0.6	0.2	0.8	1176
L-12	65	0.4	0.6	0.2	0.8	1102
L-13	70	0.4	0.6	0.2	0.8	1078
L-14	75	0.4	0.6	0.2	0.8	1043
L-15	80	0.4	0.6	0.2	0.8	986
L-16	85	0.4	0.6	0.2	0.8	854
L-17	90	0.4	0.6	0.2	0.8	728
L-18	95	0.4	0.6	0.2	0.8	547
L-19	100	0.4	0.6	0.2	0.8	475
L-20	110	0.4	0.6	0.2	0.8	425
L-21	120	0.4	0.6	0.2	0.8	378
L-22	130	0.4	0.6	0.2	0.8	354

L-23	140	0.4	0.6	0.2	0.8	326
L-24	150	0.4	0.6	0.2	0.8	287
L-25	175	0.4	0.6	0.2	0.8	254
L-26	200	0.4	0.6	0.2	0.8	251
L-27	225	0.4	0.6	0.2	0.8	205
L-28	250	0.4	0.6	0.2	0.8	200

Table II.5: Image segmentation of Quick-bird Pan image at different levels with variation in shape factor.

Level	Scale	Shape Factor	Spectral	Compactness	Smoothness	No. of Segments
L-1	10	0	1	0.2	0.8	4021
L-2	15	0	1	0.2	0.8	3689
L-3	20	0	1	0.2	0.8	3426
L-4	30	0	1	0.2	0.8	2648
L-5	50	0	1	0.2	0.8	1685
L-6	70	0	1	0.2	0.8	982
L-7	75	0	1	0.2	0.8	875
L-8	75	0.05	0.95	0.2	0.8	861
L-9	75	0.1	0.9	0.2	0.8	841
L-10	75	0.15	0.85	0.2	0.8	829
L-11	75	0.2	0.8	0.2	0.8	822
L-12	75	0.25	0.75	0.2	0.8	812
L-13	75	0.3	0.7	0.2	0.8	805
L-14	75	0.35	0.65	0.2	0.8	798
L-15	75	0.4	0.6	0.2	0.8	784
L-16	75	0.45	0.55	0.2	0.8	784
L-17	75	0.5	0.5	0.2	0.8	766
L-18	75	0.55	0.45	0.2	0.8	761
L-19	75	0.6	0.4	0.2	0.8	755
L-20	75	0.65	0.35	0.2	0.8	752
L-21	75	0.7	0.3	0.2	0.8	747
L-22	75	0.75	0.25	0.2	0.8	742
L-23	75	0.8	0.2	0.2	0.8	739
L-24	75	0.85	0.15	0.2	0.8	739
L-25	75	0.9	0.1	0.2	0.8	734

Table II.6: Image segmentation of Quick-bird Pan image at different levels with variation in compactness parameter.

Level	Scale	Shape Factor	Spectral	Compactness	Smoothness	No. of Segments
L-1	10	0.45	0.55	0	1	3954
L-2	15	0.45	0.55	0	1	3561
L-3	20	0.45	0.55	0	1	3587
L-4	30	0.45	0.55	0	1	2683
L-5	50	0.45	0.55	0	1	1506
L-6	70	0.45	0.55	0	1	888
L-7	75	0.45	0.55	0.05	0.95	821
L-8	75	0.45	0.55	0.1	0.9	802
L-9	75	0.45	0.55	0.15	0.85	796
L-10	75	0.45	0.55	0.2	0.8	791
L-11	75	0.45	0.55	0.25	0.75	782
L-12	75	0.45	0.55	0.3	0.7	775
L-13	75	0.45	0.55	0.35	0.65	765
L-14	75	0.45	0.55	0.4	0.6	762
L-15	75	0.45	0.55	0.45	0.55	757
L-16	75	0.45	0.55	0.5	0.5	752
L-17	75	0.45	0.55	0.55	0.45	752
L-18	75	0.45	0.55	0.6	0.4	747
L-19	75	0.45	0.55	0.65	0.35	741
L-20	75	0.45	0.55	0.7	0.3	732
L-21	75	0.45	0.55	0.75	0.25	724
L-22	75	0.45	0.55	0.8	0.2	722
L-23	75	0.45	0.55	0.85	0.15	722
L-24	75	0.45	0.55	0.9	0.1	721
L-25	75	0.45	0.55	0.95	0.05	719
L-26	75	0.45	0.55	1	0	718

Table II.7: Image segmentation of LISS-IV multispectral image at different levels with variation in scale parameter.

Level	Scale	Shape Factor	Spectral	Compactness	Smoothness	No. of Segments
L-1	5	0.4	0.6	0.2	0.8	2278
L-2	10	0.4	0.6	0.2	0.8	1850
L-3	12	0.4	0.6	0.2	0.8	1521
L-4	15	0.4	0.6	0.2	0.8	1354
L-5	17	0.4	0.6	0.2	0.8	1289

L-6	20	0.4	0.6	0.2	0.8	1168
L-7	22	0.4	0.6	0.2	0.8	1099
L-8	25	0.4	0.6	0.2	0.8	1042
L-9	27	0.4	0.6	0.2	0.8	954
L-10	28	0.4	0.6	0.2	0.8	921
L-11	30	0.4	0.6	0.2	0.8	914
L-12	32	0.4	0.6	0.2	0.8	899
L-13	35	0.4	0.6	0.2	0.8	874
L-14	40	0.4	0.6	0.2	0.8	853
L-15	45	0.4	0.6	0.2	0.8	784
L-16	50	0.4	0.6	0.2	0.8	715
L-17	55	0.4	0.6	0.2	0.8	665
L-18	60	0.4	0.6	0.2	0.8	621
L-19	65	0.4	0.6	0.2	0.8	587
L-20	70	0.4	0.6	0.2	0.8	546
L-21	100	0.4	0.6	0.2	0.8	514

Table II.8: Image segmentation of LISS-IV multispectral image at different levels with variation in shape factor.

Level	Scale	Shape Factor	Spectral	Compactness	Smoothness	No. of Segments
L-1	5	0	1	0.2	0.8	1252
L-2	10	0	1	0.2	0.8	1148
L-3	15	0	1	0.2	0.8	1084
L-4	17	0	1	0.2	0.8	1081
L-5	20	0	1	0.2	0.8	1069
L-6	22	0	1	0.2	0.8	1052
L-7	25	0	1	0.2	0.8	1002
L-8	28	0	1	0.2	0.8	994
L-9	28	0.05	0.95	0.2	0.8	988
L-10	28	0.1	0.9	0.2	0.8	985
L-11	28	0.15	0.85	0.2	0.8	980
L-12	28	0.2	0.8	0.2	0.8	977
L-13	28	0.25	0.75	0.2	0.8	974
L-14	28	0.3	0.7	0.2	0.8	969
L-15	28	0.35	0.65	0.2	0.8	967
L-16	28	0.4	0.6	0.2	0.8	962
L-17	28	0.45	0.55	0.2	0.8	954
L-18	28	0.5	0.5	0.2	0.8	951
L-19	28	0.55	0.45	0.2	0.8	948

L-20	28	0.6	0.4	0.2	0.8	843
L-21	28	0.65	0.35	0.2	0.8	837
L-22	28	0.7	0.3	0.2	0.8	833
L-23	28	0.75	0.25	0.2	0.8	831
L-24	28	0.8	0.2	0.2	0.8	826
L-25	28	0.85	0.15	0.2	0.8	819
L-26	28	0.9	0.1	0.2	0.8	814

Table II.9: Image segmentation of LISS-IV multispectral image at different levels with variation in compactness parameter.

Level	Scale	Shape Factor	Spectral	Compactness	Smoothness	No. of Segments
L-1	5	0.45	0.55	0	1	1246
L-2	10	0.45	0.55	0	1	1110
L-3	15	0.45	0.55	0	1	1092
L-4	17	0.45	0.55	0	1	1058
L-5	20	0.45	0.55	0	1	1012
L-6	22	0.45	0.55	0	1	985
L-7	25	0.45	0.55	0.05	0.95	927
L-8	28	0.45	0.55	0.1	0.9	888
L-9	28	0.45	0.55	0.15	0.85	885
L-10	28	0.45	0.55	0.2	0.8	884
L-11	28	0.45	0.55	0.25	0.75	878
L-12	28	0.45	0.55	0.3	0.7	874
L-13	28	0.45	0.55	0.35	0.65	871
L-14	28	0.45	0.55	0.4	0.6	858
L-15	28	0.45	0.55	0.45	0.55	857
L-16	28	0.45	0.55	0.5	0.5	848
L-17	28	0.45	0.55	0.55	0.45	842
L-18	28	0.45	0.55	0.6	0.4	835
L-19	28	0.45	0.55	0.65	0.35	833
L-20	28	0.45	0.55	0.7	0.3	828
L-21	28	0.45	0.55	0.75	0.25	824
L-22	28	0.45	0.55	0.8	0.2	824
L-23	28	0.45	0.55	0.85	0.15	820
L-24	28	0.45	0.55	0.9	0.1	818
L-25	28	0.45	0.55	0.95	0.05	815
L-26	28	0.45	0.55	1.0	0	811

Table II.10: Intermediate segmentation parameters used to fix the parameters values for linear objects from Quick-bird Pan-sharpened image.

Objects	Scale	Shape Factor	Spectral	Compact-ness	Smooth-ness	No. of sub-segments	Area of sub-segments
Object-1	15	0.4	0.6	0.2	0.8	4	178, 161, 221, 57
	40	0.4	0.6	0.2	0.8	2	235, 382
	55	0.4	0.6	0.2	0.8	2	235, 382
Object-2	15	0.4	0.6	0.2	0.8	5	145, 147, 185, 85, 157
	40	0.4	0.6	0.2	0.8	2	292, 427
	55	0.4	0.6	0.2	0.8	1	719
Object-3	15	0.4	0.6	0.2	0.8	4	181, 95, 245, 88
	40	0.4	0.6	0.2	0.8	3	181, 340, 88
	55	0.4	0.6	0.2	0.8	3	181, 88, 423
Object-4	15	0.4	0.6	0.2	0.8	7	149, 78, 116, 152, 99, 216, 82
	40	0.4	0.6	0.2	0.8	5	227, 116, 152, 315, 82
	55	0.4	0.6	0.2	0.8	2	343, 549

Table II.11: Intermediate segmentation parameters used to fix the parameters values for compact regular objects from Quick-bird Pan-sharpened image.

Objects	Scale	Shape Factor	Spectral	Compact-ness	Smooth-ness	No. of sub-segments	Area of sub-segments
Object-1	20	0.55	0.45	0.8	0.2	8	820, 519, 993, 372, 261, 218, 597, 164
	35	0.55	0.45	0.85	0.15	4	1339, 993, 633, 979
	60	0.55	0.45	0.85	0.15	1	3944
Object-2	20	0.55	0.45	0.85	0.15	4	472, 195, 272, 204
	35	0.55	0.45	0.85	0.15	3	667, 272, 204
	60	0.55	0.45	0.85	0.15	1	1143

Table II.12: Intermediate segmentation parameters used to fix the parameters values for compact irregular objects from Quick-bird Pan-sharpened image.

Objects	Scale	Shape Factor	Spectral	Compact-ness	Smooth-ness	No. of sub-segments	Area of sub-segments
Object-1	15	0.5	0.5	0.7	0.3	5	151, 104, 92, 120, 139
	40	0.5	0.5	0.6	0.4	3	151, 224, 231
	60	0.4	0.6	0.6	0.4	2	375, 231
Object-2	15	0.5	0.5	0.7	0.3	7	132, 185, 110, 114, 99, 86, 104
	40	0.5	0.5	0.6	0.4	5	317, 209, 114, 86, 104
	60	0.4	0.6	0.6	0.4	2	431, 399

Table II.13: Intermediate segmentation parameters used to fix the parameters values for linear objects from Quick-bird Pan image.

Objects	Scale	Shape Factor	Spectral	Compact-ness	Smooth-ness	No. of sub-segments	Area of sub-segments
Object-1	15	0.4	0.6	0.2	0.8	5	128, 145, 191, 107, 125
	40	0.4	0.6	0.2	0.8	3	253, 252, 191
	55	0.4	0.6	0.2	0.8	2	442, 252
Object-2	15	0.4	0.6	0.2	0.8	4	252, 184, 116, 204
	40	0.4	0.6	0.2	0.8	2	436, 320
	55	0.4	0.6	0.2	0.8	1	556

Table II.14: Intermediate segmentation parameters used to fix the parameters values for compact regular objects from Quick-bird Pan image.

Objects	Scale	Shape Factor	Spectral	Compact-ness	Smooth-ness	No. of sub-segments	Area of sub-segments
Object-1	20	0.55	0.45	0.8	0.2	7	842, 602, 1015, 384, 352, 687, 215
	35	0.55	0.45	0.85	0.15	3	1578, 1289, 1230
	60	0.55	0.45	0.85	0.15	2	1578, 2519
Object-2	20	0.55	0.45	0.8	0.2	5	182, 214, 174, 111, 204
	35	0.55	0.45	0.85	0.15	3	182, 378, 325
	60	0.55	0.45	0.85	0.15	1	885

Table II.15: Intermediate segmentation parameters used to fix the parameters values for compact irregular objects from Quick-bird Pan image.

Objects	Scale	Shape Factor	Spectral	Compact-ness	Smooth-ness	No. of sub-segments	Area of sub-segments
Object-1	15	0.5	0.5	0.7	0.3	5	139, 152, 112, 148, 97
	40	0.5	0.5	0.6	0.4	3	251, 152, 245
	60	0.4	0.6	0.6	0.4	2	397, 251
Object-2	15	0.5	0.5	0.7	0.3	5	135,148, 124, 94, 189
	40	0.5	0.5	0.6	0.4	3	135, 366, 189
	60	0.4	0.6	0.6	0.4	1	690

Table II.16: Intermediate segmentation parameters used to fix the parameters values for linear objects from LISS-IV MS image.

Objects	Scale	Shape Factor	Spectral	Compact-ness	Smooth-ness	No. of sub-segments	Area of sub-segments
Object-1	5	0.55	0.45	0.4	0.6	3	65, 41, 52
	15	0.55	0.45	0.4	0.6	2	65, 93
	30	0.55	0.45	0.4	0.6	1	158
Object-2	5	0.55	0.45	0.4	0.6	5	44,52, 64, 25, 74
	15	0.55	0.45	0.4	0.6	3	96, 64, 99
	30	0.55	0.45	0.4	0.6	1	259

Table II.17: Intermediate segmentation parameters used to fix the parameters values for compact objects from LISS-IV MS image.

Objects	Scale	Shape Factor	Spectral	Compact-ness	Smooth-ness	No. of sub-segments	Area of sub-segments
Object-1	5	0.6	0.4	0.75	0.25	4	78, 105, 91, 57
	15	0.6	0.4	0.75	0.25	2	183, 148
	30	0.6	0.4	0.75	0.25	1	331
Object-2	5	0.6	0.4	0.75	0.25	3	47, 83, 29
	15	0.6	0.4	0.75	0.25	2	83, 76
	30	0.6	0.4	0.75	0.25	1	159

Appendix III:

Table III.1: Error matrix for classified Seg-PS-I image using pruned tree.

	Reference Data							
Classified Data	Metallic road	Non-metallic road	Residential	Shadow	Trees	Grass land	Barren land	Water
Metallic road	9	0	1	0	0	0	0	0
Non-metallic road	0	5	0	0	0	0	0	0
Residential	0	1	13	0	1	0	1	0
Shadow	1	0	0	19	0	0	0	0
Trees	0	0	0	0	5	0	0	0
Grass land	0	0	0	0	1	9	0	0
Barren land	0	1	0	0	0	1	6	0
Water	0	0	0	0	0	0	0	2

Table III.2: Error matrix for classified Seg-PS-I image using unpruned tree.

	Reference Data							
Classified Data	Metallic road	Non-metallic road	Residential	Shadow	Trees	Grass land	Barren land	Water
Metallic road	7	1	1	1	0	0	0	0
Non-metallic road	0	4	0	0	0	0	1	0
Residential	0	1	12	1	0	0	2	0
Shadow	1	0	0	18	0	0	0	1
Trees	0	0	1	0	4	0	0	0
Grass land	0	0	0	0	1	8	1	0
Barren land	0	1	1	0	0	1	5	0
Water	0	0	0	1	0	0	0	1

Table III.3: Error matrix for classified Seg-PS-II image using pruned tree.

	Reference Data							
Classified Data	Metallic road	Non-metallic road	Residential	Shadow	Trees	Grass land	Barren land	Water
Metallic road	9	0	1	0	0	0	0	0
Non-metallic road	0	6	0	0	0	0	0	0
Residential	0	1	14	0	0	0	0	0
Shadow	1	0	0	19	0	0	0	0
Trees	0	0	0	0	5	1	0	0
Grass land	0	0	0	0	1	9	0	0
Barren land	0	0	0	0	0	1	8	0
Water	0	0	0	0	0	0	0	2

Table III.4: Error matrix for classified Seg-PS-II image using unpruned tree.

	Reference Data							
Classified Data	Metallic road	Non-metallic road	Residential	Shadow	Trees	Grass land	Barren land	Water
Metallic road	7	1	1	1	0	0	0	0
Non-metallic road	0	5	0	0	0	0	1	0
Residential	0	1	12	1	0	0	1	0
Shadow	1	0	2	16	0	0	0	1
Trees	0	0	1	0	4	1	0	0
Grass land	0	0	0	0	1	8	1	0
Barren land	0	1	1	0	0	1	6	0
Water	0	0	0	1	0	0	0	1

Table III.5: Error matrix for classified Seg-PS-III image using pruned tree.

	Reference Data							
Classified Data	Metallic road	Non-metallic road	Residential	Shadow	Trees	Grass land	Barren land	Water
Metallic road	10	0	1	0	0	0	0	0
Non-metallic road	0	5	0	0	0	0	0	0
Residential	0	1	14	0	0	0	0	0
Shadow	1	0	0	17	0	0	0	0
Trees	0	0	0	0	6	1	0	0
Grass land	0	0	0	0	1	9	0	0
Barren land	0	0	0	0	1	1	6	0
Water	0	0	0	0	0	0	0	2

Table III.6: Error matrix for classified Seg-PS-III image using unpruned tree.

	Reference Data							
Classified Data	Metallic road	Non-metallic road	Residential	Shadow	Trees	Grass land	Barren land	Water
Metallic road	8	1	1	1	0	0	0	0
Non-metallic road	0	4	0	0	0	0	1	0
Residential	0	1	12	1	0	0	1	0
Shadow	1	0	1	15	0	0	0	1
Trees	1	0	1	0	4	1	0	0
Grass land	0	0	0	0	1	8	1	0
Barren land	0	1	1	0	0	0	6	0
Water	0	0	0	1	0	0	0	1

Table III.7: Error matrix for classified Seg-P-I image using pruned tree.

	Reference Data							
Classified Data	Metallic road	Non-metallic road	Residential	Shadow	Trees	Grass land	Barren land	Water
Metallic road	6	1	0	0	0	1	3	0
Non-metallic road	0	4	0	0	0	0	1	0
Residential	0	1	12	0	1	0	1	0
Shadow	1	0	0	17	1	0	1	0
Trees	0	0	1	1	3	1	0	0
Grass land	1	0	0	0	1	8	1	0
Barren land	1	1	0	0	1	1	5	0
Water	0	0	0	0	0	0	0	2

Table III.8: Error matrix for classified Seg-P-I image using unpruned tree.

	Reference Data							
Classified Data	Metallic road	Non-metallic road	Residential	Shadow	Trees	Grass land	Barren land	Water
Metallic road	6	1	1	0	1	0	2	0
Non-metallic road	1	3	0	0	0	1	0	0
Residential	1	2	10	0	0	0	2	0
Shadow	3	0	0	14	1	1	1	1
Trees	1	0	0	0	4	0	1	0
Grass land	1	0	0	0	1	7	2	0
Barren land	2	0	0	0	2	1	4	0
Water	0	0	0	0	0	0	0	2

Table III.9: Error matrix for classified Seg-P-II image using pruned tree.

	Reference Data							
Classified Data	Metallic road	Non-metallic road	Residential	Shadow	Trees	Grass land	Barren land	Water
Metallic road	6	1	0	0	0	1	2	0
Non-metallic road	1	4	0	0	0	0	0	0
Residential	0	1	13	0	1	0	1	0
Shadow	1	0	0	18	1	0	2	0
Trees	0	0	0	0	4	0	1	0
Grass land	0	0	0	0	1	8	1	0
Barren land	1	0	0	0	1	1	3	0
Water	0	0	0	0	0	0	0	2

Table III.10: Error matrix for classified Seg-P-II image using unpruned tree.

	Reference Data							
Classified Data	Metallic road	Non-metallic road	Residential	Shadow	Trees	Grass land	Barren land	Water
Metallic road	6	1	1	0	1	0	1	0
Non-metallic road	1	3	0	0	0	1	0	0
Residential	1	2	10	0	1	0	2	0
Shadow	2	0	0	15	2	1	1	1
Trees	1	0	0	0	3	0	1	0
Grass land	1	0	0	0	1	6	2	0
Barren land	2	1	0	0	1	1	2	0
Water	0	0	0	0	1	0	0	1

Table III.11: Error matrix for classified Seg-P-III image using pruned tree.

	Reference Data							
Classified Data	Metallic road	Non-metallic road	Residential	Shadow	Trees	Grass land	Barren land	Water
Metallic road	6	1	0	0	0	1	1	0
Non-metallic road	1	5	0	0	0	0	1	0
Residential	0	1	13	0	1	0	1	0
Shadow	1	0	0	17	1	0	1	0
Trees	0	0	1	0	4	0	1	0
Grass land	1	0	0	0	1	8	1	0
Barren land	1	0	0	0	1	1	4	0
Water	0	0	0	0	0	0	0	2

Table III.12: Error matrix for classified Seg-P-III image using unpruned tree.

	Reference Data							
Classified Data	Metallic road	Non-metallic road	Residential	Shadow	Trees	Grass land	Barren land	Water
Metallic road	5	1	0	0	1	0	1	1
Non-metallic road	1	4	0	0	0	1	1	0
Residential	1	2	10	0	1	0	2	0
Shadow	2	0	0	14	1	1	1	1
Trees	1	0	1	0	3	0	1	0
Grass land	1	0	0	1	1	6	2	0
Barren land	1	1	0	1	1	1	2	0
Water	0	0	0	0	0	0	0	2

Table III.13: Error matrix for classified Seg-L-I image using pruned tree.

	Reference Data											
Classified Data	Apartments	Houses	Metallic road	Nonmetallic road	Metro line	Canal	Water body	Dense vegetation	Sparse vegetation	Barren land	Wet land	Sand
Apartments	10	0	1	0	0	0	0	0	1	0	0	0
Houses	0	7	1	0	0	0	1	0	0	0	1	0
Metallic road	0	1	6	0	0	0	1	0	0	1	0	0
Nonmetallic road	0	1	0	2	1	0	0	0	0	0	0	0
Metro line	0	0	0	1	2	0	0	0	0	0	0	1
Canal	0	0	0	0	1	3	0	0	0	0	0	0
Water body	0	0	0	0	0	0	3	0	0	0	1	0
Dense vegetation	0	0	0	0	0	0	0	23	2	1	0	0
Sparse vegetation	0	1	0	0	0	0	0	1	18	0	0	0
Barren land	1	1	1	0	0	0	0	0	0	18	1	0
Wet land	1	0	1	0	0	0	0	0	0	0	8	0
Sand	0	0	0	0	1	0	0	0	0	0	0	2

Table III.14: Error matrix for classified Seg-L-I image using unpruned tree.

	Reference Data											
Classified Data	Apartments	Houses	Metallic road	Nonmetallic road	Metro line	Canal	Water body	Dense vegetation	Sparse vegetation	Barren land	Wet land	Sand
Apartments	9	1	1	0	0	0	0	0	0	1	0	0
Houses	0	7	1	0	0	0	0	0	0	1	1	0
Metallic road	0	0	5	0	0	0	1	0	0	1	1	0
Nonmetallic road	0	0	0	2	1	0	0	0	0	0	0	1
Metro line	0	0	0	1	2	0	0	0	0	0	0	1
Canal	0	0	0	0	0	2	1	0	0	0	1	0
Water body	1	0	1	0	0	0	2	0	0	0	0	0
Dense vegetation	1	0	0	0	0	0	0	21	3	1	0	0
Sparse vegetation	1	1	0	1	0	0	0	1	15	1	0	0
Barren land	1	1	1	0	0	0	0	0	0	17	2	0
Wet land	1	1	1	0	0	0	0	0	0	1	6	0
Sand	0	0	0	0	1	0	0	0	0	1	0	1

Table III.15: Error matrix for classified Seg-L-II image using pruned tree.

	Reference Data											
Classified Data	Apartments	Houses	Metallic road	Nonmetallic road	Metro line	Canal	Water body	Dense vegetation	Sparse vegetation	Barren land	Wet land	Sand
Apartments	10	1	0	0	0	0	0	0	0	0	0	0
Houses	0	9	1	0	0	0	0	0	0	0	1	0
Metallic road	0	1	7	0	0	0	1	0	0	1	0	0
Nonmetallic road	0	1	0	2	1	0	0	0	0	0	0	1
Metro line	0	0	0	1	2	0	0	0	0	0	0	1
Canal	0	0	0	0	0	3	0	0	0	0	1	0
Water body	1	0	0	0	0	0	3	0	0	0	0	0
Dense vegetation	1	0	0	0	0	0	0	26	2	1	0	0
Sparse vegetation	0	1	0	0	0	0	0	1	19	1	0	0
Barren land	0	1	1	0	0	0	0	0	0	19	1	0
Wet land	1	0	1	0	0	0	0	0	0	0	8	0
Sand	0	0	0	0	1	0	0	0	0	1	0	2

Table III.16: Error matrix for classified Seg-L-II image using unpruned tree.

	Reference Data											
Classified Data	Apartments	Houses	Metallic road	Nonmetallic road	Metro line	Canal	Water body	Dense vegetation	Sparse vegetation	Barren land	Wet land	Sand
Apartments	9	0	1	0	0	0	0	0	0	1	0	0
Houses	0	7	1	0	0	0	0	0	0	2	1	0
Metallic road	0	0	7	1	0	0	1	0	0	1	0	0
Nonmetallic road	0	0	0	2	1	0	0	0	0	1	0	1
Metro line	0	0	0	1	2	0	0	0	0	0	0	1
Canal	0	0	0	0	0	2	1	0	0	0	1	0
Water body	1	0	1	0	0	0	2	0	0	0	0	0
Dense vegetation	1	0	0	0	0	0	0	24	3	1	1	0
Sparse vegetation	1	1	0	2	0	0	0	1	16	1	0	0
Barren land	1	1	2	2	0	1	0	0	0	13	2	0
Wet land	1	1	2	0	0	0	0	0	0	1	5	0
Sand	0	0	0	0	2	0	0	0	0	1	0	1

Chapter 1:

INTRODUCTION

1.1 General

Remote sensing is defined as the science and art of acquiring information about material objects or phenomenon without actually come in contact with any of them. Using various sensors, active or passive, remote sensing devices acquire data by means of energy sources (Lillesand *et al*., 2007; Campbell, 2002). The energy transmits in the form of a wave corpuscular dichotomy (Mather, 2004). These measurements are possible because sensors or instruments are designed to measure the spectral reflectance of earth objects. It is discovered that each earth surface feature (i.e., land use land cover) has a unique spectral response in a given wavelength region. The response is also known as "signature" which enable us to discern the objects from its intermixed background. After interacting with the earth's surface, the energy sources get retransmitted through the atmosphere back to the sensors.

The wavelength intervals in which the sensor can detect the features of the earth's surface is known as the spectral resolution. In addition to spectral resolution, these returned waves are stored at different electromagnetic radiation, called as radiometric resolution, which varies between 6 bits and 12 bits. An image is composed in the form of pixels; each representing a certain area, on ground approximated from the spatial resolution of the sensor too. Smaller the pixel size, higher is the spatial resolution of the image, and thus the smaller objects can be identified from the satellite image. The spectral resolution with its spatial resolution of some sensors has been shown in Fig. 1.1.

The remote sensing data acquired at different spectral, spatial and radiometric resolutions can be used to extract information about the earth surface through either visual image interpretation elements or digital image processing procedures depending upon whether it is a photographic or digital product respectively.

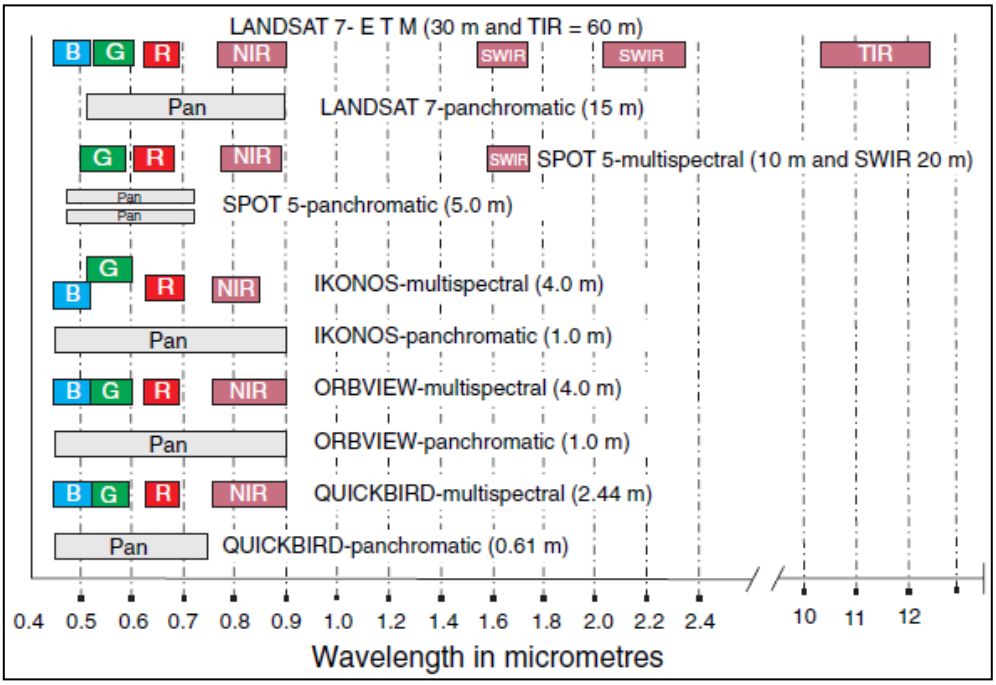

Figure 1.1: Comparison of the spectral and spatial resolution of different satellite systems (Schott, 1997)

1.2 Digital Image Classification

Digital remote sensing data are frequently used for preparing thematic maps such as land use land cover maps. Digital image classification assigns every pixel of the remote sensing data to a particular class using one of the various classification algorithms. During last 4 decades of remote sensing existence, scientists, practitioners and researchers have made enormous efforts in developing advanced classification approaches with the aim to derive accurate land use land cover information from varied remote sensing datasets under varied geographical and environmental conditions.

Digital image classification is a complex process and requires consideration of many factors. The major steps of image classification may include determination of a suitable classification system, selection of training samples, image preprocessing, feature extraction, selection of suitable classification algorithm, post-classification processing and accuracy assessment. The requirements of the users, scale of mapping, topographic conditions, and skills

of analyst are some of the key factors, which play in an important role in the design of a classification procedure under a given situation (Lu and Weng, 2007).

Since last several years, pixel based classification approaches are in vogue for classification of low and medium spatial resolution remote sensing data. Moreover, due to rapid growth in space technology, high spatial resolution images at resolutions < 5m are quite easily available now days. These images, no doubt, make visual interpretation comfortable, less tedious and precise but are also associated with other difficulties while classifying those using traditional approaches. This may partly be due to the fact that more details are resolved resulting in spectral mixing of classes. Moreover, the traditional pixel based classification approaches have limitations while incorporating the contextual attributes information like shape and size of land use features such as roads, buildings etc. in the classification process (Walker and Blaschke, 2008). Inclusion of these contextual attributes may result in production of quality land use maps from high resolution data, thus, introducing object based image analysis recently.

Land cover classification and extraction can be accomplished using either pixel-based or object-based or object oriented classification approaches. These approaches do not operate directly on individual pixels but on objects consisting of many pixels that have been grouped together in a meaningful manner by image segmentation. In addition to spectral and textural information utilized in pixel-based classification methods, image objects also allow shape characteristics and neighborhood relationships to be used for the classification of land cover or targets as objects.

1.3 Object Based Classification

Object based image analysis (OBIA) is a new concept applied for the extraction of meaningful objects of similar attributes from remote sensing images via a segmentation process. The classes involve a connection to nearby objects such as super and sub-objects in a hierarchical order. Spatial relationships such as ‘nearest neighbor’ or statistical similarities can be applied on segmented image for assigning class. At its rudimentary level, OBIA involves image segmentation, attribute selection, classification and the ability to link individual objects in hierarchy. In order to achieve this, OBIA incorporates knowledge from a vast array of

disciplines involved in the generation and use of geographic information (GI) (Blaschke and Lang, 2006). According to them the necessity of OBIA can be gauged from the following,

i. The object based analysis allows the incorporation of additional aspects in the classification such as object size, shape, position, topological relations, or distances to other objects

ii. Pixels do not sample the urban environment at the spatial scale of the features to be mapped. For example, buildings are represented by groups of pixels which should be treated as individual objects instead, in which shape characteristics could potentially enhance accuracy (Flanders *et al.*, 2003).

iii. A pixel's spatial extent may not match with the extent of the land cover feature of interest. For instance, the problem of mixed pixels is well known, whereby a pixel represents more than a single type of land cover, often leading to misclassification.

iv. The object of interest may be considerably larger than the pixel size. Consider, an agricultural agency that wishes to calculate an inventory of arable crops. Where the objective is simply to identify the crop type in each relatively large field (e.g., > 1 ha), relatively small pixels (e.g., spatial resolution = 4 m) may be inappropriately classified as a result of within-field variation.

OBIA allows inclusion of various useful features such as; shape, texture and contextual relations between objects. To achieve this, an appropriate segmentation algorithm is needed to organize an image into number of objects of varying sizes. Earlier, a threshold value was being used to segment an image into separate regions. However, now days, researchers have developed several segmentation algorithms based on different heuristics such as homogeneity measures, shape factors, scale parameters, texture, fuzzy membership values etc. Segmentation is the crucial part of OBIA. Therefore, a range of segmentation algorithms under different categories; point/threshold based, boundary based and region based, have been developed. However, segmentation is still an ill-posed problem as there is no unique solution as well as no means to assess the goodness of segmentation apart from visual assessment of quality. It varies with the perception of one analyst to the other. Hence, quantitative evaluation methods need to be developed.

In general, the quality of the image segmentation has been observed visually. Only some of the researchers applied some evaluation techniques for the quality evaluation. These techniques are categorized into three groups namely; the analytical, empirical goodness based and empirical discrepancy based approaches (Tian and Chen, 2007; Pal *et al.*, 2000). The detail descriptions are given in *Chapter 2*. Further, a number of attributes are generated for every segment during image segmentation, very little work has been done in the direction of the selection of the important attributes (Zhang *et al.*, 2010). In most of the cases the classification has been performed using all attributes. Additionally, limited number of classifiers has been used for object-based image classification. The nearest neighbor is mainly used for classification (Li and Shao, 2012; Salman *et al.*, 2008).

OBIA, since its inception, has been applied in various fields such as the wide-area monitoring of landscape areas (Laliberte *et al.*, 2007; Blaschke, 2005; Chandra *et al.*, 2005; Witheside, 2005); monitoring of densely settled urban areas (Chunyang *et al.*, 2005; Moeller, 2005); for obtaining information in the case of disasters (Heremans *et al.*, 2005; Kouchi and Yamazaki, 2005); data fusion and the establishment of geographical information system (GIS) (Cabral *et al.*, 2005; Kosugi and Kosaka, 2005; Sim, 2005; Benz *et al.*, 2004; Langanke *et al.*, 2004), road extraction (Zhang and Couloigner, 2006) and building extractions (Taubenbock *et al.*, 2010) etc.

With the advancements in OBIA, a number of software has been developed, as listed in Table 1.1. It can be seen from the table that each software has limitations and none can be regarded as complete.

Table 1.1 Overview of software for OBIA.

Software	Salient Features	Shortcomings
Machineseg program (Early 1980s) (Flanders *et al*, 2003)	• Utilization of aerial photographs to find two-lane roads. • Region growing image segmentation. • No segmentation quality assessment. • No attribute selection. • Length/width ratio, length and spectral data used for classification. • Freely available.	Worked only on aerial photographs. Useful in extraction of linear features only. Less efficient and more time consuming. Restricted by hardware and software requirements.
A road finder(ARF) (Late 1980s) (Flanders *et al*, 2003)	• Utilization of high-resolution aerial photographs for advanced object-based analysis to detect roads. • Region growing image segmentation • No segmentation quality assessment. • No attribute selection. • Freely available.	Used digital high-resolution aerial photographs. Able to extract linear features only. Limited by hardware, software, poor resolution and interpretation
SPRING (Early 1990s)	• GIS and remote sensing image processing system with an object-oriented data model. • Integrate both raster and vector data representations in a single environment. • Region growing and basin detection segmentation. • No segmentation quality assessment. • No attribute selection. • Uses ISOSEG, Bhattacharya and CLatex algorithms for classification. • Commercial software.	Not efficient in handling very large data sets.
Definiens eCognition (2000) (Baatz and Schape, 2000)	• The most promising software today. • Provides a multitude of features and techniques for OBIA. • Suitable for any kind of remote sensing data. • Region based image segmentation. • No segmentation quality assessment. • No attribute selection. • Uses nearest neighbor classifier. • Object extraction with masking. • Commercial software. • It uses advance techniques and additional parameters for quality	Segmentation is based on trial-and-error. Works with all attributes. Classifying an image by NN only.

	segmentation and classification.	
Objective (Erdas Imagine-2010)	• Provides a multitude of features and techniques for OBIA. • Suitable for all remote sensing data. • Edge based image segmentation. • No segmentation quality assessment. • No attribute selection. • Uses rule based classifier. • Object extraction with masking. • Commercial software.	Segmentation is based on threshold value.

From the above comparison table, it has been observed that most of the software's have limitation, as image segmentation somehow depends on user's defined parameter's values. Additionally, none of the software encompasses any quality measure to assess the quality of segmentation, which was indicated earlier, is the most crucial step in OBIA. Limited segmentation and classification algorithms have been used and further in all the software the classification has been performed using all attributes.

1.4 Research Gaps

On the basis of the short review provided in this chapter followed with an extensive review in chapter 2, a number of research gaps have been identified, which can be enumerated as:

i) The thresholding based segmentation algorithms are implemented on band-by-band basis, which may be insufficient for multi- and hyper-spectral remote sensing data.

ii) The edge based segmentation algorithms do not provide closed boundaries and at times, the boundaries may also be broken, which require post-processing that may be time consuming.

iii) The problem of over- and under- segmentation has been noticed in most segmentation algorithms unless the segmentation parameters are fixed judiciously.

iv) The quality of segmentation has generally been assessed by visual interpretation only. Very few attempts have been made for quantitative assessment of segmentation results.

v) A number of attributes have been suggested but the suitability of these for a given application and data has not been assessed.

vi) The use of a new generation of classifiers for object-based classification has been lacking.

1.5 Objectives of the Research

The main objective of this research is to evaluate the usefulness of object based image classification of high spatial resolution remote sensing data. Based on the research gaps identified through literature survey, following specific objectives can be enumerated as:

i) Fixation of the values of user defined segmentation parameters for segmenting the image.

ii) Study and development of quality measures for quantitative evaluation of segmented image.

iii) Study and development of a combined decision tree and ROC curve based approach for selection of attributes.

iv) Implementation of the decision tree based approach for object based classification as well as individual object extraction from remote sensing data.

v) Assessment of accuracy of classification and individual objects through suitable measures.

1.6 Overall Methodology

The overall methodology adopted in this research consists of five basic steps, as given in the form of flowchart in Figure 1.2. These include;

i) Image segmentation using multi resolution region growing segmentation and fixation of its parameters based on a new metric.

ii) Development of quality metrics, namely, segment fit index (SFI) and shape index disparity (ΔSI) for the assessment of segmentation quality.

iii) Selection of attributes using a combined decision tree and ROC curve based approach.

iv) Classification and object extraction using decision tree based classifier.

v) Accuracy assessment of classification using error matrix based measures and assessment of quality of individual objects using ROC curves.

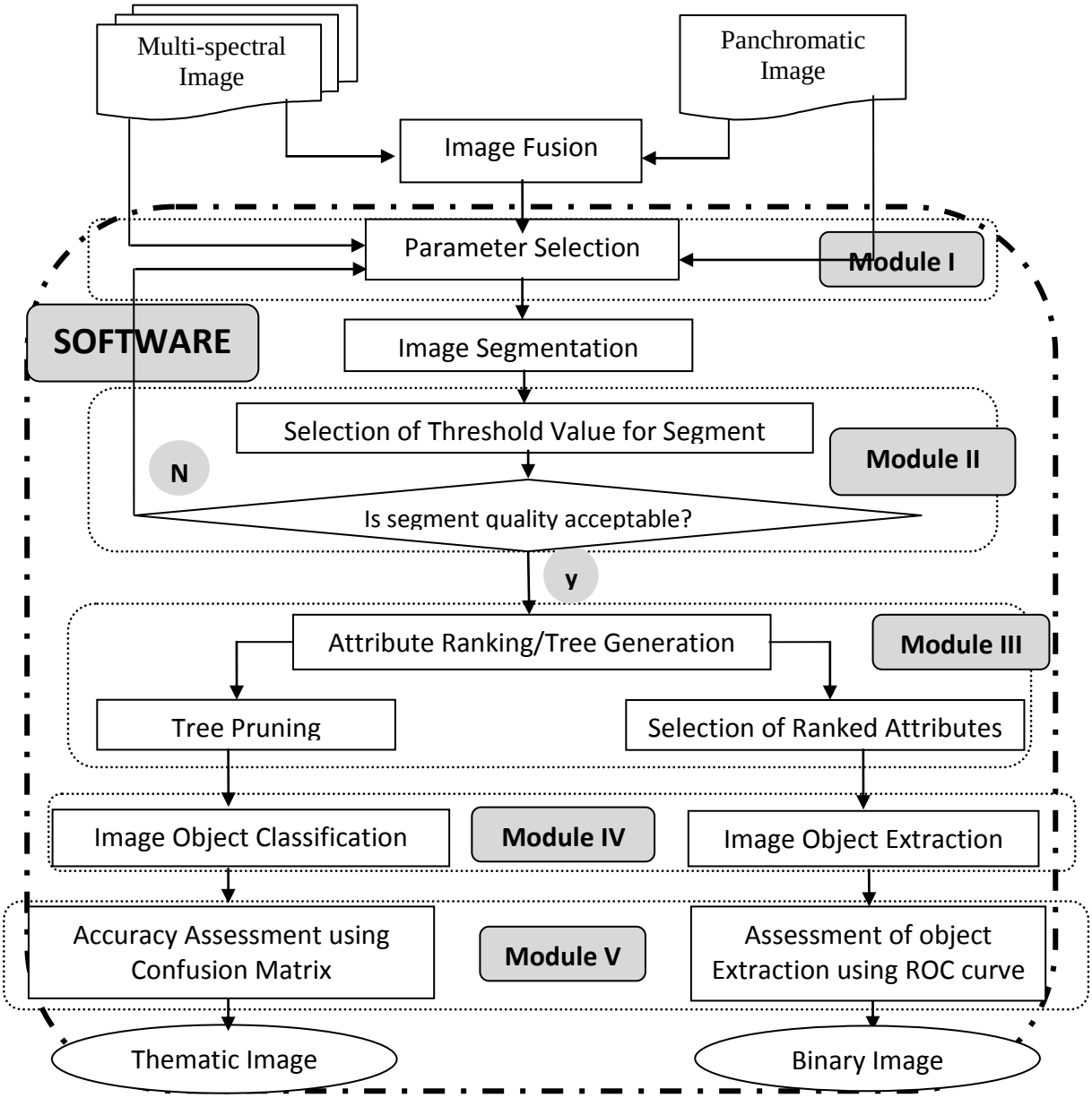

Figure 1.2: Overall methodology of the work

1.7 Organization of the Thesis

The thesis has been systematically organized into eight chapters including this present chapter of introduction. All the illustrations and tables have been inserted at appropriate place within the text. Chapter 1, after introducing the OBIA, frames the research gaps, objective of the research and an overview of the broad methodology to comply the objectives.

Chapter 2 provides a literature review of the related work and split in five parts. The first part provides the work done in the field of image segmentation for remote sensing data and also the new trends in image segmentation. The second part is related to user defined weights of parameters for proper segmentation. The evaluation approaches for the assessment of segmentation quality of the segmented image used by the authors will be covered in the third part of this chapter. The next part covers the feature reduction, in which the review on attribute selection techniques will be discussed. The fifth part of this chapter covers the literature review on the object classification and object extraction.

Chapter 3 provides the description of study area in terms of its geographic location and topography. The chapter also provides the details of experimental data sets (very high resolution Quick-bird image and high resolution LISS-IV image), image Pan-sharpening and generation of reference datasets used in this work to carry out the experiments using the algorithms.

The detailed description of the software developed to fulfill the research objectives is given in *Chapter 4*. The formats of various input and output data files required to interact with software has been explain in this chapter. The GUI functionality of the software along with the description of the information required by the various GUI elements is also provided.

Chapter 5 includes the type and mathematical description of image segmentation techniques used. It focuses on segmentation parameters, its mathematics and the generation of the fitness function for computing the segmentation parameters values for segmenting an image, and the flow diagram for obtaining it. The basis of segmentation quality evaluation techniques and generated index for evaluation with a flow diagram is also described in this

chapter. Further, the results of segmentation using fitness function and the assessment of the segmentation quality index on data sets are also described.

Chapter 6 focuses on object-based image classification, and its accuracies. The generated attributes have also been described. The chapter provides the detail of decision tree classifier, the C4.5 splitting rule of decision tree for attribute ranking, image classification and tree pruning.

Chapter 7, describes the implementation of a decision tree based approach for individual object extraction and use of ROC curve. Description and implementation of a generated 'combined decision tree-ROC curve' approach for attribute selection. The chapter also discusses about object wise attribute ranking based on its importance for object extraction from the segmented image. The extracted object and its qualities have also been discussed in this chapter.

Overall conclusions drawn from the analysis of the work have been presented in *Chapter 8*. This chapter also provides few suggestions and recommendation for future to carry this work forward.

Chapter 2:

LITERATURE REVIEW

2.1. Introduction

In recent years, due to the availability of high and very high spatial resolution remote sensing data, the concept of OBIA emerged as an alternative to pixel-based classification (De Kok *et al*, 1999; Blaschke, 2010). Earlier efforts were made on extracting mainly linear features. In early 1990s, improvements in hardware capabilities, object oriented techniques augmented its pace and various image segmentation algorithms were proposed. Optical remote sensing took a paradigm shift after 1999 with the launch of various high resolution satellite sensors (Dey *et al.*, 2010), namely, Landsat 7 (1999), IKONOS (1999), Quickbird (2001), WorldView-1 (2007), GeoEye-1 (2008), and WorldView-2 (2009). With the launch of each satellite into space the spatial resolution has been increased considerably, hence the size of the pixel becomes very small. Traditional pixel based analysis have been proved to be insufficient due to its incapability to handle the internal variability of complex scenes. This led to research on new classification algorithms, which expedite object based approach or OBIA for very high resolution remote sensing images (Hay and Castilla, 2006).

OBIA offers improvement in classification quality over per-pixel analysis and also resolves the salt-and-pepper effect, which is the most common noise (Yu *et al.*, 2006). A comparison between per-pixel classification and object based classification has clearly proved the superiority of later in many studies (Neubert, 2001; Meinel *et al.*, 2001; Flanders *et al.*, 2003; Koch *et al.*, 2003; Ehlers *et al.*, 2006).

OBIA approach has been widely used for forest classification (Dorren *et al.*, 2003; Heyman *et al.*, 2003; Shiba and Itaya, 2006; Maclean *et al.*, 2013). Xie *et al.* (2008) used an object based geographic image retrieval approach for detecting invasive, exotic Australian pine in South Florida, USA. Chubey *et al.* (2006) used OBIA to derive forest inventory parameters. Extraction of the canopy for single tree has also been done using high spatial resolution satellite images (Herrera *et al.*, 2004; Hay *et al.*, 2005; Bunting and Lucas, 2006). Maier *et al.* (2008) also incorporated LiDAR data to extract detailed information of forest classes.

The application of OBIA can be found in generation of large-scale maps also. Radoux and Defourny (2007) produced large-scale maps with delineated boundaries for forest management, using high resolution satellite images. Gergel *et al.* (2007) used OBIA to distinguish forest structural classes. Weiers *et al.* (2004), Bock *et al.* (2005), Lathrop *et al.* (2006), Diaz-Varela *et al.* (2008), Jobin *et al.* (2008) and Li and Shao (2012) demonstrated the usefulness of OBIA methods for habitat mapping tasks.

Zhong *et al.* (2005) and Kong *et al.* (2006) employed OBIA for urban land use information extraction from a high resolution image. Mo *et al.* (2007) carried out land cover classification in the Zhuzhou area, China, using a QuickBird multi-spectral image. Potential of OBIA to map urban land cover was also demonstrated by An *et al.* (2007) and Chen *et al.* (2007). Similarly, Lackner and Conway (2008) used IKONOS images to automatically delineate and classify land-use polygons in Ontario, Canada, within a diverse urban setting. Blaschke (2010) provided a review on the detail applications and recent trends of OBIA.

The introduction of eCognition software in the year 2000 has complimented the remote sensing community with a fully functional, user-friendly multi-scaled technique for object based image classification. It incorporates a knowledge based methodology for classification of image objects (Flanders *et al*, 2003). It is beyond doubt that the OBIA shall be a key image processing tool in future for extraction of information from remote sensing data. It is therefore important that the current research in OBIA is expanded further.

Majority of researchers have focused on improving the segmentation results; either by adding extra knowledge like texture, shape, contextual information or by combining two or more segmentation algorithms. Segmentation is the first and foremost step in OBIA, and the objects derived from a segmented image are the fundamental units for further processing of the image, hence the evaluation of the segmented image is an important aspect of OBIA. During the segmentation process, various attributes are generated for each of the segment. These attributes define the characteristics of the segment and are used for further processing. To increase the efficiency of algorithms, only important attributes are selected, which form the input database for an object based classification.

This chapter provides a review on various aspects of OBIA (i.e., segmentation and its quality, attribute selection and image classification).

2.2. Image Segmentation

Image segmentation is the process by which individual image pixels are grouped into partitions, according to some intrinsic properties of the image, e.g., gray levels, contrast, spectral values or textural properties. A survey of various image segmentations techniques can be found in (Haralick and Shapiro, 1985; Daida, 1991; Pal and Pal, 1993 and Le Moigne and Tilton, 1995). Efficient image segmentation is one of the most critical tasks in automatic image processing as it creates the basic units for classification of an image (Pavlidis and Liow, 1990; Zhang, 1997; Cheng *et al.*, 2001). Thus, the success of an OBIA system depends on the quality of image segmentation. Image segmentation has been interpreted differently for different applications. For example, in machine vision applications, it is viewed as a bridge between low level and high level vision subsystems (Spirkovska, 1993), in medical imaging as a tool to delineate anatomical structure and other regions of interest whose a priori knowledge is generally available (Pham *et al.*, 2000) and in statistical analysis, it is posed as a stochastic estimation problem, with assumed prior distributions on image structure (Kerfoot and Bresler, 1999). In remote sensing, it is often viewed as an aid to land use land cover classification and landscape change detection.

A large number of image segmentation algorithms are available in the literature (Trivedi and Bezdek, 1986; Gofman, E. 2006; Sramek and Wrbka, 1997; Burnett and Blaschke, 2003). These segmentation algorithms can be grouped into four broad categories as follows:

i) Pixel based algorithms
ii) Edge based algorithms
iii) Region based algorithms
iv) Hybrid algorithm

2.2.1. Pixel Based Algorithms

Pixel or threshold based algorithms are based on defining the limits on the attributes (e.g., gray level, color value, texture, etc) of pixels to form objects with attributes of similar characteristics (Lim and Lee, 1990). Other criteria such as histogram shape, clustering, entropy, spatial correlation etc. may also be used to define the thresholds (Arifin and Asano,

2006). The output from a thresholding operation is usually a binary image with ones indicating the objects and zeros indicating the background.

Thresholding is a popular technique in image segmentation as it is computationally simpler than other existing algorithms such as boundary detection or region-based techniques (Pal and Bhandari, 1992). Thus, if computational requirement is of important consideration, as in machine vision, the thresholding technique is preferred to other techniques and is widely used in image segmentation (Pratt, 1978). However, these techniques do not necessarily produce the required result and therefore the resulting output needs to be clumped. Consequently, each spatially continuous unit (often referred as connected component in machine vision literature) needs to be assigned a unique label (Weszka, 1978; Fu and Mui, 1981; Sahoo *et al.* 1988)

There are two different approaches for thresholding: global thresholding and local thresholding. In local thresholding, the image is divided into smaller sub-images and the threshold for each sub-image depends on local properties or on the position of the point (Lee *et al*., 1990). Weszka and Rosenfeld (1978), applied two techniques of threshold selection, co-occurrence based busyness (based on texture) and classification error, on synthetic as well as real image. The outputs obtained from these two techniques were compared and it was found that busyness based technique provides good result. Sahoo *et al.* (1988) evaluated the performance of several global thresholding techniques over a given set of test images. Lee *et al*., (1990) choose shape measure, and uniformity measure (Levine and Nazif, 1985) in order to evaluate the performance of global thresholding techniques quantitatively. They concluded that the performance of global thresholding techniques was limited by the object size, mean difference, contrast, variances of object, background and noise of the image. Hence, performance comparison depends on the performance criterion used.

Since remote sensing images are normally ill illuminated, highly dependent on environmental conditions and also objects in a region are ill-defined. Thus, traditional thresholding techniques may not be appropriate. Pal *et al.* (2000) applied different fuzzy thresholding techniques based on entropy of fuzzy sets, fuzzy geometry and fuzzy correlation, on IRS and SPOT images. It was found that fuzzy set based thresholding approach appeared promising to exploit the ambiguities in intensity and spatial domains in an effective manner, and produce better segmentation result than traditional thresholding techniques.

The performance of thresholding techniques depends upon various image parameters and applied on band-by-band basis. As remote sensing images are usually multispectral or hyperspectral, implementation of thresholding technique is very time consuming. Hence, other algorithms such as boundary based and edge based may be used to overcome the limitations posed by thresholding.

2.2.2. Boundary Based Algorithms

In boundary based segmentation algorithms, the boundaries among different regions are determined. Two techniques, i.e. edge based and watershed based transformation, have been used to delineate the boundaries among different image objects.

Farag (1992) examined the edge-based approach for image classification. A unified treatment of maximum energy and regularization filters for step edge enhancement was presented and a new algorithm for edge linking based on sequential search was discussed. The results indicated that linking algorithm was superior and sufficient for edge linking.

Edge detection has been extensively used for extracting features from remote sensing images and also in the segmentation of medical imagery (Pham *et al.*, 2000). In the edge based method, the edges were regarded as boundaries between image objects and were located where changes in DN values occurred. Jain *et al.* (1995) also worked on edge detection to delineate the boundaries of the objects. Three steps namely: filtering, enhancement and detection were involved. Filtering step was usually necessary in decreasing the noise present in the imagery. Image enhancement was carried out to highlight the edges and was done through high-pass filtering. The detected edge points were linked, to form the region boundaries and the regions were labeled.

A new image texture segmentation algorithm based on wavelets and the hidden Markov tree (HMT) model was proposed by Choi and Baraniuk (2001) named HMTseg. This algorithm was applied to different type of images including radar, sonar and medical images. It was observed that by concisely modeling and fusing the statistical behavior of textures at multiple scales, this algorithm produced a robust and accurate segmentation of texture images. Instead of a single segmented image, HMTseg produced a range of segmentations at different scales.

Further, it was also experimentally proved that HMTseg has a potential to segment wavelet-compressed data directly without re-expanding to the space domain.

An image segmentation system adapted to the uniform and/or weakly textured region extraction was proposed by Kermad and Kacem (2002). In this paper, authors addressed the problem of detecting low-level features in images. The proposed approach was based on two concepts (i) the integration of the information, resulting from two complementary segmentation methods; edge detection and region extraction and (ii) the active perception via the intermediate of a feedback. It was also revealed that the developed approach operates without intervention of high-level knowledge. This approach was applied to both weakly and strongly textured real images, and results demonstrated the potential of the iterative co-operation scheme.

Vitti (2012) described the Mumford–Shah variational model for image segmentation. The Mumford–Shah functional consisted of three weighted terms, the interaction of which assured that the three conditions of adherence to the data, smoothing, and discontinuity detection were meeting at once. In this, smooth approximation of the data was done to preserve the data discontinuity and then unsupervised maximum-likelihood based classifier was applied as the second step of a twofold procedure, for eventually assigning a class membership to the regions. The procedure was applied to a high-resolution aerial orthophoto. It was observed that the proposed approach produces less noisy and more homogeneous image than that of obtained by the direct classification of the original orthophoto, which showed significant improvement in classification accuracy compared to direct classification.

In recent years, several authors (Meyer and Beucher, 1990; Saarinen, 1995; Carleer *et al.*, 2005) used the watershed line as the primary tool of mathematical morphology for image segmentation. Mathematical morphology considers gray-scale images to be sets of points in a three-dimensional space, the third dimension being the gray level. The watersheds or catchment basins of the image were the draining areas of its regional minima. These areas were separated by lines called watershed line (Beucher, 1982; Merle *et al.* 1995; Vincent and Soille, 1991).

According to Bleau and Leon (2000), usually the image was over segmented into large number shallow watersheds at the starting. This work presented a novel approach of watershed

merging to solve the problem of over-segmentation. In this, the closest image that has a simpler watershed structure was used for finding the real landscape. The water first forms the tiny and shallow watershed and then flows to a nearby deeper watershed by overflow. The method presented in this paper applied the minimum extensive modifications possible to a given image to obtain a segmented image.

The widely used watershed algorithm usually has the problem of over and under-segmentation. Wang *et al.* (2005) used the texture as a separate band, to improve the segmentation quality of high resolution image. The effectiveness of this improved watershed segmentation approach for high-resolution imagery was analyzed, which partly resolves over-segmentation and under-segmentation problem.

Even though the boundary based segmentation techniques takes less time in comparison to the thresholding techniques, but still suffers with over and under segmentation problem. As the land use land cover is uneven in nature that appears as mixed classes in remote sensing data. Hence, boundaries are not clear and sometimes broken also, thus post processing is generally required to join these broken boundaries. This has led to the development of region based technique.

2.2.3. Region Based Algorithms

Region based techniques produces closed boundary region as it works on the basis of the region homogeneity. The aim of the region based technique is to form region or segment through the clustering of homogeneous pixels. Various region based techniques such as; region growing, split and merge, data clustering have been used for image segmentation. The popular methods are Hierarchical split and Merge (Hu, *et al.*, 2005; Ojala and Pietikainen, 1999) and region growing (Baatz and Schape, 2000).

Baatz and Schape (2000) brought significant development in the research of multi-resolution segmentation for remote sensing imagery. A new, Multi-resolution hierarchical segmentation technique using Fractal Net Evaluation approach (FNEA) was introduced. FNEA represents the notion of hierarchy as fractal net because of the self similarity notion of fractals. Each coarser level gets the input from finer level and if an object identified at coarser level then it repeats its representation at each finer level, which was referred as similarity. The

process started with each pixel as objects and then subsequently merged based on the criteria in which merged region should not exceed a defined heterogeneity threshold. This approach has capability to incorporate spectral, texture, spatial, shape, size, prior knowledge and contextual properties of image. This approach was incorporated in Definiens eCognition, a commercial software product. This software revolutionized the field of remote sensing image segmentation, with its immense possibility to provide GIS ready information (Benz *et al.*, 2004).

Apart from the development of eCognition, some other techniques were also developed. Chen *et al.* (2003), applied a top-down strategy for multi-scale segmentation on SPOT HRV image. They performed discrete wavelet transform on first principal component, which was obtained by applying PCT on original bands. Segmentation at fine scale used region growing procedure based on seed pixel of region. Pixels were grouped with seed pixel on the basis of spectral and textural feature vector. Grouping was based on a threshold of acceptable heterogeneity after merging. This process was performed iteratively until all coarse scale segmentation was subjected to fine scale segmentation.

Bottom–up approach was applied by many researchers for multi-scale image segmentation (Aksoy and Akcay, 2005; Zhong *et al.*, 2005). It started with seed pixel, and this seed pixel was subsequently merged with its neighbors, based on achieved homogeneity measure. The homogeneity measure was derived from color feature, smoothness feature and compactness feature. Once, every region at a particular scale was processed, the average size of objects was calculated. If this average size satisfies the threshold, the segmentation was considered optimal otherwise further segmentation was carried on.

A modified seeded-region growing (SRG) and region merging approach for segmentation of a high-resolution pan-sharpened satellite image was proposed by Byun *et al.* (2011). The initial seeds were automatically selected using the proposed block-based seed-selection method. The initial segmentation was achieved by applying the modified seeded-region growing procedure. The final segmented result was obtained by merging the homogeneous regions based on a region adjacency graph (RAG). The experimental results demonstrated that the proposed method had better performance than other approaches. Thus, had good potential for its application to the segmentation of high-resolution satellite imagery.

The region growing segmentation algorithm had been an important technique for extracting features from images (Adams and Bischof, 1994). The problem in this algorithm was to setting of desired threshold for stopping the growth of a region. Improper threshold setting usually creates over-and under-segmentation and meaningful objects cannot be created. Thus, to overcome these drawbacks, Chang and Chen (2008) proposed a multi-scale region growing segmentation technique, which considered region homogeneity as well as the edge information of different scales to improve the segmentation result. The proposed technique has removed the limitation of threshold setting and generated relatively reasonable segmentation output for different types of objects.

Li *et al.* (2008a) applied multi-scale segmentation using hybrid of statistical region merging (SRM) for initial segmentation and minimum heterogeneity rule (MHR) for merging objects of high resolution Quick-bird imagery. SRM utilizes spectral, scale and shape measures for initial segmentation. Segmentation using SRM follows region-growing technique, where region growing was based on statistical test. Minimum Heterogeneity rule was based on color (spectral) and shape property for region merging.

No doubt, multi-resolution model is the most effective technique for remote sensing image segmentation. For improvement, it is possible to combine the concept of multi-scale technique with other segmentation approaches e.g. with Markov random field (MRF) model (Bouman and Shapiro, 1994). Its success depends on its capability to incorporate spectral, shape, size, texture and contexture features of region at various scales for efficient segmentation, especially for high resolution complex landscape imageries. According to Chen *et al.* (2009), selection of appropriate scale and information extraction from image was the most typical part of this model. The developed method aids in identifying the scale of proper representation of objects.

Lizarazo and Elsner (2009) proposed an object-based image classification approach, which was based on fuzzy image-regions instead of crisp image-objects. The approach works in three steps: (a) fuzzification, in which fuzzy image-regions based on the degree of membership of each pixel to target land-cover classes were developed. (b) feature analysis, in which contextual properties of fuzzy image-regions were quantified; and (c) defuzzification, in which these fuzzy image-regions were allocated to target land-cover classes. The proposed procedure was implemented using automated statistical techniques that require very little user interaction.

The results indicated that fuzzy segmentation-based methods produced acceptable thematic accuracy and presented a viable alternative to current crisp image segmentation approaches.

In their research, Gao *et al.* (2011) used nine different parameters for segmenting the multi-spectral Landsat imagery. The aim of these parameters was to maximize intra-region homogeneity and inter-region heterogeneity between neighboring segments. The objective function was derived to evaluate the segmentation results. The segmented images were classified into eight land-cover classes and the classifications accuracy was assessed by using 600 randomly distributed independent ground points. The result indicated that the segmented image with highest objective function values produced highest classification accuracies. The result has also shown that classification accuracy directly linked with image segmentation and highest accuracy were achieved with optimal segmentation. The objective function not only worked on a single band image but also on multi-spectral imagery as tested by Espindola *et al.* (2006).

Massada *et al.* (2012) included height information collected from light detection and ranging (LiDAR) data for image segmentation. The multi-resolution segmentation technique was applied and image was segmented with varied parameters, and an area-fit approach was used to select the most successful segmentation. They assessed the feasibility of this approach in northern Israel and compared the segmented result with a traditional vegetation formations map to explore the performance of the segmentation algorithm under various parameter combinations.

Yan *et al.* (2012) proposed a new object-based analysis (OBA) method to derive digital terrain model from airborne laser scanning data, as the available methods were not so effective. In the proposed method, an unorganized cloud points were initially accelerated using grid index algorithm and the image objects were generated by segmentation using index. In this region-growing algorithm, the seed pixels were decided on the basis of their height. It was concluded that the OBA algorithm yields good results without parameter optimization and OBA method, become even more advantageous with a further increase in point densities. It was also pointed that the OBA algorithm had an ability to produce more accurate building boundaries.

A new multispectral image texture segmentation algorithm was proposed by Chen and Strobl (2013). It was based on the multi-resolution fuzzy Markov random field (MRF) model, for a variable scale in the wavelet domain. The working principal of algorithm was to constrain correlations between neighborhood features with the use of scalable wavelet coefficients combining with the fuzzy label field. The algorithm considered multi-scalar information in both vertical and lateral directions. The effectiveness of the proposed algorithm was tested on two (multispectral texture images and remote-sensing images) data sets. Segmentation results show that this new method was very convenient in achieving the homogeneity of the region and accuracy of detected boundaries compared with existing image segmentation algorithms.

Generally, the image is segmented by applying some input parameters; the selection of these parameters is complicated. In their proposed solution, Sebari and He (2013) gave a non-parametric cooperative segmentation technique, which made use of a fuzzy rule based classification on the human knowledge. This rule integrated spectral, textural, geometric and contextual object proprieties. The IKONOS images of Sherbrooke city (Canada) was classified using this proposed fuzzy rule based approach. The overall extraction accuracy for extracting building, road and parking lot classes were achieved 80%. The limitation of this approach is that it requires conformity of the geometric shape of the extracted objects to the reality.

On the other hand, Carleer *et al.* (2005) evaluated and compared the results of four algorithms, from the two main groups of segmentation algorithms (boundary-based and region-based) using empirical discrepancy based evaluation methods. The results showed that the choice of parameters plays an important role and had great influence on the segmentation results. The selected boundary-based algorithms were sensitive to the noise or texture. It was also observed that region based algorithms produces better results.

In reality, land uses present on earth surface are uneven in nature and also mixed with other surrounded features that may produce noisy image with unclear boundary. Thus, a single segmentation technique is not helpful for properly segmenting the image. Therefore, hybrid algorithms (combination of any two segmentation methods) are useful for finding meaningful segments from the image.

2.2.4. Hybrid Segmentation Algorithms

Pavlidis and Liow (1990) presented a technique which combines region growing and edge detection for image segmentation. Split-and-merge technique was initially applied on camera photographs, the parameters were set in such a way that it has produced an over-segmented image. Further, the edge detection algorithm was applied on that over segmented image, which extracted the boundaries of the meaningful objects. It was concluded that the combination of two methods yields far better segmentation results as compared to any single method.

Fan *et al.* (2001) proposed a new automatic image segmentation method which integrates color edges with seeded region growing (SRG) technique. In this method, an image with color edge was first obtained automatically by combining an improved isotropic edge detector and fast entropic thresholding technique. After the major geometric structure in an image was obtained from color edges, the centroids between these adjacent edge regions were taken as the initial seeds for SRG. These seeds were then replaced by the centroids of the generated homogeneous image regions by incorporating the required additional pixels step by step. Segmentation results show that this integrated approach provides more accurate segmentation of images.

A new object-oriented segmentation approach with special focus on shape analysis was developed by Mueller et al (2004). This approach was used for the extraction of large man-made objects especially agricultural fields, from the high-resolution panchromatic satellite imagery. The technique was divided into two parts, where essential shape information was extracted in the first part and edge-guided region growing technique in the second part. The results demonstrated the ability of the presented approach to detect long straight edges in images at their precise position, and regions with regular shape such as agricultural fields was extracted in high-resolution panchromatic image.

The generation of urban land cover maps accurately from high-resolution satellite imagery turn out to difficult within the urban region, because of the multi-scale feature and diverse composition of land cover types. Li *et al.*, (2008b) proposed a multilevel object based classification method based on hierarchical segmentation and shape descriptor. The process starts with the extraction of vegetation classes and shadow by pixel based classification and post classification processing. Secondly, it adopts a multilevel object based classification for

non-vegetation classes. It incorporated spectral and shape features at multiple segmentation levels. The experiment shows that the hierarchical object based classification method provides higher overall accuracy, compared to other methods.

Wang (2008) designed a multi-resolution image segmentation method combining spectral and shape features. The algorithm had following steps. (i) The initial segmentation parcels were obtained with rain falling watershed algorithm for its fast speed and good initial segmentation effects. (ii) A fast region merging technique has been designed to merge these parcels (sub feature units) in a hierarchical way. (iii) For controlling merging process, a scale parameter was used. The segmentation method produced highly visually homogeneous parcels in arbitrary resolution on different types of images.

Malambo (2009) developed a region based approach for image segmentation, considering both spectral and spatial information. This approach initially divides the image into several groups (in the spectral space) considering the Mahalanobis distance as a measure of similarity. The result was then segmented into regions using region growing segmentation. To overcome the problem of over and under segmentation, the edge information incorporated with region growing process. The main strength of this approach was the reduction of the mixed pixel problem suffered by most pixel based methods.

Thus, from this brief review, it appears that region based image segmentation is the most popular one. Most of the available commercial software incorporates the region-based techniques. However, any segmentation based technique relies significantly on proper selection of values of inherent parameters in their formulation and is a matter of discussion.

2.3. Segmentation Parameter Selection

The selection of parameters; scale, smoothness and compactness, for multi-resolution segmentation requires an expert knowledge. Ali *et al.* (2005) used fuzzy based semi-automatic approach to select the parameters for image segmentation. Maxwell (2005) proposed a fuzzy based approach which automatically selects the parameter of the segmentation used in multi-resolution approach.

Region-growing segmentation algorithms have been generally used for segmenting remote sensing image. The quality of the resulting segmentation is controlled by the user defined segmentation parameters. Maxwell (2005) developed a semi-automatic fitness function called as segmentation optimizer based on fuzzy logic technique for reducing the tedious trail-and-error process of object segmentation. The aim was to determine the optimal object segmentation parameters to achieve most appropriate segmentation of individual objects. In the proposed optimizer, instead of trial and error, initial segmentation parameter of the input image was used to train the segmentation optimizer. After the training, the segmentation optimizer identifies most suitable object segmentation parameters. Finally, these parameters were used to segment objects in the entire input image, achieving an optimal segmentation for all objects of interest.

Espindola *et al.*, (2006) generated a spatial autocorrelation indicator that detects separability between regions and a variance indicator, which expresses the overall homogeneity of the regions. The proposed method allows users to benefit from the potential of region-growing methods for extracting information from remote sensing data. According to Wulder and Boots (1998) and Fotheringham *et al.* (2000), spatial autocorrelation had an inherent feature of remote sensing data and also reliable indicator of statistical separability between spatial objects. This provides a high degree of flexibility but comes at the cost of extensive testing to establish the optimal system that is robust for a variety of data sets.

Boesch and Wang (2008) presented an approach named as J-segmentation (JSEG) to select optimized parameter values for segmentation. The parameter evaluation was based on finding the discrepancy between segmented regions and manually acquired ground truth. Parameter evaluation with city block optimization (CBO) was its main strengths due to its robustness and works with limited ground truth. The color quantization of the used JSEG was found very sensitive to strong lightness variations. In their work, Gao *et al.*, (2007) showed that objective function was in fact an effective way to determine the optimal segmentations to carry out the classification.

The work presented by Bo and Han (2010) was based on the selection of suitable parameters for region-growing algorithms to ensure best quality results. It considered that segmentation had two desirable properties: each of the resulting segments should be internally

homogeneous and should be distinguishable from its neighborhood. In their work, authors performed the trial and error segmentation by modifying the parameters values every time. The obtained segmented images were classified and classification accuracies were calculated. Finally, authors selected the segmentation parameters value that produced highest overall accuracy.

Thus, very little work has been done in the field of selecting the appropriate values for the segmentation parameters. The quality of segmentation is checked at each step of selection of parameters as well as their values. The segmentation quality may be assessed visually as well as through the use of quantitative measures. An account of research carried out in evaluating the quality of segmentation is also worth reporting here.

2.4. Segmentation Quality Evaluation

Various algorithms have been proposed to evaluate the quality of segmented image. The quality of the image segmentation can be assessed in two ways;

i) Goodness based approach that does not require any reference image.

ii) Discrepancy based approach in which a reference image is required

2.4.1. Goodness Based Evaluation Approach

The methods in this group evaluate the quality of segmented images based on the intra-region homogeneity of the segments. Various measures have been applied to assess the intra-region uniformity. Thus, there is no requirement of another data source (e.g., reference image or ground data) for the assessment of quality.

In their work, Borsotti *et al.* (1998) examined the issues related to the automatic evaluation of the results of color image segmentation proposed by Liu and Yang (1994), who developed an evaluation function that did not require user's interference for parameter or threshold selection. However, authors identified limitation in this automatic evaluation function, the value of which was near zero even though the image was over-segmented. They proposed two enhanced functions (the *F'* function and the Q function) that offer more realistic judgment. The

F' was the modified version of a function proposed by Liu and Yang. In their experiment, they applied the evaluation functions on ten test images segmented by six clustering methods. It was observed that the generated evaluation functions produced good evaluation results in comparison to the existing one

Pal *et al.* (2000) demonstrated the effectiveness of various fuzzy thresholding techniques for image segmentation based on the entropy of fuzzy sets, fuzzy geometrical properties, and fuzzy correlation on remotely sensed (IRS and SPOT) images. The paper presented a new index (β index) for quality evaluation using the concept of homogeneity. The intra-region homogeneity was compared with β index, higher the value of β, greater the intra-region homogeneity. It was found that value of β increases with number of classes present. If the whole image had been grouped in a single segment (c=1) then β=1, while if every DN values presented in the image were considered as class, then β becomes ∞. Results were compared with those of probabilistic thresholding, and fuzzy *c*-means and hard *c*-means clustering algorithms, both quantitatively (in terms of index value) and qualitatively (in terms of structural details). Results indicated that fuzzy set theoretic algorithms superior with respect to non-fuzzy counterparts. Fuzzy correlation, followed by fuzzy entropy performed better among all the techniques used for extracting the structures. Fuzzy C-Mean (FCM) was found superior to Hard C-Mean (HCM).

Zhang *et al.* (2004) proposed a novel objective segmentation evaluation method based on information theory. The method used entropy as the basis for measuring the uniformity of pixel characteristic (luminance was used in this paper) within a segmentation region. It provided a relative quality score, which was capable to compare different segmentation of the same image. The results showed that the proposed evaluation method was superior to the earlier quantitative segmentation evaluation by Liu and Yang (1994) and Borsotti *et al.* (1998). In the proposed approach, the region's luminance information helps in the formation of the accurate homogeneous region.

Johnson and Xie (2011) applied multi-scale approach to improve the segmentation of a high spatial resolution (30 cm) color infrared image of a residential area. A series of 25 image segmentations were performed in Definiens Professional-5 software using different scale parameters. Unsupervised evaluation method of segmentation quality that takes into account

global intra-segment and inter-segment goodness measures was used for identifying the optimal image segmentation. Further, under and over segmented regions were identified using local heterogeneity measures (variance and Local Moran's I). A heterogeneity index (H), which took into account these local statistics, was able to identify regions that were under and over segmented in the optimal single-scale image segmentation. These regions were refined by segmenting under-segmented regions at finer scales and merging over-segmented regions with spectrally similar neighbors that were also over-segmented. The method used in this study was able to overcome some of the limitations of traditional single scale segmentation approaches. To evaluate the segmentation quality it computed the global score (GS) value for each segment that was based on Moran's I. The value of GS was low for the segments that matched the border

Due to the diversity in the segmentation algorithms, the uniformity measure such as; texture, luminance, etc. within the segment vary, which affects the shape and size of the formed segments. As the goodness based evaluation approach has been based on the intra-region homogeneity measure, it may not produce good results. Therefore, a discrepancy approach, which is based on the comparative assessment of formed segment with its reference may be advantageous.

2.4.2. Discrepancy Based Evaluation Approach

Quantitative discrepancy based evaluation approach calculates deviation of the formed segment from its reference object. The deviation could be in the area, perimeter, etc. it produces the statistical measure of the quality.

Yasnoff *et al.* (1977) proposed a pixel distance error method for quality assessment. The authors also applied the percentage area misclassified method for evaluation. These algorithms were applied for evaluating the segmented image. The usefulness of both the methods in image segmentations on a single image and on multiple images by these methods was presented. The results indicated that both of these methods were helpful in the evaluation and comparison of scene segmentation procedures.

Roman-Roldan *et al.*, (2001) proposed a new model for evaluating the performance of available methods of image segmentation and edge detection. The method was intended for the evaluation of low error results and features. An objective assessment of discrepancy with respect to the theoretical edge using both the neighborhood and error-interaction criteria was done. The proposed mathematical model was a hybrid model with combination of both discrepancy and goodness. It combined the pixel-by-pixel objective discrepancy between the obtained edges and the theoretical ones with an evaluation of each mistake as assessed by human observers. The measure belongs to a class that may be called the low-error model of quality measures, not intended for excessive or aberrant (not usually found in edge images) errors. In order to implement these statements in a mathematical expression, the following bases were established; (i) the theoretical edge was defined by convention so that the mistakes produced could be detected and evaluated one by one; (ii) only strict closeness to the ideal edge was relevant; and (iii) interactions between closely clustered mistakes, should involved in the assessment of the quality.

Jiang *et al.* (2006) presented theoretical, feature-based and task-based evaluations for quality assessment. To validate the measures proposed in this paper, it was tested on 50 images. Various indices grouped into, (i) distance of clustering by counting pairs, (ii) distance of clustering by set matching and (iii) information-theoretic distance of clustering groups, were used. The results were also compared with those obtained from Hoover index. The segmentation quality results on 50 images demonstrated the usefulness of indices in both range image and intensity image domain. The paper claimed that the proposed approach was applicable in any task of segmentation performance evaluation. This includes different imaging modalities (intensity, range, etc.) and different segmentation-tasks (surface patches in range images, texture regions in gray-level or color images). In addition, the usefulness of these measures was not limited to evaluating different segmentation algorithms, but also applicable to train the parameters of a single segmentation algorithm.

Tian and Chen (2007) generated a measure termed as ‘Gs’ which takes into account both the overlapping areas and the mismatch area. The Gs was calculated as the ratio of the total overlapping areas and total dissimilarity area of segments with its reference object. The superiority of the proposed framework was tested on three artificial feature types (sports fields, roads, and residential buildings) in IKONOS multispectral images. Artificial objects included

not only intensive features (e.g. buildings) but also extensive features (e.g. roads). An intensive feature was represented by a single meaningful object taking the place of the feature, whereas an extensive feature was represented by multiple objects meaningful to the feature class. The author also addressed the issue of optimization of parameters in multi-resolution segmentation and tried to fix scale parameter to find optimal segmentations.

Neubert *et al.* (2008), developed some methodical extensions of the segmentation quality evaluation process. In the study, object differences were analyzed as topological and geometric relationships between the segment and the reference object. The overlapping area was calculated to describe the area of concurrence. Furthermore, the harmony of the segment outlines was compared with buffer zones around reference objects. The accuracy of the segmentation was evaluated with the Area Fit Index (AFI), which measures the difference between formed segments and corresponding reference objects. It also produced an indicator for the rating of over-and-under segmentation.

Liu *et al.* (2012) evaluated four existing indices (Quality Rate (QR), Over-segmentation Rate (OR), Under-segmentation Rate (UR), and Euclidian Distance 1 (ED1)) to identify optimal parameters of image segmentation that describe the discrepancy between reference polygons and corresponding segments. They proposed three new indices, Potential Segmentation Error (PSE), Number-of-Segments Ratio (NSR), and Euclidean Distance 2 (ED2) to evaluate both geometric and arithmetic discrepancies in the segmented image. They compared the effectiveness of the existing and proposed indices for identification of optimal combinations of parameters for image segmentation. The results show that the optimal combination of parameter values selected by ED2 achieves better quality of image segmentation than the optimal combination of parameter values selected by ED1. The most critical improvement of ED2-selected combinations over the ED1 selection lies in the number of corresponding segments. This happened because the ED2 selection considers both geometric and arithmetic discrepancies. It was found that the Euclidean distance ED2 and its associated PSE and NSR were more suitable for determining the optimal parameters in image segmentation.

Zhang (1997) reviewed various methods for segmentation evaluation (Yasnoff, *et al.* 1977; Yasnoff and Bacus, 1984; Nazif and Levine, 1984; Pal and Bhandari, 1992; Strasters,and

Gerbrands, 1991; Zhang, 1993a, 1993b). These methods were classified into three groups: the analytical, the empirical goodness and the empirical discrepancy groups. The paper presented comparative discussions of these different methods. The analytical method did not apply directly on the image, but assesses the algorithm by considering the principles, complexity etc., while the empirical methods applied on the segmented image. The study indicated that empirical methods were more suitable and useful than the analytical methods, for performance evaluation of segmentation algorithms as it assesses the quality qualitatively. Between empirical methods, the discrepancy methods were better for objectively assessing segmentation algorithms than the goodness methods although the former was somewhat complex in application than the latter due to the requirement for reference. Besides that the goodness based evaluation methods assess the quality by judging the intra region uniformity, inter region contrast and its shape. Therefore, only one evaluation method may not be enough to judge all properties of an algorithm and different methods should be adopted.

Visual representation produces the better judgment for the quality of segmentation as it varies with requirement. Empirical methods have been more suitable for evaluation as these produce statistical values of measures. However, discrepancy based measures have been more suitable as these compute the value by considering the reference as per requirements.

The property of the segments in the segmented image is described by the attributes, which represent the characteristics of the land uses. However, only some of the attributes are useful to discriminate a class. Thus, selection of significant attributes through a quantitative approach is a key to successful object based classification.

2.5. Attribute Selection

Each segment of a segmented image has number of attributes to represent the characteristics of the class. These attributes are typically grouped into spectral, textural, contextual categories. However, only some attributes from each group may be useful to highlight the segments belongs to one object. Extraction of an object using all attributes is very time-consuming, also requires more space for storing these values and hence reduces the efficiency of classifier. An attribute selection process reduces the number of attributes by selecting only the most

significant attributes and ignoring the redundant attributes based on certain criteria. The reduced feature space not only results into better classification accuracy but also improves the efficiency of the system.

Many attribute selection techniques have been discussed in the literature, which were applied to select the required number of attributes. However, in OBIA, only few attribute selection techniques namely; Separability and threshold (SEaTH), the Jeffries-Matusita (J-M) distance, Bhattacharyya distances, Correlation analysis, and Gini index have been used for selection of important attributes.

According to Nussbaum *et al.*, (2006), the Separability and threshold (SEaTH) technique calculates the separability and the corresponding threshold for each combination of object and the attribute. It selects the attributes that had maximum separability between two classes. The statistical measures such as the Jeffries-Matusita (J-M) and Bhattacharyya distances were used to assess the separation between a pair of objects for all attributes. Attributes with higher J-M and Bhattacharyya distances were selected.

Zhang *et al.*, (2010), generated the correlation among all attributes for each object using Pearson's correlation coefficient. The number of attributes was reduced by ignoring that attributes, which gave the highest correlation value between any two, or more attributes. Considering the characteristics of urban vegetation in IKONOS imagery, a two-scale segmentation procedure was designed to obtain objects, and the feature set for vegetation objects constructed. Redundant information among the features was removed by using correlation analysis. The Pearson coefficient of 0.9 was applied as the threshold, which reduced the number of attributes from 31 to 23. Further, J-M distance and principal component transform (PCT) were applied on the selected attributes that reduced the number of attributes to 14. Finally, the vegetation objects were identified with 87.7% accuracy by classification and regression tree (CART) model. In this study, segmentation was performed at both micro and macro scales. The correlation analysis combined with the J–M distance and PCT was found to be efficient in optimizing the feature set.

In their work, Yu *et al.* (2006) classified an image using both, the nearest neighbor of object-based and MLC for pixel-based classifier using selected attributes. The Ginni index was used to provide the statistical rank to every attribute, based on their importance to classify the

image. The gain of attributes was calculated by using Ginni index and this gain was used to assign a rank to each attribute. Total 11 feature set were generated; the first set was generated using 2 attributes and each of subsequent set was generated by adding next 5 attributes per set, ranging up to 52 attributes. It was demonstrated that the feature set with 7 attributes resulted in the highest overall classification accuracy. The accuracy of object-based classification was also found higher in comparison to pixel-based classifier.

The attribute selection is also an important step in OBIA process, which affects the efficiency of the algorithm and accuracy also. Little work has been done in the area of attribute selection. It has been noticed that number of attributes reduces very prominently by using any attribute selection methods, used thus far.

The selected attributes from the data for the final step of object classification where some work with regard to the choice of the classifier has also been reported in the literature.

2.6. Object Based Image Classification

A number of classification algorithms have been developed by the researcher; generally, these have been grouped into two parts; the parametric classifier and nonparametric classifier. The parametric classifier is one in which the statistical data is available while nonparametric classifier is useful when some data are not statistical. In case of OBIA, nonparametric classifiers have generally been used.

2.6.1. Image Classification

Shackelford and Davis (2003) presented a combined fuzzy pixel-based and object-based approach for classification of urban land cover from high-resolution multispectral IKONOS image. In this approach, first the image was classified using hierarchical pixel based fuzzy classification. This classified image was segmented using multi-resolution segmentation and then object based classification was applied to produce more detailed classified map. A significant improvement was found in the individual object classification accuracies using object-based fuzzy classification over the pixel based MLC classification. Object based

classifier achieved the individual classification accuracies as; 76% for buildings, 81% for impervious surface and 99% for roads. The corresponding accuracies from MLC classification were 72.8%, 74.5 % 70.6% respectively.

Li *et al.* (2008b) proposed a multilevel object based classification method based on hierarchical segmentation and shape descriptors. Initially, the Quick-bird image was segmented using watershed image segmentation technique. Various spectral and shape features were used jointly for classification. A hierarchical classification method was proposed, which combined pixel and object based classification methods. The various classes were extracted by pixel-based classification with overall accuracy of 78.21% and, reached to 83.04% for hierarchical pixel based classifier, which combines the shape feature. The accuracy of 83.86% was achieved using single level object-based classifier, which improves to 86.21% with the proposed (multilevel) approach.

The purpose of OBIA developed by Laliberte *et al.* (2007) was to estimate fractional cover of green and senescent vegetation using very high-resolution ground photography. The images were transformed from the RGB to IHS color space. The image was classified into soil, shadow, green vegetation, and senescent vegetation classes using nearest neighbor classifier. Shadow and soil were masked out using intensity and saturation bands. Further, the nearest neighbor classifier was used to separate green and senescent vegetations from masked image. Results obtained from OBIA were compared with data collected by field survey called as line-point-intercept (LPI) data, which revealed that this method shows high correlation (0.95) as compared to LPI method (0.88) and requires less time and labor, thus appears more effective.

A multi-scale, object-based analysis of satellite images was carried out by Mallinis and Koutsias. (2008) to delineate forest vegetation polygons in a natural forest in Northern Greece. The object was used as the primary units of classification, which provided much detailed information for the assignment of the observations to the classes. The IKONOS, ASTER and MODIS images were classified using both classification and regression trees (CART) for pixel based classification and the nearest neighbor (NN) classifier for object-based classification. Overall classification accuracies for IKONOS, ASTER and MODIS data sets were achieved 94.86%, 93.99% and 85.48%, using object based NN classifier, in comparison to 94.36%, 95.24% and 84.98% obtained from pixel-based classifier.

An experimental study was carried out by Salman *et al.* (2008) to extract land-use land cover (LULC) of greater Khartoum-Sudan using commercial eCognition software. In this experiment, two classification methods, the nearest neighbor and fuzzy membership function were used. The classification was applied on multi sensor and multi-resolution satellite images. It was observed that high degree of heterogeneity appears in building patterns in the study area, even though classification accuracy of 75-80% was achieved by using fuzzy classification, while the accuracy was less for nearest neighbor classifier.

The aim of Rahman and Saha (2008) study was to test the efficiency of both, the nearest-neighbor classifier of object-oriented approach and MLC of pixel-based approach for land use land cover classification. Overall classification accuracy of 92% was achieved with the object-based classification and 86% for the pixel-based classification, which shows better land use land cover classification was achieved using object-based rules rather than pixel-based rules.

Lu *et al.* (2011) used Quick-bird imagery for mapping impervious surface distribution. Per-pixel based supervised MLC classification, segmentation-based classification and hybrid classification (combination of these two) methods were applied on two study areas with different urban developments, sizes and spatial patterns. It was observed that per-pixel based supervised classification suffered strongly with salt-and-pepper noise compared to others. Further, by comparing classification results, it was demonstrated that the hybrid method provides the best-classified outputs. However, hybrid method required considerable time and labor, also require manual editing and refinement of the impervious surface image, whereas the segmentation-based method reduce the impact of spectral variations. However, none of these methods was efficient to eliminate spectral confusion between impervious surface and water and bare soils.

A multi-scale geographic object-based image analysis (GEOBIA) classification using only spectral bands was proposed by Kim *et al.* (2011). They discussed over three classification issues of the nearest neighbor classifier in context of segmentation scale; (i) comparison of multi and single scale GEOBIA using spectral bands, (ii) improvement in the classification accuracies by including GLCM generated texture features and (iii) the effect of quantization level of GLCM texture in multi-scale GEOBIA. From the experimental results, it was revealed that single-scale approach produced only moderately accurate classification for all marsh

classes, while multi-scale approach allowed the delineation of individual classes with increased spectral variation. It was concluded that multi scale GEOBIA performs better with an overall accuracy of 82% in comparison with 76% of single scale GEOBIA.

A recently introduced kernel called cloud basis function (CBF) of ANN classifier was investigated by Rizvi and Mohan (2011) for object-based image classification. Multiresolution watershed transform-based image segmentation followed by a modified CBF and CBF including relaxation labeling process (CBF-RLP) were applied on high-resolution satellite images for object based image classification. The image was also classified using radial basis function neural network (RBFNN). It was observed that highest classification accuracy of 89.72% was achieved using CBF-RLP post processing while modified CBF produced 88.19% accuracy. Further, the image was also classified using RBFNN and CBFNN, which gives the classification accuracies of 84.17% and 86.24% respectively.

Pu *et al.* (2011), applied ANN classifier for object-based image classification using various segment related attributes. In their work, they classified the image by using 27 and 9 feature attributes the overall accuracy (OA) of 84.58% and 76.64% was achieved respectively. The classification was also done using minimum distance classifier (MDC) with same number of attributes and OA of 77.10% and 67.57% were achieved. Similarly, the image was also classified with pixel based methods using nine attributes that gave 72.79% overall accuracy. From the comparative study, it was concluded that object-based classifier with specific number of attributes (for this case 27) had produced significant improvement in the classification accuracy. A comparison between the performances of an artificial neural network (ANN) and a MDC in urban detailed land cover classifications was also done. The results show that ANN outperforms MDC as an object based classifier.

A modified object-oriented fuzzy classification algorithm was proposed by Chen (2012), it combines multi-characteristics (such as; spectral information, geometry, texture and semantics) for object-based image classification. The classifier was applied on two IKONOS panchromatic remote-sensing imagery. Initially, the image objects was extracted by multi-scale multi-characteristics segmentation after that, those multi characteristics were extracted. The images were also classified using pixel-based MLC. It was concluded that the proposed

algorithm was an effective classifier and achieved 93% classification accuracy in comparison to 83% achieved by pixel-based MLC.

Pinho *et al.* (2012) presented an integrated OBIA strategy. In this work, main focus was to classify the intra urban area into number of classes. This strategy combines multi-resolution segmentation, data mining and hierarchical network classification techniques in order to address the problem of intra-urban land-cover mapping using high-spatial resolution imagery. The image was segmented and classified into eleven classes using nearest neighbor classifier. Overall classification accuracy of 71.91% for intra-urban land-cover map has been obtained through an object-based error matrix.

Phinn *et al.* (2012) assessed the accuracy and significance of the classification process used to derive geomorphic zone and benthic community zone maps for three western Pacific coral reefs. These maps were produced from multi-scale OBIA of high-spatial-resolution multi-spectral Quick-bird images using nearest neighbor classifier inbuilt in eCognition. Per-pixel approach was also tested for mapping benthic community zones. Author proposed a process in which, the operator field experience and a conceptual hierarchical model of the coral reef environment was linked with data and then applied object-based algorithm. Significant improvement was achieved in OBIA mapping accuracies using the proposed process in comparison with previously published work using other methods; however, the classes mapped were matched to a predetermined set of features on the reef.

Li and Shao (2012) used an object-oriented strategy for automatic/semiautomatic classifications of land use land cover using very high-resolution remote-sensing data inbuilt in eCognition software. The classification rules associated with the geometry and spatial relationships of imagery objects depend on specific objects and imagery sources. The accuracies of the land use and land cover were estimated separately and found to be 99.10% and 98.32% respectively. Authors showed that this approach not only achieves high classification accuracy, but also removes the salt-and-pepper effect found in conventional pixel-based procedures.

Very recently, Santiago *et al.* (2013) applied the OBIA on spaceborne SAR data, specifically Advanced Land Observation Satellite (ALOS), phased array L-band synthetic aperture radar (PALSAR). Single-polarized (HH) and dual-polarized (HH + HV) L-bands was

used to extract the mangroves from image. To determine the optimal color and shape ratios for the hierarchical classification, the accuracy of the object parameters were examined. In initial classification stage, the mangroves were separated from the saltpan and waters using both sets of SAR images. Object-based segmentation and classification was completed using Definiens Professional Earth 7.0 (formerly eCognition) software. The overall accuracy of 91.1% for single polarized data and 92.3% for dual-polarized data was achieved using optimal value of the objects parameters. It was observed that, all three mangrove classes were accurately identified at the second stage of classification using dual-polarized data.

Aguilar *et al.* (2013) tested the efficiency of OBIA on two pan-sharpened, very high resolution (GeoEye-1 and WorldView-2) images. The study was based on three factors: (i) sensor used, (ii) image object set, and (iii) size of the training samples. The nearest neighbor classifier was used for image classification. The best overall accuracy was achieved 89% for GeoEye-1 and 83% for WorldView-2 image respectively.

From the literature reviewed, it has been noticed that pixel-based classifier affected by salt-and-pepper noise and also not provided good result comparative to object-based image classification. However, it has been observed that limited number of classifiers are used for object-based classification. In most of the research, the nearest neighbor classifier inbuilt in eCognition software has been used.

2.6.2. Object Extraction

Object extraction differs from the image classification as the focus is on extraction of one class at a time instead of all classes. A few studies have been reported on extraction of individual objects such as regular compact and linear feature (e.g. building, road) (Tian and Chen, 2007; Zhang and Couloigner, 2006).

Zhang and Couloigner (2006) proposed an approach for object extraction, based on utilization of the spectral information and the purpose was to extract road network from multi-spectral (MS) imagery. The process starts with the segmentation of the image then an image classification using a spectral clustering algorithm was done. The fuzzy classifier was used to classify the image, after that a road centerline extraction and road network formation operation

was performed to extract the centerline of the roads and the forming a network. Three data sets, IKONOS-MS, Quickbird-MS, and color aerial imagery were used for extracting the road. Finally they evaluate the results in respects; the completeness, the correctness and the RMSE (pixels). They compared their results with Mayer *et al.*, (2005) and found that the value of completeness and correctness achieves more while RMSE (pixels) was marginally high for the proposed approach. The results showed that the proposed approach was effective for the extraction of linear objects.

To extract road network from urban areas Youn *et al.* (2008), proposed an approach that uses LIDAR data. The process starts with the subdivision of a study area into homogeneous regions based on road direction. The process worked in three steps; extraction of line segments, detection of dominant direction and image splitting with the quadtree data structure. The canny operator was applied to detect straight line. The road positive with parallelism (RPP) was used to calculate the length of the line to discriminate other smaller line. Surrounding features werebeen used as key factors for region based acupuncture method. The LIDAR point cloud was used with morphological filter to produce a building map. The image was classified and thematic map for grass area was generated and used as mask to extract road networks. The accuracy was evaluated quantitatively with respect to manually compiled road vectors. A completeness of 80% and a correctness of 79% were obtained.

Built-up areas are among the most rapidly changing and expanding elements of the landscape. For the extraction of urban features, Taubenbock *et al.*, (2010) proposed an object-based, multi-level, hierarchical classification framework that combines the shape, spectral, hierarchical and contextual information. The framework was based on a modular concept following a chronological workflow from a bottom-up segmentation optimization to a hierarchical, fuzzy-based decision fusion top-down classification. The fuzzy rule based classifier was applied on IKONOS and Quick-bird data sets. The images were initially classified and then urban features were extracted. The overall accuracy for extraction was achieved 85.14% for IKONOS and 81.57% for Quick-bird image.

Thus, a few studies on object extraction have been found in literature, but in most of the cases the extraction has been performed by applying the masking operation on the classified image, which is a lengthy process.

2.7. Summary

The present chapter described the literature reviewed on various topics grouped into five sections related to OBIA. It is clear that the number of image segmentation techniques have been developed by researchers in the past. From the above review, it has been found that the region based techniques are more popular as they provide the closed region boundary however, selection of proper segmentation parameter's value is vital. It has been noticed that quality of the segmented image generally observed by visual interpretation, while from the literature reviewed, it has been found that quantitative discrepancy based approach for the segmentation quality evaluation provides statistical measure that is more specific. After image segmentation, in general the next step is image classification, however going through very little review, which is related to the selection of the attributes, it has been found that selected attributes may increase the efficiency as well as accuracy of the classification. Additionally, it has also been observed that most of the researchers has used nearest neighbor (NN) classifier inbuilt in eCognition for image classification.

The above review points to some research gaps. It has been found that thresholding and edge based segmentation algorithms are not sufficient enough for image segmentation one is time consuming and the other one do not provide closed boundary. The most widely used region based approach suffers from over and under segmentation problem due to lack in selection of proper segmentation parameter. The research is also required in the direction of development of a measure for quantitative evaluation of the segmented output instead of as usual visual image interpretation. Very limited techniques are available for the selection of the most specific attributes. The development of new classifiers within the domain of object-based classification is also an area to explore further.

The research gaps have led to define the objectives of the present study. To achieve the objectives of the study, the algorithms have been developed/modified and applied on two datasets; very high resolution and high-resolution remote sensing data. The next chapter provides the details of study area and data sets used.

Chapter 3:

STUDY AREA AND DATA SET

3.1 Introduction

This chapter provides a description of the study area and remote sensing data used in the present work. The characteristics of study area in terms of its geographic location, topography and land-use / land-cover have been described. The remote sensing data procured from two different satellite sensors and their characteristics have been discussed.

3.2 Study Area-I and Data

Chandigarh, the Union Territory (UT) of India is located at the foothills of the Siwalik (lower ranges of Himalayas), and is about 250 km North of New Delhi. It lies between latitudes 30^{o} 40'N and 30^{o} 46'N and longitudes 76^{o} 42'E and 76^{o} 51'E (Figure 3.1). The city has an area of 114 km^2, out of which 36 km^2 is rural and remaining 78 km^2 is urban. The city is regarded as the first planned city of the India. The well planned and rectangular road network of city is the reason to select it as the study area to distinguish among various classes.

3.2.1 Type of Land use Land Cover

The Chandigarh city is covered with a number of urban land cover classes. The arranged residential colonies, well-connected road networks make the study area suitable for applying OBIA for object extraction. The other land cover classes include play ground and park, the barren land, trees, water bodies etc. In the present investigation, eight major land cover classes have been considered, as listed in Table 3.1.

Table 3.1: Land use land cover classes and their description (Study Area-I)

Class number	Class name	Class description as on Standard FCC
1	Residential	Well planned structures in the whole image appearing in greenish color.
2	Metallic roads	Greenish or cyan colored network of linear features prominently visible.
3	Nonmetallic roads	Brightest white linear network mostly appearing in the park or pathways following the metallic road.
4	Water catchment area	Irregular shape black patch in the lower left part of the image.
5	Trees	The dark red colored high texture feature at the top right side in the image.
6	Grassland	The light pink color feature spread partly in the whole image.
7	Barren land	Brown and off-white color open spaces mainly on the left side and top of the image.
8	Shadow	Black color features mostly following the shape of its tallest neighbor and appearing at the north-west of every building.

3.2.2 Physiography

The city is divided into 55 dwelling sectors. As per census 2011, the total population of the city was enumerated as 1,055,450 persons having a population density of 9258 persons/sq.km (http://www.census2011.co.in/census/district/117-chandigarh.html). Urban area covers almost 79% of the total city area. Area under forest is 2.10 km^2. There are two major streams, Sukhna Choe and Patiali ki Rao that originate from Siwalik Hills ranges and forms the natural drainage of the city. The Sukhna Choe flows north to south drains the eastern part and joins the Ghaggar River. The other important stream is Patiala-ki Rao, which flows northeast to southwest and drains the northern parts of the city. Both these streams are ephemeral in nature and carry high flows during monsoon. The N-Choe flows through the leisure valley and drains major parts of the city. It flows from northeast to southwest direction and traverses north central part of the city.

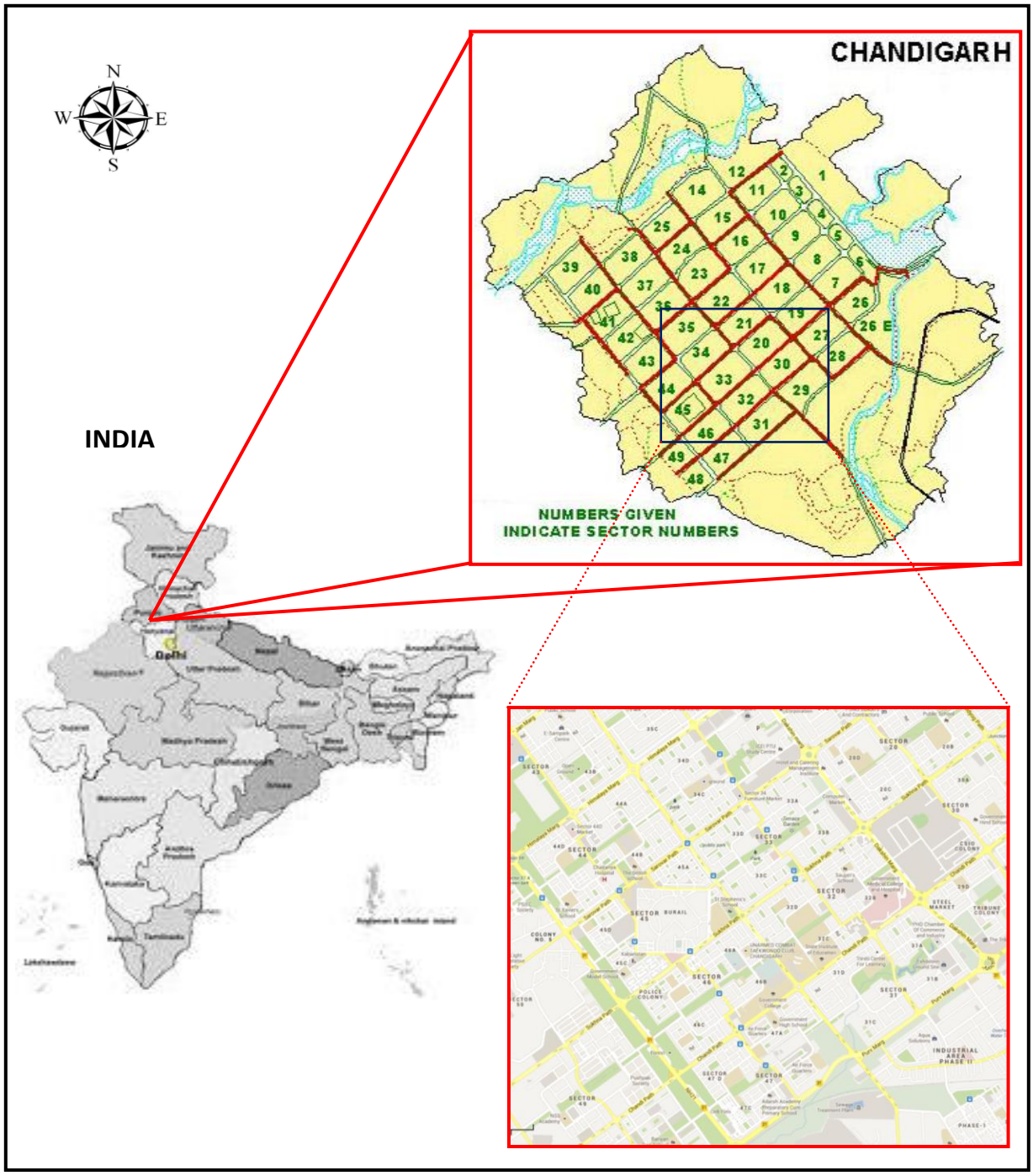

Figure 3.1: Geographical location of the study area-I (Source: http://mcchandigarh.gov.in/)

Another Choe Choi Nala originates from Sector-31 and drains southern most part of the city. The Sukhna Choe has been dammed in northeast side of the city, which has given rise to an artificial lake covering an area of about 1.62 km^2. The lake that is known as Sukhna has a water holding capacity of five million cubic meters (Gupta, 2007).

3.2.3 Experimental Data Set

Two images captured by two sensors Pan and multispectral sensors onboard Quick-bird satellite having with spatial resolution of 0.6m and 2.4m respectively have been used in this study as shown in Figure 3.2. The general specifications of Quick-bird sensor are given in Table 3.2. The image mostly covers the urban area that includes the buildings, roads vegetation and water classes. The very high spatial resolution image is taken and total eight classes including shadow as a class, as listed in Table 3.1, have been considered. The very high-resolution image has been taken for this study to assess the efficacy of OBIA approach considered here as many of the classes sparsely separable in the Chandigarh region and clear boundary appears in very high resolution image. Various algorithms of OBIA have been applied on Pan and Pan-sharpened image. The OBIA approach has been applied initially on Quick-bird Pan image to test it sharp boundary extraction. The multi-spectral image has been used here for the generation of the Pan-sharpened image. Both Pan and the Pan-sharpened image are then used as the experimental datasets to accomplish the objectives in this research.

Table 3.2: Quick-bird sensor specifications

Bands	Spectral Resolution (nm)	Spatial Resolution (m)	Temporal Resolution (days)	Radiometric Resolution (bits)	Swath Width (km^2)	Altitude (km)
Pan	450-900	0.61				
Blue	450-520	2.44				
Green	520-600	2.44	5 - 24	11	16.5 x 16.5	450
Red	630-690	2.44				
NIR	700-900	2.44				

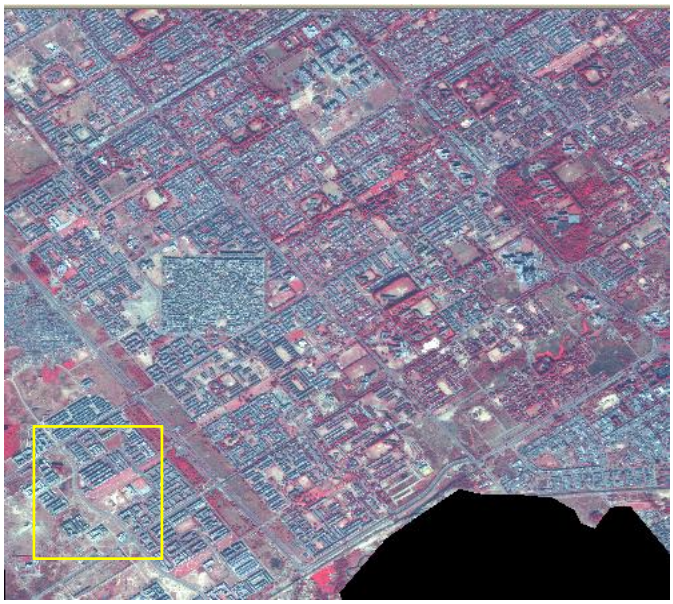

(a)

(b)

(c)

Figure 3.2: (a) Quick-bird multispectral image of Chandigarh, (b) subset of Quick-bird Pan image, and (c) subset of Quick-bird multispectral image.

3.3 Image Pan-Sharpening

Object-based image analysis is generally applied on the high and very high-resolution remote sensing images. The effectiveness of the analysis increases with the increase in spatial resolution of the image. The spatial resolution of an image can be enhanced either by an advancement in the satellite sensor or by image fusion.

Pan-sharpening is an important technique in the field of remote sensing to produce a high resolution multispectral image having the spatial resolution of Pan image and spectral resolution of multispectral image. A number of image Pan-sharpening techniques like the IHS (Intensity-Hue-Saturation) method, the PCA (Principal component analysis) method, the wavelet method, etc have been developed by the researchers. Zhang (2004) categorized these methods into three groups: the projection and substitution methods (the IHS and the PCA methods), the band ratio and arithmetic combinations (the Brovey method) and the different wavelet fusion methods. The PCA method has been used in this work for Pan-sharpening the image.

Various preprocessing steps such as; co-registration, viewing angle of the imagery and geometrically corrected are required before performing sharpening on a set of images. The panchromatic and multispectral images of Quick-bird sensor used in this study are already co-registered with the same Map projection: UTM with Datum: WGS-84. Since the two images are taken at the same time, the viewing angle of the images are same and standard geometric correction has been applied.

The PCA computes the principal components of all bands of multispectral image and the first principal component is substituted with the high-resolution panchromatic image. The inverse PCA transformation is then applied to generate the original image. Since, the panchromatic image has a high variance, which increases its effect on the final outcome, the first principal component is replaced by the panchromatic image (Solberg et al., 1996; Tso and Olsen, 2005).

Figure 3.3: Pan-sharpening of the Quick-bird image, (a) subset of Pan image, (b) unclear boundaries in unsharpened subset of multispectral image, (c) subset of Pan-sharpened image showing clear boundaries, and (d) full Pan-sharpened image.

Figure 3.4: Image showing the reference objects on Quick-bird image

The Quick-bird multispectral image of 2.4m resolution has been fused with the Quick-bird Pan image of 0.6m. The generated Pan-sharpened image has 0.6m resolution with four bands (Figure 3.3 d). A subset of panchromatic image, multispectral image and the Pan-sharpened image for representing the boundaries are shown in Figure 3.3 (a)-(c). The quick-bird Pan image has very high (0.6m) spatial resolution but have only one band, thus may not able to extract all classes. On the other hand, multispectral Quick-bird image has four bands but it suffers from the problem of unclear boundaries of the object as spatial resolution decreases but it has spectral advantage. However, the Pan-sharpened image overcomes the limitations of both by importing the spatial resolution of Pan image and spectral characteristics of multispectral image which produce sharp boundary image.

3.4 Generation of Reference Data

The purpose of the generating the reference data consisting objects is to assess the quality of the segmented image. The objects in the reference data have been generated by digitizing their boundaries onscreen.

The ArcGIS–10.0 software has been used for onscreen digitization to generate the reference data. A number of objects belonging to eight land use land cover classes have been digitized from Pan-sharpened image. The values of area, shape and shape-index of these reference objects along with their ID number are given in Table 3.3. These objects are of different shapes and sizes as can be seen from Figure 3.4.

Table 3.3: Description of reference objects as digitized from Quick-bird images.

Object	Shape	Ref-ID	A (m^2)	Shape Index
Building	Compact	26	286.14	1.56
Building	Compact	134	621.58	1.86
Building	Compact	78	1438.12	1.44
Building	Compact	485	982.50	2.04
Road	Linear	94	347.25	4.48
Road	Linear	208	775.92	3.04
Road	Linear	617	1586.35	5.24
Road	Linear	416	1124.40	5.86
Shadow	Compact	541	608.76	1.69
Shadow	Compact	721	1850.40	3.03
Shadow	Compact	47	667.80	1.56
Shadow	Compact	186	543.24	1.83
Grassland	Compact	570	896.32	2.02
Grassland	Compact	248	427.20	1.88
Barren land	Compact	310	634.60	1.78
Barren land	Compact	109	598.22	2.01
Barren land	Compact	583	548.48	1.88
Water body	Compact	875	778.56	2.05

3.5 Study Area-II and Data

Dwarka is a sub city, located in the South West of the National Capital Territory of Delhi, which lies between, 28° 33' 29"N to 28° 36' 9"N latitude and 76° 59' 47"E to 77° 3' 18"E longitude as shown in Figure 3.5. It has Asia's largest planned residential colony in urban area while unplanned in suburban part. The planned Dwarka is frequently referred to as the "Model Township" and is also thought to be the most organized and cleanest of all parts of Delhi and nearby townships (Mohan, 2002). The landscape concept of Dwarka evolves a system of open spaces which have the potential to develop into a landscape with distinctive visual qualities,

fulfilling the required ecological and recreational functions. Unlike surrounding areas of Delhi like Gurgaon or Noida, Dwarka has been developed mainly as a residential township, which has translated to only few congestion problems faced by its residents every now and then. Urban part of Dwarka has robust and well connected road network built to modern specifications to each of its sectors and adjoining areas. The sub city is well connected by metro rail with the city center and other major parts of the city by Mass Rapid Transit System.

3.5.1 Land Use Land Cover in the Study Area

The study area covers both urban and suburban regions divided by west Yamuna canal. The arranged and planned residential colonies and apartments lie in the eastern part of the canal while the densely populated region with small houses falls in the western side of the canal. The well-connected road networks are clearly visible in urban areas whereas these disappear in the dense area. The study area also contains other classes such as water bodies, barren land, vegetation etc. For the purpose of classification, 12 classes, as listed in Table 3.3 have been considered.

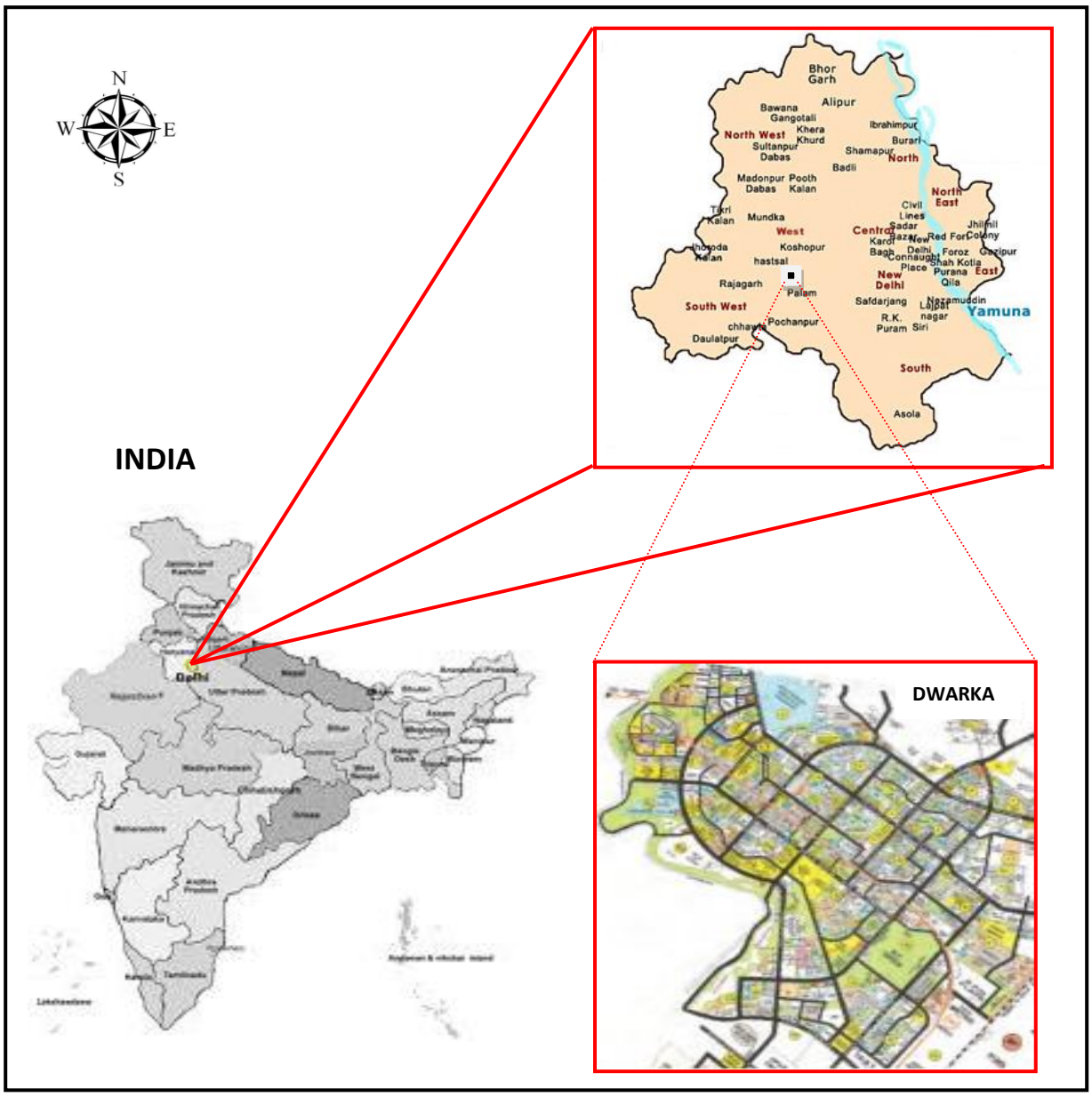

Figure 3.5: Geographical location of the study area-II (Source: dda.org.in/planning/dwarka.htm)

3.5.2 Physiography

Dwarka sub city is situated at an altitude of 210-221 m above mean sea level. This sub city is located in South-West Delhi in the vicinity of international airport. Total area of Dwarka Sub-city is around 56.48 km^2. The sub city is divided into 29 well planned sectors and each residential sector is having area of approximately 1 km^2. Each sector is bounded on all sides by arterial roads of 45 m and 60 m wide. As per Delhi development authority (http://dda.org.in/planning/dwarka_popu_area.htm), in year 2011 total population of the Dwarka was 1,100,000 and having a population density more than 20,000 persons/km^2. Dwarka has a robust road network built to modern specifications to each of its sectors and adjoining areas. The sub city is well connected by metro rail which links it with other major parts of the Delhi. The western Yamuna canal flows nearby Dwarka, which is the main source of water supply to South west Delhi (Mohan, 2002).

Table 3.4: Land use land cover classes and their description (Study Area-II).

Class number	Class name	Class description as on Standard FCC
1	Apartments	Buildings and shopping malls on the right side of the river depicted by cyan or light blue color in arranged patterns.
2	Houses	Clustered settlements mainly on the left side of the river that can be seen as cyan colored clusters.
3	Metallic roads	Greenish or cyan colored network of linear features prominently visible on the right side of the river.
4	Nonmetallic roads	Bright linear features.
5	Metro line	A very bright and thick cyan colored straight line visible at the north east of the image.
6	Canal	Thick black colored channel in the middle of the image.
7	Water catchment area	Small black patches to the west from the river.

8	Dense vegetation	The dark pink or bright red colored features spread in abundance along the river.
9	Coarse vegetation	Light pink color patches appearing in the whole image.
10	Barren land	Green color open spaces mainly on the left side of the image.
11	Wet land	Open ground nearby the river at the centre and top of the image visible as gray color.
12	Sand	White colored features mostly at the lower right of the image depicting collection of dry sand or unfinished roads or pathways.

3.5.3 Experimental Data Set

High resolution LISS-IV multispectral image with spatial resolution of 5.8m, as shown in Figure 3.6, has been used in the present study. The general specifications of LISS-IV sensor is given in Table 3.4. The image covers the urban and suburban areas that include the apartments, houses, roads vegetation and water classes. The high spatial resolution image is taken and total twelve classes, as listed in Table 3.4 have been considered.

This data set covers the Dwarka and its surrounding region that covers both highly separate and mixed classes. The LISS-IV image has low spatial resolution in comparison to the Quick-bird image Pan-sharpened image. The data will be fraught with mixed pixels. This data therefore has been used as experimental data to examine the efficacy of the proposed object based methodology on a low spatial resolution dataset and its performance evaluated with respect to Quickbird high resolution dataset.

Figure 3.6: Subset of LISS-IV multispectral image

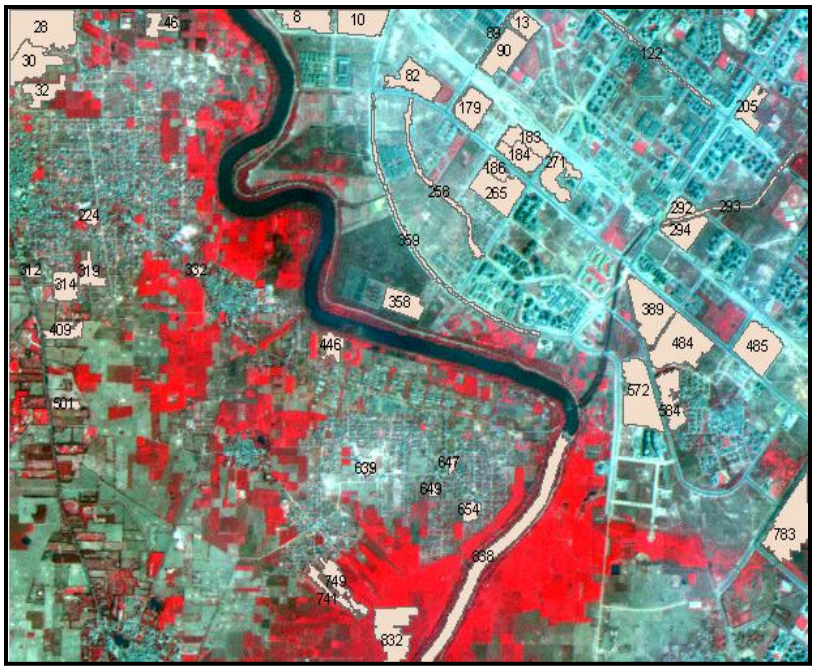

Figure 3.7: Reference objects as on LISS-IV image

Table 3.5: Resource Sat LISS-IV sensor characteristics

Bands	Spectral Resolution (nm)	Spatial Resolution (m)	Temporal Resolution (days)	Radiometric Resolution (bits)	Swath Width (km)	Altitude (km)
Pan	500-750	5.8	5 – 24	10	70	817
Green	520-590	5.8				
Red	620-680	5.8			23.9	
NIR	770-860	5.8				

3.6 Generation of Reference Data

As stated earlier in section 3.4, similar exercise has also been repeated for LISS-IV image. The reference objects as given in Table 3.6, for various objects belonging to different classes of the LISS-IV multispectral image have been generated by digitizing the image. The digitized objects as on LISS-IV image are shown in figure 3.7.

Table 3.6: Description of reference objects of LISS-IV image.

Object	**Shape**	**Ref-ID**	**A (m^2)**	**Shape Index**
Apartment	Compact	205	31677.48	1.59
Apartment	Compact	84	28978.29	1.60
Apartment	Compact	183	75520.06	1.71
Apartment	Compact	584	77447.68	2.43
Houses	Compact	28	56101.91	1.53
Houses	Compact	654	78174.80	1.86
Houses	Compact	389	78617.43	2.21
Houses	Compact	783	259068.90	2.21
Barren land	Compact	572	62748.80	2.60
Barren land	Compact	82	66319.06	3.42
Barren land	Compact	832	136373.50	1.83
Road	Linear	122	37774.62	4.44
Road	Linear	359	49500.15	4.22

Road	Linear	258	18486.71	4.58
Road	Linear	293	117606.90	5.37
Road	Linear	89	43428.77	4.35
Water body	Linear	638	227468.70	4.25
Water body	Compact	314	9394.58	1.60
Vegetation	Compact	484	47508.65	1.92
Vegetation	Compact	46	6412.54	1.47
Vegetation	Compact	179	22785.67	1.58

3.7 Summary

In this chapter, a brief description of the study areas and the land cover classes present was provided. The high and very high-resolution remote sensing data used for the study was discussed. The pre-processing of the data as well the generation of the reference data for accuracy assessment was also described.

Chapter 4:

DESCRIPTION OF SOFTWARE DEVELOPED

4.1Introduction

In the present study, an attempt has been made to develop a workable computer code for the implementation of various algorithms to fulfill the research objectives of the thesis. The related algorithms with their complete descriptions shall be discussed in subsequent chapters as appropriate.

There are few commercially available OBIA software e.g. Definiens (Germany) – eCognition, National Institute for Space Research (Brazil) - SPRING, Erdas Imagine – Imagine objective. However, each has its own merits and demerits. In this thesis, although, eCognition has been used as a tool, due to non-availability of a number of other tasks, the need for development of an associated software has arisen here. The segmentation parameter selection, its quality evaluation, and attribute selection techniques are not available in eCognition and any other commercial software. In the existing software, the segmentation parameter selection process is largely based on trial and error, which is very subjective. The developed software gets over this limitation. Further, a module for assessment of segmentation quality through quantitative measures has been developed, which is also done through visual inspection only in the current commercially available software.

Moreover, in the existing commercial software, after segmentation, the classification has been done with all the attributes. It is likely that only a few attributes may be significant and therefore it is desirable that only the useful attributes take part in the classification process. This will not only reduce the size of the data but will also improve the efficiency of the process. In the developed software, attribute selection based on a decision tree approach has been incorporated. The decision tree has further been extended for image classification as well as extraction of individual objects. A module for accuracy assessment of image classification and also for image object extraction has also been developed.

This chapter provides detailed description of the software developed, hardware and software requirements, the formats of various input and output data files required by the software, the GUI (Graphical User Interface) and the complete functionality of the software developed.

4.2 Salient Features of the Developed Software

The software has been developed in MATLAB, on Windows 7, 32 bit operating system. It is an advanced platform and provides an extensive support for software development and debugging. MATLAB can easily handle large sizes of matrices in an efficient manner. The simplicity, stability, robustness and efficient architecture make it an appropriate choice for the development of image processing application.

The input and output data files formats correspond to the ASCII format of images for their easy import/export to the module and vice versa. Definiens eCognition has been used for image segmentation, creation of training and testing data files and to export it in ASCII format. Arc GIS has been used for generating the reference objects and ERDAS Imagine has been used for generating the classified images.

The programmatic GUI for the module has been developed. It includes functionality that enables to use a default application framework. The formatting operations in the form of buttons, text box, edit box etc., have been directly used in the module to make it an excellent interface.

4.3 Software Modules

The software includes following modules,

1. Fixation of values of segmentation parameters,
2. Segmentation quality assessment
3. Attribute selection
4. Image classification and object extraction.
5. Accuracy assessment

4.4 Input and Output Data File Formats

The ASCII file format is the most common data file format supported by all the remote sensing image processing software and has been used here also.

The eCognition software has been used for image segmentation. High resolution remote sensing images are given as input to the software, wherein the images are segmented using multiresolution segmentation technique. The segmented image is exported in ASCII format and taken as the input to the developed code. The input output description of various files is given in Table 4.1.

The segmentation process via eCognition leads to generation of a set of attributes. In which, spectral and textural attributes are involved on band-by-band basis. The list of attributes along with their abbreviation is given in Table 4.2. Each attribute may have more than one value. For example, Mean () indicates mean spectral response of pixels within a segment in a given band. If there are 4 bands, there will be four mean values for that segment.

Table 4.1: Input-output description of various files used in the developed software

Module	Input Files	Input Parameters	Details of Output File
Parameter selection	Pre-segmented file	**i)** Number of bands in image file **ii)** Number of sub segments **iii)** Initial scale **iv)** Current scale	Values of Parameters
Segmentation quality evaluation	**i)** Segmented file **ii)** Reference object file	**i)** ID Number of reference object **ii)** Threshold	Quality of Segmented image
Attribute selection	**i)** Training data file **ii)** Testing data file **iii)** Reference data file	Class ID of the object to be extracted (for object extraction)	**i)** Ranked attributes with threshold values **ii)** Decision tree **iii)** ROC file and **iv)** List of selected attributes
Image classification	**i)** Segmented image file **ii)** Attribute file **iii)** Splitting rule file	Number of selected attributes	Classified image
Object extraction	**i)** Segmented image file **ii)** Splitting rule file	**i)** Number of selected attributes **ii)** Serial number of object to be extracted	Binary image
Accuracy assessment	**i)** Classified image **ii)** Object extraction file **iii)** Reference image file	Class ID of the extracted object	**i)** Error matrix **ii)** ROC file

Table 4.2: List of Attributes

Abbreviation	**Full form**
ID	Segment ID
M ()	Band wise mean value of the segment
SD ()	Band wise standard deviation of the segment
SDN ()	Band wise standard deviation to the neighbor
Ratio ()	Band wise ratio of the segment
MDN ()	Band wise mean difference to neighbor of the segment
MDN(abs.)	Band wise absolute mean difference to neighbor of the segment
MDDN() / MDBN ()	Band wise mean difference to the darker / brighter neighbor of the segment
A (Pxl)	Area in pixel units
Cmpct	Compactness
BL(Pxl)	Border length in pixel units
SI	Shape index
X min (m)	Minimum value of X
Y min (m)	Minimum value of Y
X max (m)	Maximum value of X
Y max (m)	Maximum value of Y
Cmpct (poly.)	Compactness of polygon
GLCM Homo ()	Band wise GLCM homogeneity
GLCM Cont ()	Band wise GLCM contrast
GLCM & GLDV Ent ()	Band wise GLCM and GLDV entropy
GLCM Dim ()	Band wise GLCM dissimilarity
GLCM & GLDV ASM ()	Band wise GLCM and GLDV Angular 2nd moment
GLCM Corr ()	Band wise GLCM correlation

4.4.1 Input Data Files

i) Pre- segmented file

The pre-segmented file corresponds to initially segmented multispectral image. This is an ASCII file used for calculating the value of segmentation parameters (scale, shape factor, compactness). It uses required attribute values of sub-segments of a desired segment. The file format for this input is given in Appendix-I.

ii) Segmented file

The segmented file corresponds to the multispectral segmented ASCII file used for evaluating the quality of segmentation. It uses area and shape index attributes of the formed segment with their segment ID. Table 4.3 shows the format of segmented file.

Table 4.3: Format of segmented file for segmented quality evaluation

Segment ID	Area (m^2)	Shape Index
17	248.35	1.89
31	478.51	2.98
82	57.48	3.03
83	8477.64	2.53
114	941.05	1.95
158	124785.24	3.18
246	1584.05	2.07
477	24578.88	3.26
-	-	-
-	-	-

iii) Reference object file

Similar to the segmented file there is a reference object file, which is generated in Arc GIS. The file is used for calculating the difference in values of parameters of the generated segment from the corresponding reference object. The area and shape index of the digitized object have been calculated and saved in ASCII format, as given in Table 4.4.

Table 4.4: Format of reference object file for segmented quality evaluation

Reference object ID	A (m^2)	Shape Index
26	286.14	1.56
134	621.58	1.86
78	1438.12	1.44
485	982.5	2.04
94	347.25	4.48
208	775.92	3.04
-	-	-
-	-	-

iv) Training data file

It is a file that contains details about the training segments for input to the decision tree for attribute selection. The attributes of the training segments obtained from the segmented image are assigned class values. The format of the training data file is given in Appendix-I

v) Testing data file

The testing data file is used to test the quality of generated decision tree in the attribute selection process. The format of this file is the same as the training data file except the class ID column, and is given in Appendix-I

vi) Reference data file

The reference data file is the testing file with class ID. The reference data file is used to evaluate the trained decision tree.

vii) Image file

It is the segmented image file with all attributes. The image file is used for assigning the class to every segment. The file format is similar to the testing data file, as shown in Appendix-I.

viii) Attribute file

The attribute file stores the class wise ranked attributes in descending order. This is required in classification module for image classification or object extraction. The format of the attribute file is given in Table 4.5. The row wise attributes are arranged in descending order; the number shows the attribute identity and one row depicts the values for a class.

Table 4.5: Format of the attribute file for image classification and object extraction

Rank	**1**	**2**	**3**	**4**	**5**	**6**	**7**	**8**	**9**	**10**	**--**	**--**
Class-1	81	85	77	83	84	16	35	45	54	65	--	--
Class-2	78	4	42	23	88	81	83	82	65	85	--	--
Class-3	2	11	21	30	12	18	40	49	83	86	--	--
Class-4	5	20	24	34	39	43	53	58	62	72	--	--
Class-5	10	3	2	1	11	12	19	21	20	30	--	--
--	--	--	--	--	--	--	--	--	--	--	--	--

ix) Classified image file

Classified image file is generated after the classification process it represents the assigned class value to every segment. The classified image file consists of two columns, the segment ID and its assigned class value as shown in Table 4.6. This file is used as the input to assess the classification quality.

Table 4.6: Format of the classified image file

Segment ID	Assigned Class
0	4
1	4
2	8
3	1
4	2
5	2
6	3
7	4
--	--
--	--

x) Object extraction file

Object extraction process assigned the desired class value to the extracted segment known as object and '0' to remaining background segments. Similar to the classified image file, the object extraction file is also given as the input to assess the object extraction quality. The format of the object extraction file is given in Table 4.7.

Table 4.7: Format of the object extraction file

Segment ID	Assigned Class
0	4
1	4
2	0
3	0
4	0
5	4
6	0
7	4
--	--
--	--

i) Reference image file

The classified reference image file is similar to the classified image file with selected number of segments as reference in the format as given in table 4.8. This file is used for assessment of the accuracy of classified image or extracted object.

Table 4.8: Format of the reference image file

Reference ID	Class
1	4
20	8
26	2
31	2
84	5
125	7
256	3
477	1
--	--
--	--

4.4.2 Output Data Files

On execution of various modules of the software developed, following output files are generated.

i) Values of parameters

The output file generated from the parameters selection algorithm. It is in ASCII file format that provides the value of various parameters (scale, shape-factor, compactness) for proper segmentation of the image. These values are further used in image segmentation for finding proper segmentation.

ii) Segmented image quality

The quality of the segmented image in terms of assessment parameters are written in this ASCII file.

iii) Attribute file

The output generated from the attribute selection stage provides the rank wise arranged attributes with its cutting value and the generated tree. The format of the attribute file is as given earlier in Appendix-I. The cutting value file is also generated in the intermediated operation, which provides the threshold value for all the attributes. The format of the cutting value file is given in Table 4.9. It also gives the number of selected attributes, which will produce the highest quality classification or extraction.

Table 4.9: Format of the cutting value file

Class-1	82.84	7.27	0.25	16.03	-42	20.51	1	1
Class-2	32.55	12.55	0.21	14.54	11.09	13.72	11.09	32.55
Class-3	69.79	8.08	0.25	25.69	-7.20	3.87	22.29	69.79
Class-4	93.46	7.27	0.18	27.41	-28.44	30.91	5.24	93.46
--	-	-	-	-	-	-	-	-

iv) Error matrix

The error matrix is used for assessment of image classification accuracy.

v) ROC for object extraction.

It provides the TPR and FPR values for each attribute.

4.5 Implementation Details

The software has been developed on Matlab platform and grouped in modules. Various input and output parameters are required for each module, which have been compiled in the form of member functions. The functions used in each module and their required parameters are described in Table 4.10.

Table 4.10: Member functions in various modules of the developed software

1	**Function Name**	**Parameter()**
	Module Name	Parameter selection
	Parameter Passed	fname: input file name, bnd: number of bands in the image, seg: number of sub-segments, pscale: initial/previous scale, cscale: current scale, of: output file
	Return Value	value of scale parameter, shape factor and compactness parameter.
	Description	This function is used to call the fitness functions for the selection of the segmentation parameters value and returns the values of segmentation parameters.
2	**Function Name**	**quality()**
	Module Name	Quality Evaluation
	Parameter Passed	rfname: digitized object file known as reference object file, sfname: segmented image file, of: output file
	Return Value	value of SFI and ΔSI.
	Description	It is used to call the quality measure for segmentation quality assessment and returns the values of the quality index.
3	**Function Name**	**attri_select()**
	Module Name	Attribute Selection
	Parameter Passed	train_file: training segment samples, test_file: testing segment samples, ref_file: reference file, oc: class ID to be extracted, atr: ranked attribute list as an output, roc: value of TDR and FAR for each attribute, of_attri: output file
	Return Value	cutting value, splitting rule file, number of selected attributes.
	Description	It is used for calling the attribute selection program to select the attributes based on their ranking. It returns the attributes ranking and number of selected attributes as well as cutting value and splitting rule file as an intermediate output.
4	**Function Name**	**classi_extract()**
	Module Name	Image classification
	Parameter Passed	fname: segmented image ASCII file,

		atr: ranked attribute file, of_attri: output attribute file as input, of_cls: classified output file.
	Return Value	Assigned class value to every segment.
	Description	This function is used for calling the image classification program and returns the class values assigned to all the segments.
5	**Function Name**	**classi_extract()**
	Module Name	Object extraction
	Parameter Passed	fname: segmented image ASCII file, atr: ranked attribute file, of_attri: output attribute file as input, oc: ID of class to be extracted, of_ext: extracted output file.
	Return Value	Assigned class value or 0 as background to segment.
	Description	This function is used for calling the image classification program and assigns a class value to the desired object and background value to the remaining objects.
6	**Function Name**	**classi_accuracy()**
	Module Name	Image classification accuracy
	Parameter Passed	rname_image: reference image file, cname: classified file, error_mat: error matrix with accuracies.
	Return Value	Accuracy assessment table
	Description	The use of this function is to call an accuracy assessment program to produce error matrix, user's accuracy, producer's accuracy, overall accuracy and kappa.
7	**Function Name**	**extract_accuracy()**
	Module Name	Object extraction accuracy
	Parameter Passed	rname_image: reference image file, ecname: extracted file, cls: extracted class ID roc: value of TDR and FAR.
	Return Value	Accuracy assessment table
	Description	It is used to call a program for the calculation of TDR, FAR.

4.6 The *GUI* of the Software Developed

An interactive and user-friendly graphical user interface (GUI) becomes mandatory for any software to be effective. Here the GUI has been developed in Matlab platform. The GUI allows the user to interact with the software in an easy and user-friendly manner. It represents the information and actions available to a user with the help of dialogue boxes, buttons, textboxes, etc. On running the executable file of the software, a window opens to interact with the various modules. The main window for the software developed is shown in Figure 4.1. The figures from 4.2 to 4.6 show the screen views for the dialog boxes that open for a specific module that corresponds to parameter selection, segmentation quality evaluation, attribute selection, image classification, object extraction, accuracy assessments, respectively.

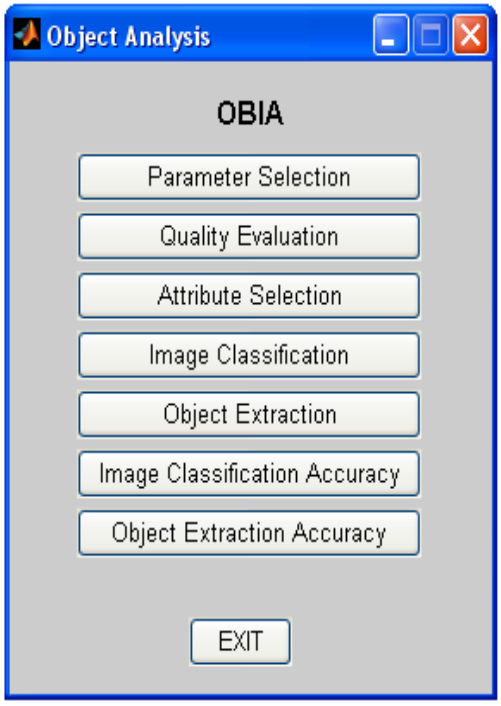

Figure 4.1: Main window for object extraction

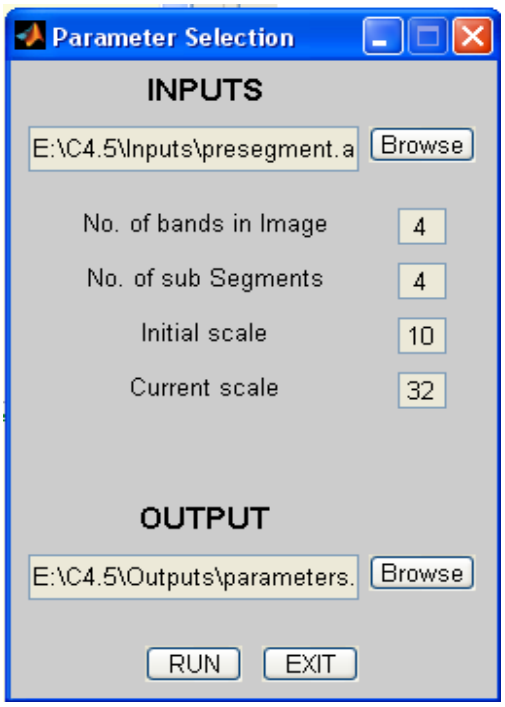

Figure 4.2: GUI of segmentation parameter selection module

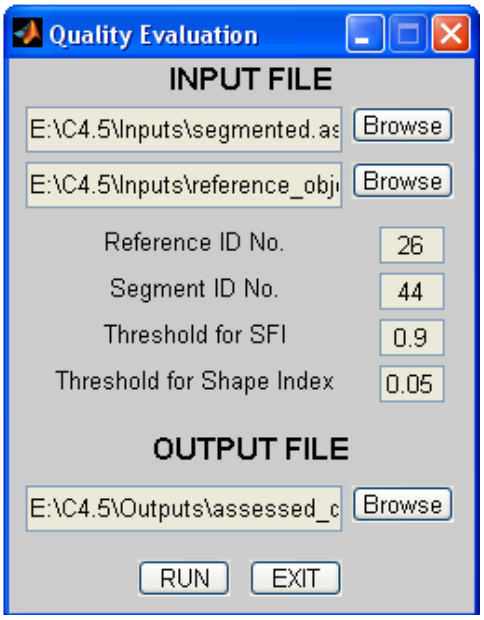

Figure 4.3: GUI of segmented quality assessment module

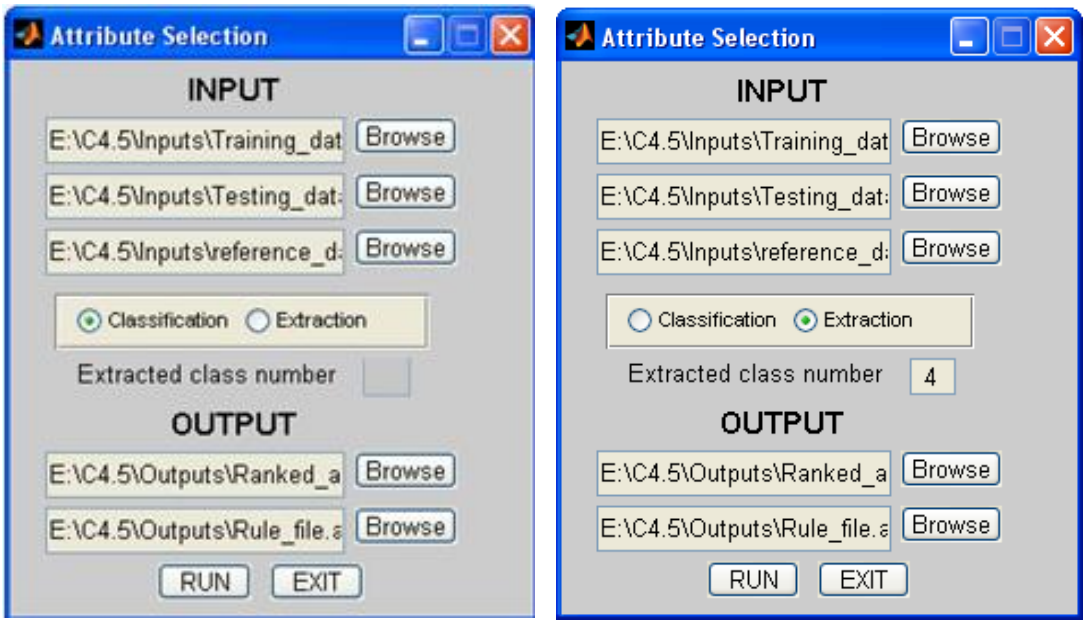

(a) (b)

Figure 4.4: GUI of attributes selection and tree generation modules for (a) image classification and (b) object extraction

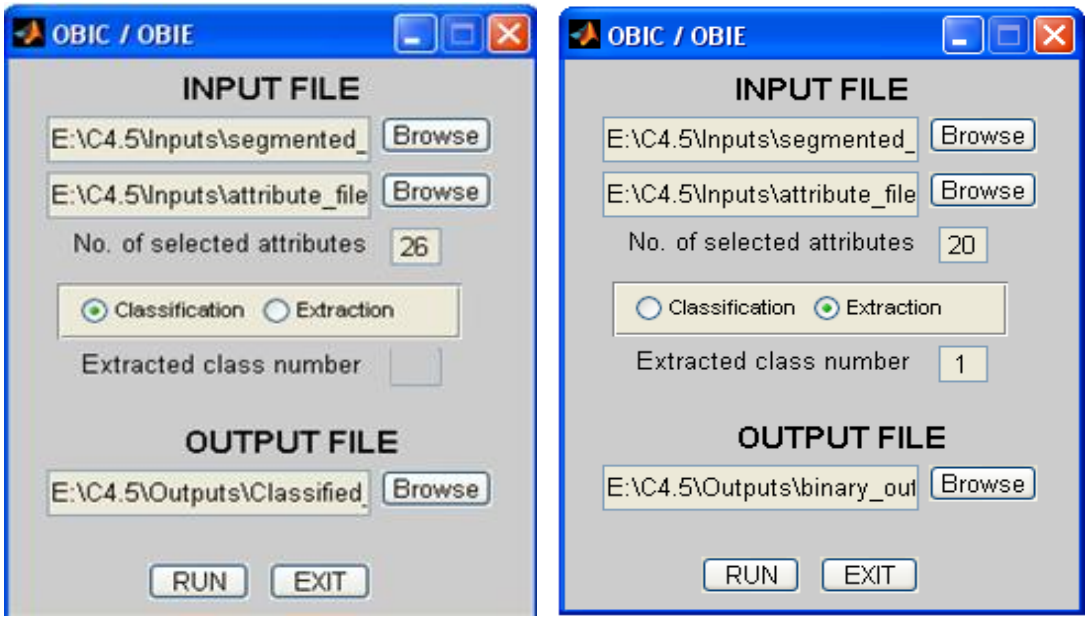

(a) (b)

Figure 4.5: (a) GUI of object based image classification and (b) GUI of object extraction

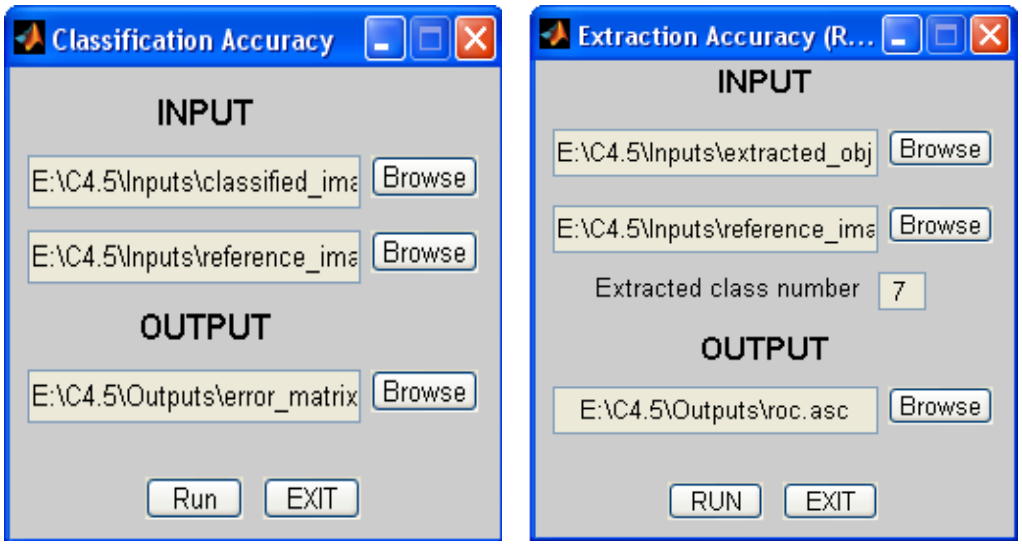

(a) (b)

Figure 4.6: Accuracy assessment module (a) GUI for classification accuracy assessment, (b) GUI for the accuracy assessment of object extraction

A brief description of the various dialogues used in various modules is provided in the following.

i) Number of bands

The user has to input the number of bands of the input remote sensing image.

ii) Number of sub segments

The user is required to give the number of sub segments of a desired segment to be formed in the next higher level as input. The intermediate segmented image file is exported and used for the selection of the segmentation parameters.

iii) Initial Scale

The default scale parameter or the scale parameter set at initial level of segmentation has to be used as the initial scale.

iv) Current Scale

The scale parameter used to segment the image at the current segmentation level.

The above four parameters are required for the module named as, parameter selection.

v) Reference ID Number

The reference image has been generated by digitizing the objects in the original image. An ID has been given to every reference object known as reference ID number. This parameter is required for the segmentation quality evaluation module.

vi) Segment ID Number

Every segment formed in the segmented image has a unique ID and used for evaluating the segmentation quality. This parameter is also required for the segmentation quality evaluation module.

vii) Threshold for SFI

The threshold for SFI lies between 0 and 1 has to be set by user. It is based on the disparity between the formed segment and the corresponding reference object. The threshold for SFI is normally set high for accurate results.

viii) Threshold for ΔSI

The threshold for ΔSI has also to be fixed by user. It calculates the variation between the shape indices of the formed segment and its corresponding reference object. A good quality segmented image is expected to have small variation (i.e., of the order of less than 0.5).

ix) Radio Buttons

Two radio buttons are available in attribute selection module. The option extraction is checked for the selection of attributes for object extraction.

x) Extracted Class ID

This option is available only for object extraction. This value refers to the ID of the class to be extracted. This is an input parameter for attribute selection and object extraction modules.

xi) Number of Selected Attributes

If the object extraction has to be done using the earlier trained tree, the attribute file and the selected number of attributes generated in the attribute selection module are required.

4.7 Summary

In this chapter, the description of the software developed, member functions used and the various file formats input to and output from the software is provided. It also provides an interaction with the graphical user interface of the software to execute the related OBIA algorithms.

Chapter 5:

IMAGE SEGMENTATION:

PROCEDURE, PARAMETERS AND QUALITY ASSESSMENT

5.1 Introduction

In the previous chapters, an overview of the various steps involved in the OBIA along with the review of work done in the field of OBIA and description of the software developed for OBIA have been presented. The work presented in previous chapters shows that, at its elementary level, OBIA has three distinct stages:

(i) Image segmentation

(ii) Attribute selection

(iii) Image classification or extraction of objects

This chapter provides the description related to image segmentation and its quality assessment. The first part focuses on the multi-resolution image segmentation technique, the steps involved in image segmentation and generation of fitness function for the fixation of the value for segmentation parameters. Various quality assessment measures, the generation of the discrepancy based measure, and the assessment of the quality of the generated segment forms the basis of the second part of this chapter.

5.2 Image Segmentation

Image segmentation is the first and crucial step in OBIA. It is the process of partitioning an image into spatially continuous, disjunctive and homogeneous regions (i.e., assigning pixels to a region having common properties). The level to which the partitioning is carried out depends on the targeted application. Segmentation leads to meaningful objects when the image is segmented into

'homogenous' areas and the homogeneity within a segment decreases with the increase in size of the segments (Gorte, 1998, Molenaar, 1998, Baatz and Schape, 2000). Image segmentation plays a fundamental role in the field of image processing, image analysis, and coding with a wide range of applications such as object matching, object recognition or object detection in remote sensing. A number of image segmentation algorithms have been proposed in the literature (Haralick and Shapiro, 1985). These algorithms work on the basis of three main criteria:

i) The homogeneity within a segment

ii) Separation from adjacent segments

iii) The shape homogeneity

According to Schiewe *et al.*, (2001) and Schiewe, (2002), though, these criteria may not be fully met simultaneously, as these, in part, are mutually exclusive to each other. This may be due to:

i). Availability of remote sensing data at varied spectral and spatial resolutions.

ii). Use of an ancillary data (e.g. information from GIS systems) at different measurement scales and units in remote sensing based study

iii). Heterogeneity in object characteristics with respect to their shape, spectral behavior, textures, etc.

iv). Large variation in size of earth surface objects.

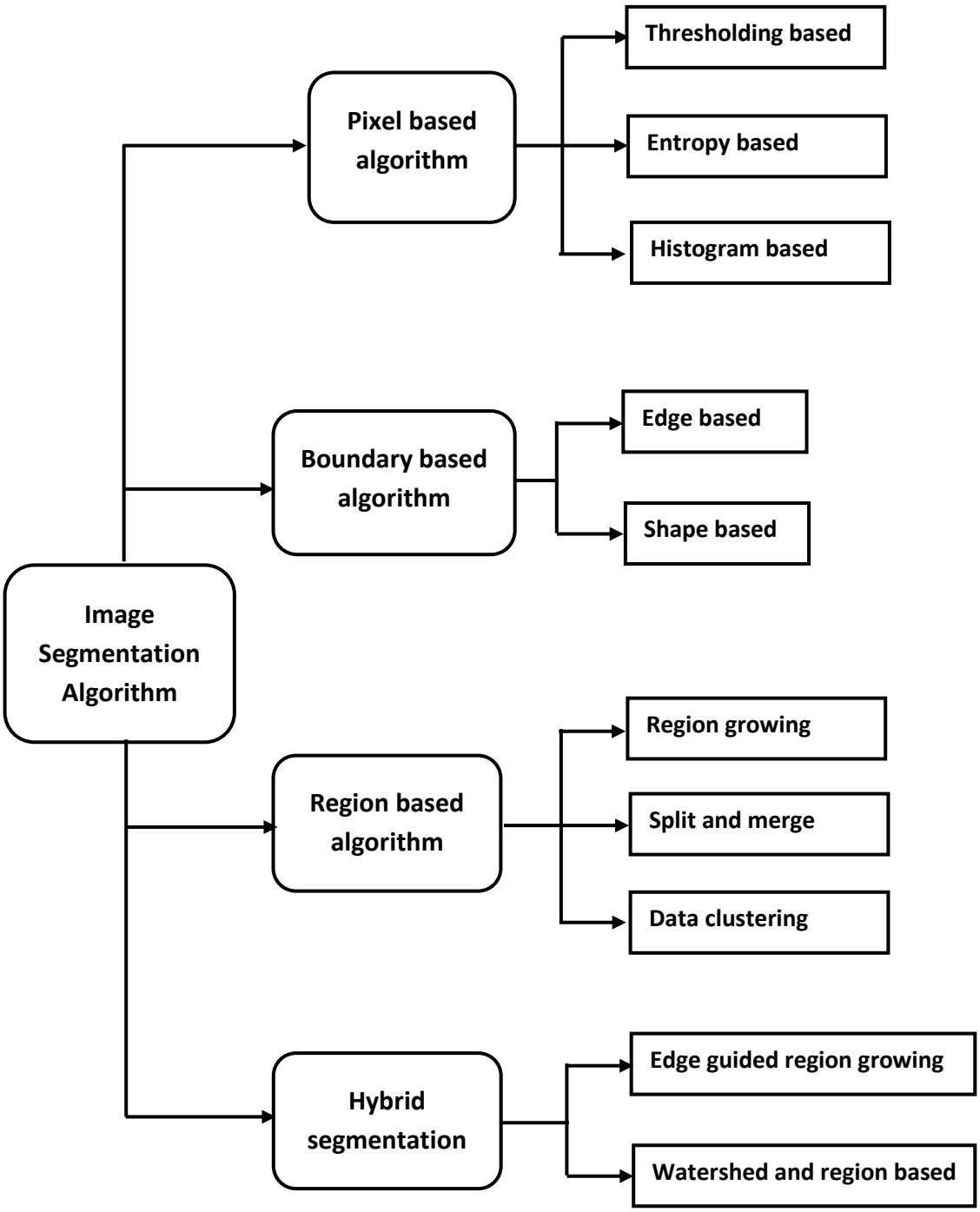

Figure 5.1: Taxonomy of image segmentation techniques

5.3 Image Segmentation Techniques

The segmentation techniques can be broadly grouped into four categories; pixel or thresholding based, boundary based, region based and hybrid image segmentation (Gonzalez and Woods, 2002; Janssen and Molenaar, 1995; Zhang, 1997; Pal *et al.*, 2000). Based on the review, taxonomy of segmentation techniques is given in Figure 5.1.

5.3.1 Thresholding Based Image Segmentation

Thresholding techniques are based on defining the limits on the attributes (e.g., gray level, color value, texture, etc) of pixels to form objects (Lim *et al.*, 1990). Other criteria such as histogram shape, clustering, entropy, spatial correlation etc. may also be used to define the thresholds (Zhang *et al.*, 2004). The output of a thresholding operation is usually a binary image.

Thresholding technique selects the threshold, either globally or locally to produce a binary image. It divides the image with ones indicating the objects and zeros indicating the background. The output from the thresholding algorithm is a binary image. A global threshold can be selected by Otsu's method (Otsu, 1975) or by any other method. The global thresholding may fail when there is a lot of variation in the background classes (Pal *et al.*, 2000). In this case, the image is first pre-processed to compensate for the illumination problem. A global threshold is then applied on the preprocessed image for segmentation.

One such thresholding technique is ***histogram-based***, in which a histogram is computed from all the pixels in the image. The peaks and valleys of the histogram are used as the thresholds to form the cluster in image. A clear separation between any peaks and valleys of histogram helps in the selection of proper threshold and hence produces better quality segmented image.

Entropy thresholding is based on the concept of Shannon entropy (Shannon, 1948). In information theory, the concept of entropy is used to quantify the amount of information necessary to describe the state of the system. In case of the image, entropy refers to the information content in a pixel. In entropy thresholding technique, the pixel uniformity is calculated using the entropy and region is formed by clustering the pixels of uniform characteristics.

5.3.2 Boundary-Based Image Segmentation

Although thresholding algorithms are computationally less complex, but have not found much attention in remote sensing image segmentation, as the data are usually multi- and hyperspectral. In such cases, the thresholding is carried out on band-by-band basis followed by integration of each segmented result, which may be inefficient. These algorithms also neglect the spatial information of the images (Fan *et al.*, 2009). Further, the thresholding algorithms consider only the point attributes of pixels. It is likely that pixel values may change rapidly at the boundaries or edges between the two objects (Palmer *et al.*, 1996). Therefore, edge detectors such as Sobel, Roberts or Canny filters (Canny, 1986) may be used to detect the edges and hence segment the image on the basis of edges. Both shape and edge based segmentation algorithms may be adopted in this category.

In the ***edge based segmentation***, the edges on the boundary of two classes are determined using any of the standard edge detection technique such as Roberts, Sobel or Prewitt edge detector. Different filter sizes and thresholds are used to detect the edges. The accuracy of segmentation depends on the selection of the appropriate value of threshold.

In edge-based methods, the local discontinuity is enhanced first and then linked to form complete boundaries. Modern edge detection is a two-stage process; edge enhancement followed by edge linking. The edge enhancement stage specifically defines the edge content of the image while in the second stage; edge linking uses the edge information to create a closed boundary of objects (Farag, 1992).

Watershed based technique find catchment basins and watershed ridge lines in an image, which in turn is used to define the shapes of the segment. A catchment basin is the geographical area of a river. Similarly, in the image it is a surface where bright pixels have a high DN value and dark pixels have low DN values, which form a region. Over segmentation is the very common problem in watershed segmentation. Advance marker-controlled watershed segmentation improves the quality of image segmentation by providing a line to differentiate the foreground objects from its background. In marker controlled watershed, there is a set of internal markers, and external markers which are used to modify the gradient image by either linear filtering, nonlinear filtering or by morphological processing.

5.3.3 Region-Based Image Segmentation

Sometimes, the edge based image segmentation algorithms may provide the broken boundaries among the segments. Some post-processing operations, such as edge tracking, gap filling, smoothing and thinning are performed to obtain the closed region boundaries. The post-processing may thus be very time consuming (Fan *et al.*, 2009). This has resulted into the development of region-based image segmentation algorithms.

Region based image segmentation is a procedure to subdivide an image to generate homogenous closed objects, called regions, using image attributes such as pixel intensity, spectral values, and textural properties (Zhang, 1997, Carleer *et al.*, 2004). Region based segmentation algorithms can be divided into three categories; region growing, split-and-merge and clustering based techniques.

The ***region growing technique*** starts with a single pixel known as seed pixel. The neighboring pixels join with the seed pixel to form a cluster, based on predefined criteria for growth (e.g. mean difference) and the process is continued till a certain threshold is met. The threshold is normally a combination of certain homogeneity and size criteria such as texture, area, etc. A region grows until all pixels in the image are accredited to any of the segments or new seeds are placed and the process is repeated. Thus, these algorithms depend on a set of given seed pixels, but sometime suffers from lack of stopping criterion, such as intensity values, texture, etc. (Gorte, 1998, Molenaar, 1998).

A region splitting-and-merging technique solves the region-growing problem in two stages; the split and the merge. The split stage is a preprocessing stage that aims to reduce the number of merge steps required to solve the problem. Initially, it subdivides the image into a set of arbitrary, disjointed regions. Later, it merges the split regions that are identical and again splits the regions which are non-homogeneous to form final segmented regions or objects. In contrast to the region growing technique, the process starts with complete image, if the segment is non-homogeneous, these segments are divided into smaller and homogeneous ones. This process continues recursively until no further splits or merges are possible.

In both, region merging and splitting techniques, the process is based on formation of

homogeneous segment. Initially, the seed pixel is selected and a distance measure is applied to calculate the heterogeneity between the seed pixel and its neighbor. If the distance is less than a threshold, these pixels are considered homogeneous and are merged. The region center is then selected as the new seed. This merging operation continues till no further merging possible.

A ***clustering technique*** starts with single pixel region and the region grows to form a cluster. It starts from the single pixel region, checks its homogeneity with neighboring regions and merges to increase the cluster if they are homogeneous. The image can be segmented by using K-means clustering, graph-based clustering (Cui and Zhang, 2011). In K-means clustering, differences between the center of the object of interest and its neighbor are calculated, while in graph-based clustering, the vertex of the weighted graph is used.

Region based segmentation techniques are commonly used for image segmentation and also provides acceptable results.

5.3.4 Hybrid Image Segmentation

Few researchers have applied the combination of different image segmentation techniques and found improvement in the image segmentation quality. In general, it could be a combination of the boundary based and region based techniques, called as hybrid image segmentation technique.

In ***Edge guided region growing technique***, the SRG technique has been applied to form the segments. However, there is a problem of over segmentation at initial level (Mueller *et al.*, 2004). The edge based technique may be now applied to that segmented image with the aim to follow the meaningful object boundary by merging the homogeneous segments.

Watershed and region based technique controls the over and under segmentation problem. Initially, the image is segmented using watershed technique and then boundaries are marked for splitting the heterogeneous regions (Bleau and Leon, 2000).

5.4 Multi-Resolution Image Segmentation

Multi-resolution image segmentation technique comes under the region based image segmentation. Both, (i) region growing, and (ii) splitting and merge process appears in multi-resolution. Region growing by merging is a bottom-up approach that groups pixels or sub-segments into larger segment. Region splitting and merge is a top-down approach. If a region does not satisfy the homogeneity criteria, then it is subdivided into sub-regions.

Definiens eCognition segmentation works on the principle of so-called 'Fractal Net Evaluation' approach (FNEA) developed by Delphi2 Creative Technology (Baatz and Schape, 2000).The FNEA incorporates an object-oriented framework and image segmentation techniques. It utilizes fuzzy set theory to extract the objects of interest, at the scale of interest, by segmenting images simultaneously at both fine and coarse scales. FNEA starts with a single pixel and a pair wise comparison of its neighbors with the aim to minimize the resulting heterogeneity. The common solution for this pair wise merging problem is described as *global mutual best fitting*. The FNEA has six aims:

i). Production of homogeneous image object-primitives

ii). Adaptability to different scales

iii). Production of similar segment sizes for a chosen scale

iv). Applicable to a variety of data sets

v). Reproducibility of segmentation results, and

vi). Requirement for reasonably fast performance

Throughout the segmentation procedure, the whole image is segmented and image objects are generated based upon several adjustable criteria of homogeneity or heterogeneity in spectral and shape characteristics of the objects. These criteria are adjusted by user defined weighting parameters such as; scale, spectral and smoothness. The scale control the merging and splitting of objects, which influences the average object size, spectral weight (varies from 0 to 1) controls the volume of spectral information and smoothness influences the shape of the objects. A larger value

of the scale parameter leads to formation of bigger object and vice versa. Pixel's spectral information majorly takes place in image segmentation. Thus, for a finer segmentation, it is required to select the spectral information as much as possible while keeping the shape information optimum. In multi-resolution image segmentation, an image is segmented at different scales, which appears as distinct resolution image at different levels. The formed segments are linked with its sub-segment at lower scale and with its super-segment at higher scale, thus a hierarchy is formed (Baatz and Schape, 2000).

One of the distinct features of multi-resolution segmentation is that it can form levels of segmented objects that may be hierarchically connected to one another as shown in Figure 5.2 (Baatz and Schape, 2000). In this hierarchical network, one level of sub-objects obtained from a particular set of scale parameter and homogeneity criteria may be merged into larger objects at higher level. Each level is build on the basis of its direct sub-objects, e.g., the sub-objects of LEVEL 1 are merged into larger objects on LEVEL 2 and so on. In addition, adjacent image objects that are the sub-objects of different super-objects cannot be merged.

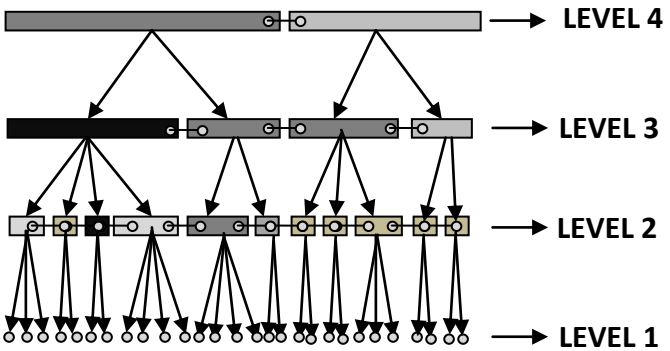

Figure 5.2 Hierarchical networks of image objects (Benz *et al.* 2004)

This feature has an ability to provide various classified maps for the extraction of different types of objects at different levels, which are divided on the basis of scales. These levels are linked to each other based on their hierarchy to sub and super objects or classes. Different hierarchical levels can be segmented based on different data. The information obtained from thematic land use can be applied to classify the image at the higher scale, whereas remote sensing data may be used to segment an image at lower scales.

Multi-resolution bottom up region-growing technique starts with one pixel as segment. It randomly picks up the starting pixel from the image and then on the basis of the weighted heterogeneity parameter '*nh'*, it decides whether the adjacent pixels should be merged or not. Here, '*n'* is the size of the segment and '*h'* is the heterogeneity. The heterogeneity criterion is based on some threshold. Adjacent segments having low heterogeneity are merged together.

As per the basic concept of region merging, it is required to establish a logical condition to evaluate whether any two adjacent image segments can be merged or not. The resulting condition is based on homogeneity criteria, which defines the degree of fitting between two segments.

To determine the degree of fitting, the algorithm focuses on two distinct features (Baatz and Schape, 2000):

(i) change in spectral heterogeneity, $\Delta h_{spectral}$

(ii) change in shape heterogeneity, Δh_{shape}

The overall change in spectral heterogeneity, $\Delta h_{spectral}$, is a measure of the segment heterogeneity difference during the merging of two segments. The process is mathematically described as,

$$\Delta h_{spectral} = \sum_{c} w_c \left[n_{merge} . \sigma_c^{merge} - \left(n_{obj1} . \sigma_c^{obj1} + n_{obj2} . \sigma_c^{obj2} \right) \right] \tag{5.1}$$

where *c* represents the number of bands, w_c are the weights associated with each band. The band weights vary from 1 to some definite value, the default weight to all bands is given as 1 (i.e., equal weight to every band). The more the weight assigned a band, more significant its contribution will be in segmentation or classification. The number of pixels comprising the segment is *n*, and σ_c is the standard deviation of segment for each band. The terms obj^1 and obj^2 represent the values related to the corresponding two segments being merged and *merge* be the segments after merging. The overall change in shape heterogeneity Δh_{shape}, is defined with the help of the weighted average change of compactness heterogeneity $\Delta h_{compact}$, and change in smoothness heterogeneity Δh_{smooth}, as given by (Baatz and Schape, 2000).

$$\Delta h_{shape} = w_{compact} . \Delta h_{compact} + w_{smooth} . \Delta h_{smooth} \tag{5.2}$$

where $w_{smooth} = (1 - w_{compact})$

where $w_{compact}$ and w_{smooth} are the weights vary from 0 to 1, and associated with the change in compactness heterogeneity and smoothness heterogeneity, respectively. Conceptually, circle describes the most compact form because the region boundary changes its direction at every pixel, whereas the rectangle describes the smoothest form as a minimum change occurs in region boundaries. Change in compactness heterogeneity $\Delta h_{compact}$ is defined as,

$$\Delta h_{compact} = n_{merge} . \frac{l_{merge}}{\sqrt{n_{merge}}} - \left(n_{obj1} . \frac{l_{obj1}}{\sqrt{n_{obj1}}} + n_{obj2} . \frac{l_{obj2}}{\sqrt{n_{obj2}}} \right) \tag{5.3}$$

where l is the border length of the formed segment. The ratio of the border length l and the square root of the number of pixels n, of the formed segment is referred as heterogeneity deviation from a compact shape.

$$h = \frac{l}{\sqrt{n}} \tag{5.4}$$

The change in smoothness heterogeneity can be determined as,

$$\Delta h_{smooth} = n_{merge} . \frac{l_{merge}}{b_{merge}} - \left(n_{obj1} . \frac{l_{obj1}}{b_{obj1}} + n_{obj2} . \frac{l_{obj2}}{b_{obj2}} \right) \tag{5.5}$$

The shape heterogeneity also depends on the ratio of the border length l and the shortest possible border length known as the bounding box b, of an image segment,

$$h = \frac{l}{b} \tag{5.6}$$

Thus, the overall heterogeneity change called as fusion value, depends on two quantities, the change in spectral heterogeneity and the change in shape heterogeneity. The fusion value *f*, for the merged segment is given by the following equation (Baatz and Schape, 2000).

$$f = w_{spectral} . \Delta h_{spectral} + w_{shape} . \Delta h_{shape} \tag{5.7}$$

where $w_{shape} = (1 - w_{spectral})$

The $w_{spectral}$ and w_{shape} are the user defined weight lies between 0 and 1.

The fusion value is then compared with the specified threshold calculated by the square of user defined scale parameter. The two segments merge, if the fusion value falls below the specified threshold.

In this segmentation technique, the merging of the two segments depends on the fusion value that is calculated by using user defined weighted parameters ($w_{spectral}$, w_{shape}, $w_{compact}$ *and* w_{smooth}), and the threshold for merging depends on the user defined scale parameter, which also controls the average size of the formed segments. A small value of the scale parameter reduces the fusion threshold, which results into over segmentation and vice-versa. Therefore, selection of suitable values for these parameters becomes essential as small variation may affect the quality of segmentation.

5.5. Generation of Fitness Function for Parameter Selection

Multi-resolution image segmentation requires three user-defined parameters (i.e., scale, shape factor and compactness) for segmenting an image. The variation in values of parameters may have bearing on the quality of segmentation. It is therefore expedient to judiciously fix these values.

5.5.1. The Fitness Function for Scale Parameter

Change in heterogeneity is a function of spectral and shape property, and the size of the segment depends on the value of scale parameter. Initial image segmentation is done on a preliminary user defined scale parameter. At the small scale, merging is less as the threshold is small, thus forming small and meaningless segments, which is known as over segmentation. To ensure the formation of meaningful segments, it is advisable to select the scale parameter as large as possible. In segmentation, a region is formed by merging the homogeneous pixels/segments, which depends on the internal and external spectral properties of that segment and is also controlled by the computed fusion value as well. The computed fusion value is compared with the threshold determined as the square of the user defined scale parameter. Internally, the spectral homogeneity is calculated by the texture attribute of the segments (Maxwell, 2005). However, an external spectral property is estimated by the *Mean_Difference_to_Neighbors* attribute (Baatz and Schape, 2000). The *Mean_Difference_to_Neighbors* is the band wise spectral mean difference between two neighboring segments. Together, these two attributes are used to estimate the current as well as the desired value of scale parameter. Texture is computed as,

$$Texture\ \ m\_segments\ = \left\{ \frac{1}{n_{merge}} \sum_{m} \left[n_{obj1} \cdot \frac{1}{c} \sum_{c} v_c^{obj_m} \right] \right\}^{1/2} \tag{5.8}$$

where $v_c^{obj_m}$ is the variance of segment *m* in spectral band '*c' and 'm'* represents the number of sub-segments comprising the meaningful object to be formed.

Texture represents the spectral variation within the segment. For small segment, spectral variation is less hence, they are more homogeneous. The intra homogeneity decreases with the increase of the spectral variation within the segment that varies with the size of the segment.

The *Mean_Difference_to_Neighbors* provide the spectral difference of a segment from its neighbors. If this value is less, the two neighbors are merged, whereas they become distinct if the spectral difference is more. It is defined as,

$$\Delta C_L = \frac{1}{l} \cdot \sum_{i=1}^{n} l_{si} \cdot \left| \bar{C}_L - \bar{C}_{Li} \right| \tag{5.9}$$

where $\bar{C}_L$ is the mean digital value of the pixels within the segment of interest, $\bar{C}_{Li}$ is the corresponding value of its neighbor *i*, *l* is the border length of the segment of interest, l_{si} is the shared border length of segment of interest with its neighbor *i*. The large value of ΔC_L indicates the heterogeneity between the two segments is more. By merging two heterogeneous segments, the size of the segment increases that further increases the intra-region heterogeneity of the formed segment. The sub-segments of an object that may have intra region homogeneity may be heterogeneous to each other. Stability is directly proportional to the heterogeneity. High heterogeneity between the sub-segments indicates that these sub-segments are more stable and thus require a high value of the scale parameter for merging. Hence, from this, a stability criterion can be introduced to evaluate stability of the segmentation that depends on the heterogeneity of its *m* neighbors. The term stability (Maxwell, 2005) is defined as,

$$Stability(m\_segments) = \frac{1}{m}\left(\sum_{m}\left[\frac{1}{c}\sum_{c} \Delta C_L \right] \right) \tag{5.10}$$

Initially, the image is segmented with some preliminary user-defined scale parameters at different levels. The texture and stability criteria are applied to the object of interest and its sub-segments to predict the desired scale. The sub-segments of an object have little variation in texture and also in mean-difference because they are the part of an object. The variation in the number of sub-segments causes the variation in texture and mean-difference values as it depends on DN values that vary with number of sub-segments. The number of sub-segments varies with change in scale parameter. The initial value of scale parameter, before the merging of the sub-segments and its current value at an intermediate level has been used to calculate its predicted value using fitness functions given Eq. (5.11). The predicted or computed value is regarded as the actual value of the scale parameter to produce quality segmentation.

$$Desired\_scale = \left(\sqrt{\frac{\pi}{2}} * Current\_scale * \left| Stability \right| / Texture \right) - Initial\_scale / \sqrt{m} \qquad (5.11)$$

5.5.2 The Fitness Function for Shape Parameter

Pixels DN value plays a dynamic role in image segmentation. Thus, to obtain meaningful segments in the image segmentation process, it is necessary to consider as much spectral information as possible, while maintaining the shape information as required (Baatz and Schape, 2000). It is critical to select an appropriate value of the object's shape related information. The shape of an object/segment depends on two factors; merging of sub-segments and the size of the formed segment. Merging of sub-segments is based on the homogeneity of the segments, which is controlled by the scale parameter as discussed in the previous section. The size of the formed segment grows by merging of the sub-segments. The shape of the grown object changes every time with merging of sub-segments.

The shape information plays an important role to control the object's shape and prevents unnecessary merging. If the neighboring segments are spectrally similar to the object of interest, they can easily merged, which in result grows the object. Merging of irrelevant segments may affect the shape of the formed segment.

The selection of shape parameter is performed in two steps; spectral difference and size difference. First, the sub segment *'a' is* selected, which has the maximum spectral difference compared to the desired object *'M'* and the *Spectral_Mean variation* of that sub segment from the desired object is computed.

$$Spectral\_Mean(a) = \max \frac{1}{c} \sum_{c} \left| C_L^{obj_a} - C_L^{obj_M} \right| \quad \text{where } a \in M \qquad (5.12)$$

In the second step, the size is considered, in which the difference in size of the selected sub-segment '*a'* and the average size of all the sub-segments of the desired object has been computed. If this size difference is large, it indicates that the sub-segment is very small in size and may not

have large effect on the shape and spectral mean after merging. Thus, the selected sub-segment will merge according to the variation in the spectral mean. In the case of large sub-segment, the size difference 'a' is small; but, the internal texture variation is more. Thus, by merging of these two sub-segments, the formed object grows more and may change in shape also. Hence, the size difference is also an important factor for merging and is given by Eq. (5.13).

$$Size\_Diff\ (m\ segments) = \left| \left(\frac{1}{m} \sum_{m} n_{obj_m} \right) - n_{obj_a} \right| \tag{5.13}$$

where *m* is the number of sub-segments forming the desired object, n_{obj_m} is the number of pixels comprising segment *m*, and n_{obj_a} is the number of pixels forming segment *a*, where segment *a* is the largest spectrally diverse sub-segment which will form desired object.

Finally, the global largest size of the segment is used to monitor the growth of sub-segments after merging. In general, shape changes rapidly with larger grow in segment thus more shape information required to control this growth. The fitness function for the calculation of shape factor is given as,

$$Shape\_parameter = \left(\frac{\left| \left(\frac{1}{m} \sum_{m} n_{obj_m} \right) - n_{obj_a} \right|}{\left| \left(\frac{1}{m} \sum_{m} n_{obj_m} \right) + n_{obj_a} \right|} \right) \Bigg/ \max \left\{ \frac{1}{c} \sum_{c} \left| \bar{C}_L^{obj_a} - \bar{C}_L^{obj_M} \right| \right\} \tag{5.14}$$

The generated fitness function depends on the two factors, the spectral mean variation of the largest heterogeneous segment, and the variation in size of that segment with the formed segment. The shape factor controls the merging of a sub-segment with its neighbor to obtain the ideal object.

5.5.3 The Fitness Function for Compactness Parameter

The generated fitness function for scale parameter controls the merging of spectral similar sub-segments whereas the shape related function controls the size variation of the formed segment while merging. Further, compactness and smoothness are the properties of the object's shape. As the importance of shape increases, the compactness and smoothness parameters also become important as they describe the shape of an object. Any object can be compact as well as smooth. The shape of an ideal object is fixed and hence it is likely that the values of smoothness and compactness will not change every time, thus fixed at the start. The compactness parameter provides the information about the selection of weight regarding compactness factor, based on the shape of the object of interest (Maxwell, 2005). The smoothness of the object is generally equated to a rectangle, whereas the compactness of the object is equated to a circle. The compactness function of an object is given in Eq. (5.15) is used for the calculation.

$$Compactness\_Parameter = \sqrt{\frac{\sum_{i=1}^{m} l_i - \sum_{\substack{j=1 \\ i \neq j}}^{m} {}_s l_{i,j}}{n_{obj_M}}} \tag{5.15}$$

where l_i is the border length of the sub-segment and ${}_s l_{i,j}$ is the shared border length between a sub-segment (i) and its neighboring sub-segment (j).

The value of the compactness function for every segment has been calculated using Eq. 5.15. The shared border length between two sub-segments of a segment of interest has been calculated. The difference between the total border length of all the intra sub-segments and the intra sub-segment shared border length is the border length of the formed segment. The value of the border length of compact object is low in comparison to that of the linear object. Additionally, the border length is low for smooth object and high for irregular shaped object. If the segment of interest is compact, value of the compactness function is high. The value of the compactness function for a model object can be calculated by the ratio of the border length to the area of the model object.

5.6 Methodology of Segmentation Parameter Fixation

For many years, image segmentation has been a main research focus in the area of image analysis, and a number of algorithms have been proposed so far. Most of the image segmentation algorithms require a set of user-defined parameters to control the quality of the resulting segmentation. Selecting suitable value for parameters is a challenging task. In this study, the region-growing algorithm has been used for image segmentation, which depends on three user-defined parameters as described earlier in section 5.4. Generally, parameter selection is carried out by trial and error. Here, in this work a fitness function is proposed to fix the values of the user defined parameters.

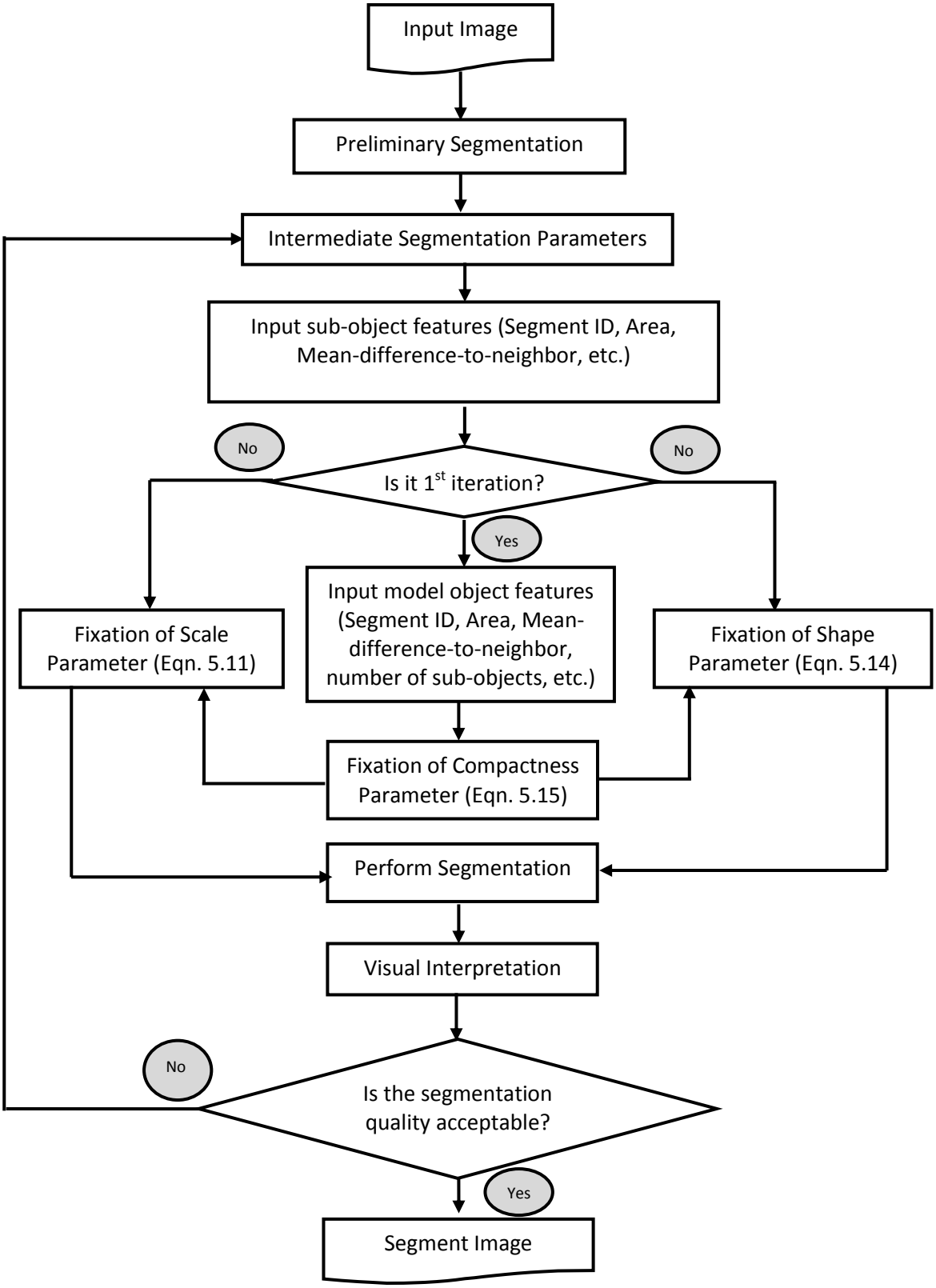

Figure 5.3: Flow diagram for parameter selection process

The flowchart of the methodology for fixation of segmentation parameter is given in Figure 5.3. The process starts with initial segmentation, in which the image is given as the input and the preliminary segmentation is done with initial set of the parameters values (e.g., very low value of scale parameter). At this level, the object is subdivided in a number of sub-segments. The proposed method retains the required information of all sub-segments to calculate the optimum value of the parameters. As the shape of the particular object is not changing, the compactness parameter's value is computed and set in the first iteration only. However, the size of the object varies every time with the fusion of sub-segment. Hence, to optimize the scale and shape parameter values, numbers of iterations are required. To obtain the meaningful object, the desired values of the scale parameter and shape factor can be set iteratively, by making use of generated fitness functions. Finally, the image is segmented again with the help of the generated parameter's value. The quality of the segmented image is analyzed visually. If the object of interest is obtained in the form of single segment, then the generated parameter's value may able to segment the image correctly, otherwise the process is repeated.

In the process of image segmentation, the shape and size of the formed segment may vary every time due to merging. Apparently, varying any parameter may result into over and under segmentation. It is therefore a necessity to assess the segmentation quality at each step via a set of quantitative measures.

5.7 Fixation of Segmentation Parameters

Various classes present on the earth's surface have different characteristics. Thus to extract a particular class in object based environment, values of segmentation parameters need to be set judiciously, which also depends upon the spatial resolution of the image. During segmentation, the image is initially segmented using trial-and-error process of eCognition.

The generated fitness function is now used to fix the segmentation parameters value. The initial segmentation parameters value used in trial-and-error segmentation and corresponding outcomes have been used for fixing these values of the segmentation parameters. These generated values are further used to extract a meaningful object of interest. As the shape of the object of

interest (e.g. compact or linear) is fixed, the value of the compactness is fixed once for all the iterations. However, the other two parameters are modified till an appropriate object is obtained because the size and the intermediate shape of the object changes every time by the merging of two segments.

5.7.1 Segmentation Parameters Value Fixation: Study Area-I

Bottom-up region growing multi-resolution image segmentation has been used for segmenting an image at different levels by varying values of segmentation parameters. These parameters are set in such a manner that meaningful segments corresponding to the objects are generated. As each constituent land use objects may have different spectral, spatial and shape characteristics and hence variation in segmentation parameters these have been grouped as,

i. Linear objects

ii. Regular compact objects

iii. Irregular compact objects

Thus, for extracting particular group of objects, the values of segmentation parameters may be different than those of other groups. Therefore, the Pan-sharpened image has been segmented three times, once for each group using eCognition software by varying values of segmentation parameters. The segmentation parameters values for each group are given in Appendix-II. Although, the image will be segmented in objects belonging to all the classes, but it is expected that the classes belonging to one group will be extracted accurately by utilizing the values of the parameters set for that group. It has been observed that at small scale, the objects of interest are over-segmented and the resulting sub-segments are small and spectrally homogeneous. The values of set of parameters selected by trial and error process for different groups are given in Table 5.1.

The three corresponding segmented images, referred as Seg-PS-I, Seg-PS-II and Seg-PS-III, for linear, regular and irregular compact objects, are shown in Figure 5.4.

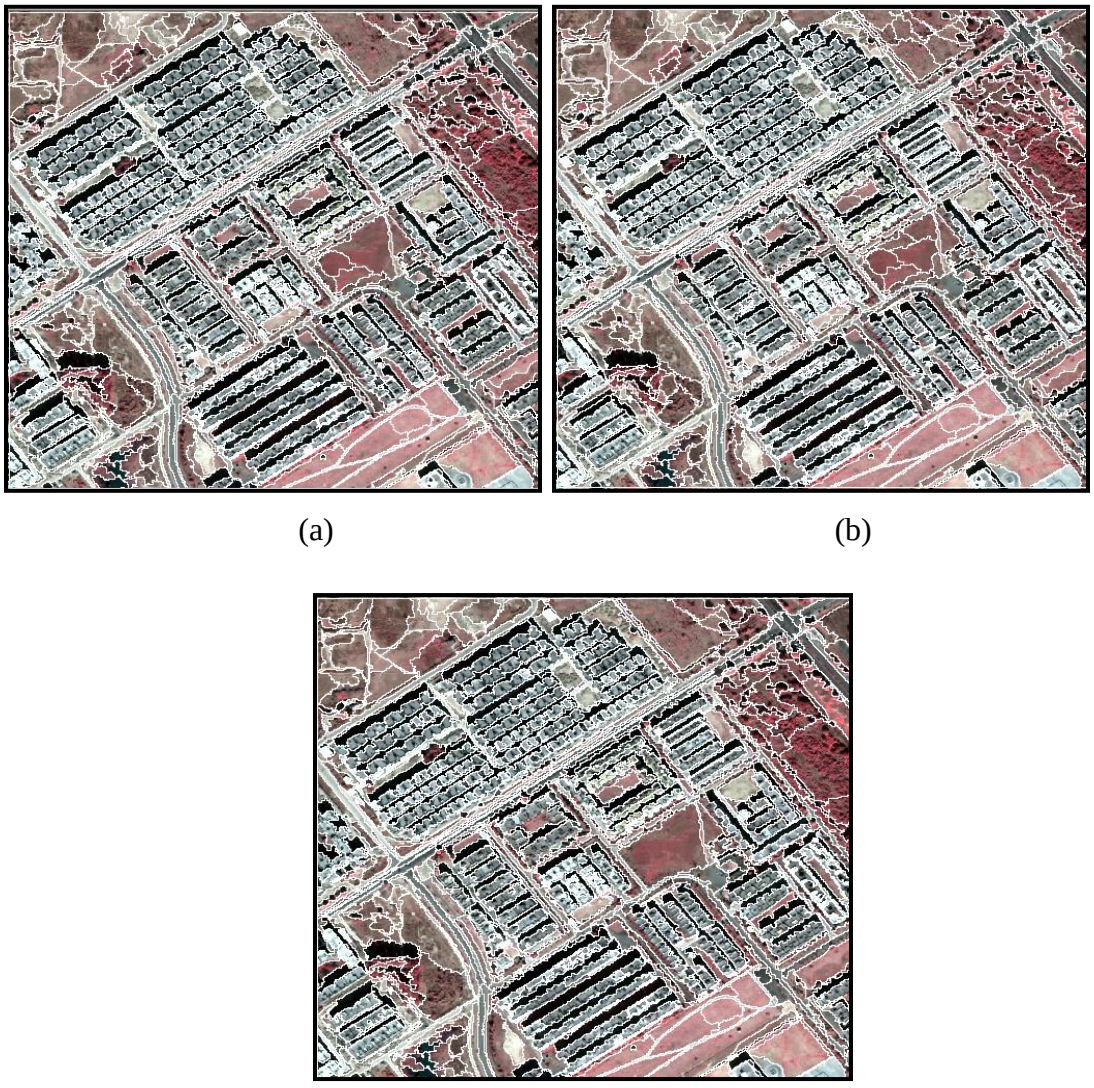

(a) (b)

(c)

Figure 5.4: The segmented images using trial and error methods. (a) Seg-PS-I: linear object extraction, (b) Seg-PS-II: regular compact object extraction and (c) Seg-PS-III: irregular compact object.

As it can be seen from image Seg-PS-I, the segments closely follow the boundaries of linear objects whereas for another group of objects, exact boundaries have not been obtained. In case of Seg-PS-II, regular compact objects, such as buildings, have been segmented clearly than the other objects. Same kind of observations has been noticed in case of Seg-PS-III image, where irregular objects have been properly segmented. This exercise has been completed using the trial and error

process, which is time consuming and the values of parameters may not set properly. Thus to reduce this complexity the generated fitness functions have been applied. It uses the intermediate values of segmentation parameters to obtain the required optimal value for segmentation.

Table 5.1: Values of segmentation parameter found experimentally for extracting different types of objects from Quick-bird Pan-sharpened image.

Feature group	Parameter values			Number of Segments	Segmented image
	Scale	Color/Shape	Smoothness / Compactness		
Linear object	70	0.6/0.4	0.55/0.45	814	Seg-PS-I
Compact regular object	58	0.374/0.626	0.35/0.65	881	Seg-PS-II
Compact irregular object	75	0.58/0.42	0.4/0.6	805	Seg-PS-III

5.7.1.1 Fixation of Segmentation Parameters for Quick-Bird Pan-Sharpened Image

The required parameter's value has been computed using the derived fitness functions. The desired scale parameter computed using Eqn. 5.11 and Eqn. 5.14 has been used to calculate the shape parameter. The parameter value for compactness has been obtained from Eqn. 5.15.

The image is first segmented by varying the initial set of segmentation parameters. The intermediate segmentation parameters value and its corresponding outcomes set in trial-and-error experiment have been used to fix the optimum value of these parameters. The segmentation parameters value, number of sub-segments and its areas, which have been used for generation of the parameters value for linear object extraction, have been given in appendix-II Table II.10. Similarly, the intermediate values for the extraction of compact-regular and irregular shapes object have been given in appendix-II Table II.11 and Table II.12.

To check the suitability of the desired parameters generated using the fitness function, the image has been again segmented using the computed optimum value. In Table 5.2, details of segmentation parameters using trial-and-error and computed using fitness function have been

given. For the linear object, the value of the scale parameter using the commercial software is 70, and the computed value is 66.7. Similarly, the experimental value of shape-factor is 0.4 and from the fitness function it is 0.37. While the value of compactness is fixed to 0.45 based on the regularity of the object's shape and its computed value is 0.27.

Similar experiments have also been done to regular shape compact and irregular shape compact object. The image has also been segmented individually to extract these objects experimentally. The shape and smoothness parameter values play an important role in this case. From the initial experiments, the scale parameter is set to 58, shape-factor is 0.626 and the value of compactness is 0.65 to extract regular shape compact object. The computed values for these parameters are 55.4, 0.46 and 0.582 respectively. The smoothness parameter value is very less for irregular shaped object, as they do not follow any ideal shape. The experimentally obtained segmentation parameter's value for extracting irregular shaped compact object in Pan-sharpen image are 75, 0.42 and 0.6, while the computed values are 68.4, 0.481 and 0.627 for scale, shape-factor and compactness parameters respectively.

Segmented image using the optimum value obtained through fitness function has been compared to the segmented image obtained through trial and error. The comparison result shows that there is little variation in these values, and the computed parameter's value produces an appropriate object of interest. The results in Table 5.2 show that the generated parameter's value is acceptable under certain conditions; (i) if the number of segments for any object of interest is less than obtain by trial-and-error, as segment is meaningful if object is segmented in one segment, (ii) the value of the generated scale parameter is also less than the experimental value. The three corresponding segmented images, referred as Seg-PS-I, Seg-PS-II and Seg-PS-III, for linear, regular and irregular shape objects with computed parameters value, are shown in Figure 5.5. Objects with red boundaries depict the extracted objects shape.

Table 5.2: Variation in parameters value with trial and error and the generated parameters value from fitness function for Quick-bird Pan-sharpened image.

Process	Scale	Shape-factor	Compactness	No. of segments	Remarks (Acceptable: Yes/No)
Trial and error	70	0.4	0.45	1	-
Fitness function	66.7	0.37	0.27	1	Yes
Trial and error	58	0.65	0.65	1	-
Fitness function	55.4	0.46	0.582	1	Yes
Trial and error	58	0.35	0.8	1	-
Fitness function	52.5	0.27	0.84	3	No (more segments)
Trial and error	75	0.45	0.6	1	-
Fitness function	68.4	0.481	0.627	1	Yes
Trial and error	50	0.65	0.40	1	-
Fitness function	58.4	0.62	0.64	1	No (larger scale)

Table 5.3: Selected image segmentation parameter's values from the computed values for extracting three types of objects from Quick-bird Pan-sharpened image.

Feature group	Parameter values			No. of Segments	Segmented image
	Scale	Color/Shape	Smoothness / Compactness		
Linear object	66.7	0.63/0.37	0.73/0.27	853	Seg-PS-I
Compact regular object	55.4	0.54/0.46	0.42/0.582	922	Seg-PS-II
Compact irregular object	68.4	0.519/0.481	0.373/0.627	788	Seg-PS-III

(a) (b)

(c)

Figure 5.5: The segmented images with optimal value of segmentation parameters (a) Seg-PS I. linear object extraction, (b) Seg-PS II. regular compact object extraction and (c) Seg-PS III. irregular compact object.

It has been observed that there is minute variation in number of segments formed, when segmenting the image with trial-and-error process and with computed parameters. The visual interpretation of the image also justifies the segmentation quality. It can also be observed from the segmented image shown in Figure 5.5 (a), that all types of roads are segmented almost accurately while the large compact shape grounds are sub-segmented and small buildings merged. However,

for the extraction of small buildings (compact regular shape) the problem occurs with large irregular shape compact object, which are divided in many sub-segments. Similarly, when the parameters are set to extract large irregular shape compact objects smaller objects appear under segmented while the linear road features are merged with surrounding.

5.7.1.2 Fixation of Segmentation Parameters for Quick-Bird Pan Image

Similar exercise has been performed on Quick-bird Pan image. The image has been segmented three times, once for each group, with different values of parameters (Appendix-II). The values of parameters thus set experimentally for different groups are given in Table 5.4.

Table 5.4: Experimentally selected image segmentation parameter's values for extracting three types of objects from Quick-bird Pan image.

Feature group	Parameter values			No. of Segments	Segmented image
	Scale	Color/Shape	Smoothness / Compactness		
Linear object	75	0.55/0.45	0.65/0.35	765	Seg-P-I
Compact regular object	53	0.35/0.65	0.35/0.65	894	Seg-P-II
Compact irregular object	68	0.7/0.3	0.2/0.8	831	Seg-P-III

Various intermediate segmentation parameters value and its corresponding outcomes set in trial-and-error experiment to fix the optimum value of these parameters are shown in tables. Table II.13 in appendix-II shows the values for linear object extraction, while parameters values for extracting compact regular and irregular shape objects are shown in appendix-II, Table II.13 and Table II.15

The generated fitness functions have been used for the computation of the required parameter's value to extract linear object, regular shape and irregular shape compact objects. The

experimentally obtained segmentation parameter's value and the computed values using fitness function for extracting these three types of objects are given in Table 5.5.

Table 5.5: Variation in parameters through experiments and the computed parameters through fitness function for Quick-bird Pan image.

Process	Scale	Shape-factor	Compactness	No. of segments	Acceptable: Yes/No
Trial and error	75	0.45	0.35	1	-
Fitness function	72.4	0.39	0.24	1	Yes
Trial and error	68	0.75	0.45	1	-
Fitness function	71.1	0.62	0.53	1	No (larger scale)
Trial and error	68	0.3	0.8	1	-
Fitness function	66.9	0.22	0.18	1	Yes
Trial and error	53	0.65	0.65	1	-
Fitness function	51.2	0.68	0.68	1	Yes
Trial and error	65	0.35	0.2	1	-
Fitness function	66.4	0.47	0.58	1	No (larger scale)

Table 5.6: Computed image segmentation parameter’s values for extracting three types of objects from Quick-bird Pan image.

Feature group	Parameter values			No. of Segments	Segmented image
	Scale	Color/Shape	Smoothness / Compactness		
Linear object	72.4	0.71/0.39	0.56/0.44	802	Seg-P-I
Compact regular object	51.2	0.32/0.68	0.32/0.68	895	Seg-P-II
Compact irregular object	66.9	0.78/0.22	0.82/0.18	839	Seg-P-III

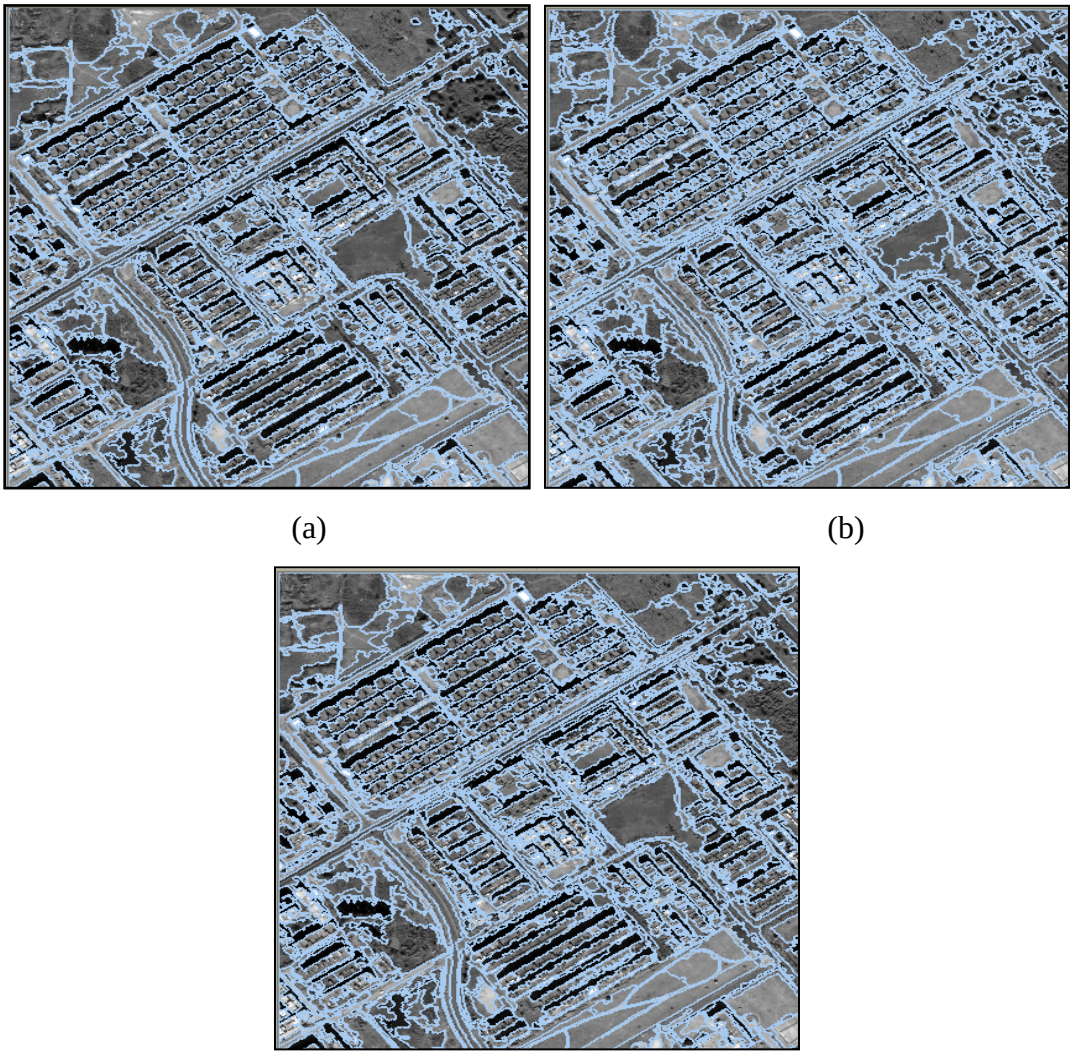

(a) (b)

(c)

Figure 5.6: Segmented Quick-bird Pan image with optimum value of segmentation parameters (a) Seg-P-I: linear object extraction, (b) Seg-P-II: regular compact object extraction and (c) Seg-P-III: irregular compact object.

The Quick-bird Pan image is segmented using these computed values of segmentation parameters using respective fitness function as given in Table 5.6. It has been observed that similar result has been obtained in case of Pan-sharpened image; also there is minimum variation in total number of generated segments obtained through the computed parameter value in comparison to that of the trial-and-error method. Generated segmented image using the optimum

value obtained through fitness function, referred as Seg-P-I, Seg-P-II and Seg-P-III, for linear, regular and irregular shape objects, are shown in Figure 5.6.

With the help of visual interpretation, it is clearly visible that segments follow the border of the linear object when the parameters values set for linear object extraction. The value of the scale parameter is high in comparison to that for the case of compact shape and compactness weight is low. However, it has also been observed that at this value of parameters, small objects are merged while, larger compact shapes become sub-segmented.

By comparing the computed values of Quick-bird pan-sharpened image with Quick-bird image for all three types of features, it has been observed that the successfulness of the fitness function is almost similar. However, at some places the computed values are not suited and in result produces poor quality segmented image.

5.7.2 Segmentation Parameters Value Fixation: Study Area-II

The multispectral LISS-IV image has also been segmented using bottom up region growing image segmentation technique. Various segmentation parameters have been set judiciously after several experimental trials. Due to the low spatial resolution of LISS-IV image, in comparison to that of Pan-sharpened Quick- bird image, the image objects are divided only in linear and compact groups. The variation in values of parameters for segmenting the image has been carried out as given in Table II.7 to Table II.9 of Appendix-II. The experimentally selected values of parameters for segmenting the LISS-IV image are given in Table 5.7. Additionally, the values of the segmentation parameters have also been computed with the help of the generated fitness functions and listed in Table 5.8.

Table 5.7: Experimentally determined image segmentation parameter's values for extracting two types of objects from LISS-IV (MS) image.

Feature group	Parameter values			No. of Segments	Segmented image
	Scale	Color/Shape	Smoothness / Compactness		
Linear object	28	0.55/0.45	0.6/0.4	858	Seg-L-I
Compact object	26.5	0.64/0.36	0.25/0.75	990	Seg-L-II

Table II.16 in appendix-II shows the values for linear object extraction, while values of parameters for extracting compact regular shape objects are shown in Table II.17 of appendix-II.

Table 5.8: The values of parameters through experiments and the computed parameters through fitness function for LISS-IV (MS) image.

Process	Scale	Shape-factor	Compactness	No. of segments	Acceptable: Yes/No
Trial and error	28	0.45	0.4	1	-
Fitness function	25.7	0.156	0.242	1	Yes
Trial and error	26.5	0.36	0.75	1	-
Fitness function	24.2	0.53	0.837	1	Yes
Trial and error	26.5	0.36	0.75	3	-
Fitness function	24.2	0.53	0.837	4	No (More segments)
Trial and error	32	0.65	0.54	1	-
Fitness function	33.9	0.61	0.52	1	No (larger scale)
Trial and error	28	0.45	0.4	1	-
Fitness function	25.7	0.156	0.242	1	Yes

The fitness functions have been applied to compute the segmentation parameter's values for LISS-IV segmented image at different levels and to consider different segment of interest. From Table 5.8, it has been noticed that similar to Quick-bird image, in most of the cases the computed parameters values fit suitably. It has also been observed that computed parameters value for one

type of feature may not suitable for other and it may be computed on the size of the segment of interest.

The computed values of parameters have been selected for final segmentation of the image. These values are; shape-factor-0.156, compactness-0.242 and scale of 24.2 for extraction of linear features. The corresponding values for extraction of compact features are 0.53, 0.837 at scale 25.7 respectively (Table 5.9). The segmented LISS-IV images using these values are shown in Figure 5.15.

Table 5.9: Computed image segmentation parameter's values for extracting two types of objects from LISS-IV (MS) image.

Feature group	Parameter values			No. of Segments	Segmented image
	Scale	Color/Shape	Smoothness / Compactness		
Linear object	24.2	0.844/0.156	0.758/0.242	1014	Seg-L-I
Compact object	25.7	0.47/0.53	0.163/0.837	885	Seg-L-II

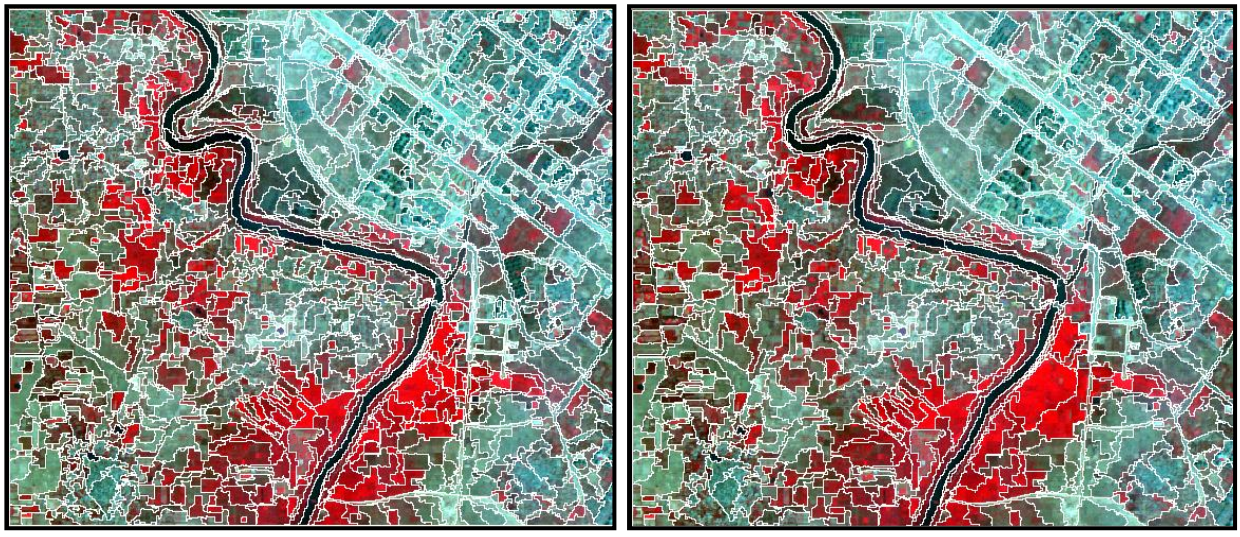

(a) (b)

Figure 5.7: Segmented LISS-IV MS image with optimum value of segmentation parameters (a) Seg-L-I. linear object extraction, and (b) Seg-L-II. compact object extraction.

As the image covers both extremely separable classes as well as mixed classes, the focus is to find the boundaries to separate the classes. In the image, it is almost impossible to extract houses from urban colonies but at the same value of parameters an apartment can be segmented, thus urban colonies and also some vegetation areas suffers with over-segmentation problem. However, at larger values of parameters, the apartments and some other small classes mixed with surroundings and image becomes under-segmented. Additionally, under-segmentation produces worst quality in classification. Similar to results of segmentation of the Quick-bird image segmentation, the linear and compact group of objects have been found to be accurately segmented using the computed values of parameters.

From these experiments, it may be concluded that selection of proper segmentation parameters is an important task but not an easy one. Number of segments may vary with the small variation in the segmentation parameters, especially by varying scale parameter. From Tables 5.2, 5.5 and 5.8, it may be clearly seen that the appropriate values of segmentation parameters obtained through fitness function appear low in comparison to the experimentally selected. There is not much variation in the values obtained from trial-and-error and through fitness function. However, fixation of values through proposed fitness functions requires not only less efforts of the user but also produces optimal values for segmentation. This may be treated as a semi-automatic approach for the selection of the parameters values in region based image segmentation.

Nevertheless, the computed values may always not satisfy all the cases and may not be accepted under the following circumstances, as these may deteriorate the segmentation quality, (i) if the computed scale parameter value becomes higher than the experimental value, (ii) the computed value is less, but the object of interest is divided into more sub-segments.

With regard to the fixation of values of parameters, the quality of the segmented image has been assessed through visual interpretation of the segmented images. It is, however, necessary that an appropriate quantitative measure of quality assessment be utilized. Next section focuses on the assessment of the segmentation quality.

5.8 Assessment of Segmentation Quality

The qualitative and quantitative assessment of segmentation result is very important for any object based classification (Neubert *et al.*, 2008). Most of the time, the quality of the image segmentation has only been assessed by visual interpretation. In few studies (e.g., Borsotti *et al.*, 1998, Lucieer, 2004), the segmentation quality of remote sensing data has been assessed quantitatively.

The quality assessment approaches may be categorized into three different groups,

i) Analytical approaches

ii) Empirical goodness-based approaches

iii) Empirical discrepancy-based approaches

Analytical approaches assess the segmentation quality without directly applying the algorithm on the data set. It measures the successfulness of the algorithm for image segmentation based on their principles and characteristics used (Everingham *et al.*, 2002). In contrast, the goodness-based measures calculate the homogeneity within the region or segment by applying some desirable goodness properties. These properties could be intra region uniformity, inter region contrast and object shape, which measure the empirical goodness of segmented image (Pal *et al.* 2000; Roman-Roldan *et al.* 2001; Sahoo *et al.*, 1988). The empirical discrepancy based approach measures the quality of segmentation with respect to a reference data to calculate the discrepancy between the reference object and segmented image (Jiang *et al.*, 2006, Borsotti *et al.*, 1998, Zhang, 1997, Tian and Chen, 2007, Carleer *et al.*, 2005, Lucieer, 2004, Neubert *et al.*, 2008).

A general diagram of the segmentation quality evaluation is shown in Figure 5.8, which describes the implementation details of the algorithm, necessity of pre-and-post processing and the requirement of reference data.

5.8.1 Analytical Approaches

The analytical approaches directly focus on the segmentation algorithms by considering the principles, requirements, utilities, complexity, etc. of the applied algorithms. The analytical methods avoid the concrete implementation of these algorithms on the data set. The results can be exempted from the influence caused by the arrangement of evaluation experiments as the empirical methods do. The analytical methods work only with some particular models or desirable properties of algorithms.

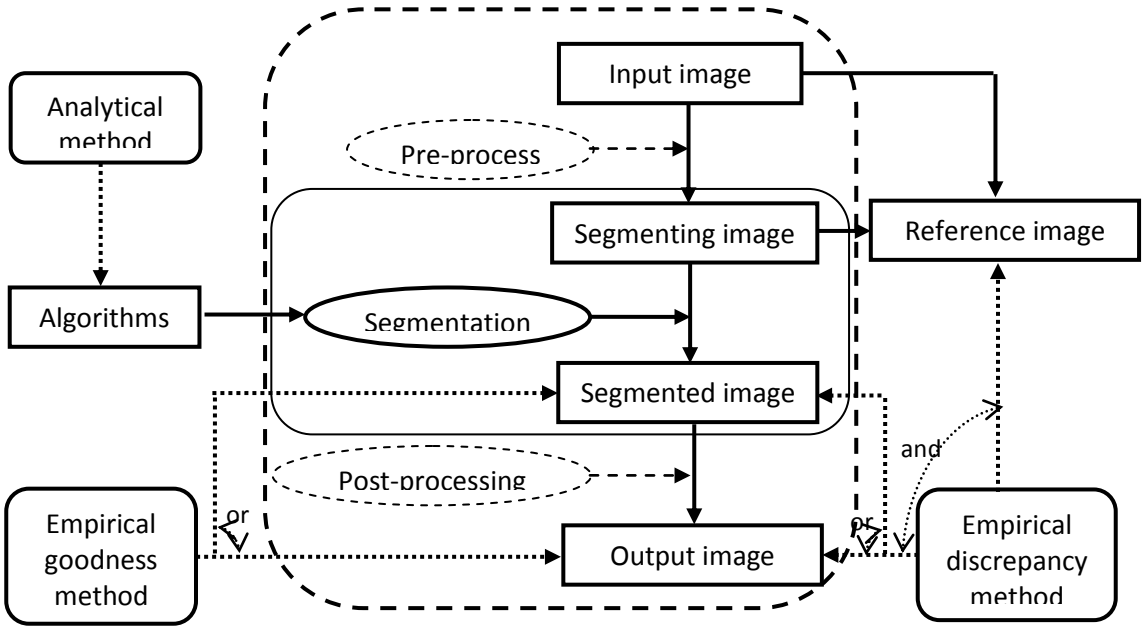

Figure 5.8: General sketch for segmentation and its evaluation (Zhang, 1997)

5.8.2 Empirical Goodness-Based Approaches

Empirical goodness based methods assess the performance of algorithms by evaluating the quality of segmented images. These methods characterize different segmentation algorithms by simply computing the goodness measures based on the segmented image without any *a priori* knowledge of the reference data. Some goodness measures are intra region homogeneity, the inter

region heterogeneity that calculates the uniformity within the segment and also separation from the neighboring segments.

5.8.3 Empirical Discrepancy-Based Approaches

These approaches work to measure the difference. If the segmented image is complex and the algorithm used is fully automatic, the error is expected. The disparity between segmented image and a reference image is used to assess the performance of these algorithms. Higher the value of the discrepancy measure is, larger the error in segmented image (Zhang, 1997).

Empirical discrepancy based approaches normally provides the numerically calculated value of quality measure. Several literature demonstrates the discrepancy based approaches, which are related to over-and-under segmentation e.g. the Fragmentation index *FRAG* (Strasters and Gerbands, 1991); the Area based index (Lucieer, 2004, Liu 2004, Tian and Chen, 2007); distance based approach (Boesch and Wang, 2008) and difference in shape (Neubert *et al.*, 2008) Fragmentation index is computed on the basis of number of segments, area based index calculates discrepancy between reference and segmented region, shape based index finds the variation in shape, and distance based approaches computes the homogeneity within the segments. Some of the quantitative techniques for quality measures are described briefly in Table 5.10

Table 5.10: Quantitative approaches for assessment of segmentation quality (Neubert *et al.*, 2008)

Evaluation Approach / Cited Reference	Method	Mathematical Formulation	Description
Fragmentation (*FRAG*) Strasters and Gerbrands (1991)	ED	$FARAG = \frac{1}{1 + p.\left\|T_N - A_N\right\|^q}$ where T_N is the number of objects in the image and A_N the number of regions in the reference; p and q are scaling parameters	Finding the over-and-under segmentation by analysing the number of segmented and reference regions
Area-Fit-Index *(AFI)* Lucieer (2004)	ED	$AFI = \frac{A_{reference\ object} - A_{largest\ segment}}{A_{reference\ object}}$	
Geometric features Circularity Yang *et al.* (1995)	ED	$Circularity = \frac{4\pi A}{P}$ where A is the area and P is the perimeter	Addresses the shape conformity between segmentation and reference regions (scaling invariant shape feature)
Geometric features Shape Index Neubert and Meinel (2003)		$Shape\ Index = \frac{P}{4\sqrt{A}}$ where A is the area and P is the perimeter	
Empirical Evaluation Function Borsotti *et al.* (1998)	EG	$Q(I) = \frac{1}{1000(N \cdot M)} \sqrt{R} \sum_{i=1}^{R} \left[\frac{e_i^2}{1 + \log A_i} + \left(\frac{R(A_i)}{A_i} \right)^2 \right]$ where $N \cdot M$ is the size of the image I, e_i is the color error of the region i and $R(A)$ the number of regions of the size A	Calculates the uniformity feature within segmented regions (color deviation)
Pal *et al.*, (2000)	EG	where, n_i is the number of pixels in the ith segment, X_{ij} be the gray value of the jth pixel in segment i, n is the size of the image, is the mean gray value of image.	β index is directly proportional to the intra-region homogeneity. β =1 if c=1, and β= ∞ if every DN value forms separate segment. thus, β should be in between.

Fitness function Everingham *et al.* (2002)	A, ED	Probabilistic hull, Potential accuracy *f(a,I)* Multidimensional fitness-cost-space	Addresses multiple criteria and parameterizations of algorithms by a probabilistic Fitness/Cost Analysis
Entropy-based evaluation function and a weighted disorder function Zhang *et al.* (2004)	EG	$E = H_l ( ) + H_r ( )$ where H_l is the layout entropy and H_r is the expected region entropy of the image I	It checks for the uniformity within segmented regions (luminosity) using the entropy as a criterion of disorder within a region
Liu (2004)	ED	$Index = \frac{S'}{S} = \frac{2S'}{S_s + S_r}$ where S_r is the area of reference, S_s is the area of segment and S' is the intersected area	Addresses the fitting criteria between segment and reference region
Tian and Chen (2007)	EG	$G_s = \frac{\sum A_i^{overlap}}{A_{ref} . e^{\sum A_i^{diff} / A_{ref}}}$ where $A^{overlap}$ is the intersected area, A^{diff} is the non-intersected area for region i and A_{ref} is the area of the reference image	Calculates the matching between segment and its reference

Analytical (A), Empirical Goodness (EG), Empirical Discrepancy (ED)

All the above-mentioned empirical discrepancy based approaches use different methods for quality assessment of segmentation, but have not considered errors of omission and commission while assessing the quality of segmentation.

In the proposed empirical discrepancy based quality assessment approach, the area and the shape index have been used together for assessment of segmentation quality. The segment and its corresponding reference object have been used in quality assessment. The correctly segmented area has been calculated by overlapping the segments of the two data sets to estimate the size related index whereas the difference in shape has been computed by comparing the shape indices of segmented object and the corresponding reference object.

It is therefore expected that by taking the area and shape indices together, and by considering the errors of omission and commission, a realistic estimate for quality of segmentation can be achieved. Its performance has also been evaluated with a competitive segmentation quality index (Zhang *et al.*, 2010). The existing index is the ratio of the correctly segmented area with the mean area of the segment and corresponding reference object.

A user-defined threshold is generally used for the assessment of segmentation quality. The threshold selection is based on spatial resolution of the image i.e. high threshold value may be selected for high and very high-resolution images and slightly low threshold value may be selected for medium resolution images (Zhang *et al.*, 2010).

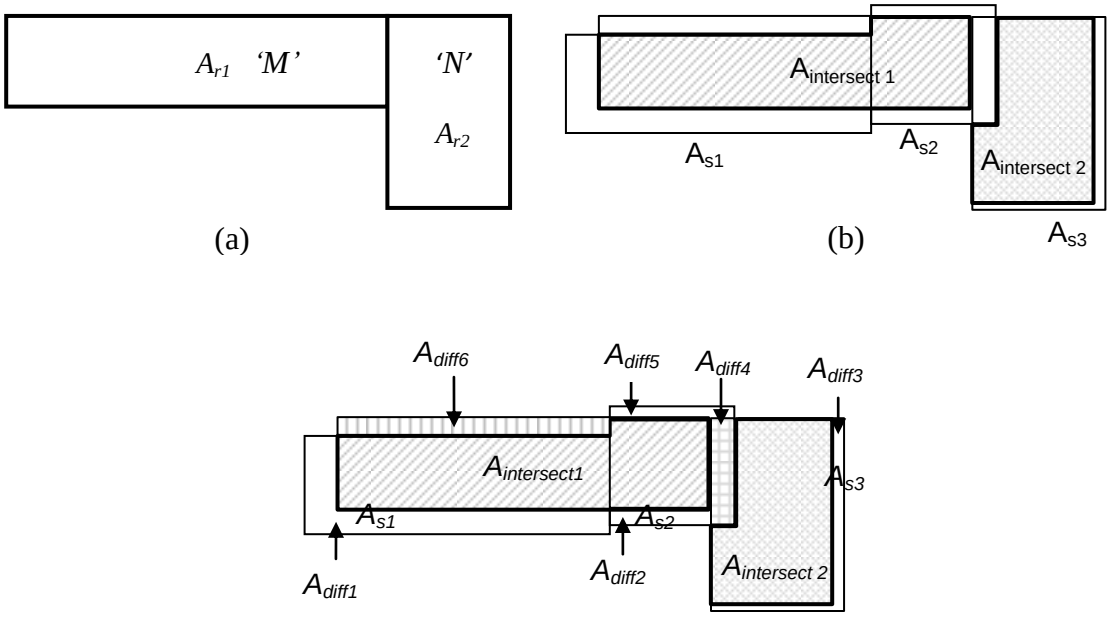

Figure 5.9: A schematic diagram of the segmentation quality evaluation, (a) reference object, (b) segments of the object *'M'* and *'N'*, and (c) intersection part showing calculation of errors of omission and commission.

A quality measure named as segment fit index (SFI) represents the fitness of the segment with its corresponding reference object and is given as the ratio of the correctly segment area with area covered by segment to the reference object. If SFI is 0, it indicates no match whereas an SFI value 1 indicates complete matching of the segment with its reference object.

As an example, a pictorial representation for calculation of errors of omission and commission is given in Figure 5.9. The shaded region shows the area of the reference objects A_{r1} and A_{r2}, which have been segmented into three segments A_{s1}, A_{s2} and A_{s3}. The region A_{diff1} to A_{diff6} represents mismatched areas and the regions surrounded by thick boundary represents the correctly segmented areas. During the segmentation process, a part of an object which may get omitted from its corresponding segment is referred as error of omission. In addition, a segment of an object may include a part of neighboring objects, which has been referred as error of commission. Figure 5.9 (c) displays A_{diff6} as the error of omission for reference object A_{r1} (with segment A_{s1} and A_{s2}) whereas error of commission for object A_{r1} is represented by A_{diff1}, A_{diff2}, A_{diff4}, A_{diff5}. The detailed description of the figure is given in Table 5.11.

Table 5.11: General description of evaluation technique used in Figure 5.9

Description of Figure	**Representation in Figure**
The reference object A_{r1} & A_{r2} (Figure: 5.9 a)	Thick boundary
Segments of object *'M'* (A_{s1} and A_{s2}) (Figure: 5.9 b)	Bounding box with thin line
Segments of object *'N'* (A_{s3}) (Figure: 5.9 b)	Bounding box with thin lines
Intersection part of object *'M'* and *'N'*(Figure: 5.9 b)	Shaded region
Reference objects that are not covered in the segments of that object (error 1) (Figure: 5.9 c)	The portion shaded by vertical lines, outside the bold boundary of the object *'M'* (represented by A_{diff6})
Outer part of the segments that are not covered by reference object (error 2) (Figure:5.9 c)	White region between reference objects and segment boundary (A_{diff1}, A_{diff2}, A_{diff3}, A_{diff5})
For ex., in Figure 5.9 c Part of reference object A_{r2} is segmented as in segment (A_{s2}) of object *'M'*. This region is neither the part of the object *' N'* as it is a segment of an object *'M'* nor the part of the object *'M'* as it is a part of reference object A_{r2}, thus produce an error.	The portion of the joint of object *'M'* and object *'N'* shaded by horizontal and vertical strips (A_{diff4})

The SFI can be computed by using the reference area (A_r), the segment area (A_s) and the area of the correctly segmented region (A_i) as shown in Eq. 5.16. The *SFI* is thus directly proportional to the actual area.

$$SFI = \frac{A_i}{A_t} = \frac{A_i}{(A_r + A_s - A_i)} \quad and \qquad SFI = \begin{cases} 1, & Perfect\ Fit \\ 0, & No\ Fit \\ Else, & Partly\ Fit \end{cases} \tag{5.16}$$

The shape index (SI) defines the geometry of the segment and provides the information regarding the shape of each segment. The segments of similar shapes will have a little variation in shape index. Generally, the value of the shape index is small for compact objects and large for linear objects. Therefore, the difference in the shape index (ΔSI) of the segment and its respective reference object provides information about the variation in shape of the segment. The value of ΔSI is 0 for a segment which exactly follow the shape of the corresponding reference object. Its value increases with the increase in mismatch of shapes. The SI and ΔSI are given as,

$$SI = \frac{Perimeter}{4\sqrt{Area}} \quad and \qquad \Delta SI = \begin{cases} Low, & Matching \\ High, & Not\ Matching \end{cases} \tag{5.17}$$

The quality of segmentation is expected to be high when the value of SFI is large and the overall difference of Shape Index (ΔSI) between the segment and associated reference object is small. Thus, in the proposed approach, empirical discrepancy is jointly calculated using both; segment fit index (SFI) and difference in the shape index (ΔSI).

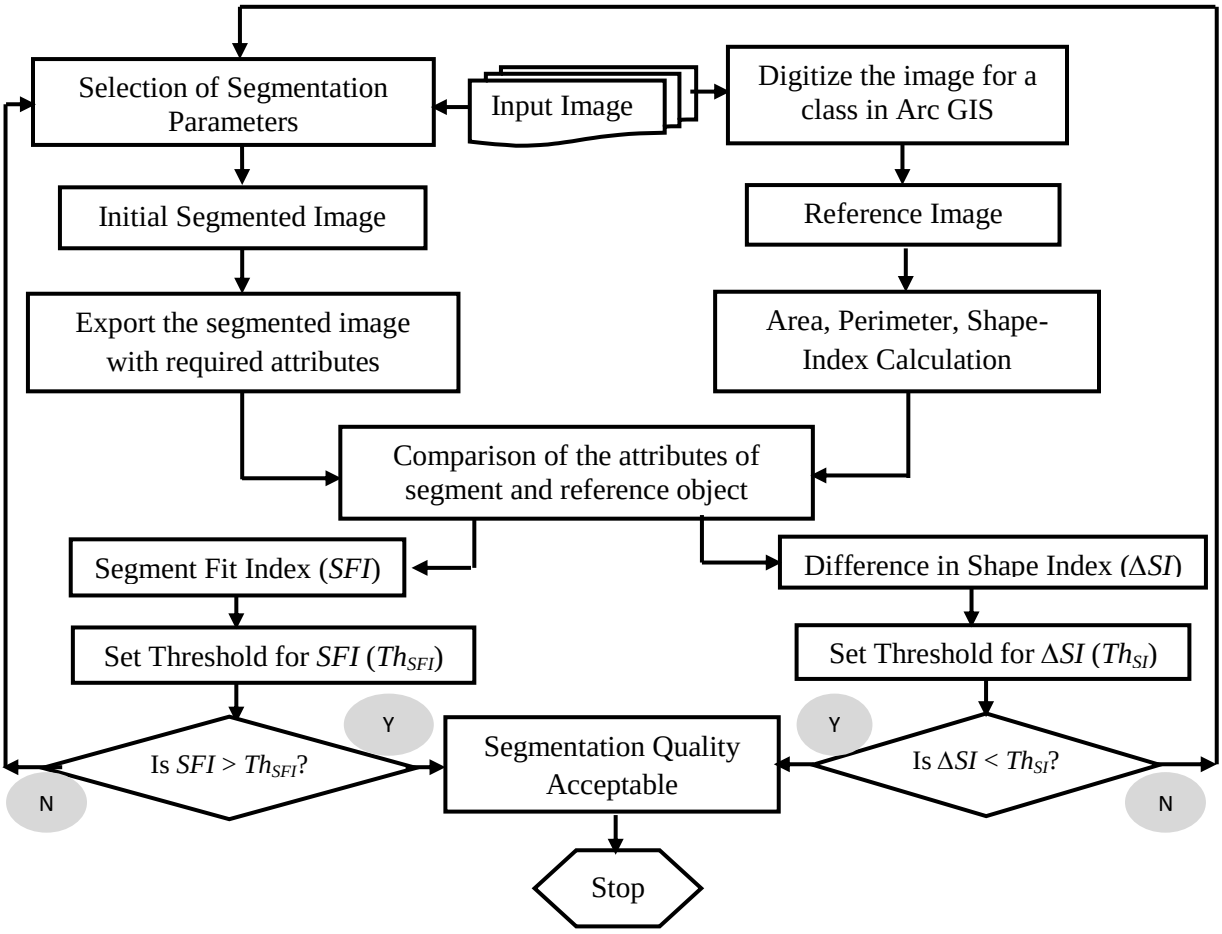

Figure 5.10: Flowchart of the methodology adopted for segmentation quality assessment

Earlier, Zhang *et al.* (2010) also assessed the quality of the segmented image quantitatively. The empirical discrepancy based approach as given in Eq. 5.18 has been used by the author for the assessment of segmentation quality. The index is the ratio of the correctly segmented area (A_i) to mean of the reference and segmented area (A_m). The limitation of the approach is that it does not consider the errors of omission and commission for calculation.

$$Existing\ Index = \frac{A_i}{A_m} = \frac{A_i}{A_r + A_s \quad / 2} \tag{5.18}$$

5.9 Implementation of Proposed Segmentation Quality Assessment Measures

The workflow for implementing the proposed quality assessment approach is given in Figure 5.10. The process starts with the segmentation of the remote sensing image with various computed segmentation parameters, which are set on the basis of shape (linear or compact) of the object. The multi-resolution region growing technique, inbuilt in eCognition software has been used for segmenting the image. The segmentation process starts with small initial values of parameters and gradually incrementing it till the desired segmentation quality is achieved, as discussed in section 5.7. At the same time, a reference map for various linear and compact shape objects has been generated by digitizing a sample of objects in Arc GIS. The generated reference objects have been shown in chapter 3. Based upon the attributes of the segments in the reference map as well as the segmented image, the values of SFI and ΔSI have been computed. Thresholds for these measures are set based on the recommendations given in the literature (e.g., Zhang *et al.*, 2010) to assess the segmentation quality. If the value of SFI is greater than the SFI threshold (Th_{SFI}) and ΔSI is less than the ΔSI threshold (Th_{SI}), then the quality of the segmentation is considered as acceptable. If these thresholds are not satisfied, the image is segmented again by adjusting the parameters.

For quality assessment purposes, the generated reference data corresponding to a sample of objects of various land uses falls into two categories, linear shape and compact shape have been used. The area and the shape index (SI) of each reference object are computed.

5.10 Results and Discussion

5.10.1 Assessment of Segmentation Quality: Study Area - I

Generated quality measures SFI and ΔSI has been applied jointly on the segmented images of very high resolution Quick-bird images to assess the quality of the segmented images.

5.10.1.1 Quality Evaluation of Quick-Bird Pan-Sharpened Image

Both the images of data set-I have been segmented by considering the optimal values of the parameters for regular and irregular compact shape category as well as for linear shape category features. Thus, six segmented images, referred as Seg-PS-I (Pan-sharpened: linear), Seg-PS-II (Pan-sharpened: compact regular), Seg-PS-III (Pan-sharpened: compact irregular) from Pan-sharpened image; Seg-P-I (PAN: linear), Seg-P-II (PAN: compact regular), Seg-P-III (PAN: compact irregular) from Pan image have been used. A total of 18 segments corresponding to different land use and shadow as classes has been sampled from Seg-PS I to Seg-PS III images for quality assessment for Quick-bird Pan-sharpened image. The values of SFI and ΔSI for the sample segments are given in Table 5.12 to 5.15.

It can be seen from Table 5.12 that for Seg-PS-II and Seg-PS-III images, the value of SFI is very high for compact shape objects, whereas it is low for linear objects. Considering SFI threshold of 0.95, it can be seen that almost all the compact shape segments have high SFI value than its threshold whereas linear shape segments have significantly lower values than the threshold. Thus, the SFI has been clearly able to distinguish between the quality of segments belonging to two different groups.

Similar outcome has been observed in case of existing index (Zhang *et al.*, 2010). However, the values of existing index are higher than the proposed index, since the latter takes into account errors of commission and omission. Thus, the proposed index portrays realistic values to assess the quality of segmentation.

Additionally, Table 5.12 shows that compact shaped segments have lower values of ΔSI and these values are near to the threshold value of 0.05, whereas linear shape segments have high ΔSI values, it is because that segment have formed in compact shape while they are linear in reference. Thus, joint analysis of SFI and ΔSI may be quite useful in assessing the quality of a segmented image.

The results of segmentation of Seg-PS-I image are represented in Table 5.13. In this case, the values of SFI for linear shape objects are higher than those obtained for the compact shape objects. Similarly, the values of ΔSI for linear shape objects are lower than those obtained for compact

Table 5.12: Quality assessment of segmented images produced from the optimum values of parameters defined for compact shape features (Quick-bird Pan-sharpened image).

Shapes	A_r (m^2)	A_s (m^2)	A_i (m^2)	$A_t = A_r + A_s - A_i$	$A_m = (A_r + A_s)/2$	Existing Index (A_i/A_m)	Proposed Index $SFI = A_i/A_t$	SI_r	SI_s	ΔSI
Compact	286.14	273.58	270.98	288.74	279.86	0.97	0.94	1.56	1.54	0.02
Compact	621.58	612.31	610.80	623.09	616.95	0.99	0.98	1.86	1.84	0.02
Compact	1438.12	1382.25	1382.25	1438.12	1410.19	0.98	0.96	1.44	1.42	0.02
Compact	982.5	901.1	865.26	1018.34	941.8	0.92	0.85	2.04	2.16	0.12
Linear	347.25	412.50	347.25	412.50	379.88	0.91	0.84	4.48	1.89	2.59
Linear	775.92	926.14	743.20	958.86	851.03	0.87	0.78	3.04	2.4	0.64
Linear	1586.35	1982.16	1502.50	2066.01	1784.26	0.84	0.73	5.24	1.58	3.66
Linear	1124.40	1586.35	1105.81	1604.94	1355.38	0.82	0.69	5.86	1.68	4.18
Compact	608.76	617.33	599.71	626.38	613.04	0.98	0.96	1.69	1.72	0.03
Compact	1850.4	1829.86	1796.33	1883.92	1840.13	0.98	0.95	3.03	3.12	0.09
Compact	667.8	661.10	658.16	670.74	664.45	0.99	0.98	1.56	1.54	0.02
Compact	543.24	530.54	514.65	559.13	536.89	0.96	0.92	1.83	1.75	0.08
Compact	896.32	889.59	889.59	896.32	892.96	1.00	0.99	2.02	2.03	0.01
Compact	427.20	434.80	422.96	439.04	431.00	0.98	0.96	1.88	1.93	0.05
Compact	634.60	619.83	619.83	634.60	627.22	0.99	0.98	1.78	1.77	0.01
Compact	598.22	610.50	596.91	611.81	604.36	0.99	0.98	2.01	1.83	0.18
Compact	548.48	546.32	538.86	555.94	547.40	0.98	0.97	1.88	1.864	0.016
Compact	778.56	765.91	763.40	781.07	772.24	0.99	0.98	2.05	2.04	0.01

Table 5.13: Quality assessment of segmented image produced from the optimum values of parameters defined for linear shape features (Quick-bird Pan-sharpened image).

Shape	A_r (m^2)	A_s (m^2)	A_i (m^2)	$A_t = A_r+A_s-A_i$	$A_m = (A_r+A_s)/2$	Existing Index (A_i/A_m)	Proposed Index $SFI=A_i/A_t$	SI_r	SI_s	ΔSI
Linear	347.25	339.86	336.84	350.27	343.56	0.98	0.96	4.48	4.5	0.02
Linear	775.92	814.11	768.8	821.23	795.02	0.97	0.94	3.04	3.01	0.03
Linear	1586.35	1584.56	1534.2	1636.71	1585.46	0.97	0.94	5.24	5.23	0.01
Linear	1124.4	1104.88	1026.58	1202.7	1114.64	0.92	0.85	5.86	5.84	0.02

shape objects. This shows that judicious selection of parameters based on the shape of the objects definitely has bearing in producing accurate segmentation. The proposed indices (i.e., SFI and ΔSI) are clearly able to reflect this.

The above arguments can also be corroborated from the visual inspection of two segmented images shown in Figure 5.11, which shows the best and the worst segmented images obtained from the Pan-sharpened image. The compact irregular shape object representing grassland has been segmented as a single entity in the best-segmented image with set of parameters for compact shape whereas it has been segmented into number of small sub-segments when using parameters fixed for linear group of features. The values of SFI and ΔSI for the best segmented image are 0.96 and 0.02, respectively, whereas the corresponding values of the worst segmented image are 0.84 and 2.59 respectively. Thus, the visual evaluation also supports the utility of proposed indices for the assessment of quality of segmentation of high spatial resolution remote sensing data.

5.10.1.2 Quality Evaluation of Quick-Bird Pan Image

The quality of the segmented images obtained from Quick-bird Pan data has also been assessed. A total of 18 segments corresponding to different land uses and shadow class have been sampled. Segmented images Seg-P-I, II and III have been used for generating the statistics of quality assessment for Quick-bird Pan image. The values of SFI and ΔSI for the sample segments are given in Table 5.14 and 5.15. By evaluating the value of SFI and ΔSI, it has been found that the segments obtained from Seg-P-II and Seg-P-III images are qualified for compact objects, whereas segments of Seg-P-I follow the linear objects.

The above arguments can also be corroborated from the visual inspection of two segmented images shown in Figure 5.12, which shows the best and the worst segmented images obtained from the Pan image. The object (residential building) has been segmented as a single entity in the best-segmented image whereas it has been segmented into several segments in the worst segmented image. The values of SFI and ΔSI for the best segmented image are 0.98 and 0.03 respectively, whereas the corresponding values of the worst segmented image is 0.31 and 0.64 respectively.

On comparing the segmentation results obtained from Pan-sharpened image with those obtained from Pan image, it has been observed that value of SFI appears more for Pan-sharpened image. The reason for this may be that Pan-sharpened image has four bands and hence have been able to produce more close boundaries than the Pan image due to single wide band data.

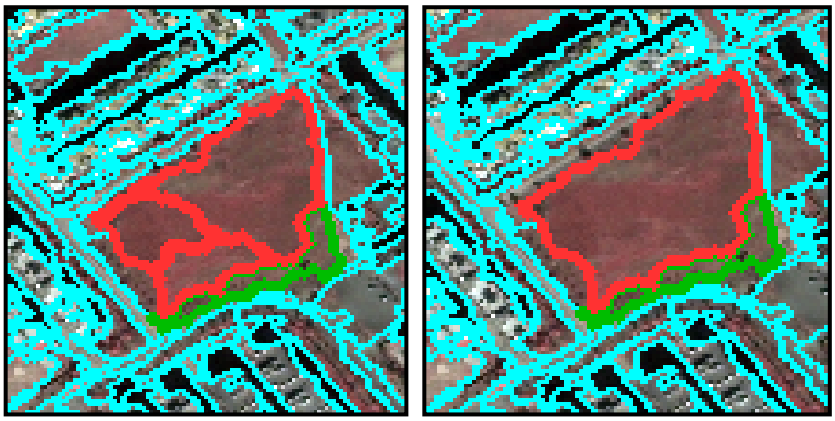

(a) (b)

Figure 5.11: Visual representation of segmentation quality of Pan-sharpened image; green line represents the boundary of an object in the reference map and the red line represents the boundary of the same object in the segmented image (a) the best segmentation at SFI = 0.96 and ΔSI = 0.02 (b) the worst segmentation at SFI = 0.84 and ΔSI = 2.59.

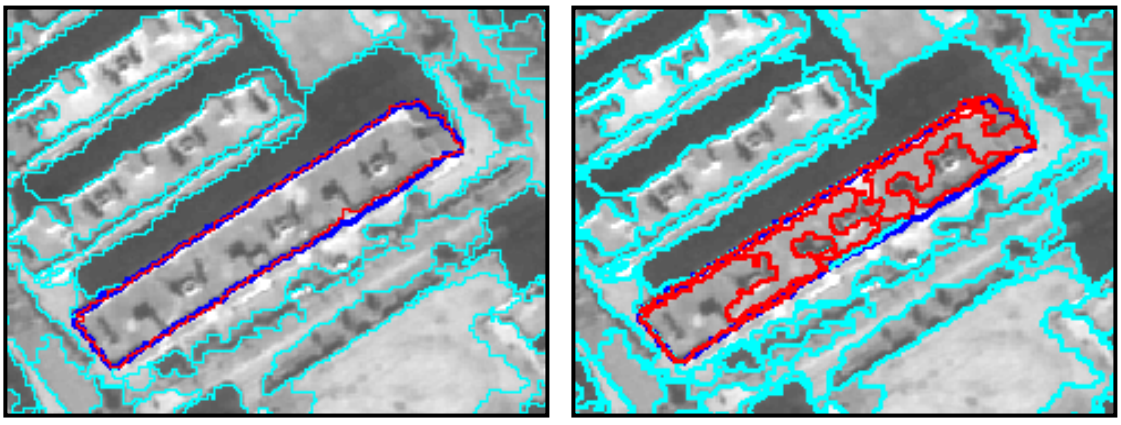

(a) (b)

Figure 5.12: Visual representation of segmentation quality of Pan image; blue line represents the boundary of an object in the reference map and the red line represents the boundary of the same object in the segmented image (a) the best segmentation at SFI = 0.98 and ΔSI = 0.03 (b) the worst segmentation at SFI = 0.31 and ΔSI = 0.64.

Table 5.14: Quality assessment of segmented images produced from the optimum values of parameters defined for compact shape features (Quick-bird Pan image).

Shapes	A_r (m^2)	A_s (m^2)	A_i (m^2)	$A_t = A_r + A_s - A_i$	$A_m = (A_r + A_s)/2$	Existing Index (A_i/A_m)	Proposed Index $SFI = A_i/A_t$	SI_r	SI_s	ΔSI
Compact	286.14	283.58	280.98	288.74	284.86	0.99	0.97	1.56	1.54	0.02
Compact	621.58	630.54	618.6	633.52	626.06	0.99	0.98	1.86	1.89	0.03
Compact	1458.12	1407.5	1358.89	1506.73	1432.81	0.95	0.90	1.44	1.49	0.05
Compact	982.5	970.64	865.26	1087.88	976.57	0.89	0.80	2.04	2.1	0.06
Linear	347.25	406.78	336.25	417.78	377.015	0.89	0.80	4.48	2.19	2.29
Linear	775.92	844.25	717.2	902.97	810.085	0.89	0.79	3.04	1.78	1.26
Linear	1586.35	1902.87	1436.45	2052.77	1744.61	0.82	0.70	5.24	1.61	3.63
Linear	1124.4	1435.85	1075.21	1485.04	1280.125	0.84	0.72	5.86	2.47	3.39
Compact	608.76	621.02	599.71	630.07	614.89	0.98	0.95	1.69	1.72	0.03
Compact	1850.4	1835.12	1799.58	1885.94	1842.76	0.98	0.95	3.03	3.07	0.04
Compact	667.8	658.42	639.35	686.87	663.11	0.96	0.93	1.56	1.51	0.05
Compact	543.24	530.54	514.65	559.13	536.89	0.96	0.92	1.83	1.79	0.04
Compact	896.32	847.29	840.58	903.03	871.805	0.96	0.93	2.02	1.96	0.06
Compact	427.2	424.76	414.61	437.35	425.98	0.97	0.95	1.88	1.93	0.05
Compact	634.6	650.8	619.83	665.57	642.7	0.96	0.93	1.78	1.74	0.04
Compact	598.22	576.25	555.89	618.58	587.235	0.95	0.90	2.01	2.11	0.1
Compact	548.48	546.32	538.86	555.94	547.4	0.98	0.97	1.88	1.82	0.06
Compact	778.56	765.91	763.4	781.07	772.235	0.99	0.98	2.05	2.01	0.04

Table 5.15: Quality assessment of segmented image produced from the optimum values of parameters defined for linear shape features (Quick-bird Pan image).

Shape	A_r (m^2)	A_s (m^2)	A_i (m^2)	A_t= $A_r+A_s-A_i$	A_m= $(A_r+A_s)/2$	Existing Index (A_i/A_m)	Proposed Index $SFI=A_i/A_t$	SI_r	SI_s	ΔSI
Linear	347.25	339.86	336.84	350.27	343.56	0.98	0.96	4.48	4.51	0.03
Linear	775.92	782.14	768.80	789.26	779.03	0.99	0.97	3.04	3.08	0.04
Linear	1586.35	1521.50	1521.50	1586.35	1553.93	0.98	0.96	5.24	5.22	0.02
Linear	1124.40	1095.87	1084.73	1135.54	1110.14	0.98	0.96	5.86	5.84	0.02

5.10.2 Assessment of Segmentation Quality: Study Area - II

In order to further substantiate the usefulness of the proposed index to assess the quality of the segmentation of the image at any spatial resolution, it is tested on medium resolution LISS-IV image. The multispectral image of LISS-IV sensor was segmented as Seg-L II and Seg-L I images using the compact shape parameters and linear shape parameters respectively. The corresponding results for 19 testing segments are given in Table 5.16 and Table 5.17, respectively. The behavior of SFI and ΔSI reported in these tables is almost similar to those analyzed for high resolution Quick-bird images earlier. This clearly shows the applicability of the proposed indices for images acquired at different spatial resolutions.

A comparison of SFI values obtained for segmented Quick-bird images and segmented LISS-IV image shows that these values are higher for the former. Similarly, the values of ΔSI are lower for segmented Quick-bird images and higher for the segmented LISS-IV image. This is logical since the geometry of the objects in high spatial resolution images is expected to be well defined than that in medium resolution images. Thus, the proposed indices are able to highlight this proposition also. The value of the threshold for LISS-IV image has been selected to 0.9 for SFI and 0.1 for ΔSI.

For medium resolution image also, the segmentation results of an object with two different sets of segmentation parameters have been evaluated visually. It can be seen from Figure 5.13 (a) representing the best quality segmentation and Figure 5.13 (b) representing the worst quality segmentation. The object (grassland) has been segmented as a single entity in the best-segmented image whereas it has been segmented into several segments in the worst segmented image. The values of SFI and ΔSI for the best segmented image are 0.97 and 0.04 respectively, whereas the corresponding values of the worst segmented image are 0.47 and 0.69 respectively. Thus, the visual evaluation also supports the utility of proposed indices for the assessment of quality of segmentation of remote sensing image acquired at any spatial resolution.

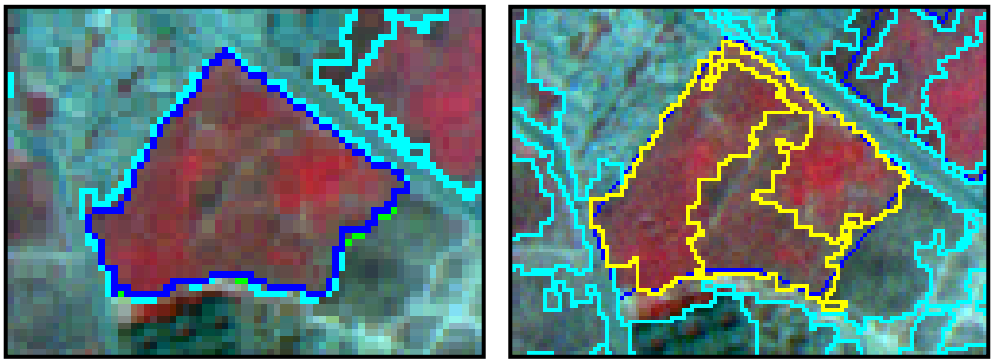

(a) (b)

Figure 5.13: Visual representation of segmentation quality of LISS-IV image; blue line represents the boundary of an object in the reference map and the yellow line represents the boundary of the same object in the segmented image (a) the best segmentation at SFI = 0.97 and ΔSI = 0.04 (b) the worst segmentation at SFI = 0.47 and ΔSI = 0.69.

Table 5.16: Quality assessment of segmented image produced from the optimum values of parameters defined for compact shape features (Resourcesat LISS-IV image).

Shapes	A_r (m^2)	A_s (m^2)	A_i (m^2)	$A_t = A_r + A_s - A_i$	$A_m = (A_r + A_s)/2$	Existing Index (A_i/A_m)	Proposed Index $SFI = A_i/A_t$	SI_r	SI_s	ΔSI
Compact	31677.48	31216.08	30379.79	32513.77	31446.78	0.97	0.93	1.59	1.68	0.09
Compact	28978.29	31967.2	28892.64	32052.85	30472.745	0.95	0.90	1.6	1.57	0.03
Compact	75520.06	77573.84	72454.33	80639.57	76546.95	0.95	0.90	1.71	1.67	0.04
Compact	77447.68	78995.92	74730.99	81712.61	78221.8	0.96	0.91	2.43	2.38	0.05
Compact	56101.91	60252.4	50341.2	66013.11	58177.155	0.87	0.76	1.53	1.39	0.14
Compact	78174.8	82194.88	76874.75	83494.93	80184.84	0.96	0.92	1.86	1.95	0.09
Compact	78617.43	82396.72	77450.05	83564.1	80507.075	0.96	0.93	2.21	2.11	0.1
Compact	259068.9	233583.2	228461.7	264190.4	246326.05	0.93	0.86	2.21	2.01	0.2
Compact	62748.8	63943.6	60935.85	65756.55	63346.2	0.96	0.93	2.6	2.63	0.03
Compact	66319.06	176946.4	65287.77	177977.69	121632.73	0.54	0.37	3.42	3.35	0.07
Compact	136373.5	134119.5	132702.2	137790.8	135246.5	0.98	0.96	1.83	1.75	0.08
Linear	37774.62	150000.8	30944.97	156830.45	93887.71	0.33	0.20	4.44	2.17	2.27
Linear	49500.15	125073.5	44106.45	130467.2	87286.825	0.51	0.34	4.22	2.05	2.17
Linear	18486.71	36970.86	18485.4	36972.17	27728.785	0.67	0.50	4.58	1.62	2.96
Linear	117606.9	236623.8	115438.1	238792.6	177115.35	0.65	0.48	5.37	1.97	3.4
Linear	43428.77	82249.8	192.01	125486.56	62839.285	0.00	0.00	4.35	2.32	2.03
Linear	227468.7	244226.4	205345.5	266349.6	235847.55	0.87	0.77	4.25	1.31	2.94
Compact	9394.58	9654.68	9258.22	9791.04	9524.63	0.97	0.95	1.6	1.58	0.02
Compact	47508.65	46986.43	46608.24	47886.84	47247.54	0.99	0.97	1.92	1.96	0.04

Table 5.17: Quality assessment of segmented image produced from the optimum values of parameters defined for linear shape features (Resourcesat LISS-IV image).

Shapes	A_r (m^2)	A_s (m^2)	A_i (m^2)	$A_t = A_r + A_s - A_i$	$A_m = (A_r + A_s)/2$	Existing Index (A_i/A_m)	Proposed Index $SFI = A_i/A_t$	SI_r	SI_s	ΔSI
Linear	37774.62	36986.21	36523.47	38237.36	37380.415	0.98	0.96	4.44	4.52	0.08
Linear	49500.15	50752.85	49004.54	51248.46	50126.5	0.98	0.96	4.22	4.25	0.03
Linear	18486.71	17895.06	17654.89	18726.88	18190.885	0.97	0.94	4.58	4.49	0.09
Linear	117606.9	109857.5	109857.5	117606.9	113732.2	0.97	0.93	5.37	5.28	0.09
Linear	43428.77	65325.95	33857.29	74897.43	54377.36	0.62	0.45	4.35	3.54	0.81
Linear	227468.7	227801.24	227354.54	227915.4	227634.97	1.00	1.00	4.25	4.24	0.01

5.11 Summary

In this chapter, different types of image segmentation algorithms, the segmentation techniques used by various investigators and technique available in the software were discussed. Region growing image segmentation techniques are frequently used in the OBIA based applications. The selection of most appropriate parameters for segmenting an image is a crucial task. In this chapter, the fitness functions for fixing the values of the scale, shape and smoothness parameters were proposed. The proposed method allows the users to compute the value of these parameters to segment a remote sensing image for an object of interest. The values computed via fitness functions were found to be efficient in improving the quality of segmentation for all types of features; linear, compact-regular and compact-irregular features on three data sets; the Pan-sharpened Quick-bird image, Quick-bird Pan image and the LISS-IV MS image at different spatial and spectral resolutions.

A set of quality assessment techniques for segmentation were also discussed. Quality evaluation indexes, SFI, that includes the errors of commission and omission and ΔSI which include discrepancy in objects shape, were proposed. The efficacy of these quality indices was examined on the three datasets. The results obtained from the proposed index were also compared with that of existing competitive quality index.

The results clearly indicated that the two indices in combination produced more realistic values of segmentation quality and showed robustness in assessing the quality of segmentation for all kinds of features.

The best quality segmented images have now been considered for further processing to accomplish the other objectives; attribute selection and image classification, which form the basis of subsequent chapters.

Chapter 6:

OBJECT BASED IMAGE CLASSIFICATION

6.1 Introduction

The segmented images after having assessed for its quality evaluation are now further processed. Each segment of a segmented image is accompanied with a number of attributes representing characteristics of classes within that segment. The selection of appropriate attributes therefore becomes crucial for subsequent image classification and individual object extraction.

The C4.5 algorithm of decision tree has been used for attribute selection as well as object based image classification. As the attributes may be both parametric and non-parametric, decision tree approach has been preferred, since it is essentially a non-parametric approach that does not depend on statistical data distribution assumptions. The classification has been performed in two ways; using the unpruned tree and by using pruned decision tree. The error matrix based measures have been used for classification accuracy assessment.

6.2 Description of Attributes

In the segmentation process, the segments are formed by merging the surrounding homogeneous pixels. Each segment in the segmentation stage has a number of attributes. These attributes are typically grouped as spectral, shape, contextual and textural categories. The data pertaining to these attributes form the basis for image classification and object extraction.

6.2.1 Spectral Characteristics

The spectral response of Panchromatic, multi spectral and hyperspectral images in a wavelength region facilitates fine discrimination between different objects or classes. A number of parameters such as mean, standard deviation, brightness etc., computed from the spectral response represented as DN values or reflectance are computed to form the spectral attribute set, as defined in Table 6.1 (Baatz and Schape, 2000)

Table 6.1: Description of the spectral attributes

Attribute	Description	Range
i). Mean	Average DN value of all pixels forming an image object in a band.	0 to (2^{bit} -1)
ii). Brightness	Sum of the mean values of the bands divided by the number of bands used to compute an image object.	0 to (2^{bit} -1)
iii). Max Difference	Difference between the minimum mean value belonging to an object and its maximum value.	0 to (2^{bit} -1)
iv). Std Deviation	Standard deviation is the square root of its variance. In OBIA, it is calculated from the band values of all n pixels forming an image object.	0 to (2^{bit} -1)
v). Ratio	It is a band wise ratio of the mean value of an image object of a band divided by the sum of all spectral bands mean values.	0 to1
vi). NDVI	Normalized difference vegetation index is the ratio of the difference in the near-infrared and red reflectance, over the sum of those and varies from -1 to +1. In practice, extreme negative values represent water and high positive values represent the vegetation while its value is around zero for bare soil.	-1 to +1

6.2.2 Shape Characteristics

Shape refers to the general form, configuration, or outline of an individual object. The shape of some objects is so distinctive that their images may be identified exclusively from this criterion. The use of shape becomes a key when objects in an image are spectrally similar but spatially different on the ground (Van der Werff and Van der Meer, 2008). The main advantage of using shape characteristic is the spatial information which is not interpreted by an end-user from

separate pixels but measured automatically. The set of shape attributes along with their definitions are given in Table 6.2.

Table 6.2: Description of the shape attributes.

Attributes	Description	Attribute value range
i). Area	In raw image, the area of an image object is the number of pixels forming it. In case of georeferenced image, the area of an image object is the true area covered by one-pixel times the numbers of pixels forming the image object.	0-to-scene size
ii). Length-width ratio	There are two ways to compute the length/width ratio of an image object. (a) The ratio length/width is identical to the ratio of the eigenvalues of the covariance matrix with the largest eigenvalue being the numerator of the fraction. (b) The ratio length/width can also be approximated using the bounding box. The bounding box is a rectangle box of the size (X_{min} to X_{max}) to (Y_{min} to Y_{max}) of the image object.	0-to-1
iii). Border length	The border length of an image object is defined as the sum of the edges of the image object that are shared with other image objects or are situated on the edge of the entire scene. In raw image, the length of a pixel edge is 1.	4 to depending on shape of the image object
iv). Shape index	Mathematically, the shape index is the border length of the image object divided by four times the square root of its area. The shape index is used to describe the smoothness of the image object borders. The more fractal an image object appears, the higher its shape index.	1 to depending on shape of the image object
v). Density	The density can be expressed by the area covered by the image object divided by its radius (the intra circle has been drawn by considering the object as a square). The density is used to describe the compactness of an image object. The ideal compact form on a pixel raster is the square.	0 to depending on shape of the image object
vi). Compactness	It is a product of the length and the width of the corresponding object and divided by the number of its inner pixels.	0 to ∞

vii). Elliptic Fit	Elliptic fit is the creation of an ellipse with the same area as the considered object. In the calculation of the ellipse, the area of the object outside the ellipse is compared with the area inside the ellipse that is not filled out with the object. While 0 means no fit, 1 stands for a complete fitting object.	0 to 1
viii). Rectangular fit	A rectangle with the same area as the object is used. In the calculation of the rectangle, the proportion of the length to the width of the object is considered. The area of the object outside the rectangle is compared with the area inside the rectangle, which is not filled out with the object. While 0 means no fit, 1 stands for a complete fitting object.	0 to 1
ix). Asymmetry	The lengthier an image object, the more asymmetric it is. For an image object, an ellipse is approximated which can be expressed by the ratio of the lengths of minor and major axes of this ellipse. The attribute value increases with the asymmetry.	0 to 1

6.2.3 Contextual Characteristics

Contextual characteristic describes the geometric relationships between the objects or the whole scene, such as being left, right, or in a certain distance to a certain object, or being in a certain area within the image (Baatz and Schape, 2000). In consequence, the resulting contextual network has a big advantage as it permit the efficient propagation of many different kinds of relational information. The Contextual relation of single, adjacent pixels is given implicitly by the raster structure. The set of contextual attributes along with their definitions are given in Table 6.3.

Table 6.3: Description of the contextual attributes

Attribute	Description	Range
i). Mean difference to neighbors	For each neighboring object, the layer mean difference is computed. The range of the mean difference is twice the bit depth of the data.	-2^{bit} to 2^{bit}
ii). Mean	It is similar to "Mean difference to neighbors," but only	0 to 2^{bit}

difference to neighbors (abs)	absolute values of the differences are averaged.	
iii). Mean difference to brighter neighbors	This attribute is computed in the same way as "Mean difference to neighbors," but only image objects with a layer mean value larger than the layer mean value of the desired object are regarded.	0 to 2^{bit}
iv). Mean difference to darker neighbors	This attribute is also computed in the same way as "Mean difference to neighbors," but only image objects with a layer mean value less than the layer mean value of the desired object are regarded.	0 to 2^{bit}
v). Relative border to brighter neighbors	It is the ratio of shared border with image objects of a higher mean value in the selected layer and the total border of the concerned image object.	0 to 1

6.2.4 Textural Characteristics

Texture is the frequency of tonal change in an image. Texture is produced by an aggregation of unit extent that may be too small. It determines the overall visual smoothness or coarseness, rippled, molled, irregularity of image features (Haralick et al., 1973, Avery and Berlin, 1992). Texture plays an important role in an image segmentation and object recognition, as well as in the interpretation of images in a variety of applications. Texture depends on the scale of the image segmentation. As the scale is reduced, the texture of any given object or area becomes progressively finer and ultimately disappears. In the literature, wavelet transforms (Zhu and Yang, 1998) and gray tone spatial co-occurrence matrix (Haralick, et al., 1973) has been used to analyze texture. In this study, gray level co-occurrence matrix (GLCM) and gray level difference vector (GLDV) of the spatial co-occurrence matrix have been used to compute texture. In the following section, GLCM and GLDV have been discussed.

6.2.4.1 Gray Level Co-occurrence Matrix (GLCM)

GLCM is one of the most widely used methods to compute texture. It contains relative frequencies of the two neighboring pixels in an image. Various statistical measures can be computed from the (GLCM) matrix.

The GLCM is a matrix showing how often different combinations of gray level values occur in an image (Hall-Beyer, 2000). It considers the relation between two pixels at a time, called the reference and the neighbor pixel. Say, for a 2-bit image, given in Figure 6.1, the neighboring pixel is chosen to be the one to the right of each reference pixel.

0	0	1	1
0	1	1	1
0	1	2	2
2	2	3	3

Figure 6.1 Example data

Consider a 3 x 3 pixels moving window over the image. Each pixel within the window becomes the reference pixel in turn, starting with the upper left corner and proceeding to the lower right. Pixels along the right edge have no right hand neighbor, so they are not used for this count. The cells of a co-occurrence matrix (of a size corresponding to its number of gray levels) are filled with the number of times a particular combination of neighbor and reference pixel occurs within the window. Hence, the corresponding co-occurrence matrix is obtained as given in Figure 6.2.

	Neighbor pixel			
Reference pixel	0	1	2	3
0	1	3	0	0
1	0	3	1	0
2	0	0	2	1
3	0	0	0	1

Figure 6.2 Gray-level co-occurrence matrix

The GLCM takes into consideration neighbor to the right of the reference matrix thus the count of occurrences of two consecutive pixels, say (*I, j*), is not similar to the occurrence of (*j,i*). This implies that the matrix should be symmetrical. Therefore, to compute texture from GLCM, the symmetrical transpose of the co-occurrence matrix is required. Thus, the transpose the GLCM is computed and added to the original GLCM to make it symmetrical along the diagonal.

2	2	1	0
0	2	0	0
0	0	3	1
0	0	0	1

+

2	0	0	0
2	2	0	0
1	0	3	0
0	0	1	1

=

4	2	1	0
2	4	0	0
1	0	6	1
0	0	1	2

a) GLC Matrix b) Transpose GLCM c) Symmetrical Matrix

Fig. 6.3 Generation of a symmetrical matrix

The values of the matrix are then converted into probabilities by the process of normalization given as,

$$P_{i,j} = \frac{V_{i,j}}{\sum_{i,j=0}^{N-1} V_{i,j}} \tag{6.1}$$

where, $P_{(i,j)}$ is the probability and $V_{(i,j)}$ refers to the cell values of the GLCM, i.e. count.

The normalized GLCM for the example taken is given in Figure 6.4.

0.166	0.083	0.042	0
0.083	0.166	0	0
0.042	0	0.25	0.042
0	0	0.042	0.083

Figure 6.4 Normalized GLCM

In this study, eight GLCM measures namely homogeneity, contrast, dissimilarity, entropy, mean, angular second momentum, standard deviation and correlation have been used as texture attributes because they render distinct information (Haralick et al., 1973). From the normalized GLCM, different texture may be defined as

i). The **GLCM homogeneity** of an image provides the information regarding the homogeneity between the diagonal neighboring pixels and varies from 0 to 1. Homogeneity is 1 for a diagonal GLCM.

$$GLCM\_HOMO = \sum_{i,j=0}^{N-1} \frac{p_{i,j}}{1 - (i - j)^2} \tag{6.2}$$

ii). The **GLCM contrast** returns a measure of the intensity contrast between a pixel and its neighbor over the whole image. The minimum value of contrast is 0 for a constant image. A low contrast image presents a GLCM concentration term around principal diagonal and, consequently a low value of GLCM contrast.

$$GLCM\_CON = \sum_{i,j=0}^{N-1} P_{i,j} (i - j)^2 \tag{6.3}$$

iii). The **GLCM dissimilarity** is similar to the contrast. It is high when the local region has a high contrast.

$$GLCM\_DISM = \sum_{i,j=0}^{N-1} P_{i,j} |i - j| \tag{6.4}$$

iv). The **GLCM entropy** measures the disorder of an image. When the image is not texturally uniform, many GLCM elements have very small values, which imply that entropy is very large.

$$GLCM\_ENT = \sum_{i,j=0}^{N-1} P_{i,j} (-\ln P_{ij}) \tag{6.5}$$

v). The **GLCM mean** represents the average gray level in the local window.

$$GLCM\_MEAN = \frac{1}{m}\sum_{i,j=0}^{N-1} i, j \left(P_{ij} \right) \quad (6.6)$$

vi). The **GLCM angular second momentum**, also called as energy, checks the pixel pair's repetitions. It returns the sum of the squared elements in the GLCM and falls between 0 and 1. A constant image has a value of ASM is 1.

$$GLCM\_ASM = \sum_{i,j}^{N-1} \left(P_{i,j} \right)^2 \quad (6.7)$$

vii). The **GLCM standard deviation** is high when there is a large gray level standard deviation in the local region.

$$GLCM\_SD = \sigma_{ij}^2 - \sum_{i,j=0}^{N-1} P_{i,j} \left(j - \mu_{ij} \right) \quad (6.8)$$

viii). The **GLCM correlation** returns a measure of how correlated a pixel is to its neighbor over the whole image. The value of correlation is 1 for a perfect positively correlated image and for perfectly negatively correlated image its value is -1.

$$GLCM\_CORR = \sum_{i,j=0}^{N-1} P_{ij} \left[\frac{\left(i - \mu_{ij} \right)\left(j - \mu_j \right)}{\sqrt{\left(\sigma_i^2 \right)\left(\sigma_j^2 \right)}} \right] \quad (6.9)$$

6.2.4.2 Gray Level Difference Vector (GLDV)

The GLDV is the sum of the diagonal elements of the GLCM matrix. The GLDV method estimates the probability density function for differences taken between the image function values. Some GLDV attributes are:

i). The **GLDV angular second momentum** is similar to GLCM_ASM, it measure the local homogeneity.

$$GLDV\_ASM = \sum_{i,j=0}^{N-1} V_k^2 \tag{6.10}$$

ii). The **GLDV entropy** is opposite to the GLDV angular second momentum.

$$GLDV\_ENT = \sum_{i,j=0}^{N-1} V_k \left(\ln V_k \right) \tag{6.11}$$

There are a number of attributes that come under the above four categories. These attributes represent different characteristics of the land use land cover classes on ground. The property of the segments in the segmented image is described by these attributes. However, some of the attributes appear similar for more than one segment type, thus those attributes may become redundant and their introduction may produce noise in the dataset. Additionally, some other attributes that describe the segment property, such as information regarding the number of neighbors, location of the segment, number of segmentation levels, etc. may also be meaningless for image classification and object extraction. Therefore, before applying any technique for attribute selection, it is required to ignore these ineffectual attributes. The list of the attributes, which may be used for further processing of image classification, is listed in Table 6.4.

However, the number of attributes may still be pruned via some quantitative approaches such as Separability and threshold (SEaTH) (Nussbaum *et al.* 2006), Ginni index (Yu *et al.*, 2006), Pearson correlation coefficient (Zhang *et al.*, 2010). The decision tree approach has been used here for attribute selection.

From the literature reviewed it has been found that Yu *et al.,* (2006) applied Gini impurity index of classification and regression tree (CART) for attribute ranking and image classification.

In the proposed research, gain-ratio instead of the Gini index splitting rule has been used for the ranking of the input attributes of the segments. The gain-ratio is the normalized version of information gain that provides global variation in gain and appears to be more practical. C4.5 decision tree has been used for the classification and also for the extraction of the objects.

Table 6.4: List of useful attributes generated in the image segmentation process.

Sl. No.	Attributes of segment	Sl. No.	Attributes of segment
1	Mean (All bands)	20	GLDV Entropy (All bands)
2	Std Dev (All bands)	21	Length
3	Ratio (All bands)	22	Width
4	Std Dev. to neighbor pixels (All bands)	23	Area
5	Mean diff. to neighbors (All bands)	24	Length/width
6	Mean diff. to neighbors (abs) (All bands)	25	Compactness
7	Mean diff. to darker neighbors (All bands)	26	Elliptic Fit
8	Mean diff. to brighter neighbors (All bands)	27	Rectangular Fit
9	Relative border to brighter neighbors (All	28	Border length
10	Min and max pixel value (All bands)	29	Shape index
11	GLCM Homogeneity (All bands)	30	Density
12	GLCM Contrast (All bands)	31	Asymmetry
13	GLCM Dissimilarity (All bands)	32	Area (excluding inner polygons)
14	GLCM Entropy (All bands)	33	Perimeter (polygon)
15	GLCM Ang. 2nd moment (All bands)	34	Compactness (Polygon)
16	GLCM Mean (All bands)	35	Length/width (line so)
17	GLCM Std Dev (All bands)	36	Indices
18	GLCM Correlation (All bands)		
19	GLDV Ang. 2nd moment (All bands)		

6.3 Decision Tree Approach

The basic concept of a decision tree is to split a complex decision into several simple decisions, which may lead to a solution that resembles the reality (Pal and Mather, 2003). A Decision Tree is defined as a classification method that recursively partitions a data set into smaller subdivisions on the basis of a set of test defined at each branch (Friedl and Brodley, 1997). The tree is composed of a root node (consisting of the entire data), a set of internal nodes (splitting criteria) and a set of terminal nodes (leaves). Each node in the decision tree has only one parent node and two or more descendant nodes.

In this framework, a data set is classified by sequentially subdividing it according to the decision framework defined by the tree. Specifically, the decision tree is strictly nonparametric and do not require a prior assumption as regards to the distribution of input data. In addition, they can handle nonlinear relations between attribute and classes, and are capable of handling numeric as well as categorical data. Generally, the splits defined at each internal node of a decision tree and these splits are estimated from training data based on the learning algorithms. In the generation of decision tree, attributes that have maximum information are automatically selected. Further, one has the flexibility of selecting a subset of attributes at different internal nodes of the tree such that the subset discriminates the classes in an optimal way (Quinlan, 1986).

In a decision tree, it is assumed that the input attributes and the desired classes for a sample of segments (i.e., training data) are given. The problem is then to construct a decision tree that optimizes a cost function (e.g., the average number of nodes in a tree) such that the training data is partitioned. There are several ways in which optimization can be performed.

To construct a decision tree from a set T of training data having m classes denoted by $\{C_1, C_2, ..., C_m\}$, there are three possibilities (Han and Kamber, 2006),

i). If T contains one or more objects, all belonging to a single class C_i, and then the decision is a leaf identifying class C_i.

ii). If T contains no data, the decision tree is again a leaf determined from information other than T.

iii). If *T* contains data that belongs to a mixture of classes then a test is chosen, based on a single attribute or a combination of attributes, that has one or more mutually exclusive outcomes $\{O_1, O_2, ..., O_k\}$. *T* is partitioned into subsets $T_1, T_2, ..., T_k$ where T_k contains all the data in *T* that have outcome O_k of the chosen attribute selection measure. The decision tree for *T* consists of a decision node identifying the test, and one branch for each possible outcome. The same tree building process is applied recursively to each subset of training data.

It is obvious that if rules on the node are not enough to complete after tracing through the decision tree, some segments will remain unclassified. Therefore, the efficiency and performance of this approach is strongly affected by tree structure and choice selected for training. The main part of the whole process is the attribute selection measures, which are utilized for the splitting of tree nodes. An example decision tree is given in Figure 6.5.

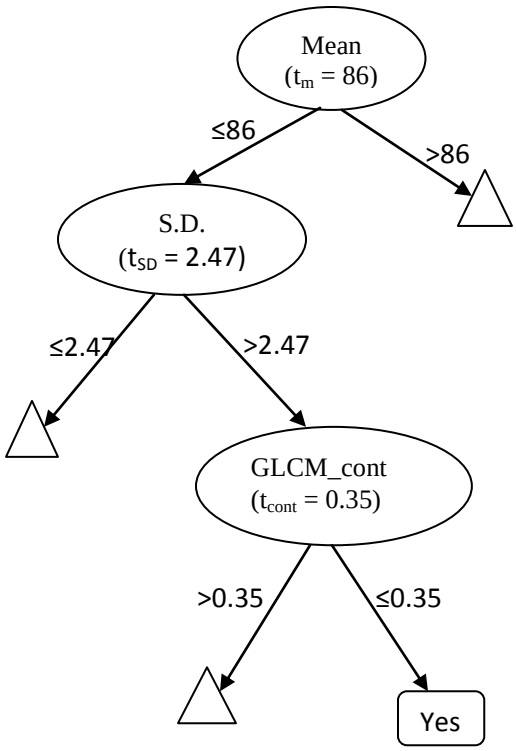

Figure 6.5: Example of top down decision tree approach

6.3.1 Attribute Selection Measures

As decision trees are iteratively built by recursively partitioning the data into leaf nodes, the primary issue encountered is the selection of the suitable index which arranges the attributes in their importance to extract a class at the leaf node. The frequently used indices in decision tree induction are *information gain* (Quinlan, 1979, 1993), *gain ratio* and the *Gini impurity index* (Breiman *et al*., 1984).

6.3.1.1 Information Gain

Quinlan (1979, 1993) proposed a measure called information gain for tree induction based on Shannon's entropy measure expressed as ($-\log_2 \times$ probability) bits, which is used in information theory (Shannon, 1948). The probability of a set of training data for a particular class is the relative frequency of the observations in class (e.g., if training data of class *j* contain 8 segments and the total number of training segments is 32, then the probability of class *j* is 0.25). The concept of information theory is used to evaluate all possible tests for the subdivision of the tree and the test that produces the largest information gain is selected.

During the tree induction process, for a node *t*, the information gain for each attribute is calculated based on the split at node *t* on that attribute. The attribute with the largest information gain is chosen for splitting at that node. In order to compute information gain, the entropy I_E for node *t* must first be calculated, which is expressed by

$$I_E(t) = -\sum_{j=1}^{m} f(t, j) \log_2 f(t, j) \qquad (6.12)$$

where $f(t, j)$ is the proportion of training samples belonging to class *j* and *j* varies1, 2, …, *m*, within node *t*. Here, *m* is the number of classes i.e., if node *t* contains samples, then $f(t, j)$ is calculated by the following expression:

$$f(t,j) = \frac{1}{N_t}\sum_{i=1}^{N_t} \Gamma(y_i,j) \tag{6.13}$$

$$\text{where} \quad \Gamma(y_i,j) = \begin{cases} 1, & \text{if } y_i = j \\ 0, & \text{Otherwise} \end{cases} \tag{6.14}$$

Finally, the information gain associated with a split on attribute *X* is calculated by the following equation:

$$Gain(t,X) = I_E(t) - \sum_{r=1}^{c}\left(\frac{n_r}{N_t}\right) I_E\left(t_{X(x_r)}\right) \tag{6.15}$$

6.3.1.2 Gain Ratio

The gain ratio "normalizes" the information gain as follows (Quinlan, 1993):

$$Gain\_Ratio(t,X) = \frac{Gain(t,X)}{Split\_I(t,X)} \tag{6.16}$$

where, *Split_I(t, X)* is obtained from the Eqn (6.17), in which is the cutting value, $f(t,$ is the proportion of portioned attribute values of training samples with its cutting value used for extracting a class at node *t.*

$$Split\_I(t,X) = -\sum_{i=1} f(t,x_i)\log_2 f(t,x_i) \tag{6.17}$$

The split is obtained in two stages. The information gain is calculated for all attributes. Consequently, taking into consideration only attributes that have performed at least as good as the

average information gain, the attribute that obtains the best ratio gain is selected. This ratio is not defined when the denominator is zero. The ratio may tend to favor attributes for which the split value is very small. Consequently, it has been found that the gain ratio tends to outperform information gain criteria, both from the accuracy aspect, as well as from classifier complexity aspects (Quinlan, 1986).

6.3.1.3 Gini Index

The Gini impurity index (named after Italian economist Corrado Gini, and originally used for measuring income inequality) measures the impurity of an input feature with respect to the classes (Breiman et al., 1984). When all attributes in the node fall into a single information class, the Gini impurity index becomes zero. The Gini index associated with attribute set X (= {x_1, x_2, …, x_r}) for node t is denoted by $I_G(t_{X($ and is expressed as

$$I_G\left(t_{X(x_i)}\right) = 1 - \sum_{j=1}^{m} f\left(t_{X(x_i)}, j\right)^2 \tag{6.18}$$

where $f(t_{X(x_i}$ is the proportion of samples with the value x_i belonging to class j at node t as defined in Equation (6.12). The decision tree splitting criterion is based on choosing the attribute with the lowest Gini impurity index of the split (Tso and Mather, 2009). Let a node t be split into r children, n_i be the number of records at child i, and N_t be the total number of samples at node t. The Gini impurity index of the split at node t for attribute X is then computed as

$$Gini(t, X) = \left(\frac{n_1}{N_t}\right) I_G\left(t_{X(x_1)}\right) + \left(\frac{n_2}{N_t}\right) I_G\left(t_{X(x_2)}\right) + ... \left(\frac{n_r}{N_t}\right) I_G\left(t_{X(x_r)}\right) \tag{6.19}$$

6.3.2 The C4.5-Decision Tree Algorithm

Quinlan (1986) noted that the building of a decision tree requires a "divide and conquer" strategy that uses a recursive testing procedure with the aim of generating a small tree. C4.5 uses either information gain or a normalized version of gain called the gain ratio to choose attributes as candidates for splitting. From Equation (6.15), it may be seen that the information gain measure tends to favor attributes that have multiple values. For instance, in an extreme case, if attribute X holds a different value for each class, Equation (6.12) will always be 0, which in turn results in maximal gain in Equation (6.15), and thus this attribute becomes the first candidate for splitting (Tso and Mather, 2009). The implementation steps of C4.5 algorithm are given in the following section.

i. Arrange the attribute values in increasing or decreasing order.
ii. Each value of an attribute is set as cutting value (x_i).
iii. Partition the data, such that one partition includes attributes with values $\geq x_i$, and the other partition with attribute values $< x_i$.
iv. Compute the gain ratio for each partition.
v. Repeat steps i to iv for all values of an attribute taking one at a time.
vi. Select that cutting value as a threshold that produced partitions with highest gain ratio.
vii. Repeat the step i to vi for remaining attributes and assign the rank.

Algorithm:

Notations: 1. A: a set of attribute types used as predictors, originally, $A=\{A_1,A_2,....,A_n\}$, where $A_1,A_2,....,A_n$ are the segment property of in a remote sensing image.
2. t: the tree node with corresponding attributes.

C4.5 (A, t)

Begin

1. If t consists of samples of the same class, label the node with that class then exit the program;
2. If A is empty, label the node t as the most frequent of the class contained at the node t then exit the program;
3. Compute the gain ratio for each attribute type and let Ak be the attribute with

largest gain ratio among *A*;
4. Let *{Ak(i)| i*=1, 2, …, r*}*, be the values of attribute *Ak*;
5. Let *{tk(i)| i*=1, 2, …, r*}*, be the child nodes of *t* consisting respectively of attribute according to *Ak(i)*;
6. Label node *t* as *Ak* and branches labeled *Ak(1), Ak(2), …., Ak(r)*;
7. For *i*=1 to *r*
   C4.5(*A-{Ak}, tk(i)*);
   End.

End.

6.3.3 Pruning of Decision Tree

Decision tree classifiers divide the training data into subsets, which contain only a single class. The result of this procedure is often a very large and complex tree. In most cases, fitting a decision tree until all leaves contain data for a single class might overfit to the noise in the training data, as the training samples may not be representative of the population they intend to represent. If the training data contain errors, then overfitting of the tree to the data in this manner may lead to poor performance on unseen cases. To reduce this problem, the original tree can be pruned to reduce classification errors when data outside of the training set are to be classified.

The steps to remove the least reliable branches are called as pruning. There are two common approaches of tree pruning: pre-pruning and post-pruning (Han and Kamber, 2006). In the pre-pruning approach, a tree is "pruned" at the time of construction (e.g., by deciding not to further split at a given node) and the node becomes a leaf. The leaf may hold the most frequent class among the subset. The second and more common approach is post-pruning, which removes sub-trees from a "fully grown" tree. A sub-tree at a given node is pruned by removing its branches and replacing it with a leaf. The leaf is labelled with the most frequent class among the sub-tree being replaced.

To produce the shortest tree, C4.5 algorithm removes unnecessary nodes through the pessimistic pruning that is a post-pruning procedure (Witten and frank, 1999; Pinho *et. al*., 2008). In addition, the number of occurrences in each leaf also controls the size of the tree. The lower is the number of occurrences the higher is the classification precision for the training set. However,

the algorithm can produce a complex tree with more inaccurate results for another set of samples. An alternative is to test various threshold values and to observe when the tree stabilizes.

6.3.3.1 Pessimistic Error Pruning (PEP)

The pessimistic error pruning (PEP) estimates the error directly from the training segment (Tso and Mather, 2009). The error for leaf node *t* denoted as $Error_{PEP}\ (t)$ is estimated as

$$Error_{pEP}(t) = \frac{N(t) - n_j(t) + 0.5}{N(t)} \tag{6.20}$$

where $N(t)$ is the number of segments within leaf node *t*, and $n_j(t)$ is the number of segments belonging to the most likely class *j* within node *t*. The error at sub-tree *s* can be computed the sums of the errors at each leaf node within the sub - tree as

$$Error_{pEP}(s) = \frac{\sum N(i) - n_j(i) + 0.5}{\sum N(i)} \tag{6.21}$$

The PEP compares the errors occurred at node *t* and sub-tree *s*. If $Error_{pEP}(t) \leq Error_{pEP}$, then pruning is performed.

6.3.4 Decision Tree for Object Based Image Classification

Decision tree classification algorithms can be defined according to whether a uniform or a heterogeneous set of algorithms is used to estimate the splits at internal nodes. Such algorithms are described as having a homogenous or heterogeneous hypothesis space, respectively. Traditional approaches for the design of decision trees are based on homogenous classification models for which a single algorithm is used to estimate each split. There are two types of decision trees based on homogenous hypothesis space: univariate decision trees and multivariate decision

trees. The C4.5 technique can mount both the univariate and multivariate decision trees. (Tso and Mather, 2009)

Object based image classification algorithm does not classify single pixels, but rather image object primitives called as segments, formed in image segmentation step. Every class has its own unique characteristic that is represented by the attributes of the segment. In classification process, the segments are assigned to a class based on their attributes value. The gain ratio (GR) of all attributes for providing a segment to a class is calculated. A tree with a root node, the number of intermediate nodes and leaf nodes equal to the classes is generated. An attribute having highest GR is set as root node while others except the lowest GR attribute are used as intermediate nodes. In the image classification process, all segments are passing through the root node of the tree and appear to their corresponding leaf nodes of the tree through different intermediate nodes.

6.4 Methodology for Object Based Image Classification

6.4.1 Attribute Ranking and Training of Decision Tree

The proposed methodology for attribute ranking is shown in Figure 6.6. The data file is divided into three groups, training file, reference file and the testing file. Training file and the reference files are generated with the help of known segment samples by assigning the class values to the selected segments. For each class, arrange the samples of the training file in ascending order, according the attribute values. Starting from the smallest, select each value of the attribute one by one and divide the training samples into two parts. The attribute value greater than or equal to the selected value is considered as one part and the attribute values less than the selected value is considered as another part. Calculate the gain ratio for every selected value one by one and compare. The value of the attribute for which the gain ratio is the highest, is selected as the cutting value of that attribute for a class. This step continues until the last attribute is processed. After that it arranges the attributes according to their obtained gain ratio.

The gain ratio is used as the splitting criteria in the process of the generation of the decision tree. The highest ranked attribute is selected as the root node and remaining are treated as the sub-

nodes. The generated ranked attributes with their cutting values are used for splitting. All the training segments are passed through the root node. The value of the selected attribute of all segments is compared with the cutting value of root node attribute. The segment is split in two parts; one part is greater than or equal to the cutting value and the other part is lower than the cutting value. Now the generated sub-node is selected as the splitting node and then second ranked attribute is selected for splitting. This process is repeated for all ranked attributes, and finally a trained decision tree is generated. In image object classification, the generated decision tree has number of leaf nodes that are equal to the number of available classes. The segments of the testing file are now given as the input to the trained tree to get their class values. Once the class values are obtained, the quality of the testing segments is evaluated vis a vis class values of these segments obtained from the reference file.

All attributes are checked in order of their assigned rank in the generated tree, to allocate a class for any segment. Only some attributes may be useful to assign the class value to the segments however, including more attributes may introduce noise. Thus, a tree pruning operation is useful to reduce the size of the tree. The pruning operation has been done using PEP in the present research.

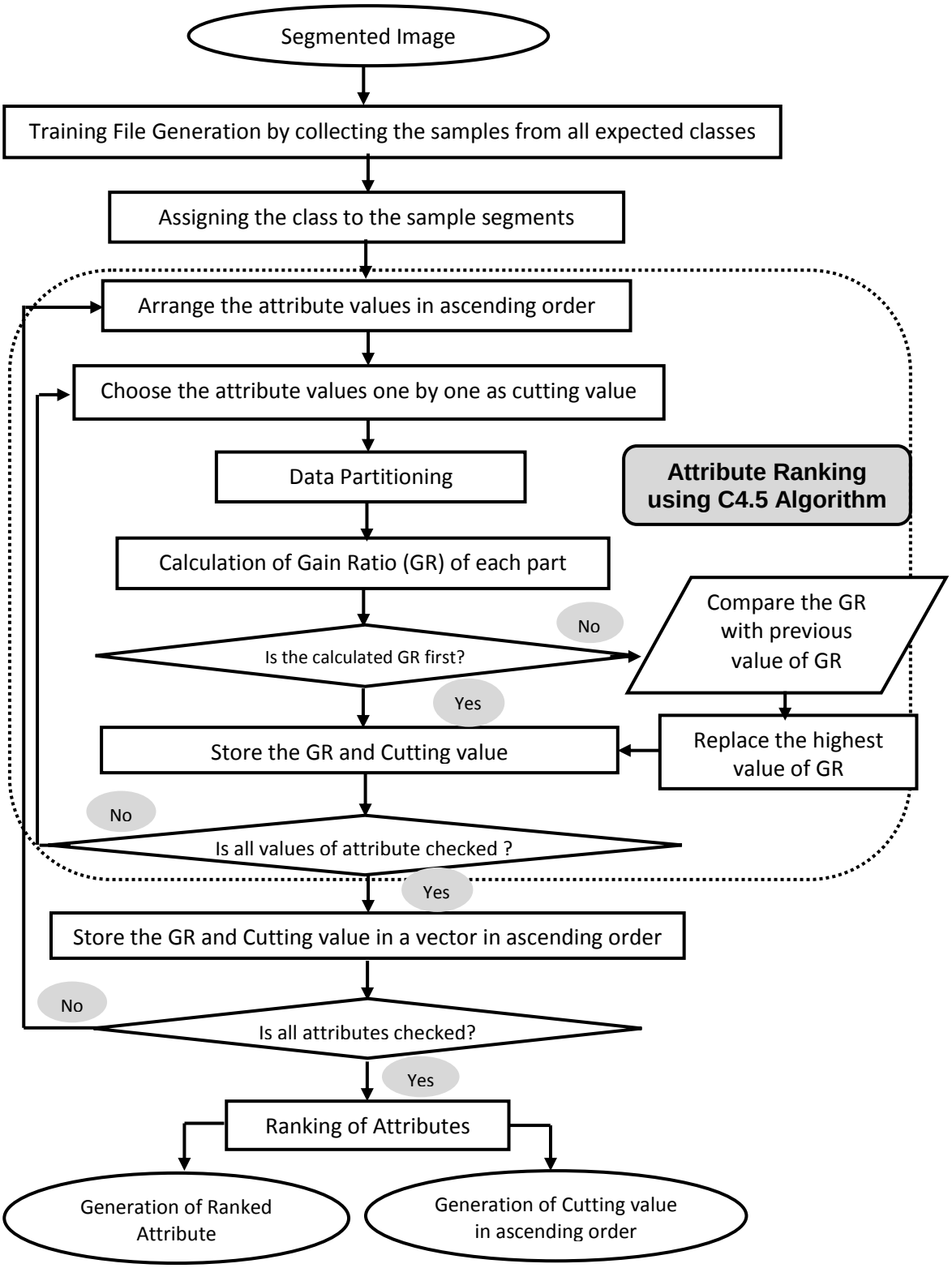

Figure 6.6: Flow chart demonstrating methodology for attribute ranking.

6.4.2 Object Classification

Both unpruned and pruned trained decision trees are used for object classification. In the classification process, as given in Figure 6.7, the attributes of segments of the segmented image are given as the input to the root node of the trained tree. The attributes value of the segments is compared with the cutting value of desired node attribute in their sequence of trained tree. The segment is then passed to the next node for splitting. In this manner, the segment is tested at all possible nodes of the trained decision tree and is assigned to a desired class. The segment is not assigned to any class if there is mismatch in splitting criteria. The desired class number is assigned to the segment if it is matched, else '0' is assigned and it is represented as 'unclassified'. Finally, a classified image has been generated by assigning unique colors to individual classes.

6.4.3 Classification Accuracy Assessment

A classified image produced from remote sensing data using decision tree based classification technique is a crisp one as each segment is classified into one and only one class. A typical strategy for accuracy assessment of hard classification similar to the pixel-based classification is used. In object based image classification, the minimum unit is segment instead of pixel as in pixel-based classification. Samples from the classified segmented image are taken as testing segments. Reference segments are also generated to match the class assigned to that segment matches with the actual class represented by that segment. An error matrix similar to pixel based has been generated using these samples to calculate various accuracies obtained through a decision tree based classifier (Congalton, 1991).

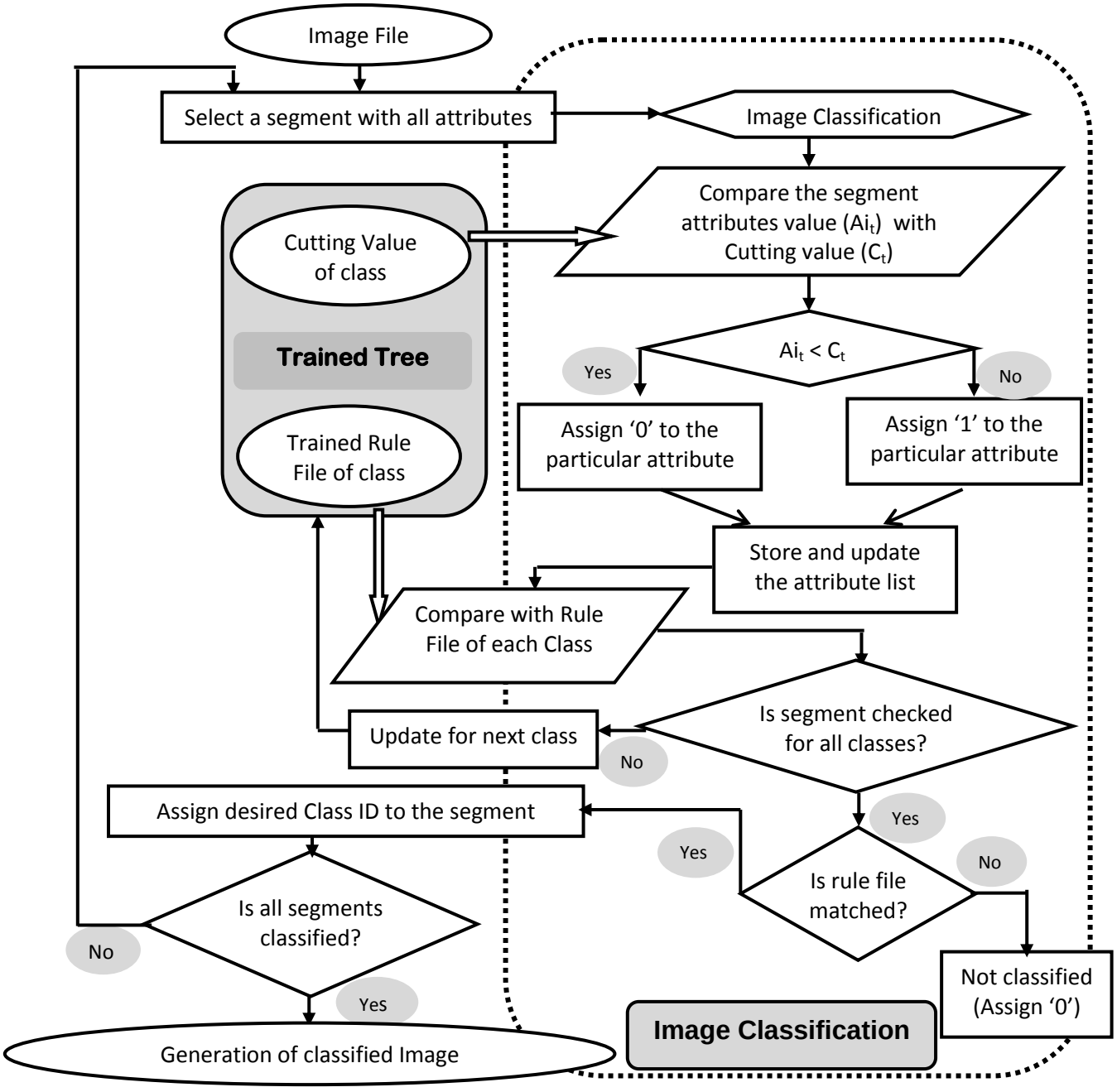

Figure 6.7: Flow chart of image classification

6.4.3.1 The Error Matrix

An error matrix is a cross-tabulation of classes on the classified image and on the reference data(Foody, 2010). It is represented by a $c \times c$ matrix (where c is the number of classes). The elements of this matrix indicate the number of samples in the testing data. The columns of the matrix generally define the reference data, and the rows define the classified image, but they can be interchanged. A typical error matrix is shown in Table 6.5.

Table 6.5: A typical error matrix

Classified image	Reference data				Row total
	Class 1	Class 2	…	Class c	
Class 1	n_{11}	n_{12}	…	n_{1c}	n_{1+}
Class 2	n_{21}	n_{22}	…	n_{2c}	n_{2+}
…	⋮	⋮	…	⋮	⋮
Class c	n_{c1}	n_{c2}	…	n_{cc}	n_{c+}
Column Total	n_{+1}	n_{+2}	…	n_{+c}	$n = \sum_{i=1}^{c} n_{i+}$
Definition of terms: n is the total number of testing samples, c is the number of classes, n_{ii} is the number of samples correctly classified, n_{ij} is the number incorrectly classified samples for class j in reference data and class i in classified output, n_{i+} is the row total for class i and n_{+j} is the column total for class j.					

For an ideal classification, it is expected that all points lie on the diagonal of the error matrix. This indicates that the same class has been observed both on the reference data as well as on the classified image. An error of omission occurs when a class on the reference data is incorrectly recorded in the classified image. An error of commission occurs when the class recorded in the classified image does not match on the reference data.

Various individual class related accuracies, average accuracy and overall accuracy are calculated for quantitative assessment. The overall accuracy (OA) is the most commonly adopted measure (Arora and Ghosh, 1998). OA is a measure of classification as a whole and not of individual classes while user's accuracy and producer's accuracy are the individual class accuracies. Another measure is the Kappa coefficient (K), which is based on all elements of the error matrix and not just the diagonal elements (as is the case with OA), therefore, K may sometimes be an appropriate candidate for accuracy assessment of classification (Foody, 1992). These accuracies are calculated as,

$$Overall\ Accuracy = \frac{1}{n}\sum_i^c n_{ii} \tag{6.22}$$

$$User's\ Accuracy = {}^{n_{ii}}/_{n_{i+}} \tag{6.23}$$

$$Producer's\ Accuracy = {}^{n_{ii}}/_{n_{+j}} \tag{6.24}$$

$$Kappa\ Coefficient = \frac{P_o - P_e}{1 - P_e} = \frac{\left(\frac{1}{n}\sum_i^c n_{ii}\right) - \left(\frac{1}{n^2}\sum_i^c n_{i+} n_{+j}\right)}{1 - \left(\frac{1}{n^2}\sum_i^c n_{i+} n_{+j}\right)} \tag{6.25}$$

6.5 Results and Analysis

6.5.1 Object-Based Classification: Study Area-I

6.5.1.1 Classification of Quick-Bird Pan-Sharpened Image

It is expected that every segment of the segmented image belongs to a class. The supervised classification technique has been applied to classify the Pan sharpened Quickbird image into eight classes (metallic and nonmetallic road, residential, shadow, grassland, trees, barren land and water) as mentioned in *Chapter 3*. From three segmented images, 32 segments from all classes (as listed in Table 6.6) have been taken as training samples. Individual decision trees have been generated and trained to classify these three segmented images (Seg-PS-I, Seg-PS-II and Seg-PS-III). The generated trees have been pruned using PEP to reduce the length and complexity of the tree without much effect on the accuracy.

Each segmented image produces a classified image after classification. Seg-PS-I image has been used for linear object classification, Seg-PS-II for compact regular shape object classification and Seg-PS-III for the compact irregular shape object classification.

Table 6.6: Description of training samples of segmented Quick-bird Pan-sharpened image-I, II and III used for attribute ranking

Seg-PS-I image		Seg-PS-II image		Seg-PS-III image	
Class	Samples	Class	Samples	Class	Samples
Metallic road (1)	5	Metallic road (1)	6	Metallic road (1)	4
Nonmetallic road (2)	4	Nonmetallic road (2)	4	Nonmetallic road (2)	4
Residential (3)	4	Residential (3)	4	Residential (3)	4
Shadow (4)	5	Shadow (4)	5	Shadow (4)	5
Grassland (5)	5	Grassland (5)	4	Grassland (5)	5
Trees (6)	3	Trees (6)	3	Trees (6)	4
Barren land (7)	4	Barren land (7)	4	Barren land (7)	4
Water (8)	2	Water (8)	2	Water (8)	2

In Quick-bird Pan-sharpened image, a total 100 attributes, as listed in Table 6.7, related to four categories has been generated.

Table 6.7: Generated attribute set for each segment of segmented Pan-sharpened Quick-bird image (numbers in brackets represent the band number and 'all dir.' Represents the 'all direction').

Sl. No.	Attributes of segment	Sl. No.	Attributes of segment
1	Mean (4)	38	GLDV Entropy (all dir.) (3)
2	Stddev (4)	39	Mean (2)
3	Ratio (4)	40	Stddev (2)
4	StdDev. to neighbour pixels (4)	41	Ratio (2)
5	Mean diff. to neighbors (4)	42	StdDev. to neighbour pixels (2)
6	Mean diff. to neighbors (abs) (4)	43	Mean diff. to neighbors (2)
7	Mean diff. to darker neighbors (4)	44	Mean diff. to neighbors (abs) (2)
8	Mean diff. to brighter neighbors (4)	45	Mean diff. to darker neighbors (2)
9	Rel. border to brighter neighbors (4)	46	Mean diff. to brighter neighbors (2)
10	GLCM Homogeneity (all dir.) (4)	47	Rel. border to brighter neighbors (2)
11	GLCM Contrast (all dir.) (4)	48	GLCM Homogeneity (all dir.) (2)
12	GLCM Dissimilarity (all dir.) (4)	49	GLCM Contrast (all dir.) (2)
13	GLCM Entropy (all dir.) (4)	50	GLCM Dissimilarity (all dir.) (2)
14	GLCM Ang. 2nd moment (all dir.) (4)	51	GLCM Entropy (all dir.) (2)
15	GLCM Mean (all dir.) (4)	52	GLCM Ang. 2nd moment (all dir.) (2)
16	GLCM StdDev (all dir.) (4)	53	GLCM Mean (all dir.) (2)
17	GLCM Correlation (all dir.) (4)	54	GLCM StdDev (all dir.) (2)
18	GLDV Ang. 2nd moment (all dir.) (4)	55	GLCM Correlation (all dir.) (2)
19	GLDV Entropy (all dir.) (4)	56	GLDV Ang. 2nd moment (all dir.) (2)
20	Mean (3)	57	GLDV Entropy (all dir.) (2)
21	Stddev (3)	58	Mean (1)
22	Ratio (3)	59	Stddev (1)
23	StdDev. to neighbour pixels (3)	60	Ratio (1)
24	Mean diff. to neighbors (3)	61	StdDev. to neighbour pixels (1)
25	Mean diff. to neighbors (abs) (3)	62	Mean diff. to neighbors (1)
26	Mean diff. to darker neighbors (3)	63	Mean diff. to neighbors (abs) (1)
27	Mean diff. to brighter neighbors (3)	64	Mean diff. to darker neighbors (1)
28	Rel. border to brighter neighbors (3)	65	Mean diff. to brighter neighbors (1)
29	GLCM Homogeneity (all dir.) (3)	66	Rel. border to brighter neighbors (1)
30	GLCM Contrast (all dir.) (3)	67	GLCM Homogeneity (all dir.) (1)
31	GLCM Dissimilarity (all dir.) (3)	68	GLCM Contrast (all dir.) (1)
32	GLCM Entropy (all dir.) (3)	69	GLCM Dissimilarity (all dir.) (1)
33	GLCM Ang. 2nd moment (all dir.) (3)	70	GLCM Entropy (all dir.) (1)
34	GLCM Mean (all dir.) (3)	71	GLCM Ang. 2nd moment (all dir.) (1)
35	GLCM StdDev (all dir.) (3)	72	GLCM Mean (all dir.) (1)
36	GLCM Correlation (all dir.) (3)	73	GLCM StdDev (all dir.) (1)
37	GLDV Ang. 2nd moment (all dir.) (3)	74	GLCM Correlation (all dir.) (1)

Sl. No.	Attributes of segment	Sl. No.	Attributes of segment
75	GLDV Ang. 2nd moment (all dir.) (1)	88	Length/width (line so)
76	GLDV Entropy (all dir.) (1)	89	Compactness (Polygon)
77	Brightness	90	GLCM Homogeneity (all dir.)
78	Max.Diff.	91	GLCM Contrast (all dir.)
79	Area	92	GLCM Dissimilarity (all dir.)
80	Length/width	93	GLCM Entropy (all dir.)
81	Compactness	94	GLCM Ang. 2nd moment (all dir.)
82	Elliptic Fit	95	GLCM Mean (all dir.)
83	Rectangular Fit	96	GLCM StdDev (all dir.)
84	Border length	97	GLCM Correlation (all dir.)
85	Shape index	98	GLDV Ang. 2nd moment (all dir.)
86	Density	99	GLDV Entropy (all dir.)
87	Asymmetry	100	NDVI (Calculated)

The process to train the decision tree starts with the selection of the segments as training samples. Initially, values of an attribute for all 32 training samples have been arranged in ascending order, then the process of selection of cutting value for the particular attribute starts. In this process, starting with the highest segment attribute value, one value has been selected every time and the data set is divided into two parts; the value less than the selected value has been considered as one part and greater than or equal to the selected value has been considered as another part. The gain ratio has been calculated for both the parts. The selected value that has the highest gain ratio has been chosen as the cutting value for that attribute. The selection of cutting value process is repeated for all 100 attributes. Further, the cutting value selection process is repetitive for all classes present in the image. The rank has been assigned to all 100 attributes based on their gain ratio, which shows the importance of the attribute for the selection of a class of the image. The attribute that gives the highest gain ratio, is selected as the first candidate attribute for splitting.

In the generation of the decision tree, these attributes are selected as the nodes and their corresponding cutting values are considered as the split threshold. Thus, a tree with 100 attributes as the node has been generated. The pruning operation is now applied to the generated tree. The image is classified using both pruned and unpruned trees.

After the image classification using the pruned and unpruned trees, various testing samples have been collected from segmented images, for all eight classes (as shown in Table 6.8.). These testing samples have been used for assessment of the accuracies of the classified images.

The classification error matrices for these three segmented images classified using unpruned and pruned tree are given in Appendix III Table III.1 to III.6. The user's and producer's accuracies have been calculated from all classified images, which are as shown in Table 6.9 and 6.10. It has been observed that higher overall accuracies of the image have been achieved by using the pruned tree classifier. Moreover, it has also been analyzed that the both metallic and nonmetallic roads have been classified perfectly using segmented image Seg-PS-I. It is because of their high segmentation quality. Similarly, classification using Seg-PS-II image and Seg-PS-III image has demonstrated good result for compact regular shape and irregular shaped objects respectively. The classes, water and the nonmetallic roads have been classified accurately in all three images using reduced trees, which may be due to its spectral characteristics.

Table 6.8: Object wise testing samples of Quick-bird Pan-sharpen the image for accuracy assessment.

Desired object	Seg-PS-I image	Seg-PS-II image	Seg-PS-III image
Metallic road	10	10	11
Non metallic road	5	6	5
Residential	16	15	15
Shadow	20	20	18
Grassland	5	6	7
Trees	10	10	10
Barren land	8	9	8
Water	2	2	2
Total Samples	76	78	78

Table 6.9: User's Accuracies for different classified images

Class names	User's accuracy (%) for classified image					
	Seg-PS-I image		Seg-PS-II image		Seg-PS-III image	
	Pruned tree	Unpruned tree	Pruned tree	Unpruned tree	Pruned tree	Unpruned tree
Metallic road	90.00	70.00	90.00	70.00	90.91	72.73
Non-metallic road	100.00	80.00	100.00	83.33	100.00	80.00
Residential	87.50	75.00	86.67	80.00	93.33	80.00
Shadow	95.00	90.00	95.00	80.00	94.44	83.33
Trees	100.00	80.00	83.33	66.67	85.71	57.14
Grass land	90.00	80.00	90.00	80.00	90.00	80.00
Barren land	75.00	62.50	88.89	66.67	75.00	75.00
Water	100.00	50.00	100.00	50.00	100.00	50.00

Table 6.10: Producer's Accuracies for different classified images

Class names	Producer's accuracy (%) for classified image					
	Seg-PS-I image		Seg-PS-II image		Seg-PS-III image	
	Pruned tree	Unpruned tree	Pruned tree	Unpruned tree	Pruned tree	Unpruned tree
Metallic road	90.00	87.50	90.00	87.50	90.91	80.00
Non-metallic road	71.43	57.14	85.71	62.50	83.33	57.14
Residential	93.33	80.00	92.86	70.59	93.33	75.00
Shadow	100.00	85.71	100.00	84.21	100.00	83.33
Trees	83.33	80.00	83.33	80.00	75.00	80.00
Grass land	90.00	88.89	81.82	80.00	81.82	88.89
Barren land	85.71	55.56	88.89	66.67	100.00	66.67
Water	100.00	50.00	100.00	50.00	100.00	50.00

The results obtained from Seg-PS-I image classified using a pruned and unpruned trees have been compared. It has been observed that both metallic and nonmetallic roads have been extracted distinctly in case of image classified using pruned tree whereas there is confusion between these

classes in the classified image obtained from unpruned tree. The similar observation can be seen for other classes also.

Table 6.11: Overall Accuracies and Kappa Coefficient for classified images

	Overall accuracy and Kappa coefficient for classified images					
	Seg-PS-I image		Seg-PS-II image		Seg-PS-III image	
	Pruned tree	Unpruned tree	Pruned tree	Unpruned tree	Pruned tree	Unpruned tree
Overall Accuracy	90.79	77.63	91.03	75.64	90.79	76.32
Kappa Coefficient	0.891	0.731	0.893	0.71	0.891	0.719

Error matrices for all classified images produced using pruned and unpruned trees have been generated. It may be observed from Table 6.11 that overall accuracy and the kappa coefficient for classified images with pruned tree (i.e., more than 90%) is always higher than those produced from unpruned tree (i.e., 76%).

While comparing the overall accuracy and the kappa coefficient of these three classified images with selected number of attributes, it has been found that Seg-PS-II image has achieved the highest 91.03% overall accuracy and 0.893 kappa coefficient.

The classified images for all segmented images Seg-PS-I, Seg-PS-II and Seg-PS-III are shown in Figure 6.8 (a-f). From these images, it has been observed that misclassification occurs generally in the classified image obtained through unpruned tree. It has also been noticed that some segments of class shadow have been misclassified to class water when the unpruned tree has been used for classification while some places other classes are wrongly classified as class tree. Both types of roads have been classified correctly in Seg-PS-I image using pruned tree whereas compact shape objects such as buildings, shadows etc. have been classified accurately in Seg-PS-II and Seg-PS-II images.

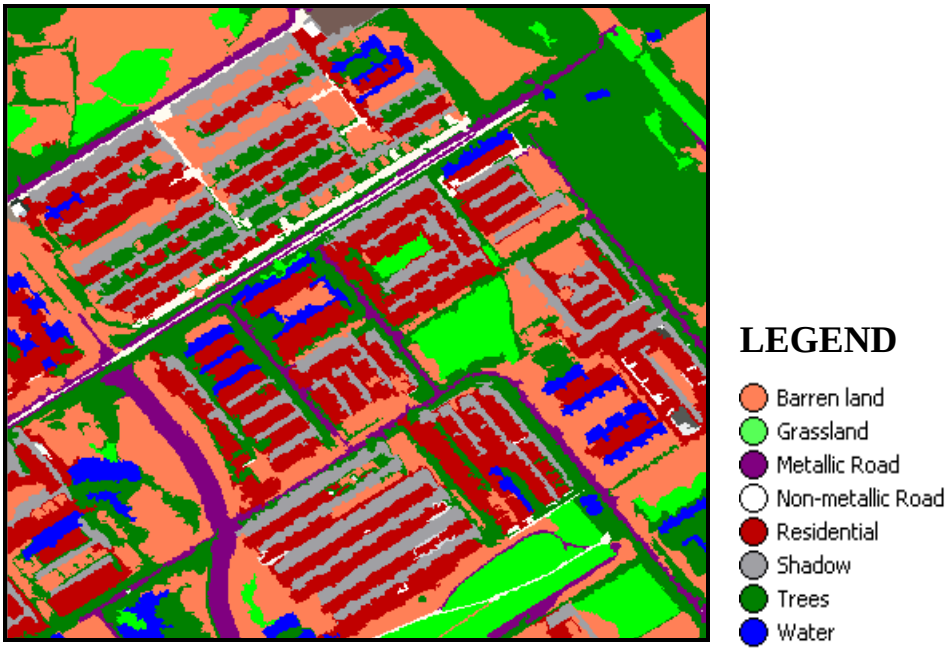

Figure 6.8 (a): Classified Seg-PS-I of Quick-bird Pan-sharpen image using an unpruned tree

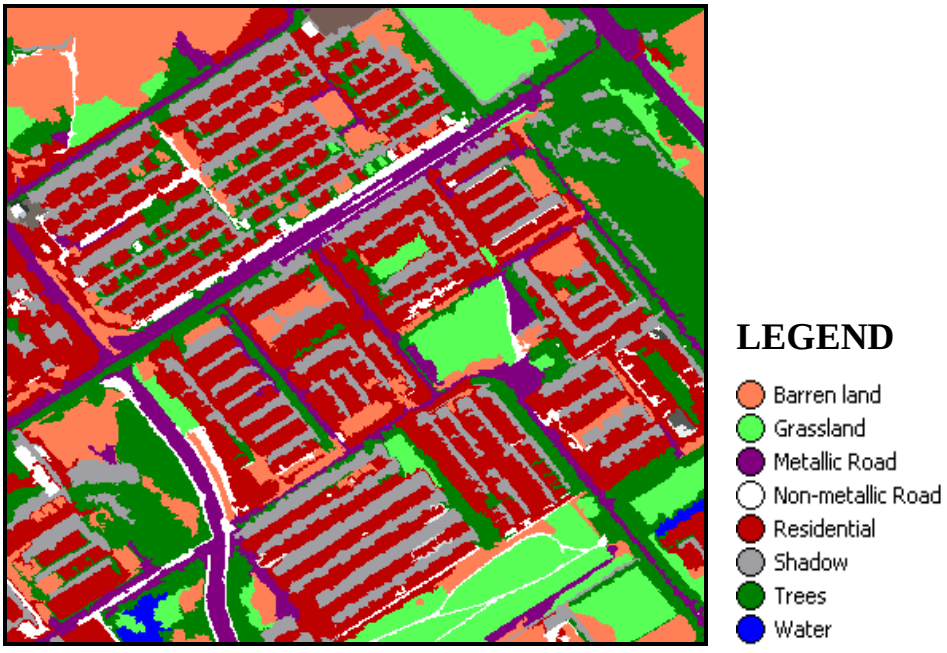

Figure 6.8 (b): Classified Seg-PS-I of Quick-bird Pan-sharpen image using a pruned tree

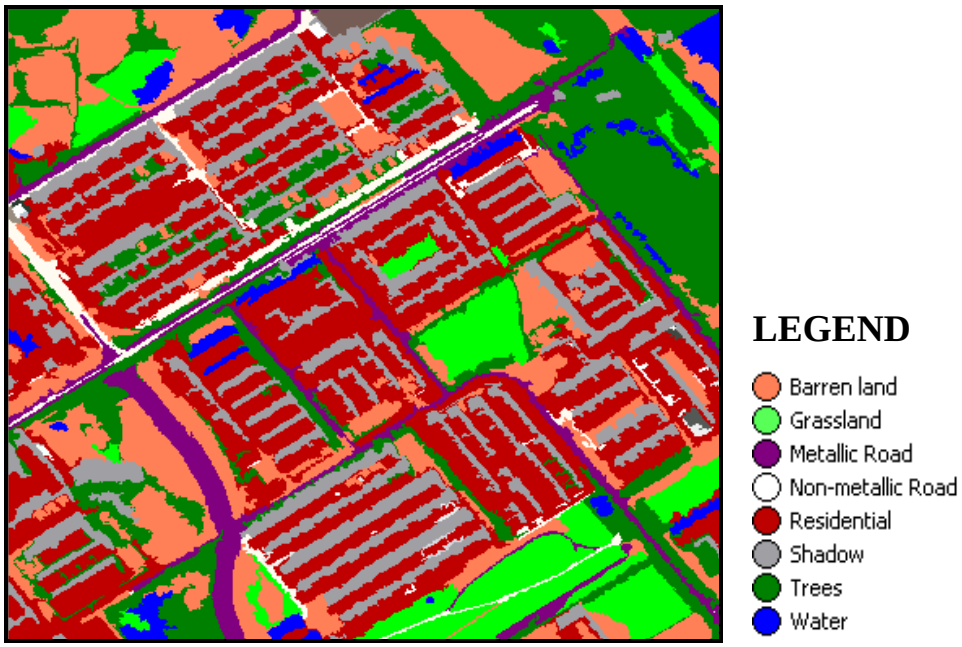

Figure 6.8 (c): Classified Seg-PS-II of Quick-bird Pan-sharpen image using an unpruned tree

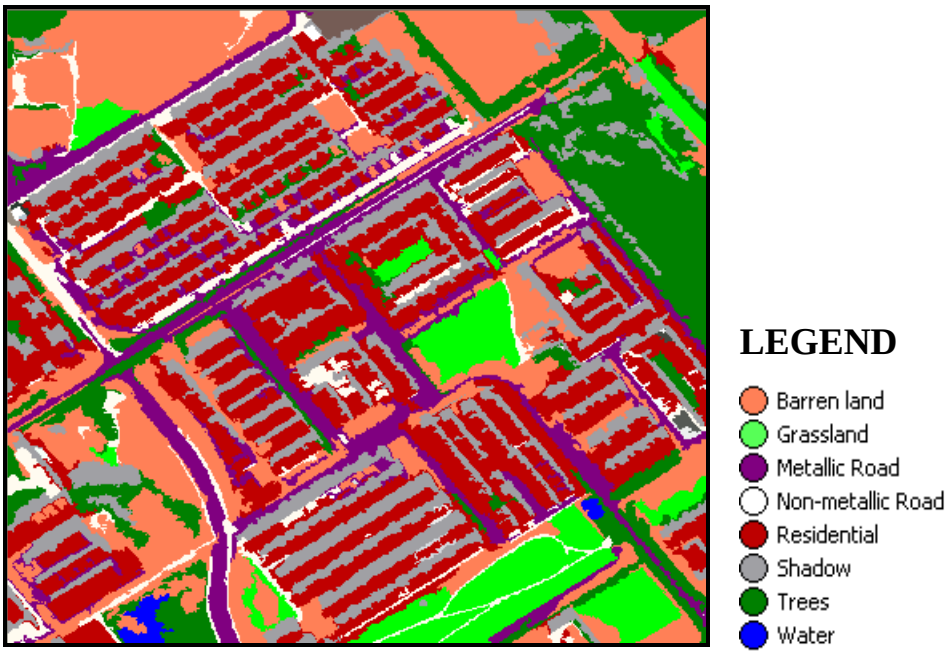

Figure 6.8 (d): Classified Seg-PS-II of Quick-bird Pan-sharpen image using a pruned tree

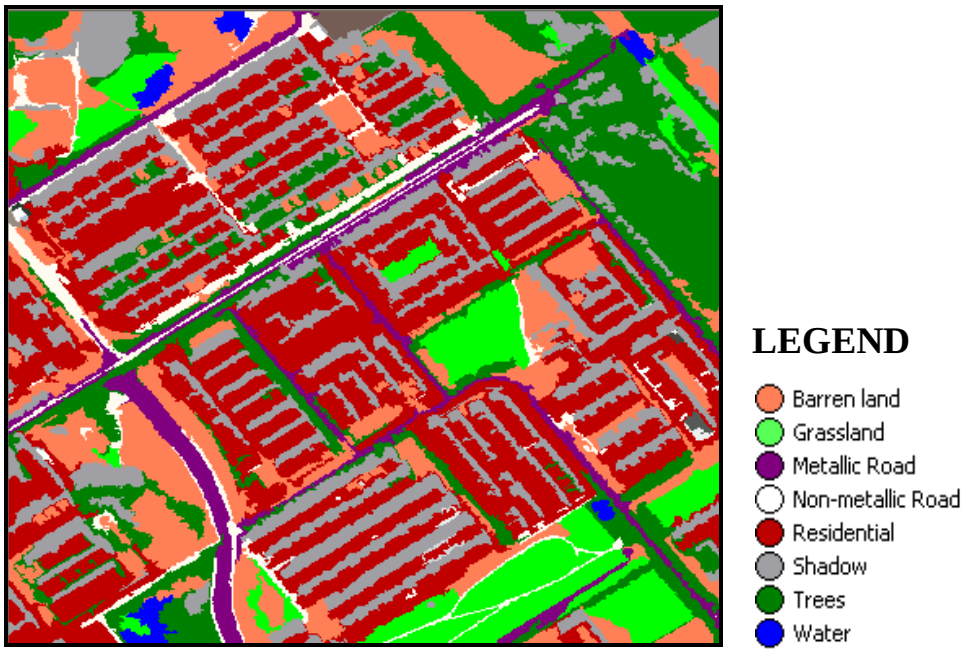

Figure 6.8 (e): Classified Seg-PS-III of Quick-bird Pan-sharpen image using an unpruned tree

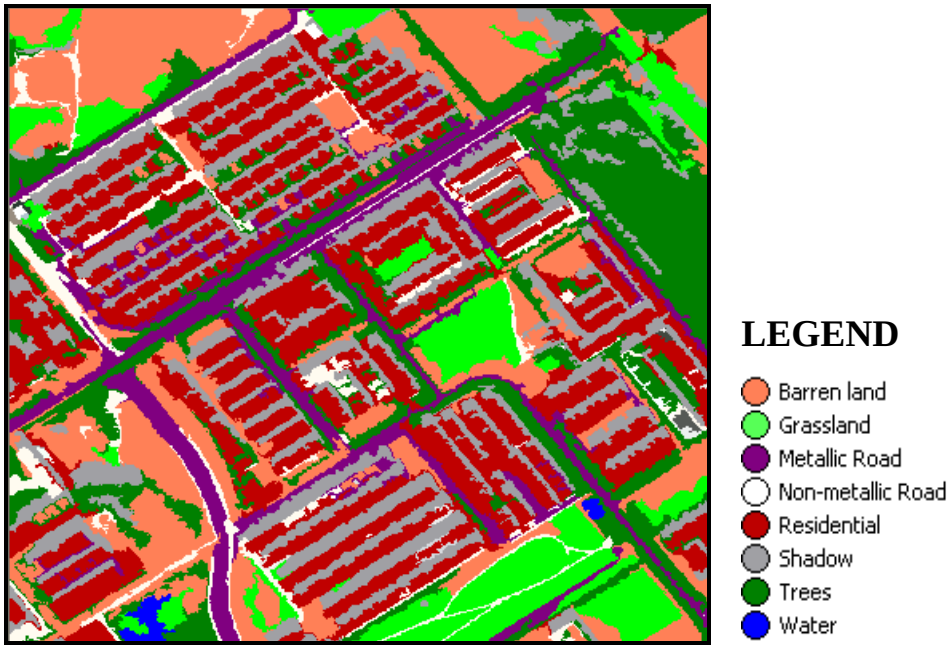

Figure 6.8 (f): Classified Seg-PS-III of Quick-bird Pan-sharpen image using a pruned tree

6.5.1.2 Classification of Quick-Bird Pan Image

Similarly, the Quick-bird Pan image has been segmented using three sets of parameters. These segmented images (as given Figure 5.10) have been used for image classification. A number of segments as listed in Table 6.12 taken as training samples to classify the images. In case of Seg-P-I, 44 training samples have been taken, which includes 11 samples of linear objects and remaining 33 samples belong to other objects. For Seg-P-II image, 47 training samples have been selected, out of which 18 samples belong to compact regular shaped objects and rest 29 samples belong to other objects. For the Seg-P-III image, out of the 46 samples selected samples 20 samples belong to compact irregular shaped object and remaining 26 samples belong to other objects.

Table 6.12: Description of training samples of segmented image-I, II and III used for attribute ranking (Quickbird Pan image).

Seg-P-I image		Seg-P-II image		Seg-P-III image	
Object	Samples	Object	Samples	Object	Samples
Metallic road (1)	7	Metallic road (1)	6	Metallic road (1)	6
Nonmetallic road (2)	4	Nonmetallic road (2)	4	Nonmetallic road (2)	4
Residential (3)	8	Residential (3)	8	Residential (3)	6
Shadow (4)	8	Shadow (4)	10	Shadow (4)	10
Grassland (5)	5	Grassland (5)	6	Grassland (5)	6
Trees (6)	4	Trees (6)	5	Trees (6)	5
Barren land (7)	6	Barren land (7)	6	Barren land (7)	6
Water (8)	2	Water (8)	2	Water (8)	3

The Quick-bird Pan image is a single band image, thus less number of attributes are available to represent the characteristic of the segments. The 43 attributes, as given in Table 6.13, have been used for further processing. The C4.5 decision tree based classification algorithm has been applied on these three data sets and tree has been trained. Further, the trained tree has been used to classify the segmented images. These generated trees have been pruned using PEP method and the pruned trees have further been used for classifying the images. Similar to the results of Pan-sharpened image, it has been observed that the images classified using pruned tree produced more

accurate results as compared to that obtained from the unpruned trees. The classified outputs for these three sets of images are shown in Figures 6.9 (a) to 6.9 (f).

Table 6.13: Generated attribute set for each segment ('all dir.' Represents the 'all direction')

Sl. No.	Attributes of segment	Sl. No.	Attributes of segment
1	Mean	24	Elliptic Fit
2	Stddev	25	Rectangular Fit
3	StdDev. to neighbour pixels (m)	26	Border length (m)
4	Mean diff. to neighbors (m)	27	Shape index
5	Mean diff. to neighbors (abs)(m)	28	Density
6	Mean diff. to darker neighbors	29	Asymmetry
7	Mean diff. to brighter neighbors	30	Length/width (line so)
8	Rel. border to brighter neighbors	31	Area (excluding inner poly) (m^2)
9	GLCM Homogeneity (all dir.)	32	Perimeter (polygon) (m)
10	GLCM Contrast (all dir.)	33	Compactness (polygon)
11	GLCM Dissimilarity (all dir.)	34	GLCM Homogeneity (all dir.)
12	GLCM Entropy (all dir.)	35	GLCM Contrast (all dir.)
13	GLCM Ang. 2nd moment (all dir.)	36	GLCM Dissimilarity (all dir.)
14	GLCM Mean (all dir.)	37	GLCM Entropy (all dir.)
15	GLCM StdDev (all dir.)	38	GLCM Ang. 2nd moment (all dir.)
16	GLCM Correlation (all dir.)	39	GLCM Mean (all dir.)
17	GLDV Ang. 2nd moment	40	GLCM StdDev (all dir.)
18	GLDV Entropy (all dir.)	41	GLCM Correlation (all dir.)
19	Area (m^2)	42	GLDV Ang. 2nd moment (all dir.)
20	Length (m)	43	GLDV Entropy (all dir.)
21	Width (m)		
22	Length/width		
23	Compactness		

A testing data with reference file for very high resolution Quick-bird Pan image has been generated. The reference file includes 80 samples for Seg-P-I, 77 samples for Seg-P-II and 78 samples for Seg-P-III, from all eight classes (as given in Table 6.14) and used to assess the classification accuracy.

Table 6.14: Object wise testing samples of Quick-bird Pan image for accuracy assessment.

Desired object	**Seg-P-I image**	**Seg-P-II image**	**Seg-P-III image**
Metallic road	11	10	9
Non metallic road	5	5	7
Residential	15	16	16
Shadow	21	22	20
Grassland	6	5	6
Trees	11	10	11
Barren land	9	7	7
Water	2	2	2

The error matrices have been generated for these three classified outputs. Similar to the Pan sharpened classified image, the significant improvement in accuracies has been observed when image is classified using a pruned tree as compared to the accuracy obtained with unpruned tree. However, the overall accuracies from classification of Pan image are lower than those obtained from Pan-sharpened image. This is due to less number of attributes to represent the object characteristics (43 as there have only one band in the image) as well as very little variation in the attribute values for different classes also. It has also been noticed that the class water has been classified more accurately in all the data sets while the class barren land has the poor classification accuracy.

The error matrices for all three data sets classified with pruned tree and unpruned tree are given in Appendix-III Table III.7 to Table III.12. User's and producer's accuracies for these six outputs are given in Table 6.15 and Table 6.16 respectively. The overall accuracies and the kappa coefficient are tabulated in Table 6.17. The highest overall accuracy and kappa co-efficient has been obtained as 76.32% and 0.72 respectively for classification produced using the pruned tree.

Table 6.15: User's Accuracies for different segmented images

Class names	User's accuracy (%) for classified image					
	Seg-PS-I image		Seg-PS-II image		Seg-PS-III image	
	Pruned tree	Unpruned tree	Pruned tree	Pruned tree	Unpruned tree	Pruned tree
Metallic road	54.55	54.55	60.00	60.00	66.67	55.56
Non-metallic road	80.00	60.00	80.00	60.00	71.43	57.14
Residential	80.00	66.67	81.25	62.50	81.25	62.50
Shadow	85.00	66.67	81.82	68.18	85.00	70.00
Trees	50.00	66.67	80.00	60.00	66.67	50.00
Grass land	72.73	63.64	80.00	60.00	72.73	54.55
Barren land	55.56	44.44	50.00	28.57	57.14	28.57
Water	100.00	100.00	100.00	50.00	100.00	100.00

Table 6.16: Producer's Accuracies for different segmented images

Class names	Producer's accuracy (%) for classified image					
	Seg-PS-I image		Seg-PS-II image		Seg-PS-III image	
	Pruned tree	Unpruned tree	Pruned tree	Pruned tree	Unpruned tree	Pruned tree
Metallic road	66.67	40.00	66.67	42.86	60.00	41.67
Non-metallic road	57.14	50.00	66.67	42.857	71.43	50.00
Residential	92.31	90.91	100.00	90.91	92.86	90.91
Shadow	94.44	100.00	100.00	100.00	100.00	87.50
Trees	42.86	44.44	50.00	30.00	50.00	37.50
Grass land	72.73	70.00	80.00	66.67	80.00	66.67
Barren land	41.67	33.33	30.00	22.22	40.00	20.00
Water	100.00	66.67	100.00	50.00	100.00	50.00

Table 6.17: Overall Accuracies and Kappa Coefficient for different segmented images

	Overall accuracy and Kappa coefficient for classified image					
	Seg-PS-I image		Seg-PS-II image		Seg-PS-III image	
	Pruned tree	Unpruned tree	Pruned tree	Pruned tree	Unpruned tree	Pruned tree
Overall Accuracy	72.15	62.5	76.32	59.74	75.64	58.97
Kappa Coefficient	0.67	0.56	0.72	0.53	0.71	0.52

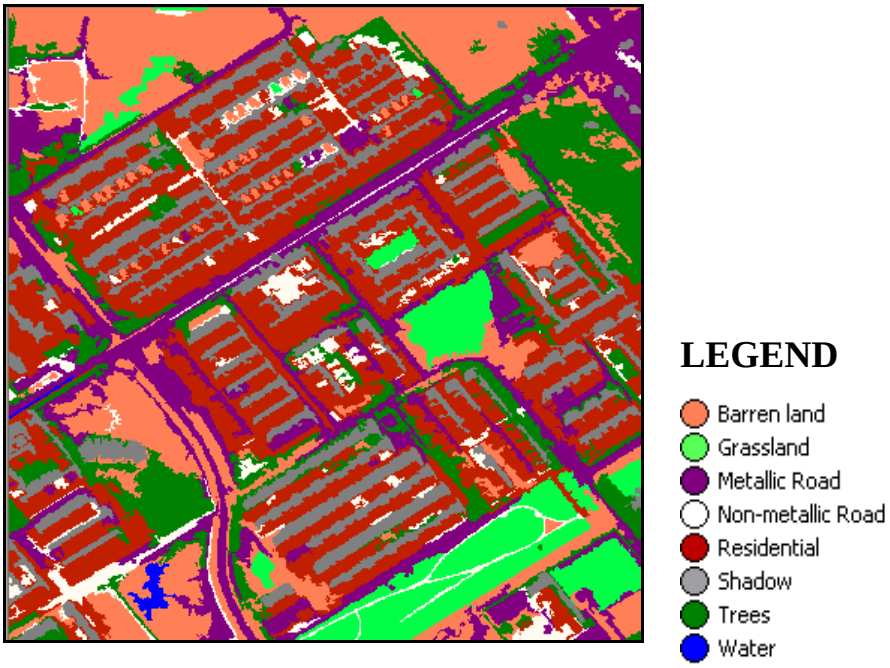

Figure 6.9 (a): Classified Seg-P-I of Quick-bird Pan image using pruned tree

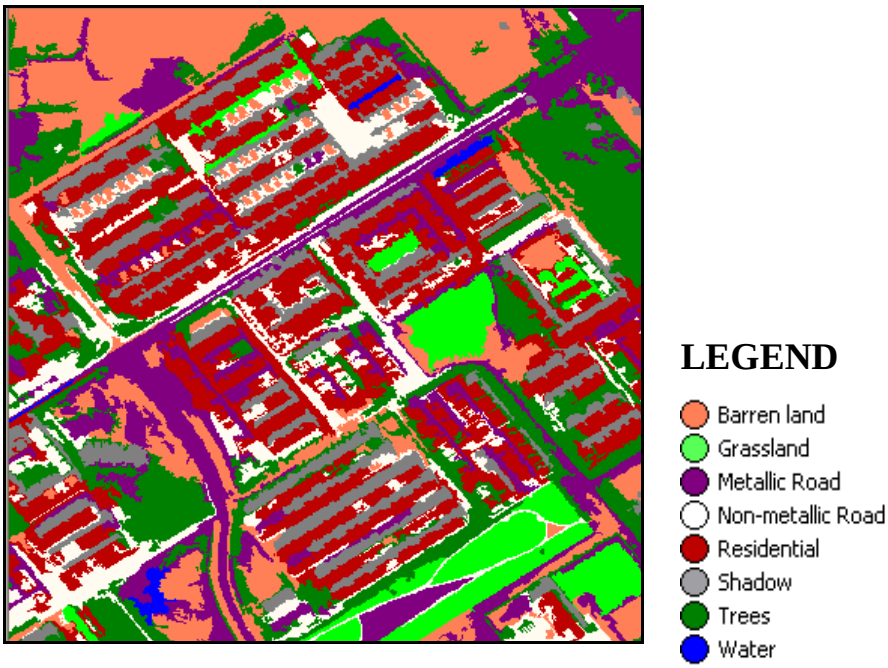

Figure 6.9 (b): Classified Seg-P-I of Quick-bird Pan image using unpruned tree

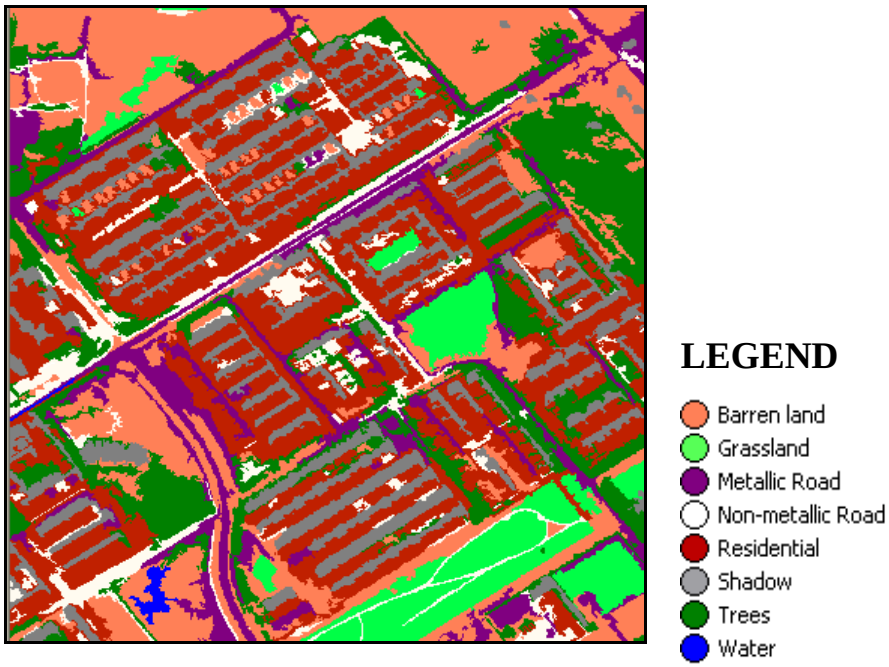

Figure 6.9 (c): Classified Seg-P-II of Quick-bird Pan image using pruned tree

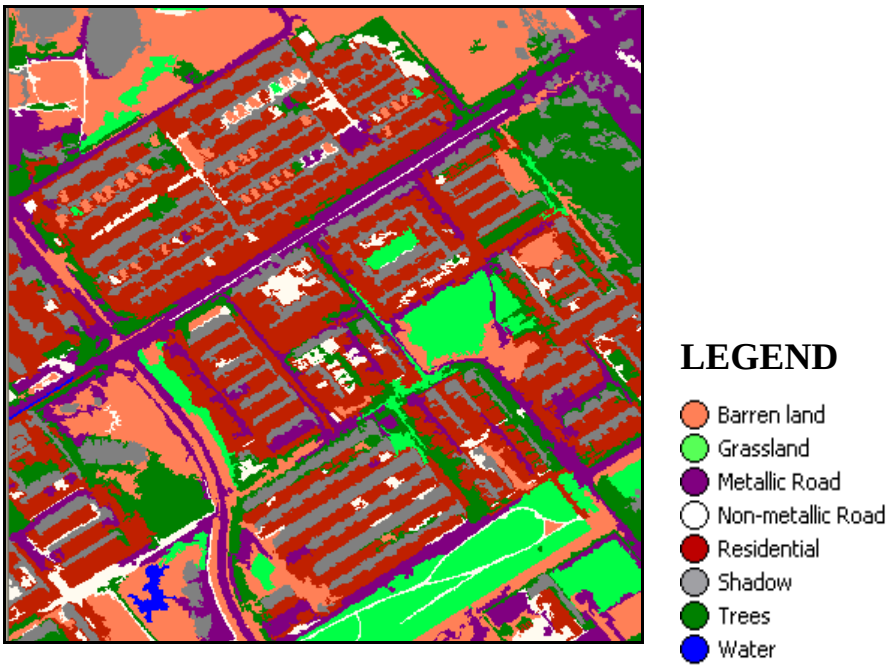

Figure 6.9 (d): Classified Seg-P-II of Quick-bird Pan image using unpruned tree

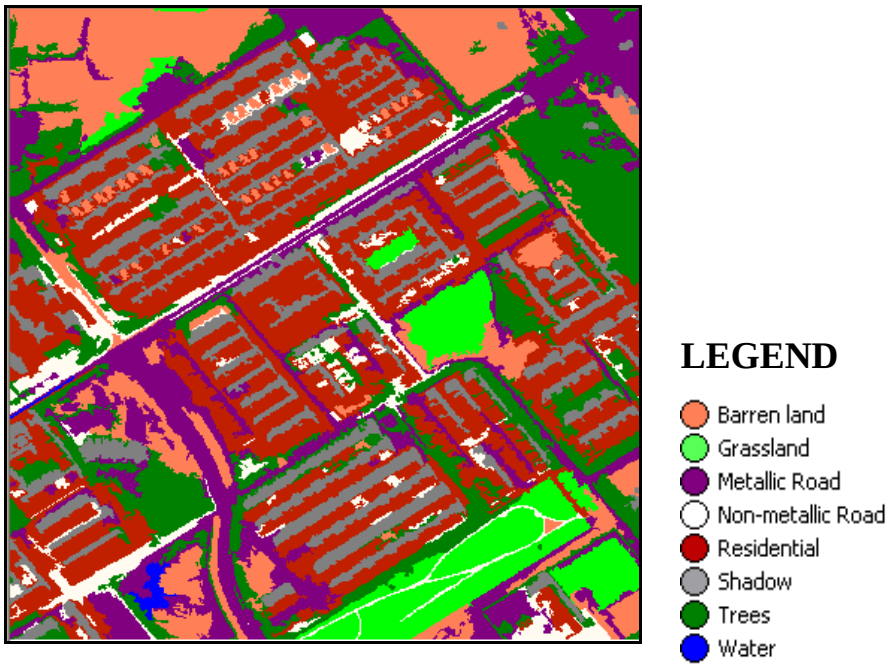

Figure 6.9 (e): Classified Seg-P-III of Quick-bird Pan image using pruned tree

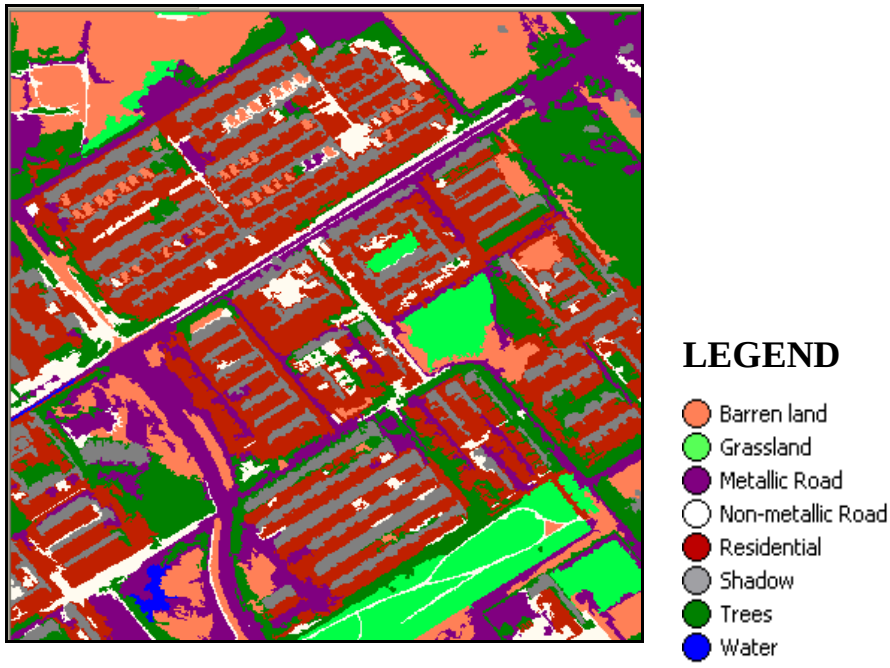

Figure 6.9 (f): Classified Seg-P-III of Quick-bird Pan image using unpruned tree

6.5.2 Object-Based Classification: Study Area II

The image classification process has also been performed on LISS-IV multispectral-segmented images of the Delhi region (Study Area II). The image has been segmented using two set of parameters. These segmented images (Figure 5.11, as given in *Chapter 5*) have been used for attribute selection. The numbers of segments, taken as training samples, to classify these images are listed in Table 6.18. In case of segmented image Seg-L-I, 15 segments belong to linear objects and remaining 58 samples belongs to compact shape objects. To extract the compact object, segmented image Seg-L-II has been considered. In this image, 64 samples belong to compact object and rest 18 samples belong to other objects. A total of 85 attributes, as listed in Table 6.19, as generated in the segmentation process, have been used for classification.

Table 6.18: Description of training samples for segmented image-I and II used for attribute ranking

Seg-L-I image		**Seg-L-II image**	
Object	**Samples**	**Object**	**Samples**
Apartments (1)	8	Apartments (1)	10
Houses (2)	7	Houses (2)	8
Metallic road (3)	4	Metallic road (3)	5
Nonmetallic road (4)	4	Nonmetallic road (4)	4
Metro line (5)	3	Metro line (5)	4
Canal (6)	4	Canal (6)	5
Water body (7)	3	Water body (7)	4
Vegetation (8)	10	Vegetation (8)	11
Grassland (9)	10	Grassland (9)	12
Barren land (10)	11	Barren land (10)	10
Playground (11)	5	Playground (11)	6
Sand (12)	4	Sand (12)	3

Table 6.19: Generated attribute set for each segment (numbers in brackets represent the band number of multi spectral image and 'all dir.' represents the 'all direction')

Sl. No.	Attributes of segment	Sl. No.	Attributes of segment
1	Mean (1)	39	Mean (3)
2	Stddev (1)	40	Stddev (3)
3	Ratio (1)	41	Ratio (3)
4	StdDev. to neighbour pixels (1)	42	StdDev. to neighbour pixels (3)
5	Mean diff. to neighbors (1)	43	Mean diff. to neighbors (3)
6	Mean diff. to neighbors (abs) (1)	44	Mean diff. to neighbors (abs) (3)
7	Mean diff. to darker neighbors (1)	45	Mean diff. to darker neighbors (3)
8	Mean diff. to brighter neighbors (1)	46	Mean diff. to brighter neighbors (3)
9	Rel. border to brighter neighbors (1)	47	Rel. border to brighter neighbors (3)
10	GLCM Homogeneity (all dir.) (1)	48	GLCM Homogeneity (all dir.) (3)
11	GLCM Contrast (all dir.) (1)	49	GLCM Contrast (all dir.) (3)
12	GLCM Dissimilarity (all dir.) (1)	50	GLCM Dissimilarity (all dir.) (3)
13	GLCM Entropy (all dir.) (1)	51	GLCM Entropy (all dir.) (3)
14	GLCM Ang. 2nd moment (all dir.) (1)	52	GLCM Ang. 2nd moment (all dir.) (3)
15	GLCM Mean (all dir.) (1)	53	GLCM Mean (all dir.) (3)
16	GLCM StdDev (all dir.) (1)	54	GLCM StdDev (all dir.) (3)
17	GLCM Correlation (all dir.) (1)	55	GLCM Correlation (all dir.) (3)
18	GLDV Ang. 2nd moment (all dir.) (1)	56	GLDV Ang. 2nd moment (all dir.) (3)
19	GLDV Entropy (all dir.) (1)	57	GLDV Entropy (all dir.) (3)
20	Mean (2)	58	Brightness
21	Stddev (2)	59	Max.Diff.
22	Ratio (2)	60	Area (Pxl/m^2)
23	StdDev. to neighbour pixels (2)	61	Length (m)
24	Mean diff. to neighbors (2)	62	Width (m)
25	Mean diff. to neighbors (abs) (2)	63	Length/width
26	Mean diff. to darker neighbors (2)	64	Compactness
27	Mean diff. to brighter neighbors (2)	65	Elliptic Fit
28	Rel. border to brighter neighbors (2)	66	Rectangular Fit
29	GLCM Homogeneity (all dir.) (2)	67	Border length (m)
30	GLCM Contrast (all dir.) (2)	68	Shape index
31	GLCM Dissimilarity (all dir.) (2)	69	Density
32	GLCM Entropy (all dir.) (2)	70	Asymmetry
33	GLCM Ang. 2nd moment (all dir.) (2)	71	Length/width (line so)
34	GLCM Mean (all dir.) (2)	72	Area (excluding inner polygons) (Pxl or m^2)
35	GLCM StdDev (all dir.) (2)		
36	GLCM Correlation (all dir.) (2)	73	Perimeter (polygon) (m)
37	GLDV Ang. 2nd moment (all dir.) (2)	74	Compactness (polygon)
38	GLDV Entropy (all dir.) (2)	75	GLCM Homogeneity (all dir.)

Sl. No.	Attributes of segment	Sl. No.	Attributes of segment
76	GLCM Contrast (all dir.)	81	GLCM StdDev (all dir.)
77	GLCM Dissimilarity (all dir.)	82	GLCM Correlation (all dir.)
78	GLCM Entropy (all dir.)	83	GLDV Ang. 2nd moment (all dir.)
79	GLCM Ang. 2nd moment (all dir.)	84	GLDV Entropy (all dir.)
80	GLCM Mean (all dir.)	85	NDVI (calculated)

A testing data with reference file for high-resolution LISS-IV image has been generated. The reference file includes 127 and 137 samples from across all 12 classes from segmented images Seg-L-I and L-II, respectively, as given in Table 6.20, has been used to assess the classification accuracy.

Table 6.20: Object wise testing samples of LISS-IV Multispectral image for accuracy assessment.

Desired object	Seg-L-I image	Seg-L-II image
Apartments	12	11
Houses	10	11
Metallic road	8	10
Nonmetallic road	4	5
Metro line	4	4
Canal	4	4
Water body	4	4
Dense vegetation	26	30
Sparse vegetation	20	22
Barren land	22	22
Wetland	10	10
Sand	3	4

Table 6.21: User's Accuracies for different segmented images

User's accuracy (%) for classified image				
Class names	Seg-L-I image		Seg-L-II image	
	Pruned tree	Unpruned tree	Pruned tree	Unpruned tree
Apartments	83.33	75.00	90.91	81.81
Houses	70.00	70.00	81.82	63.64
Metallic road	66.67	62.50	70.00	70.00
Nonmetallic road	50.00	50.00	40.00	40.00
Metro line	50.00	50.00	50.00	50.00
Canal	75.00	50.00	75.00	50.00
Water body	75.00	50.00	75.00	50.00
Dense vegetation	88.46	80.77	86.67	80.00
Sparse vegetation	90.00	75.00	86.36	72.73
Barren land	81.82	77.27	86.36	59.10
Wet land	80.00	60.00	80.00	50.00
Sand	66.67	33.33	50.00	25.00

Table 6.22: Producer's Accuracies for different segmented images

Producer's accuracy (%) for classified image				
Class names	Seg-L-I image		Seg-L-II image	
	Pruned tree	Unpruned tree	Pruned tree	Unpruned tree
Apartments	83.33	65.32	76.92	64.29
Houses	63.64	63.64	64.29	70.00
Metallic road	60.00	50.00	70.00	50.00
Nonmetallic road	66.67	50.00	66.67	25.00
Metro line	40.00	50.00	50.00	40.00
Canal	100.00	100.00	100	66.67
Water body	60.00	50.00	75.00	50.00
Dense vegetation	95.83	95.45	96.30	96.00
Sparse vegetation	85.71	83.33	90.48	84.21
Barren land	90.00	70.83	82.61	59.10
Wet land	72.73	54.55	72.73	50.00
Sand	66.67	33.33	50.00	33.33

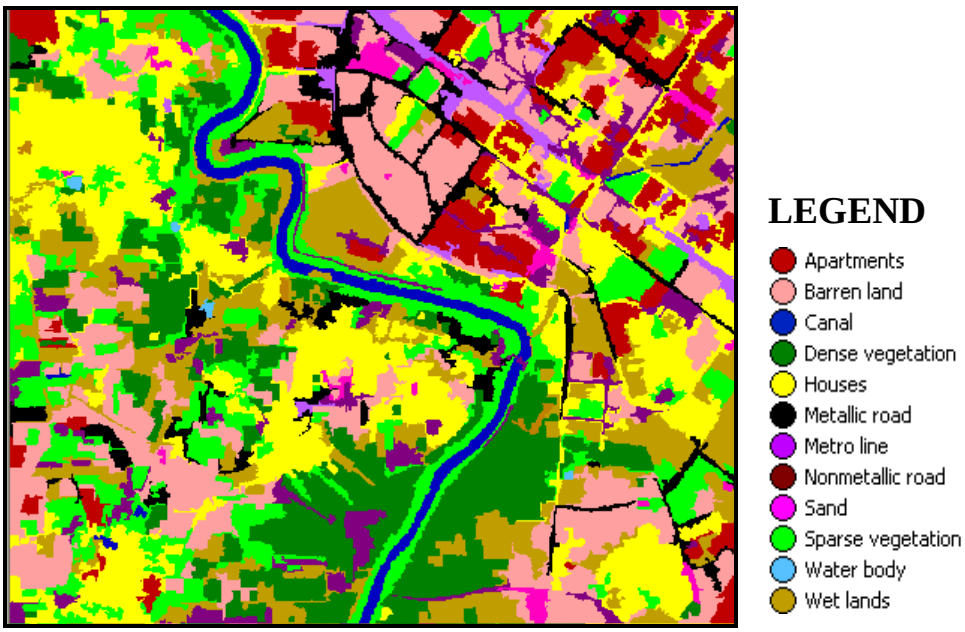

Figure 6.10 (a): Classified Seg-L-I of LISS-IV image using pruned tree

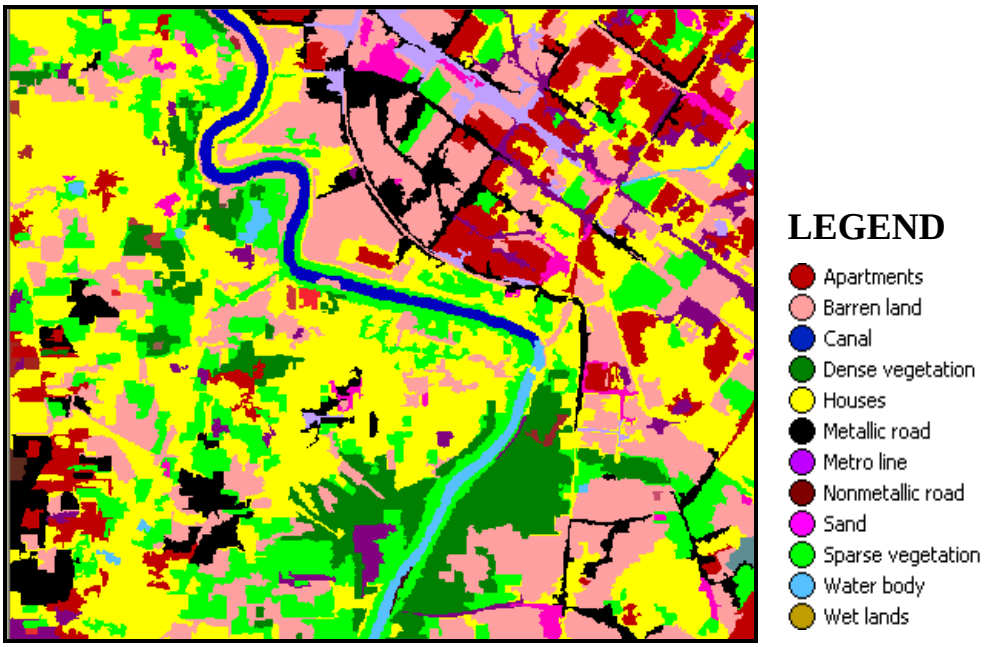

Figure 6.10 (b): Classified Seg-L-I of LISS-IV image using unpruned tree

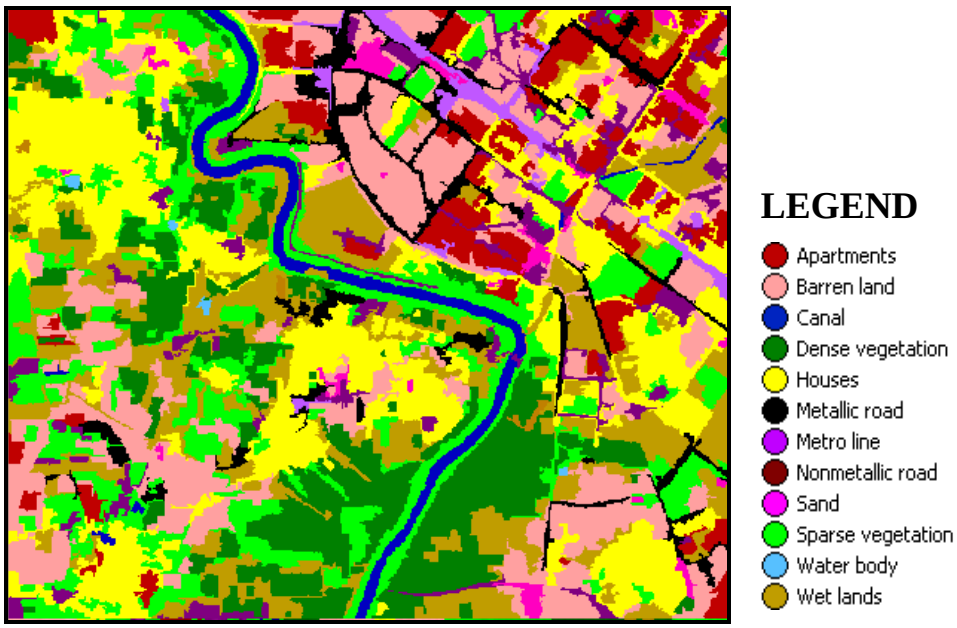

Figure 6.10 (c): Classified Seg-L-II of LISS-IV image using pruned tree

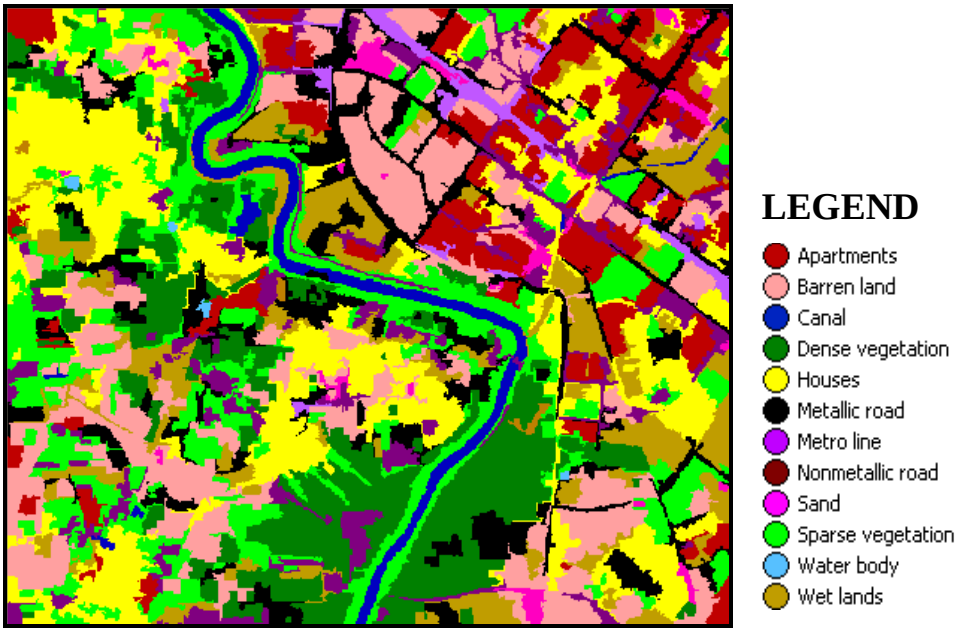

Figure 6.10 (d): Classified Seg-L-II of LISS-IV image using unpruned tree

Table 6.23: Overall Accuracies and Kappa Coefficient for different segmented images

Overall accuracy and Kappa coefficient for classified image				
	Seg-L-I image		Seg-L-II image	
	Pruned tree	Unpruned tree	Pruned tree	Unpruned tree
Overall Accuracy	79.69	70.10	80.29	65.69
Kappa Coefficient	0.769	0.659	0.775	0.610

The images have been classified using both, pruned tree and with unpruned tree. The classified images are shown in Figure 6.10 (a-d). From the classified images, it may be observed that both types of vegetation, canal, barren land and houses have been classified more accurately as compared to other classes. Error matrices have been given in Appendix-III, Table III.13 to Table III.16. The user's accuracies, producer's accuracies and the overall accuracy are given in Table 6.21 to Table 6.23. The overall accuracy and kappa coefficients for classified image with reduced set of attributes have been found higher than that of image classified with unpruned tree. It has also been observed that Seg-L-I image has produced more accurate results as compared to others.

The classification results of the LISS-IV image has been compared with that of the Quick-bird images. It has been observed that due to more number of attributes and fine resolution, Quick-bird Pan-sharpened image provides higher classification accuracy. However, the LISS-IV MS image is classified more accurately when compared with Quick-bird Pan image. It is because of the single band Pan image, thus classes are not easily separable.

6.6 Summary

In this chapter, the results of the image classification produced from different remote sensing data sets were provided, analyzed and discussed. Experiments using C4.5 decision tree techniques on

segmented images with pruned and unpruned tree were conducted. The results show that C4.5 decision tree provides acceptable accuracies. The accuracy increases with the use of pruned tree, which shows the effectiveness of the C4.5 decision tree algorithm in OBIA for attribute selection. The object classification results can be summarized in the following.

i). Object based image classification and their accuracy assessment using the error matrix have been performed on three data sets namely; Quick-bird Pan-sharpened image, Quick-bird Pan image and LISS-IV multispectral image.

ii). For assessing classification quality, various accuracy measures such as overall accuracy, individual class accuracies and Kappa coefficient, have been calculated. For Quick-bird Pan-sharpened image, Pan image and LISS-IV image; highest overall accuracy have been obtained as 91.03%, 62.5%, 78.91%, and Kappa coefficient as 0.893, 0.572 and 0.76 respectively.

iii). Highest classification accuracy is achieved for the Quick-bird Pan-sharpened image, due to its fine spatial resolution and multispectral data. Quick-bird Pan image produces low classification accuracy as compared to other images. This is due to single band data, where classes create confusion. The LISS-IV multispectral image produced better results in comparison to Quick-bird Pan image due to its multi band characteristics and poor result in comparison to Pan-sharpened image, because of its low spatial resolution.

iv). It has been observed that highest classification accuracies have been obtained with pruned tree.

Additionally, the C4.5 algorithm of decision tree has also been used for object extraction. The next chapter explains the complete process of the object extraction with its attribute selection criteria.

Chapter: 7

IMAGE OBJECT EXTRACTION

7.1 Introduction

The present chapter discusses the attribute selection and image object extraction. The decision tree C4.5 algorithm has been used for extracting the objects from the image. The segmented images are again used and the objects have been extracted. It is clear from the classification results obtained in the previous chapter, that the accuracy of classification produced from a pruned tree is higher than the unpruned tree. This clearly shows that if more number of attributes are used for classification (as in case of unpruned tree), it creats confusion and produces misclassification. Therefore, selection of proper attribute is very important.

The segmented images, after having assessed for its quality evaluation, are now further processed. Each segment of the segmented image is accompanied with a number of attributes representing characteristics of objects/classes within that segment. As the number of attributes is typically large, it is always expedient to identify the significant attributes for image classification or object extraction. The aim of this chapter is to propose a methodology, named as ***"a combined decision tree-ROC curve approach"*** for attribute selection. In this methodology, the C4.5 decision tree algorithm has been used to assign ranks to all attributes, which is followed by receiver operating characteristic (ROC) curve analysis to select those ranked attributes that provide unique characteristic of the desired class/object.

Further, the C4.5 algorithm of decision tree has been used for object extraction. A number of decision trees equal to the number of objects have been generated. Object extraction has been performed in two ways; using a selected number of attributes and using all attributes. The ROC curve has been drawn for object extraction using all attributes to assess the object extraction quality.

7.2 Attribute Reduction

Attribute reduction can be performed in two ways; attribute extraction and attribute selection. Attribute extraction may be employed on segmented image to generate new data statistics from pixels within the segmented regions. The attribute extraction transforms the data in other feature space where the objects may be segregated distinctly. The objects are then classified in the reduced and/or transformed data space thereby optimizing the classification process. The principal component analysis (PCA), wavelet transform, etc. may be used to extract the attributes (Zhang *et al*., 2010; Blaschke and Lang, 2006; Zhu and Yang, 1998).

As stated earlier, after the image segmentation process, the attribute selection strategy may be applied to select the most significant attributes of objects belonging to a given land use class, for their subsequent input in the classification stage. In general, various techniques for attribute selection have been given in the literature (Hu *et al.*, 2005; Gao *et al.*, 2007). The reduced set of attributes not only results into better classification and extraction accuracy but also improves the efficiency of the algorithm.

In case of OBIA, attributes are selected by computing the correlation using Pearson correlation coefficient (Zhang *et al.*, 2010), by using the Jeffries-Matusita (J-M) distance and the Bhattacharyya distances. A high correlation coefficient indicates that the two attributes contain similar information. So, the attributes which show a high correlation coefficient with the other attributes are removed from the attribute set. Attributes can also be selected by applying the Separability and threshold (SEaTH) technique to find the separation between classes (Nussbaum *et al.* 2006). It calculates the separability and the corresponding threshold for every object combination with attributes and selects the attributes that comprise maximum separability between two classes. The Ginni index (Yu *et al.*, 2006) has also been used for attribute selection. It provided the statistical rank to every attribute, based on their importance to classify the image. The gain of attributes have been calculated by using Ginni index and this gain values were used to assign a rank to each attribute. These attributes are typically grouped as spectral, shape, textural and topological categories derived under the attribute selection stage.

7.3 Receiver Operating Characteristic (ROC) Curves

In general, ROC curve is a 2D representation of the accuracy of extracting an individual class from the image. When working with ROC curve, it is required that source data must be classifiable into two categories and the ground truth label for each data event is available. It is also desirable that the output of the detector is continuous and the decision threshold of the detector can be varied continuously. The ROC curve is mainly used to,

i). Visualize the differentiated accuracy of a class extraction over its decision threshold.
ii). Recognize the role of the decision threshold in extraction quality.
iii). Compare multiple detectors.

The segmented image is considered in two groups; the segments of the desired class and the background segments. In the ROC curve, the rate of extraction known as a true positive rate (TPR) is plotted on the y-axis, and false-positive rate (FPR) or false alarm rate (FAR) is plotted on x-axis. ROC curve with more TPR value than the FAR value results in the rise of the curve in upward direction.

When the TP rate is much higher than the FP rate, then the curve will have a more extreme jump and represent the performance of a superior detector (Maxion and Roberts, 2004). It is worth remembering that it is not always just the overall shape that matters, but sometimes the shape of a curve in a particular region also matters. For instance, if the task imposes maintaining a false-positive rate below 5% (or < 0.05 error given a noise event), then the only part of the curve of interest is that region which lies to the left of the vertical line passing through $x = 0.05$ on the graph. Thus, looking at the shape of the curve in a particular region is more important than the overall curve shape.

Limitations of an ROC curve:

i). The ROC curve of testing data may vary from ROC curve of training data and also different for various data sets. Since an object detector's accuracy on one set of testing data may vary dramatically from its accuracy on a different set of testing data, no direct generalizations can be guaranteed.

ii). The ROC curve assumes that the allotment of object and background (within each class) is constant. While it is not necessary that number of object and background remains constant for all datasets and for all classes.

In this work, the ROC curve has been implemented with a dual aim; the selection of the proper decision threshold for obtaining highest extraction accuracy, and also for the assessment of the extraction accuracy.

7.3.1 Selection of Threshold Using ROC curve

Each point along the ROC curve corresponds to a different operating mode, or decision threshold. Points closer to the origin (0,0) indicate a more exclusive criterion; points closer to the upper-right (1,0) indicate a more inclusive one.

Every ROC curve is based on the measurement of detector performance at various decision thresholds as shown in Figure 7.1. On the ROC curve, the strict thresholds appear closer to the point (0,0) and the more lenient thresholds appear closer to the point (1,0). The point (0,0) corresponds to a low false-positive rate but also missing many true positives, and the point (1,0) corresponds to capturing nearly all the true positives, but at the expense of a high false-positive rate (Maxion and Roberts, 2004).

In order to select a threshold using ROC curve, it is required to choose a fixed *FP rate* and then look at the corresponding coordinate for the *TP rate*. This action is analogous to assuming a maximum level of error for false positives, and then seeing how much true-positive success has been achieved.

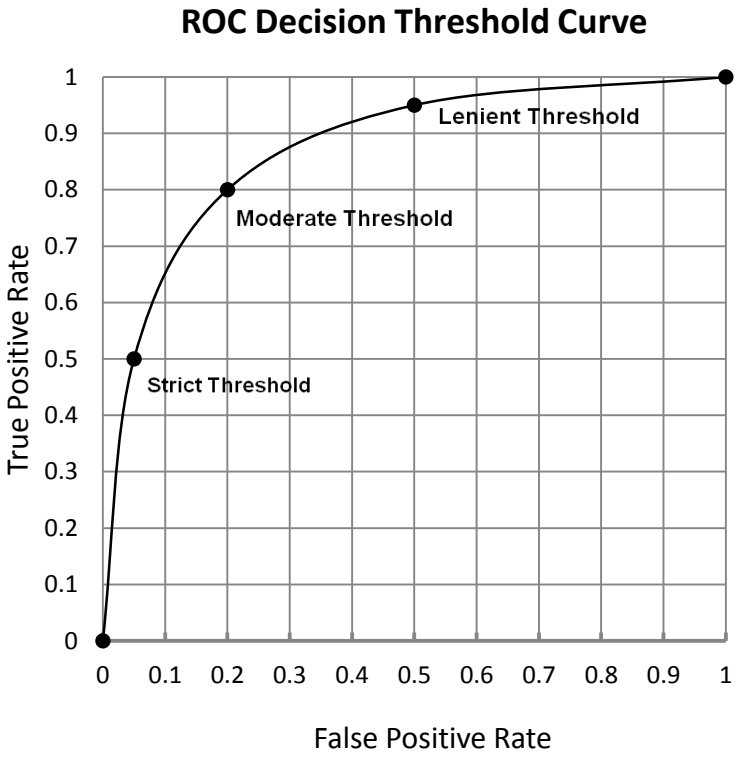

Figure 7.1: Representation of ROC decision threshold curves (Maxion and Roberts, 2004).

7.3.2 Assessment of Object Extraction Quality Using ROC curve

The ROC curve can be used for the assessment of the extraction accuracy of a class, when two classes are present in the image. An ROC curve plots the true-positive rate of detection or TP rate, against the corresponding false-positive rate of error, or FP rate. These two numbers varies with the variation in the threshold. Whenever the rate of true positives is the highest, the rate of false positives is at the lowest, and vice versa. An ideal ROC curve will have a TPR of 1.0 and FAR of 0.0. While a positive diagonal line from (0, 0) to (1, 1) represents the worst ROC curve. The extraction accuracy depends on two components, the TPR and FAR values and will vary in a different way from one detector to the other, and from one data set to another. This makes the shape of each ROC curve look different, as shown in Figure 7.2.

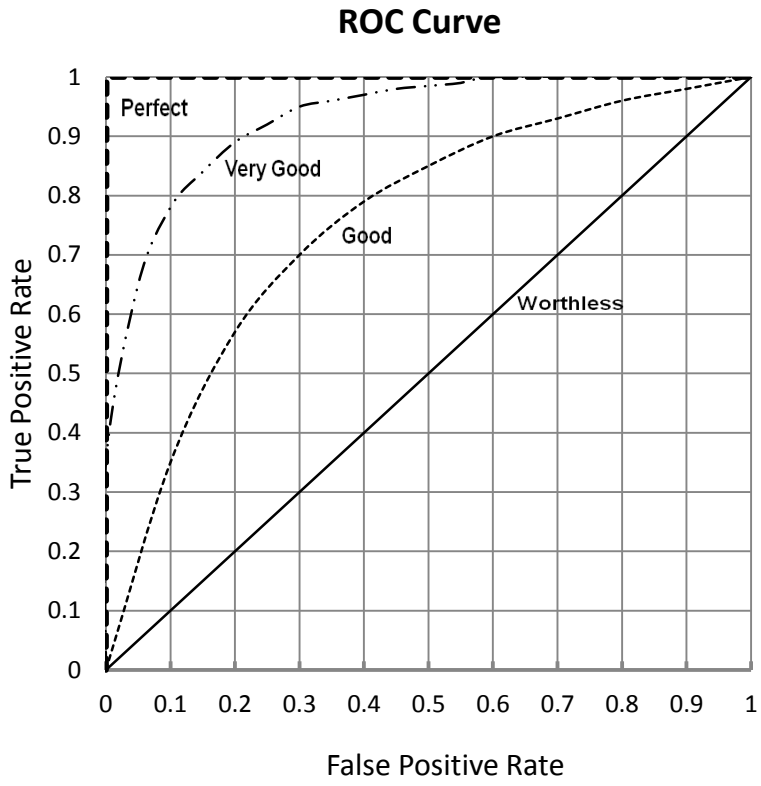

Figure 7.2**:** Representation of different ROC curves (Maxion and Roberts, 2004).

In this study, the TPR and FAR values have been calculated for each of the selected attribute, which are considered in order of their corresponding rank given by the decision tree. The TPR and FAR values change with the variation in the threshold. Here, the threshold is the number of attributes used to extract the desired object. Therefore, TPR and FAR values can be used to select the minimum number of attributes. The minimum number of attributes, which gives the highest TPR at the low value of FAR, is selected. This minimum number of attributes can be used as selected attributes for object extraction.

True positive rate (TPR) in the present context is given as,

$$TPR = \frac{\text{Total number of segments of target class extracted as object}}{\text{Total number of segments of target class present in testing data}} = \frac{TP}{TP + FN} \qquad (7.4)$$

False alarm rate (FAR) in the present context is given as,

$$FAR = \frac{\text{Total number of segments of background selected as an object}}{\text{Total number of segments of background in testing data}} = \frac{FP}{TN + FP} \tag{7.5}$$

7.4 Combined Decision Tree-ROC Curve Approach for Attribute Selection

In general, ROC curve is used for the assessment of the extraction accuracy, when a data set is divided into two classes. Extraction accuracies have been checked at various thresholds. It has been noticed that extraction quality depends on the selected threshold and best extraction quality has been observed at moderate threshold, while extraction quality starts decreasing beyond this threshold value.

In the proposed combined decision tree-ROC curve approach, the decision tree has been used for attribute ranking based on gain ratio measure. Starting from the lowest ranked attribute, the TPR and FAR values have been calculated for all ranked attributes by removing one sub-tree in every step. It thus gives an equal number of TPR and FAR values as that of the number of attributes. The ROC curve is drawn using these calculated values of TPR and FAR. Finally, moderate threshold for ROC curve at which highest value of TPR is obtained at low value of FAR, is selected. The moderate threshold provides the number of selected attributes. The decision tree with this selected number of attributes is used to extract the desired object. Further, the ranking of the attributes may vary from class to class.

Various attributes generated in the image segmentation process and grouped into four categories (spectral, shape, contextual and textural) as discussed in *Chapter 6*, have been used for object extraction. Similar to the image classification, C4.5 algorithm has been applied and decision trees have been generated and trained. Individual decision trees have been generated to extract various objects/classes present in the image.

7.5 Decision tree for object extraction

In object extraction (OE) framework of OBIA, the focus is only on one class called as object and remaining are known as background. The object extraction from the segmented image is performed by assigning the segments either as objects or as background. The generated output is a binary image in which the object appears bright on a dark background. In order to extract an object, OBIA incorporates knowledge from both local and global properties in the form of attributes of the image. All attributes of the segment are arranged for a given desired object. This arrangement of attributes is based on the extraction quality of a class. The attributes of the segments are given as input at the root node and the desired object is obtained at the farthest leaf node through different selected attributes, while the segments appear to other leaf nodes belong to the background. Several decision trees equal to the number of objects to be extracted have been designed.

7.6 Proposed Methodology

7.6.1 Methodology for Attribute Selection

The segmented image is used for object extraction. Initially, gain ratios of all attributes for extracting one class have been calculated as previously described in s*ection 6.3*. According to their gain ratio, ranks to the attributes have been assigned. Further, tree has been generated to extract an object. A similar exercise has been repeated for generation of all trees, which are equal to the number of objects to be extracted.

All attributes are checked in order of their assigned rank in the generated tree to allocate a class for the segment. However only some attributes are useful to assign the class value to the segments, thus selection of the required attributes is an important step. The proposed methodology for attribute selection has been shown in Figure 7.3. In the proposed method, the ROC curve is employed to select the optimal number of attributes, which correctly assign the class to the segments. The selection of the number of attribute is based on the TPR and FAR values of ROC curves.

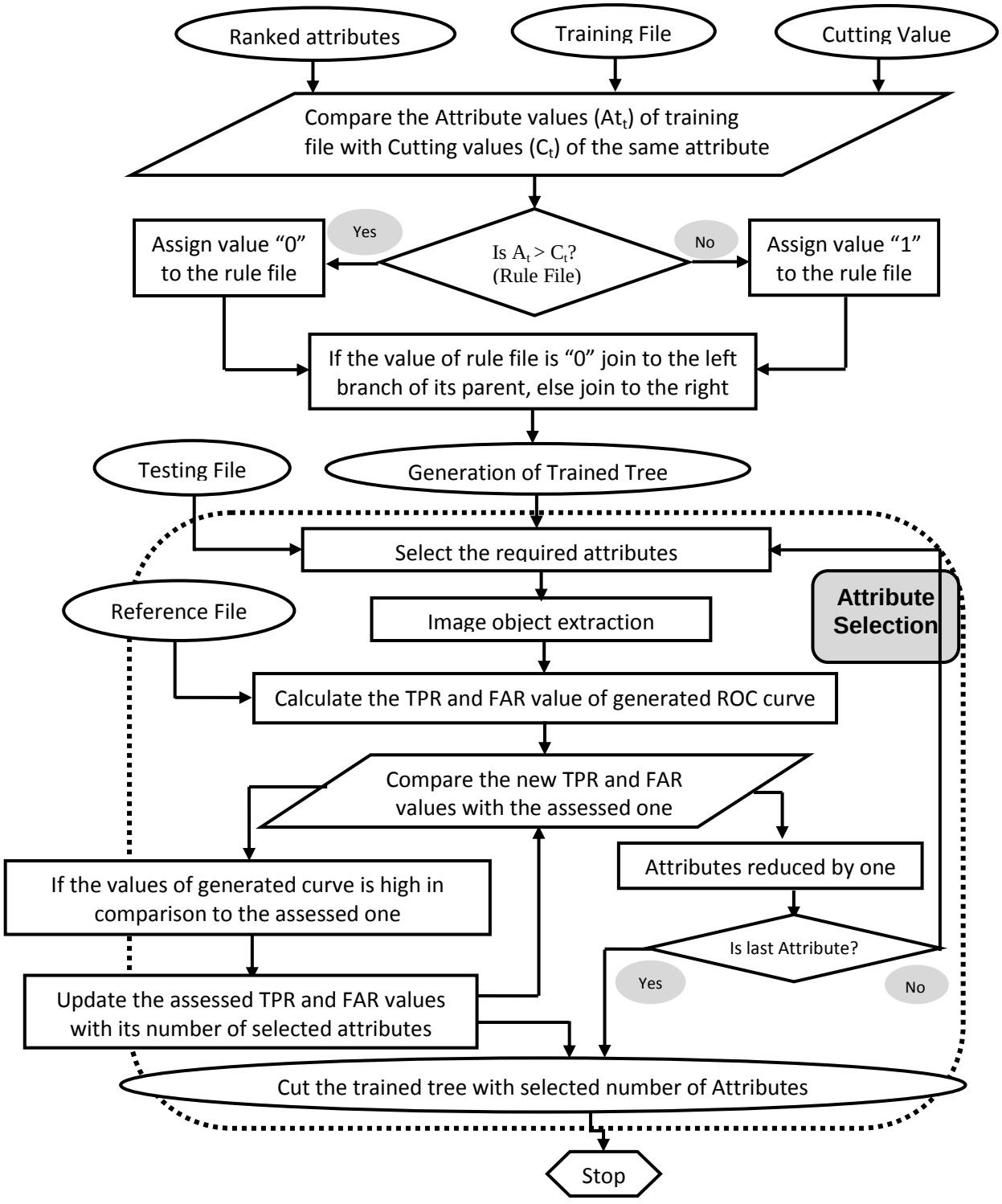

Figure 7.3: Flow chart for tree generation and attribute selection.

Starting from all attributes the TPR and FAR values are calculated for the highest ranked attribute by removing the least ranked attributes one by one. Those ranked attributes that give highest TPR with low FAR value are selected. Finally, a tree with the selected number of attributes in their order of importance is used for the extraction of an object. A similar exercise has been performed for all generated trees.

7.6.2 Methodology for Object Extraction

Trained decision trees have been generated by using training segments and attributes selected for object extraction. The split decision file (rule file) with 0 and 1 has been generated, in which 0 indicates the value less than the cutting value and 1 for vice versa. The flowchart for object extraction using decision tree has been shown in Figure 7.4. The decision tree is selected to extract an object, in which the cutting values of the selected attributes appear as a threshold at a particular node. The attribute values for all segments are now given as input to the root node of the desired decision tree. For object extraction, value of the ranked attributes has been compared with the cutting value of that attribute for the extraction of the desired object. The ‘0’ is assigned to the attribute that value appears less than the cutting value, otherwise the value ‘1’ is assigned to that attribute. After passing through all nodes of desired tree, a binary file with values ‘0’ and ‘1’ has been obtained for a segment.

Every class has its individual characteristic, which is represented by a trained rule file in the decision tree. To check the similarity in the character of a segment, the generated rule file is compared with the trained rule file of the desired class. If matched, assign the particular class number to the segment, which is considered as the desired object class, otherwise it is treated as background and ‘0’ value assigned. Using this process, all segments are assigned either to an object or to the background class, and a binary image is generated. This process has been repeated for all desired objects. Finally, the individual binary image has been generated for various extracted objects.

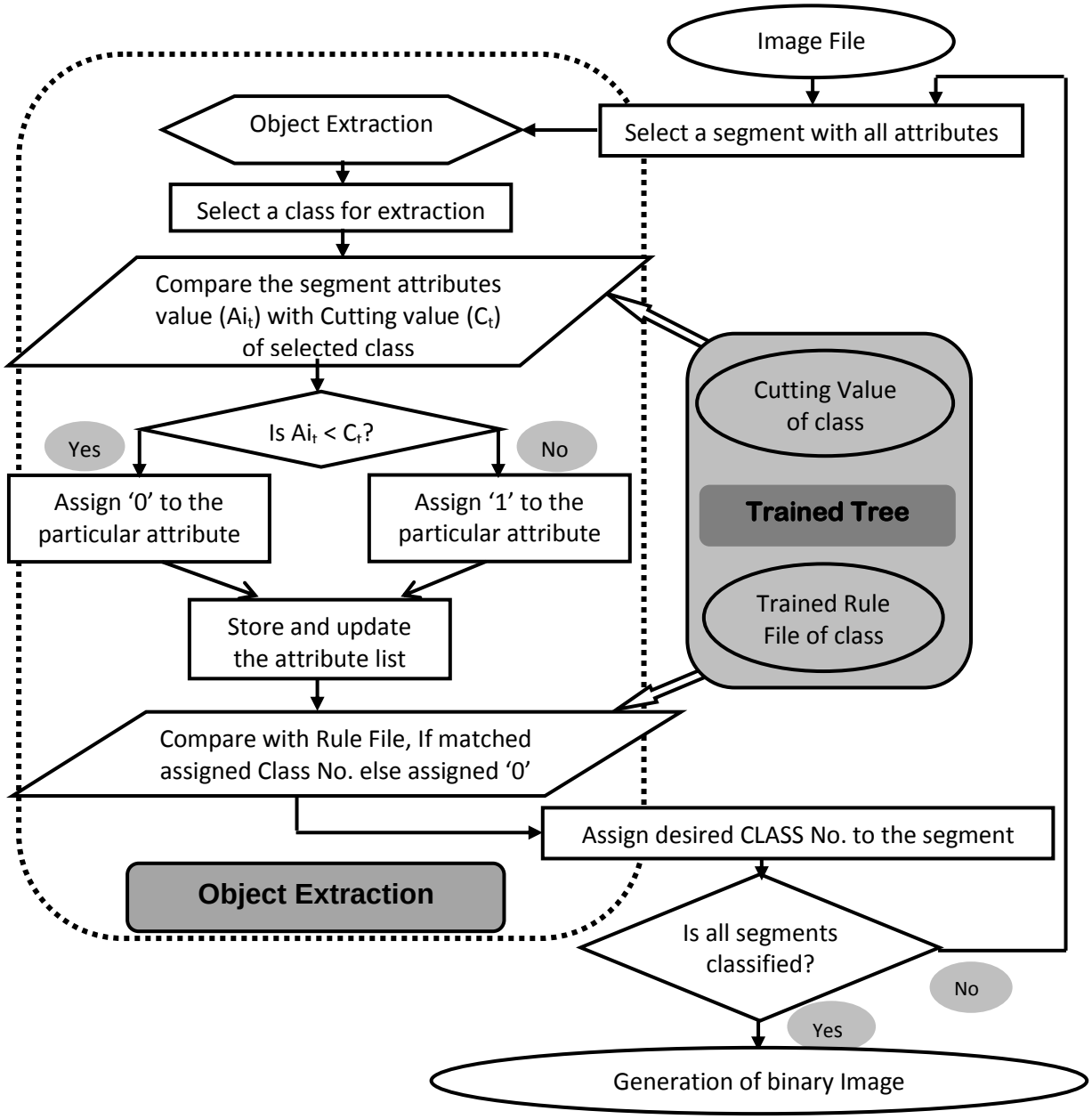

Figure 7.4**:** Flow chart of methodology for object extraction.

7.7 Results and Analysis

7.7.1 Object Extraction: Study Area-I

7.7.1.1 Quick-bird Pan-Sharpened Image

Attribute Selection

In the segmented Pan-sharpened image, each segment may belong either to the desired object or to the background. From each segmented image, 32 segments as already discussed in chapter 6 have been taken as training samples. These samples are collected from both objects as well as background. Segmented image-I is used to extract linear feature by considering one object at a time. When extracting the metallic road, 5 samples belonging to this are considered as object, remaining 27 samples (belongs to other objects and nonmetallic road) are considered as background. Next, when nonmetallic road is to be extracted, 4 samples belonging to it are considered as object and the rest 28 samples are taken as background. Segmented image-II is used to extract regular shaped features such as residential and shadows. For the class residential, number of the object and background samples are 5 and 27, and for shadow it is 4 and 28 respectively. To extract irregular shaped features, segmented image-III is used. For grassland extraction, the 5 samples of grassland are considered as objects and 27 samples as background. While for tree and barren land the number of samples for an object and background are 4 and 28, for water it is 2 and 30 samples, respectively.

All the 100 attributes as described in Table 6.7, have been assigned ranks according to their gain ratio. The attribute that gives the highest gain ratio is selected as the first candidate attribute for splitting. The rank of an attribute may vary from object (compact) to object (linear) (e.g. attribute rank for compactness and shape index are 1 and 2 for metallic road, while for residential its rank are 25 and 49 respectively).

The tree has been generated by considering the splitting decision and ranked attributes of training samples. The combined decision tree-ROC curve approach has been applied to select the important attributes. In this way, eight individual trees have been generated, one for each class and trained for extracting the classes. It has been found that out of 100 ranked attributes, maximum 20 attributes are required for extracting metallic road while only 5 attributes are required for extracting non-metallic

road, 9 attributes are required for extracting residential. Shadow and tree can be extracted with 15 attributes whereas 12 attributes are required for grassland extraction, 10 attributes are used for barren land and 4 attributes are required for extracting water body from the image. The attributes for extracting each object in order of their importance are given in Table 7.1. In this table, the selected attributes for extracting each object individually are highlighted with a gray shade.

Two curves, the ROC curve and the attribute selection curve with common X-axis have been drawn. The ROC curve has been plotted between the TPR on Y-axis and FAR on X-axis, while the attribute selection curve has been plotted between the attributes on secondary Y-axis and FAR on X-axis. In case of attribute selection, the ROC curve has been used to find out the value of FAR on the X-axis at the specific value of TPR and the second curve uses that FAR value to find the number of selected attributes on secondary Y-axis. The plotted curves are shown in Figure. 7.5 (a) to (h).

It is evident from the ROC curve that initially the TPR increases as attributes are included up to selected value, but it decreases steadily with the further inclusion of more attributes. The shape of the plotted curve demonstrates that the FAR increases rapidly when the number of attributes decreases from the selected value and it decreases gradually with increase in number of attributes. The square box at the point on the ROC curve in graphs (Figure. 7.5 (a) to (h)) represents the selected attribute, which shows that for selected attributes maximum TPR with a minimum value of FAR is obtained. Analysis of ROC curve shows that the objects residential, shadow and water follow the ideal characteristic of ROC and hence perfect extraction may be obtained. In addition, for objects trees and barren land, the value of TPR is quite low whereas the value of FAR is high at selected attributes, thus reducing the accuracy of extraction. It has also been seen that for objects grassland, metallic and nonmetallic road, the value of TPR is high and FAR is quite low at selected attributes thereby, producing high extraction accuracy.

Table 7.1: Rank wise position of first 20 selected attributes for each class combined from the three segmented images (selected attributes in gray shade and the numbers represents the attribute Serial Number in Table 6.7).

	Segmented image-I		Segmented image-II		Segmented image-III			
Rank	Metallic road	Non-metallic road	Residential	Shadow	Grassland	Trees	Barren Land	Water
1	81	78	2	5	100	22	36	77
2	85	4	11	20	3	2	20	41
3	77	42	21	24	2	100	34	58
4	83	23	30	34	1	16	77	21
5	84	88	12	39	11	20	17	30
6	16	81	18	43	12	34	15	31
7	35	83	40	53	19	53	96	50
8	45	82	49	58	21	58	95	68
9	54	85	83	62	20	72	1	69
10	65	86	31	72	30	76	4	11
11	80	80	32	77	31	78	8	91
12	96	87	35	81	38	99	23	87
13	87	100	37	91	41	13	27	29
14	82	1	38	96	44	3	42	35
15	6	15	16	95	49	6	46	48
16	73	29	48	1	50	25	61	54
17	74	20	19	15	57	44	65	67
18	97	72	50	60	61	63	80	73
19	4	77	51	8	63	64	84	10
20	17	95	54	46	64	87	82	90

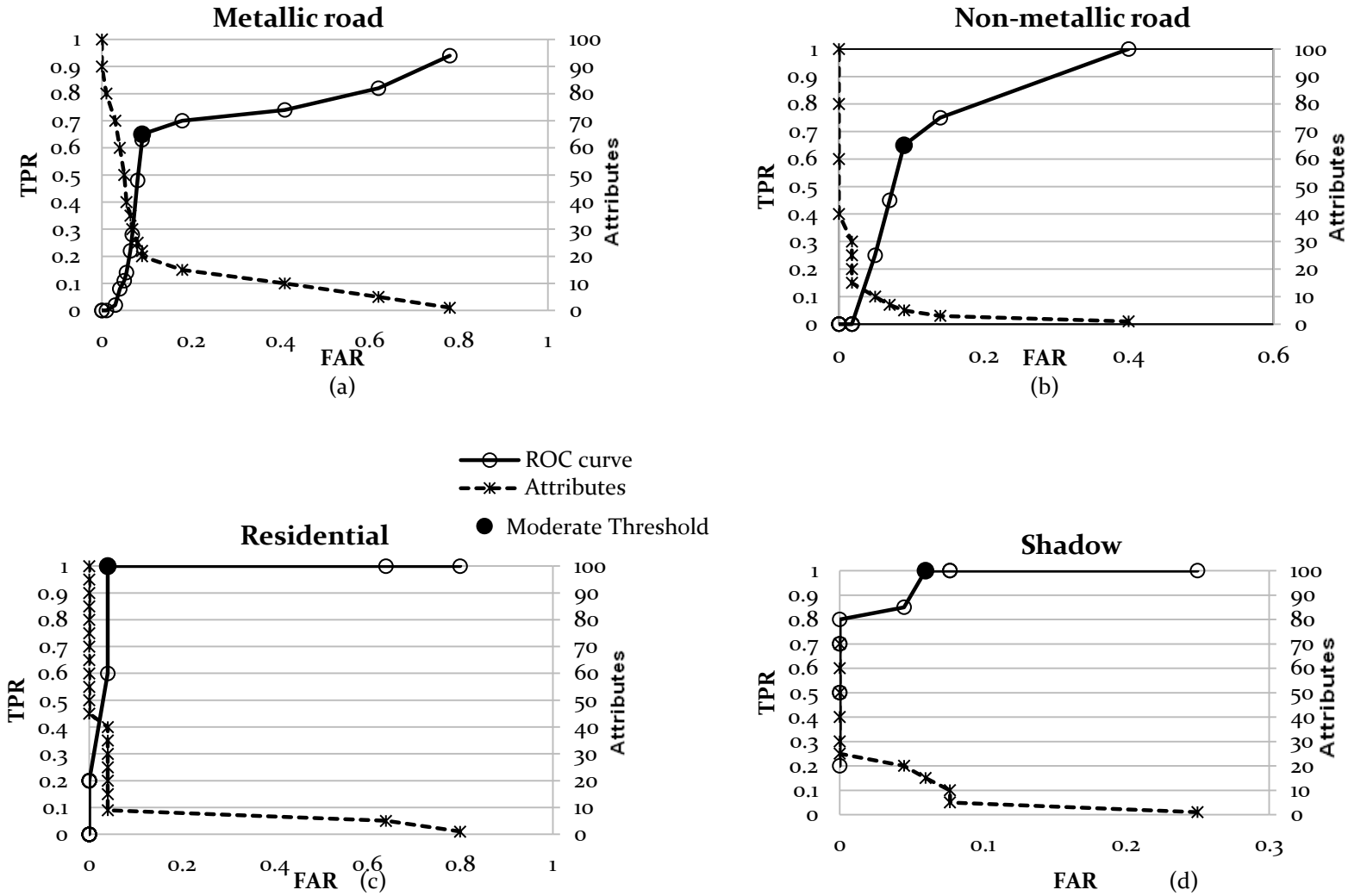

Figure 7.5: ROC curve and attribute selection curve for moderate threshold selection from Quick-bird Pan-sharpened image for; (a) Metallic road, (b) Non-metallic road, (c) Residential, (d) Shadow.

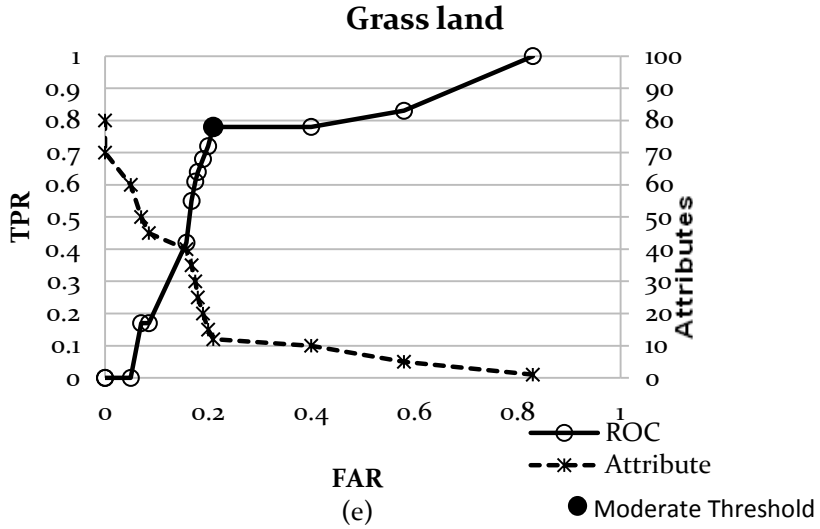

(e)

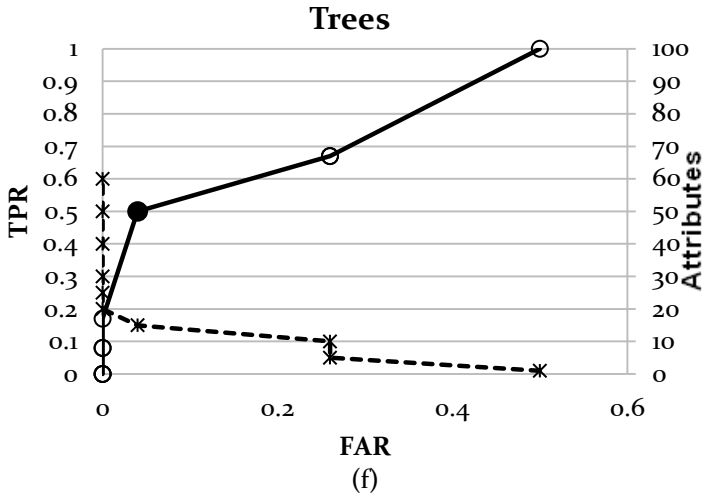

(f)

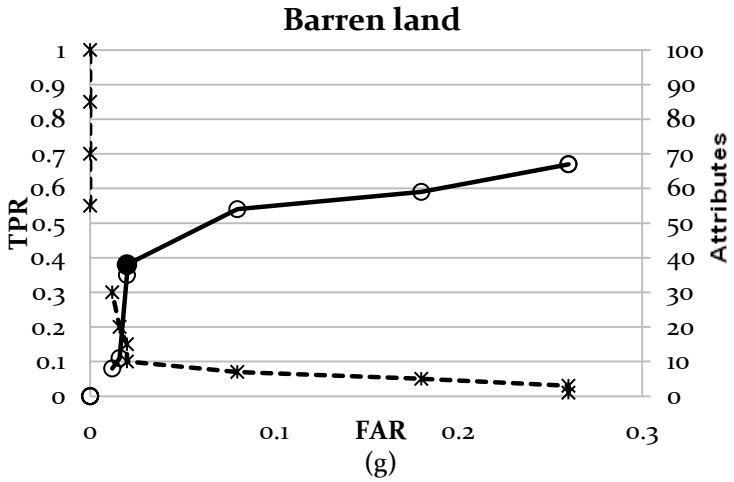

(g)

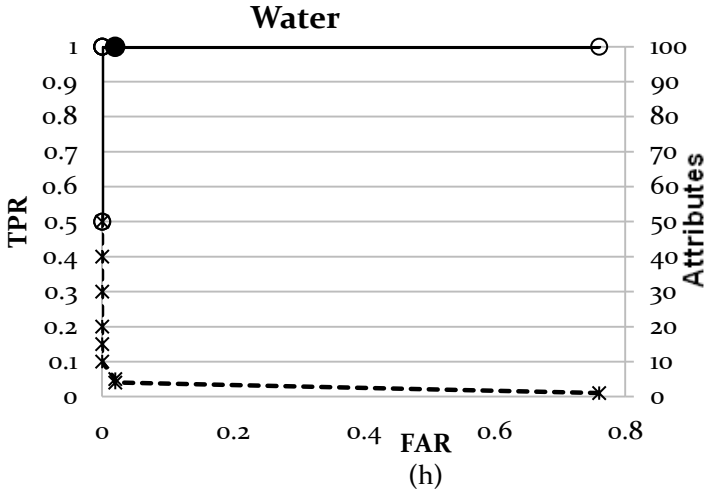

(h)

Figure 7.5: ROC curve and attribute selection curve for moderate threshold selection from Quick-bird Pan-sharpened image for; (e) Grassland, (f) Tree, (g) Barren land, and (h) Water.

Extraction of Objects

The bar chart shown in Figure 7.6 (a) represents the number of selected attributes used to extract each object. Using this set of attributes eight separate decision trees have been generated. Figure 7.6 (b) displays a trained decision tree for the extraction of non-metallic road by treating the remaining classes as background. Linear feature (nonmetallic road) has been extracted accurately using five selected attributes (compactness, shape index, brightness, rectangular fit and border length) from segmented image 'Seg-PS-I'. In general, the non-metallic road is made of cement, soil or tiles. It is linear in shape, appear whitish bright and having the smooth texture feature. It has been found that for extracting non-metallic road, compactness has the highest gain ratio thus, considered as the root node attribute to extract segments of non-metallic road object. The segments for which compactness attributes values are less than their thresholds belong to non-compact object. The next important attribute is shape index. The shape index attribute of all non-compact shape segments has been compared with its cutting value. The segments with high shape index value are treated as a linear feature and belong to metallic and non-metallic roads. Next, the segments that fulfill the shape index criteria have been checked for brightness value to separate both types of roads. Non-metallic roads have high brightness value as compared to metallic road, thus linear segments that have high brightness value than its threshold may belong to non-metallic roads. Further, some residential rooftops also appear white, but rectangular and compact in shape, hence, the rectangular fit attributes have been selected to disregard the segments of bright compact rooftop. The rectangular fit attribute values of the segments have been compared with its cutting value, the segments with low value of attribute belong to the linear feature. Finally, all bright linear features are passed through the attribute mean-diff-to-neighbor to extract the metallic roads, the segments having high value of mean-diff-to-neighbor than its cutting value have been assigned as non-metallic road object. Thus, a decision tree with selected attributes for extracting non-metallic road has been generated and trained.

Similarly, separate decision trees with selected attributes have been used for the extraction of each individual object. The decision trees with all (100) attributes have also been used for extracting the objects. All three segmented images; Seg-PS-I, II and III have been taken as the input for object extraction. The extraction qualities of objects with selected attributes and with all attributes have also been assessed.

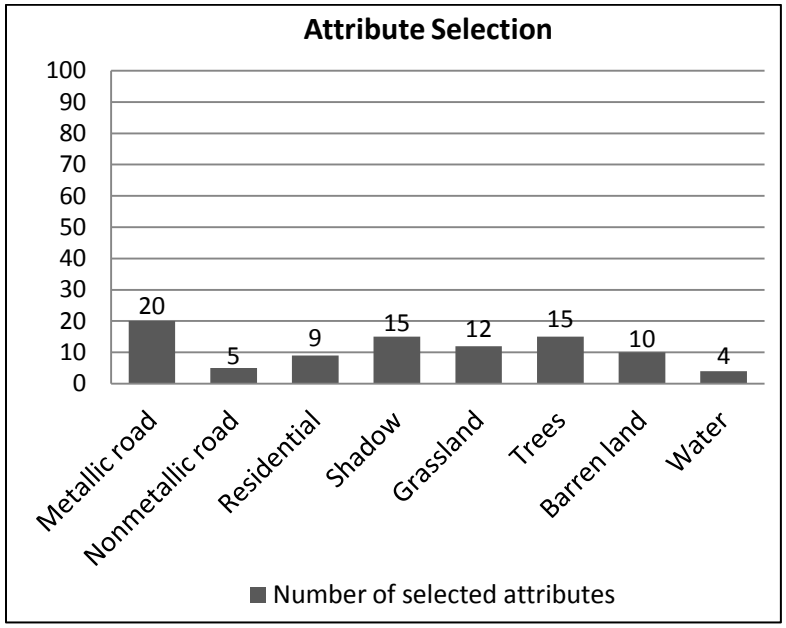

(a)

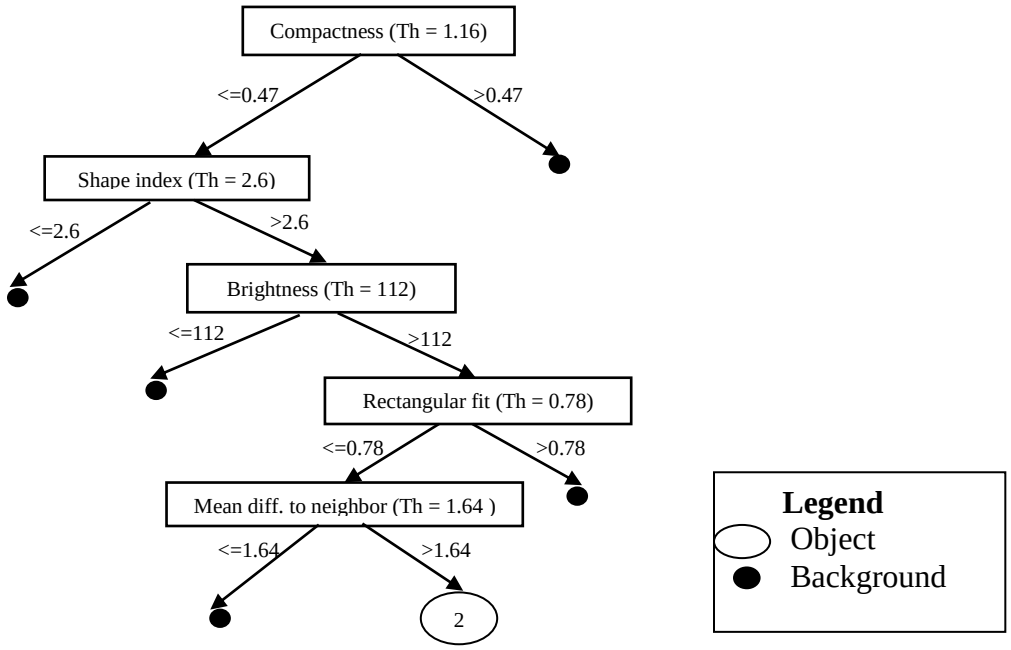

(b)

Figure 7.6: (a) Bar chart of class wise selected attributes used for object extraction (b) shorted decision tree to extract linear object (non-metallic road).

Assessment of Object Extraction Quality

A total of 76, 78 and 78 segments of all classes from Seg-PS-I, II and III respectively, as shown in Table 7.2, have been used as testing samples to assess the accuracy of the object extraction. The object has been extracted using the selected attributes and value of TPR and FAR for extraction has been calculated.

ROC curve has been used to assess the quality of the object extraction when it has been extracted using all attributes. From the analysis of the ROC curve, it has been observed that quality of object extraction depends on the variation in number of attributes. It has also been observed that with a certain number of attributes, the quality of object extraction is high. Whereas using less number of attributes, the object extraction quality reduces, it is because number of background segments may wrongly get classified as the desired object. Also if more number of attributes is used, some segments of the object may not be extracted. Therefore, the quality of object extraction also depends on the number of attributes selected by ROC curve as discussed earlier.

Table 7.2: Object wise number of testing samples of Quick-bird Pan-sharpen image.

Desired object	**Seg-PS-I**	**Seg-PS-II**	**Seg-PS-III**
Metallic road	10	10	11
Non metallic road	5	6	5
Residential	16	15	15
Shadow	20	20	18
Grassland	5	6	7
Trees	10	10	10
Barren land	8	9	8
Water	2	2	2

The TPR and FAR values have been calculated for testing samples of all eight objects. The selected attributes and their corresponding TPR and FAR values, for both training and testing image, are given in Table 7.3. It has been observed that the overall quality of the extracted objects, namely, residential (i.e., TPR=1, FAR=0.04), shadow (i.e., TPR=1, FAR=0.06) and water (i.e., TPR=1,

FAR=0.02) is very high, while trees and barren land objects have lowest quality of extraction. For each extracted object from training and testing samples, value of TPR and FAR at selected attributes have been compared. Change in TPR and FAR values for testing samples with training samples estimate the deviation in extraction quality of each object. From the results shown in Table 7.3, it has been observed that in the final extracted binary image, maximum degradation has been seen in extraction quality of grassland, while a small decrease in the extraction quality of metallic and non-metallic road, trees and barren land has been observed.

The image objects are further extracted using all attributes in the order of their ranking. It has been found that the extraction quality of objects is the lowest when they are extracted using all attributes. The ROC curves for assessment of object extraction quality have been shown in Figure 7.7.

Table 7.3: Quality comparison of extracted object with selected and with all attributes.

Object	**No. of selected attributes**	**Training sample with selected attributes**		**Testing sample with selected attributes**		**Testing sample with 'All (100)' attributes**	
		TPR	**FAR**	**TPR**	**FAR**	**TPR**	**FAR**
Metallic road	20	0.58	0.04	0.56	0.06	0.07	0.05
Non metallic road	5	0.65	0.09	0.62	0.10	0.08	0.05
Residential	9	1.00	0.04	1.00	0.05	0.11	0.07
Shadow	15	1.00	0.06	1.00	0.06	0.07	0.03
Grassland	12	0.75	0.21	0.72	0.26	0.07	0.05
Trees	15	0.45	0.04	0.41	0.07	0.01	0.04
Barren land	17	0.52	0.21	0.48	0.24	0.04	0.08
Water	4	1.00	0.02	1.00	0.03	0.05	0.03

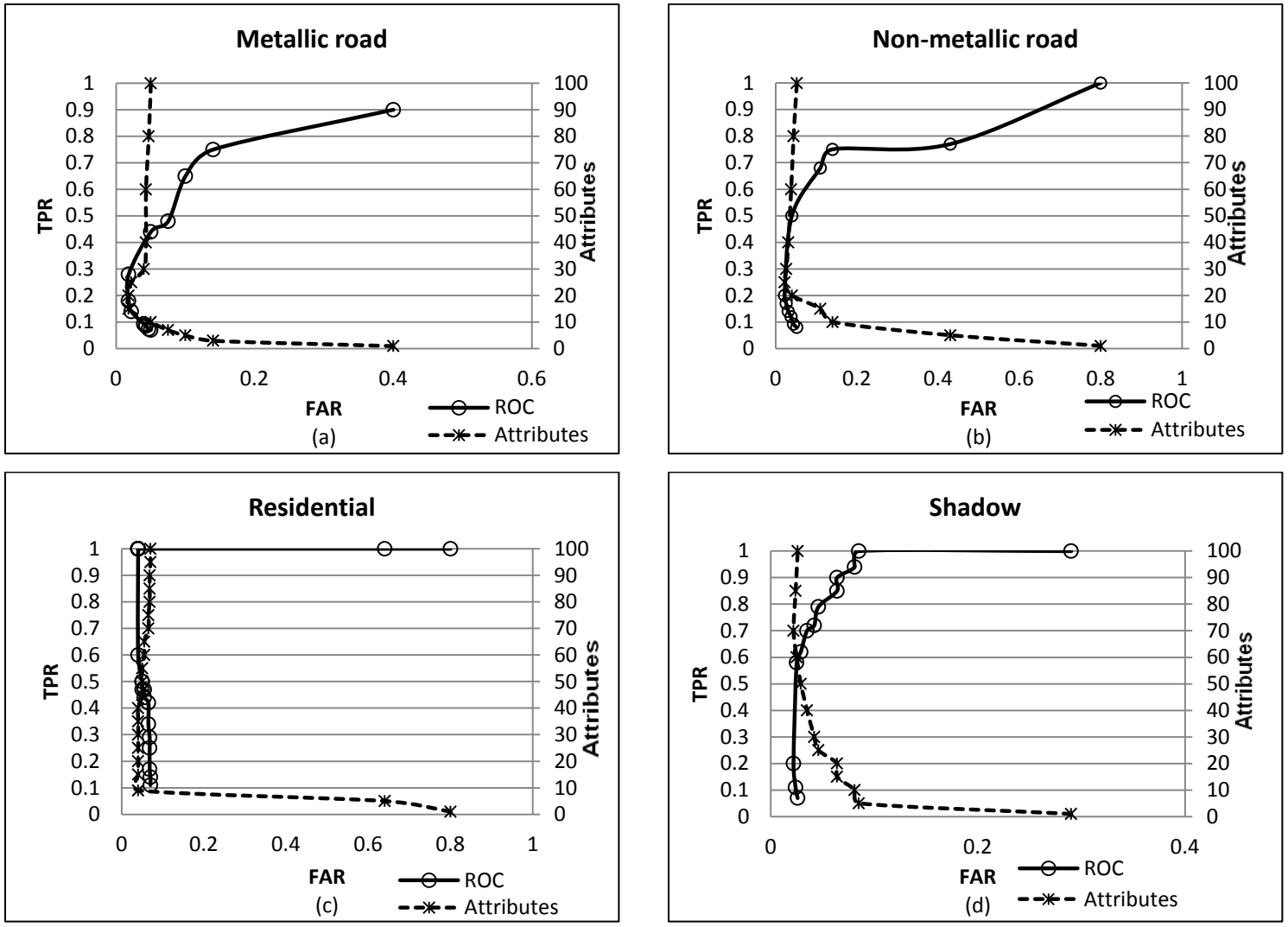

Figure 7.7: ROC and attribute selection curves for; (a) Metallic road, (b) Non-metallic road, (c) Residential, (d) Shadow.

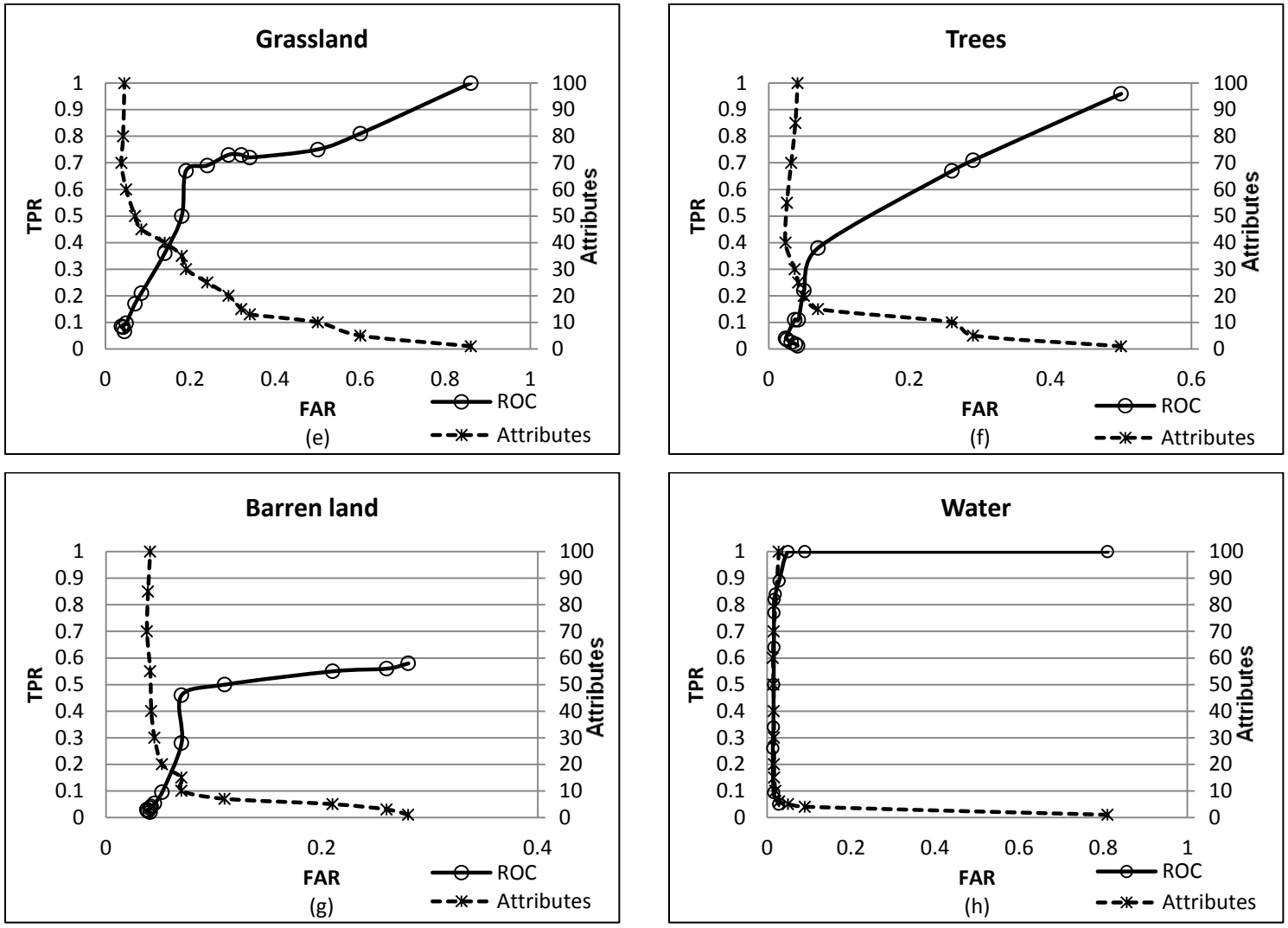

Figure 7.7: ROC and attribute selection curves for; (e) Grassland, (f) Trees, (g) Barren land, and (h) Water.

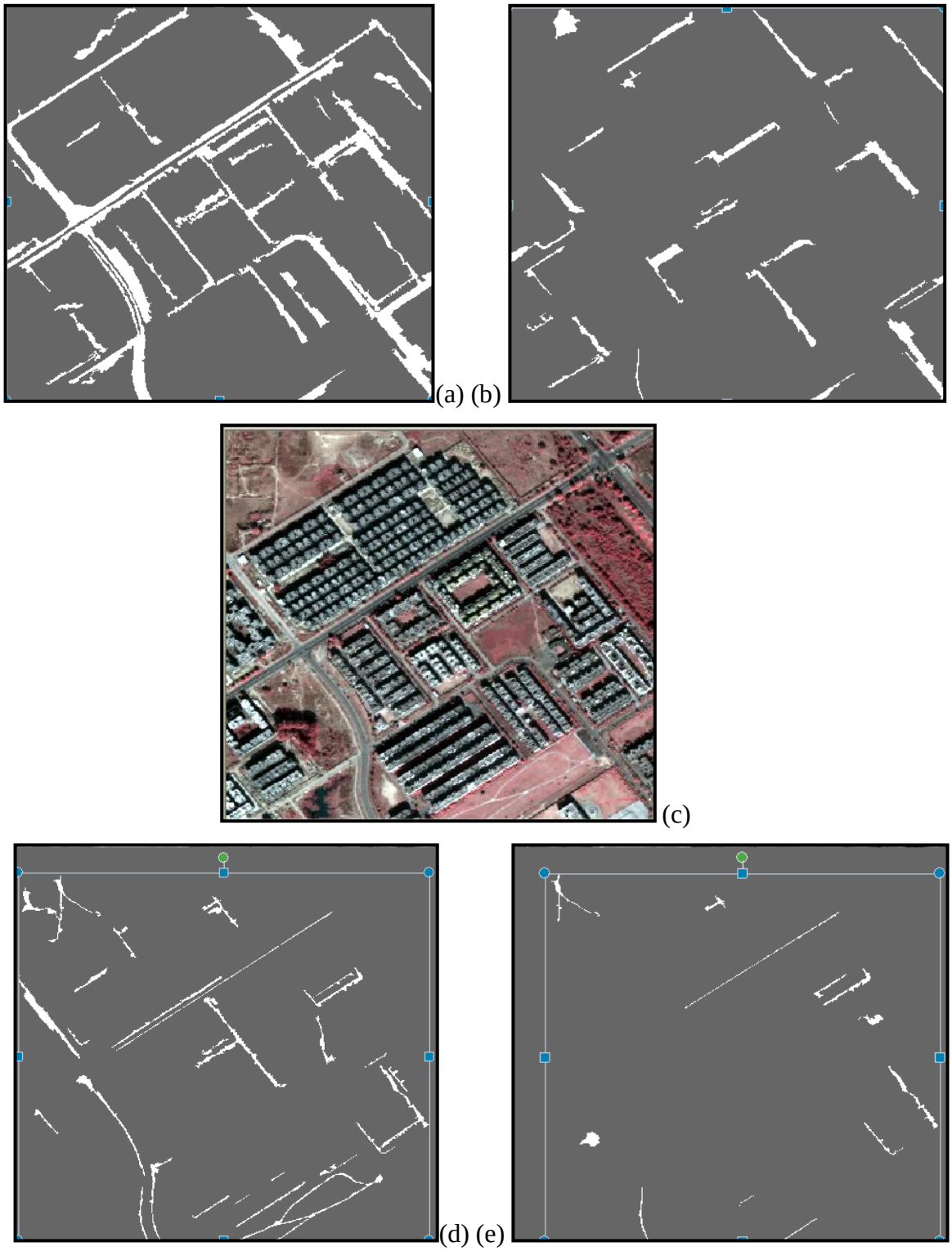

Figure 7.8: Extracted metallic road (a) with 20 attributes, (b) with all 100 attributes, (c) original image, and extracted nonmetallic road (d) with 5 attributes and (e) with all 100 attributes.

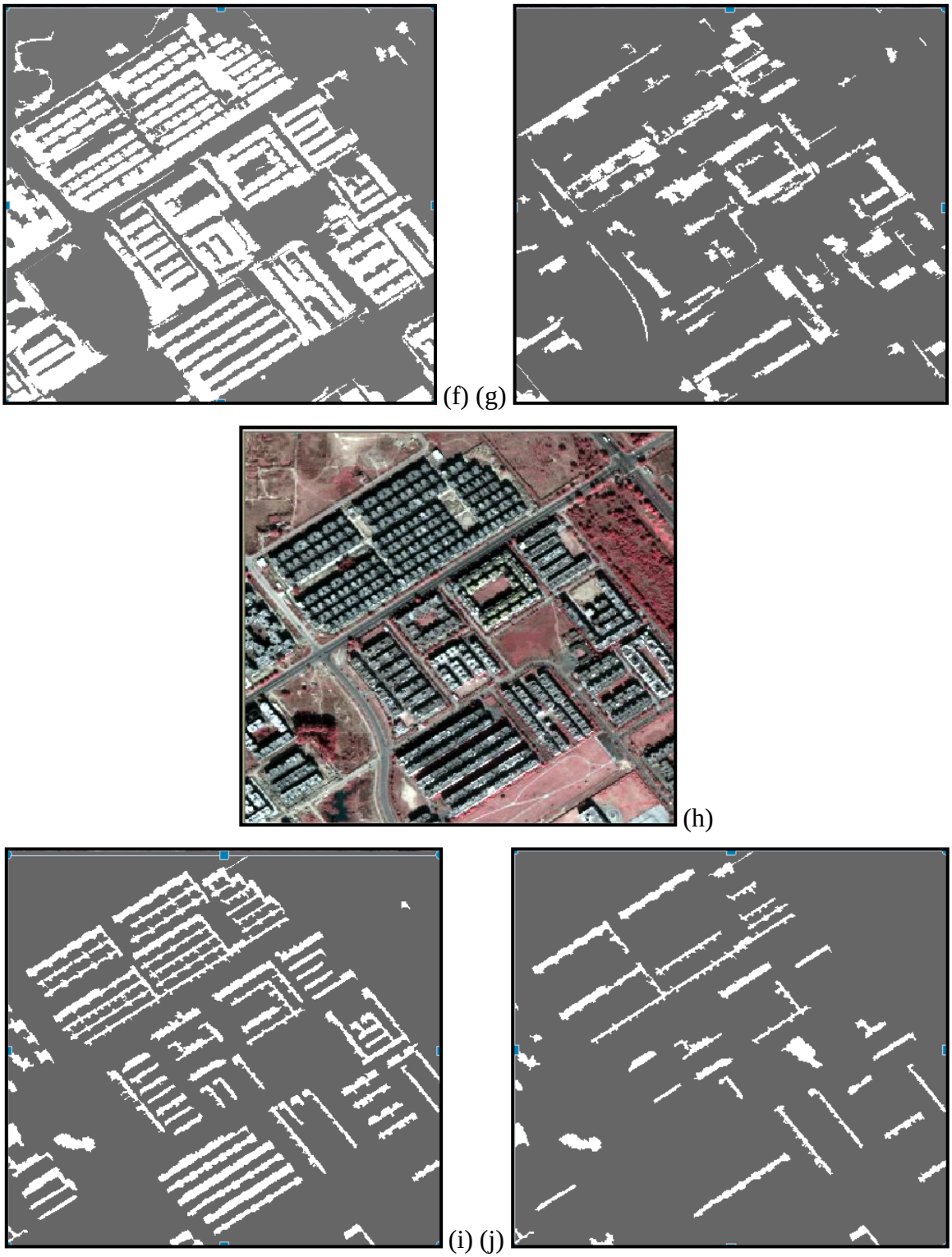

Figure 7.8: Extracted residential (f) with 9 attributes, (g) with all 100 attributes (h) original image, and extracted shadow (i) with 15 attributes and (j) with all 100 attributes.

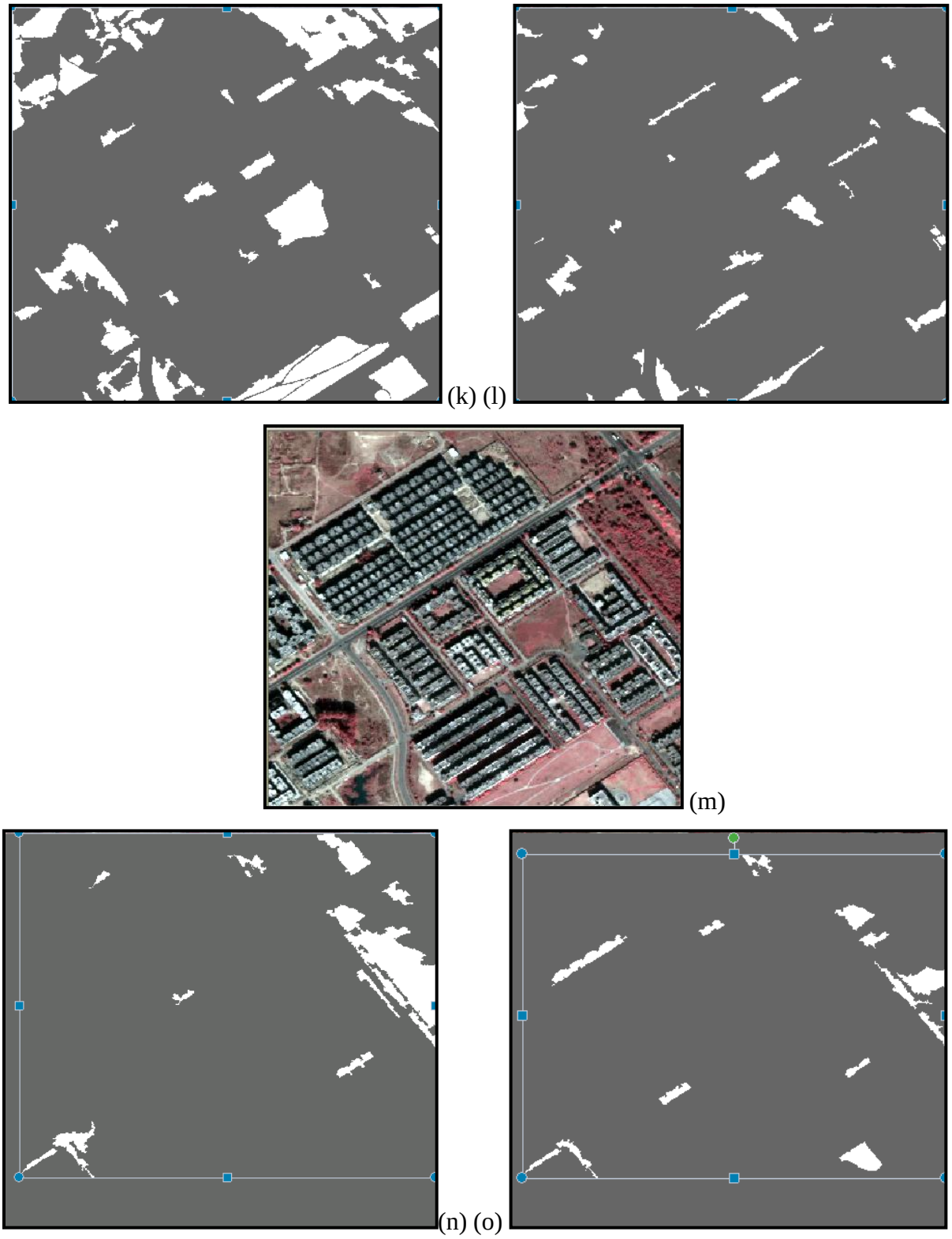

(k) (l) (m) (n) (o)

Figure 7.8: Extracted grassland (k) with 12 attributes, (l) with all 100 attributes (m) original image, and extracted trees (n) with 15 attributes and (o) with all 100 attributes.

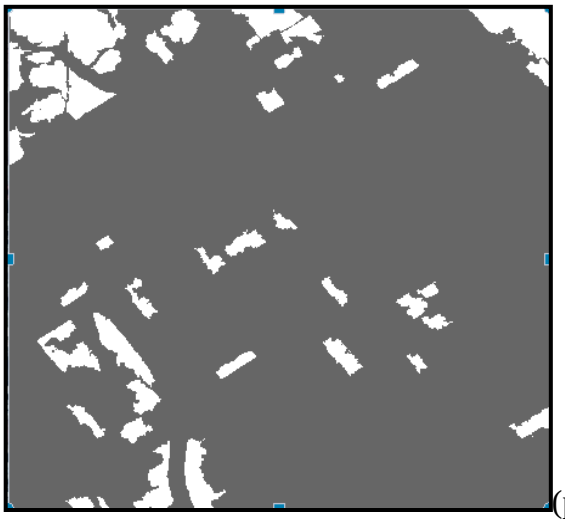
(p)
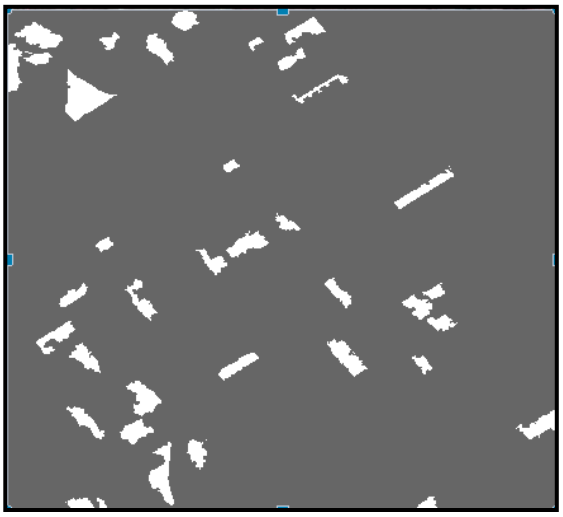
(q)


(r)

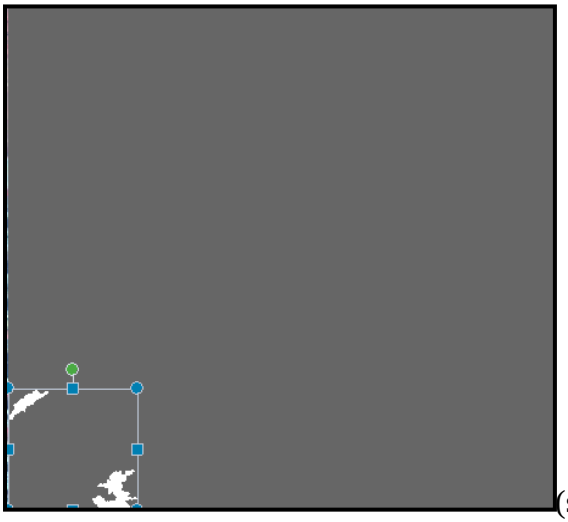
(s)
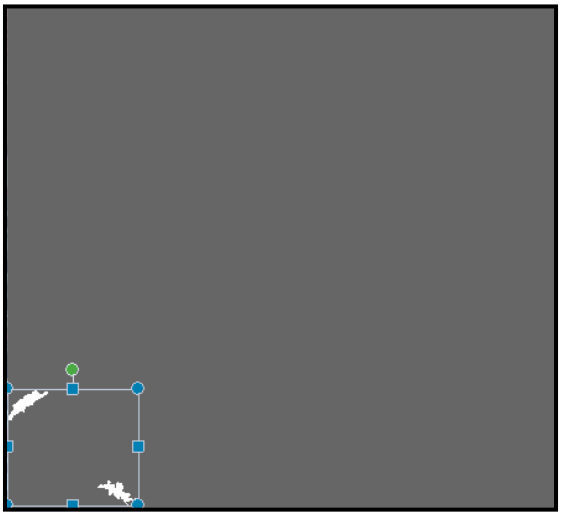
(t)

Figure 7.8: Extracted barren land (p) with 10 attributes, (q) with all 100 attributes, (r) original image, and extracted water body (s) with 4 attributes and (t) with all 100 attributes.

The ROC curves shown in Figure 7.7 have been drawn by using the testing samples. It has been observed that the ROC curves follow the same trend as obtained by using training samples, but the value of TPR is slightly less in comparison to that of training samples for every attribute. The graph also shows that using less number of attributes, objects are extracted with very high accuracy but at the same time also suffer with high noise. However, the extraction rate decreases with the increase in the number of attributes and falls to its minimum when the object has been extracted using all attributes.

The binary images, as shown in Figure 7.8, have been generated for objects extracted using selected attributes as well as using all attributes. The binary image shows that few segments of other classes are wrongly classified as an object when extraction has been performed with selected attributes. However, a number of segments that belong to the object have not been extracted as an object when using all 100 attributes. It can be seen from these binary images that the objects residential, shadow and water have been extracted very accurately, while worst accuracy has been obtained for the object barren land.

7.7.1.2 Object Extraction from Quick-bird Pan Image

Attribute Selection

Similar to Quick-bird Pan-sharpened image, Quick-bird image Pan has also been segmented using three sets of parameters. These segmented images have been used for attribute selection. A number of training segments, as described in the previous chapter, has been considered to extract desired objects from the image. Segmented image (Seg-P-I) having focus on linear objects includes 7 samples of metallic road, 4 of non-metallic road and remaining 33 samples of other objects. To extract regular shape compact objects from Seg-P-II image, 8 samples of residential, 10 for shadow and rest 29 samples belonging to other objects have been considered. Seg-P-III has been used to extract irregular shape compact object. Here, 6 samples of grassland, 5 of trees, 6 of barren lands, 3 of water and remaining 26 samples of other objects have been considered.

All 43 generated attributes, as given in Table 6.13, have been assigned the rank according to their splitting importance for object extraction. The rank wise attributes to extract objects from Quick-bird Pan image are tabulated in Table 7.4. In comparison to Pan-sharpened image, here more attributes are required to extract each object. In Table 7.4, only first 25 attributes have been tabulated. It has been observed that for the extraction of metallic road from image, 21 attributes are required, while 13 attributes are required for extracting non-metallic road, 16 attributes are required for residential, 17 attributes are required for extraction of shadow and barren land. Grassland can be extracted with the set of 18 attributes, 24 attributes are needed for extracting trees and 10 attributes are required for the extraction of water from the image. The selected attributes of an object have been represented in gray shade in Table 7.4.

Class-wise ROC curves for attribute selection to extract different object from the Panchromatic Quick-bird image have been drawn in Figure 7.9 (a) to (h). Analysis of ROC curves shows that non-metallic road, residential, shadow and water objects have high value of TPR and low FAR value of selected attributes, and thus produce high extraction quality. For metallic road, grassland, trees and the barren land, the value of TPR is quite low whereas the value of FAR is high at selected attributes, which reduces the accuracy of object extraction. Additionally, from the ROC curve and attribute selection curve, it can also be observed that objects tree and barren land have produced the worst extraction quality with low TPR and high FAR. Further, the reduction in extraction quality is due to the fact that Pan is a single band image. So, there are less number of attributes available to represent a class and thus confusion may occur between the desired object extraction and other objects. Although, more number of attributes has been selected for object extraction, in comparison to that of Pan-sharpened image, but the extraction quality is comparatively less.

Table 7.4: Rank wise position of first 25 selected attributes for each class (selected attributes in gray shade) combined from the three segmented images.

	Segmented image-I		Segmented image-II		Segmented image-III			
Rank	Metallic road (1)	Non-metallic road (2)	Residential (3)	Shadow (4)	Grassland (5)	Trees (6)	Barren Land (7)	Water (8)
1	27	1	2	5	34	22	15	17
2	22	4	11	1	38	2	36	41
3	9	42	12	24	6	1	35	43
4	13	23	16	34	8	16	34	1
5	10	18	18	39	11	20	37	36
6	16	21	17	43	12	34	14	38
7	35	23	21	33	17	23	16	40
8	43	40	9	28	23	18	18	7
9	14	35	36	42	35	35	11	39
10	1	26	31	12	36	36	17	11
11	19	30	32	37	31	38	38	13
12	2	27	35	20	28	41	39	37
13	7	2	37	9	41	43	24	33
14	30	5	38	11	18	13	42	35
15	6	15	40	29	2	17	40	18
16	12	18	10	17	9	4	2	16
17	17	16	13	18	10	12	4	34
18	18	15	14	40	18	5	5	42
19	42	43	10	38	40	28	13	12
20	37	39	3	36	16	40	43	15
21	36	37	34	4	1	8	29	10
22	30	18	43	16	37	10	12	2
23	34	30	42	10	43	42	9	3
24	38	38	25	13	28	25	29	23
25	33	36	29	41	19	9	3	28

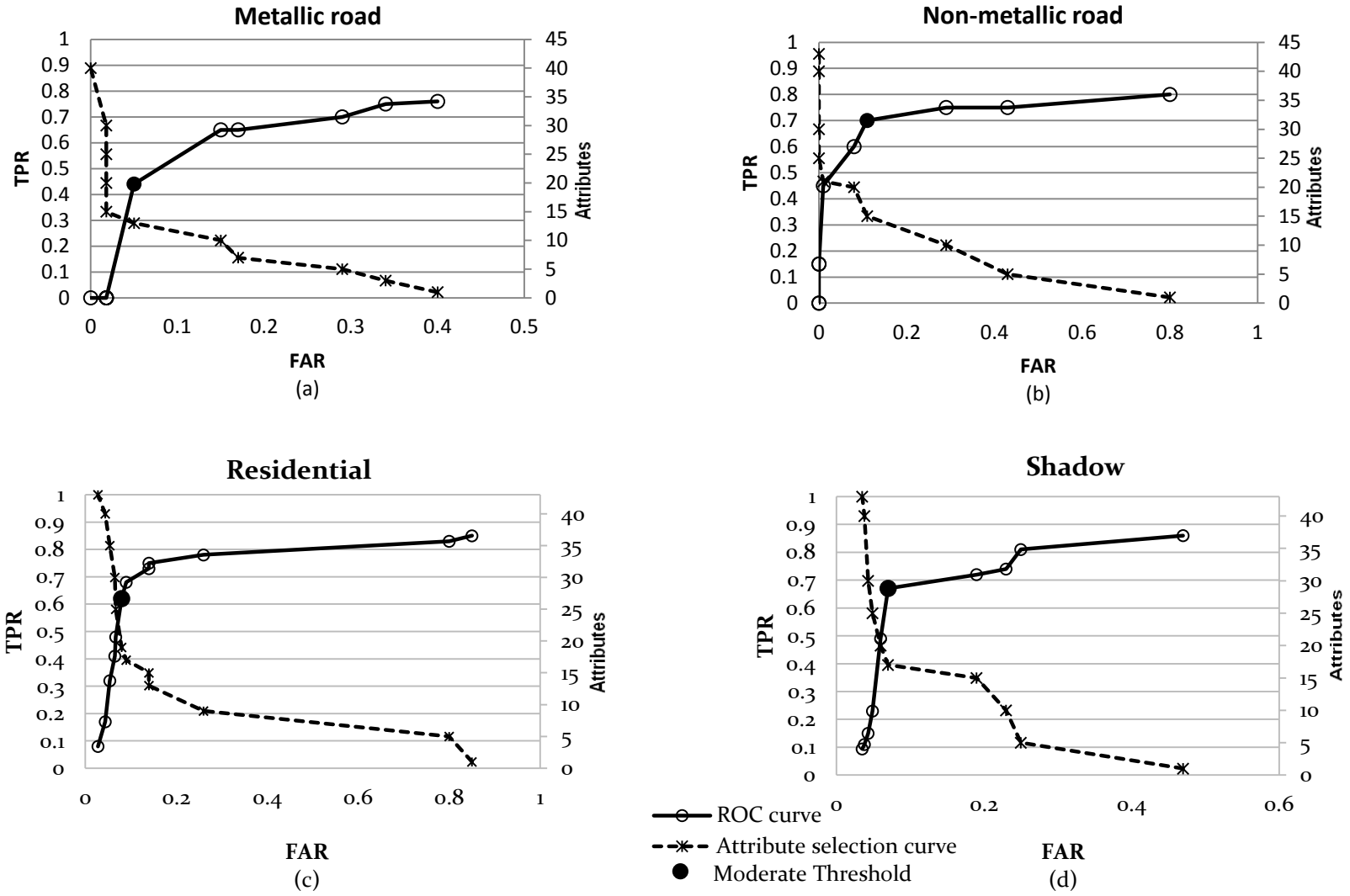

Figure 7.9: ROC curve and attribute selection curve for moderate threshold selection from Quick-bird Pan image for; (a) Metallic road, (b) Non-metallic road, (c) Residential, (d) Shadow.

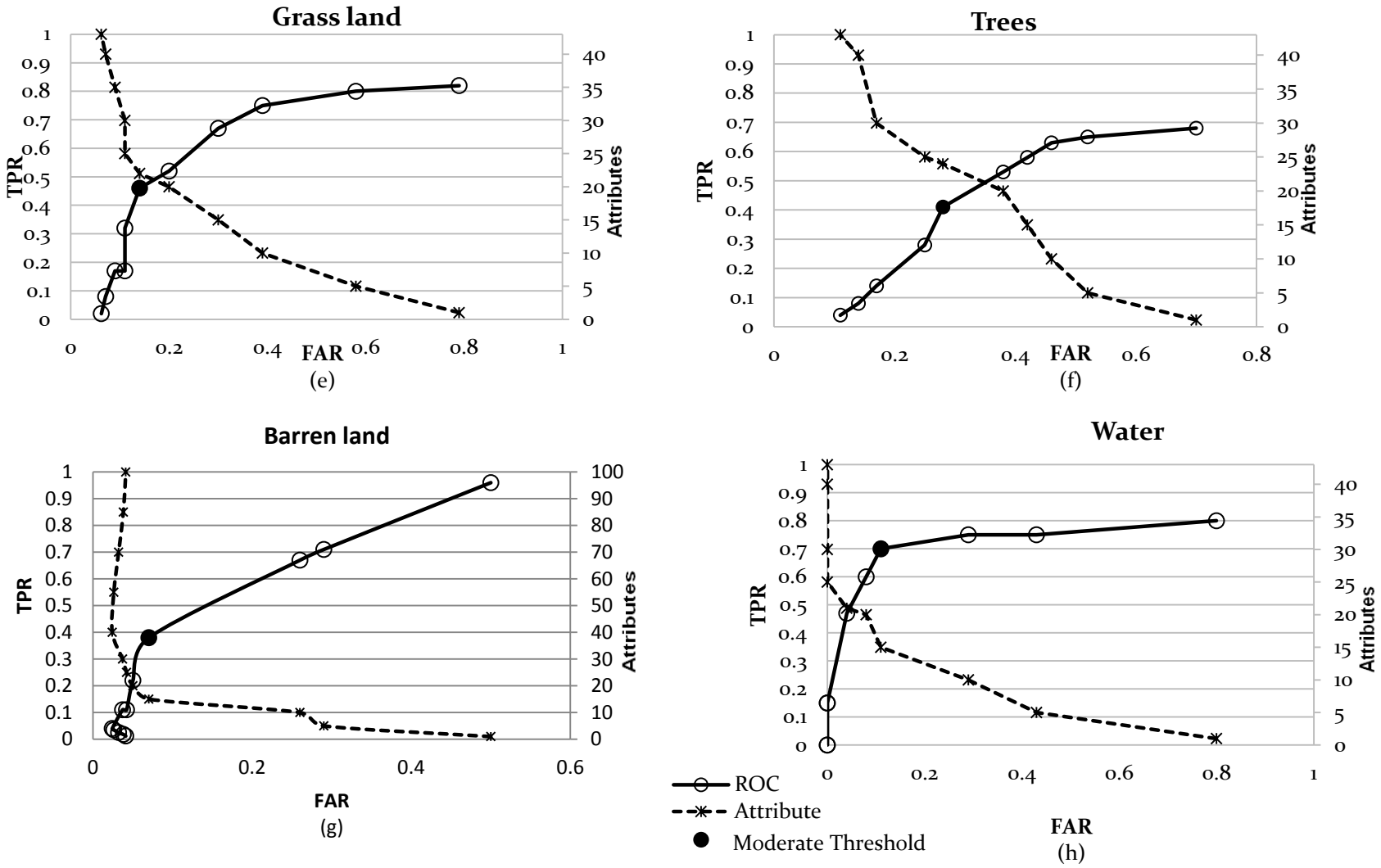

Figure 7.9: ROC curve and attribute selection curve for moderate threshold selection from Quick-bird Pan image for; (e) Grassland, (f) Trees, (g) Barren land and (h) Water.

Extraction of Objects

C4.5 algorithm has been applied once again to the Quick-bird Pan segmented image, for the desired object extraction using ranked attributes. A total of eight decision trees have been generated. The number of selected attributes to extract all eight objects has been represented by a bar chart as shown in Figure 7.10.

The bar chart shows the variation in the required number of attributes for various classes extraction. It has been observed that more number of attributes in comparison of Pan-sharpened image are required to extract an object from the Quick-bird Pan image.

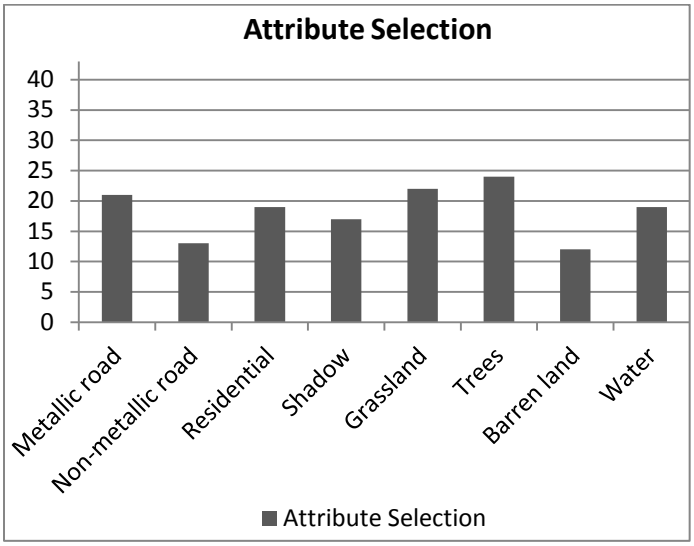

Figure 7.10: Bar chart of class wise selected attributes used for object extraction.

Assessment of Object Extraction Quality

A set of testing segments representing their actual object identification have been generated from the reference file created for high-resolution Quick-bird Pan image. It includes 80, 77 and 78 samples across all 8 objects corresponding to Seg-P–I, II and III, images respectively, as given in Table 7.5. This testing dataset has been used for the assessment of the extraction quality for every object, the assessed values are given in Table 7.6.

The ROC curve for training data has been generated at the time of attribute selection and the number of attributes for the highest fraction of TPR and FAR has been selected. The values of TPR and FAR for testing samples for the object extraction using selected number of attributes have been determined. To find the change in extraction quality and the efficiency of the generated tree, the TPR and FAR values for both training and testing samples have been compared. The result shows that the extraction quality of testing data decreases slightly. The object extraction has also been performed using all attributes and the TPR and FAR values for every attribute have been calculated. It has been found that the extraction quality of all objects decreases when extraction is done with all attributes. The ROC curves for extraction of all eight objects are as shown in Figure 7.11.

The ROC curves show that the extraction quality of objects varies with the number of attributes used for object extraction. The highest value of TPR has been obtained when extraction is done using a single attribute, but at a high FAR. The TPR as well as FAR starts decreasing by introducing more attributes. The highest extraction accuracy has been achieved when extracting objects using selected attributes. The highest extraction accuracies have been observed for non-metallic road (TPR = 0.65, FAR = 0.1), residential (TPR = 0.58, FAR = 0.1) and shadow (TPR = 0.66, FAR = 0.09), while the extraction accuracy is low for metallic road (TPR = 0.45, FAR = 0.12), grassland (TPR = 0.44, FAR = 0.19), trees (TPR = 0.35, FAR = 0.34) and barren land (TPR = 0.36, FAR = 0.08). The binary images corresponding to each object have been shown in Figure 7.12.

Table 7.5: Object wise testing samples (Quick-bird Pan image).

Desired object	**Seg-P-I**	**Seg-P-II**	**Seg-P-III**
Metallic road	11	10	9
Non metallic road	5	5	7
Residential	15	16	16
Shadow	21	22	20
Grassland	6	5	6
Trees	11	10	11
Barren land	9	7	7
Water	2	2	2

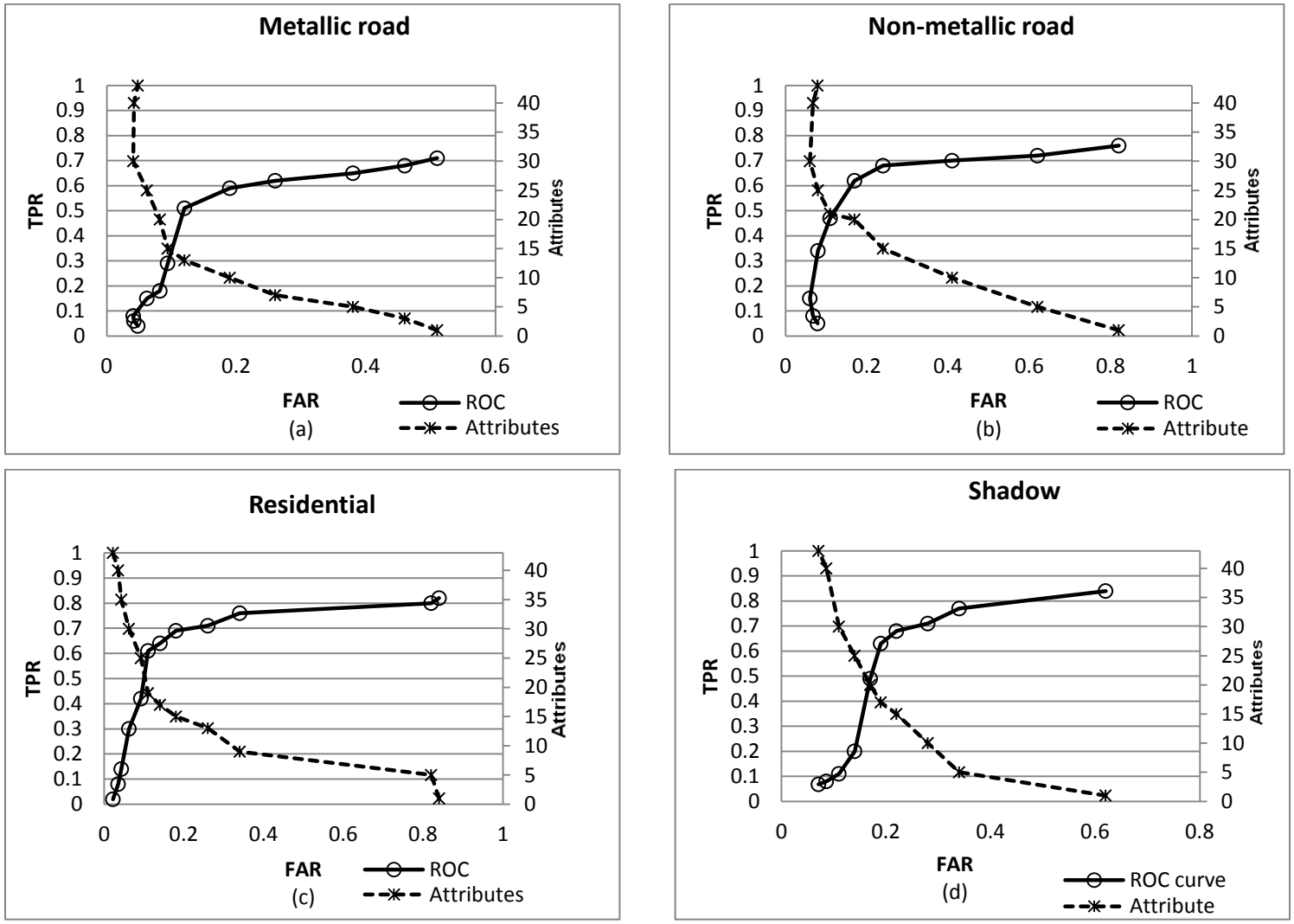

Figure 7.11: The ROC and attribute selection curves for (a) Metallic road, (b) Non-metallic road, (c) Residential, (d) Shadow.

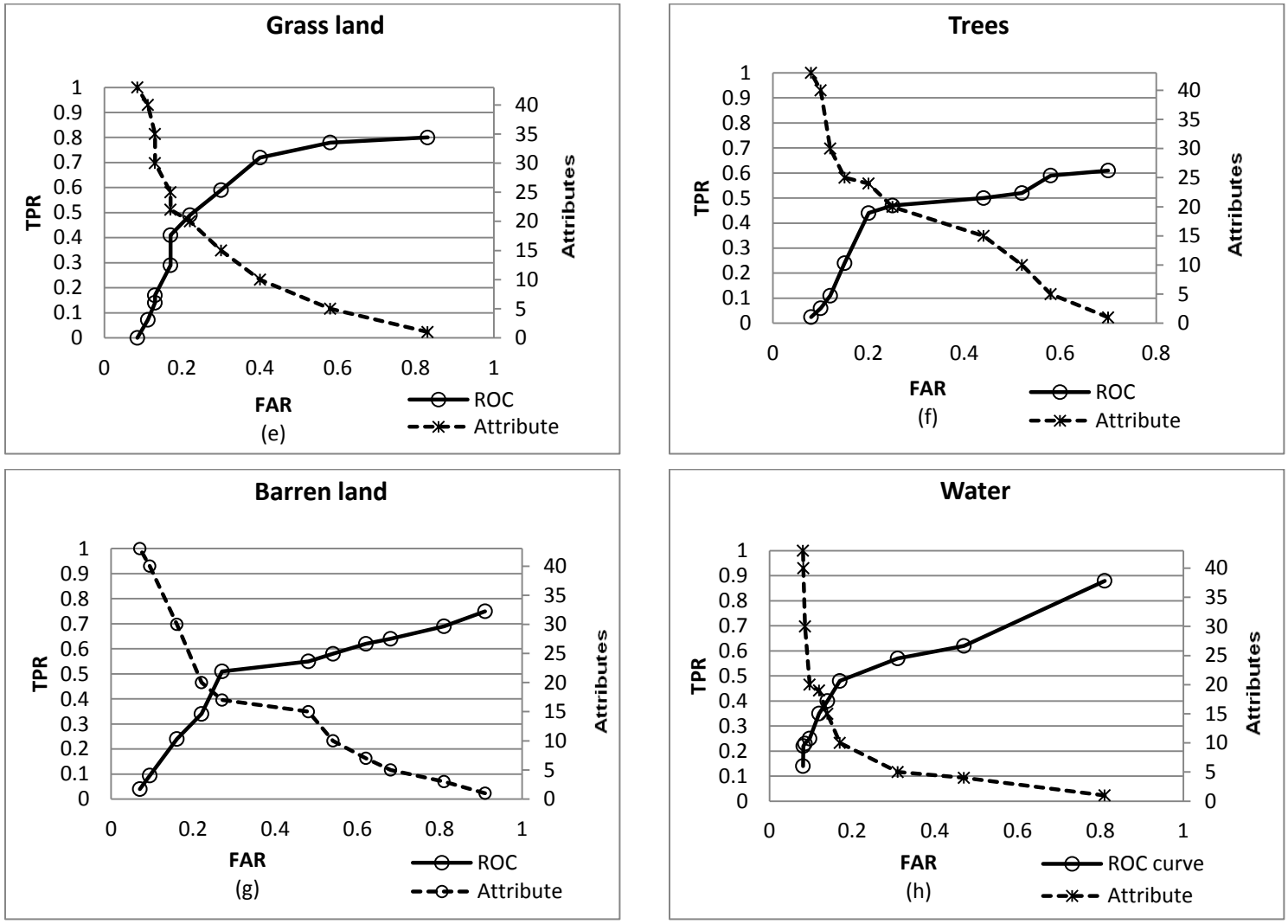

Figure 7.11: The ROC and attribute selection curves for (e) Grassland, (f) Tree, (g) Barren land and (h) Water.

Table 7.6: Quality comparison of extracted object with selected and with all attributes.

Object	No. of selected attributes	Training sample with selected attributes		Testing sample with selected attributes		Testing sample with 'All (43)' attributes	
		TPR	FAR	TPR	FAR	TPR	FAR
Metallic road	21	0.47	0.04	0.45	0.12	0.05	0.06
Non-metallic road	13	0.67	0.07	0.62	0.10	0.07	0.14
Residential	19	0.62	0.08	0.58	0.10	0.18	0.11
Shadow	17	0.68	0.07	0.66	0.09	0.16	0.07
Grassland	22	0.46	0.17	0.44	0.19	0.05	0.07
Trees	24	0.41	0.28	0.35	0.34	0.07	0.06
Barren land	12	0.38	0.02	0.36	0.08	0.02	0.04
Water	19	0.68	0.08	0.49	0.10	0.09	0.02

Binary images extracted with selected number of attributes and with all attributes have been compared. The visual inspection of binary images shows that the extraction quality of object is always high when it is extracted with selected number of attributes. Further, from the comparison of images, it is clear that a number of objects have not been extracted when extraction has been performed using all the attributes.

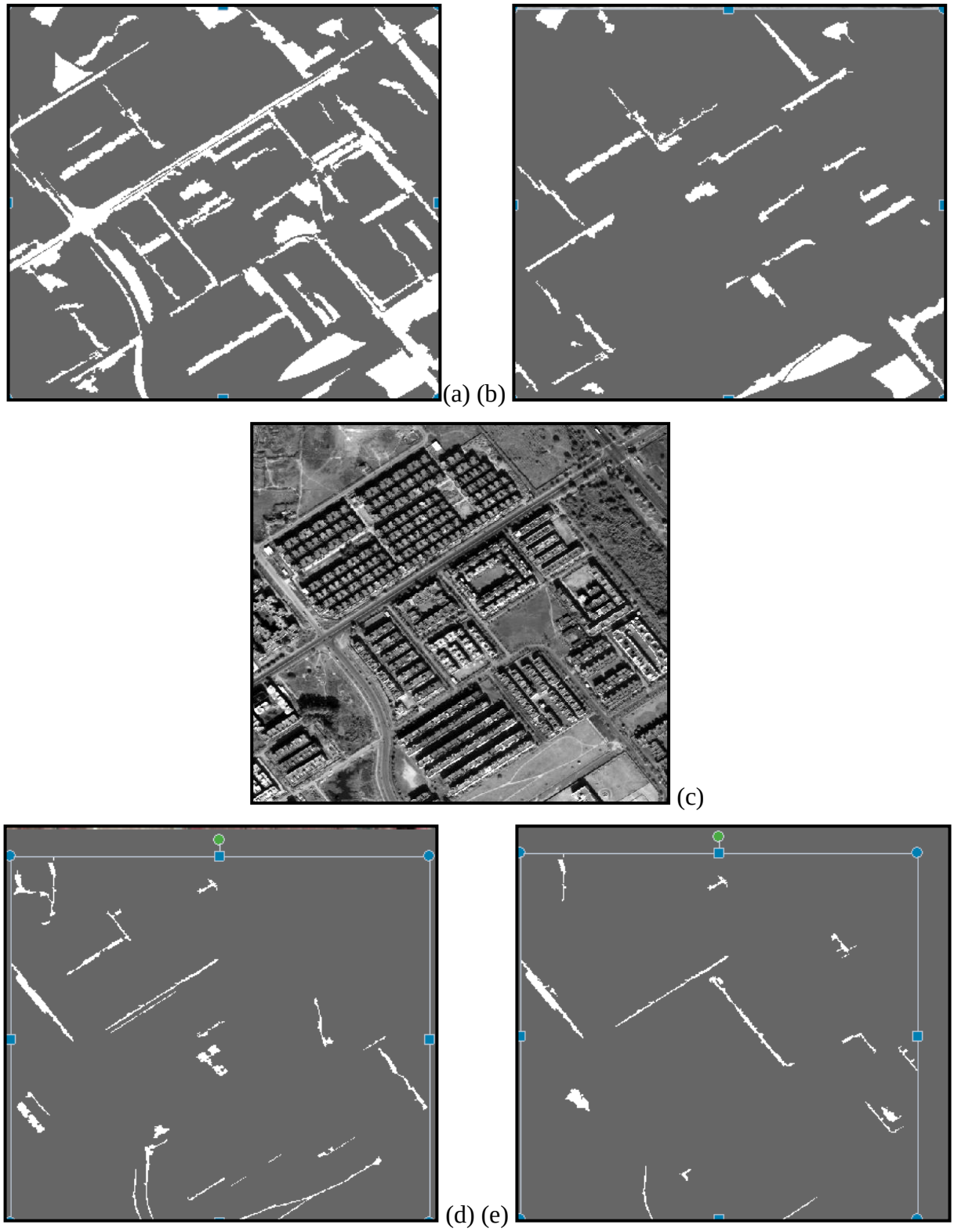

Figure 7.12: Extracted metallic road (a) with 21 attributes, (b) with all 43 attributes, (c) original image, and extracted nonmetallic road (d) with 13 attributes and (e) with all 43 attributes.

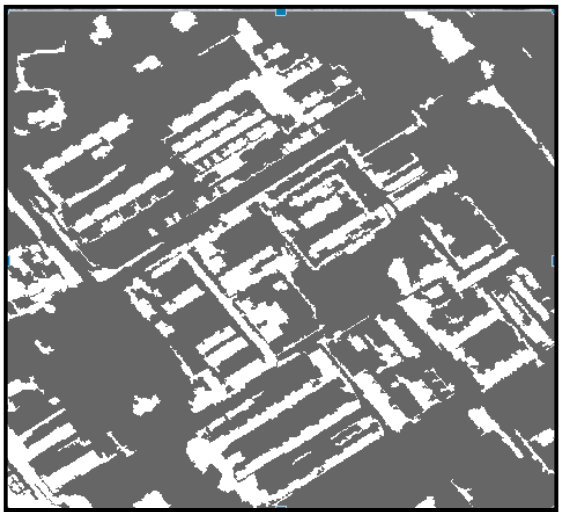
(f)
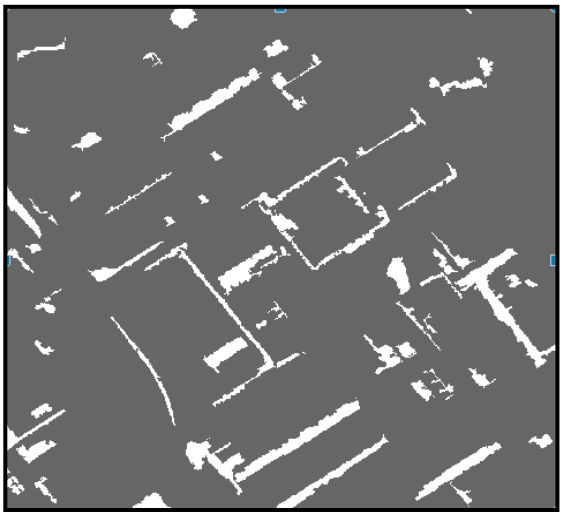
(g)

(h)
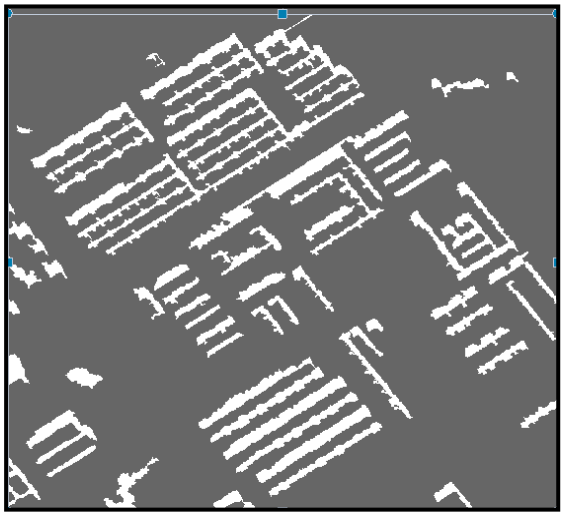
(i)
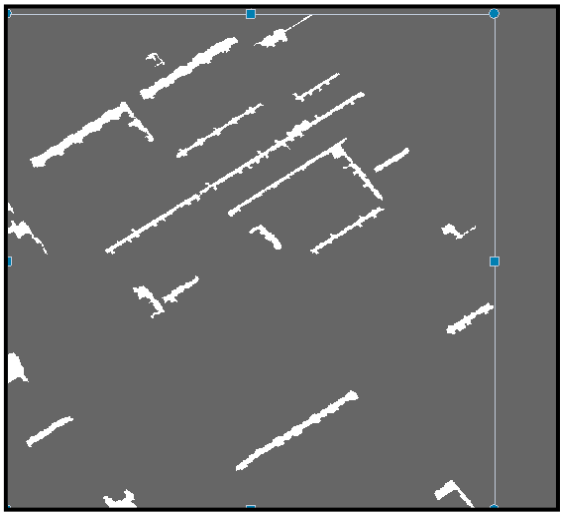
(j)

Figure 7.12: Extracted residential (f) with 16 attributes, (g) with all 43 attributes, (h) original image, and extracted shadow (i) with 17 attributes and (j) with all 43 attributes.

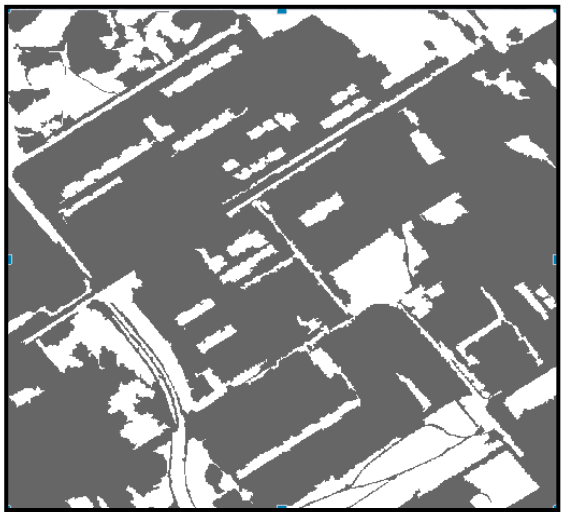

(k)

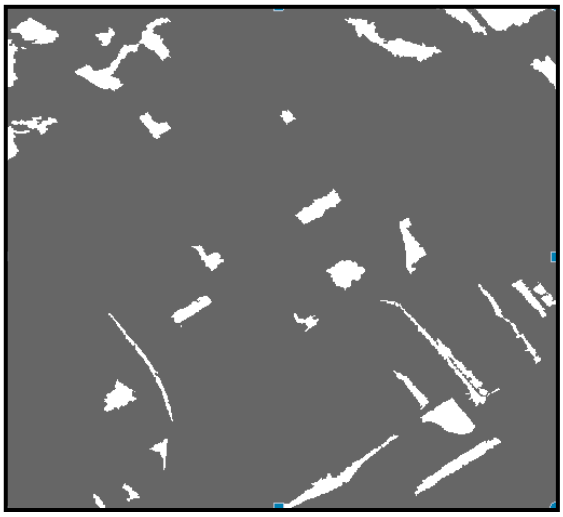

(l)

(m)

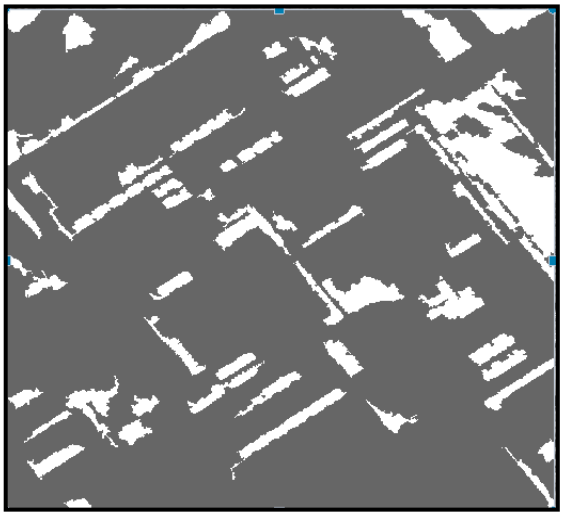

(n)

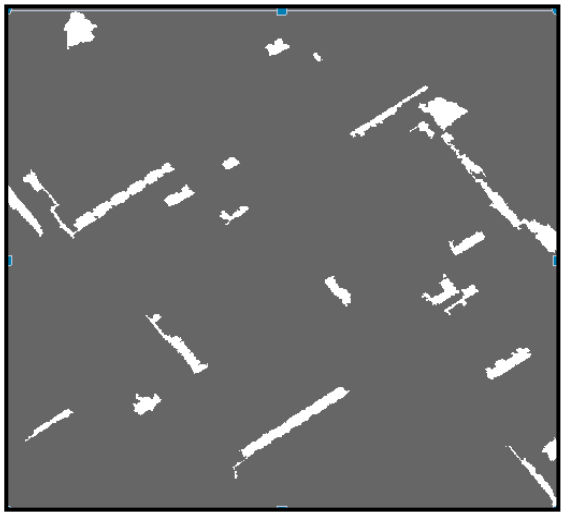

(o)

Figure 7.12: Extracted grassland (k) with 18 attributes, (l) with all 43 attributes, (m) original image, and extracted trees (n) with 24 attributes and (o) with all 43 attributes.

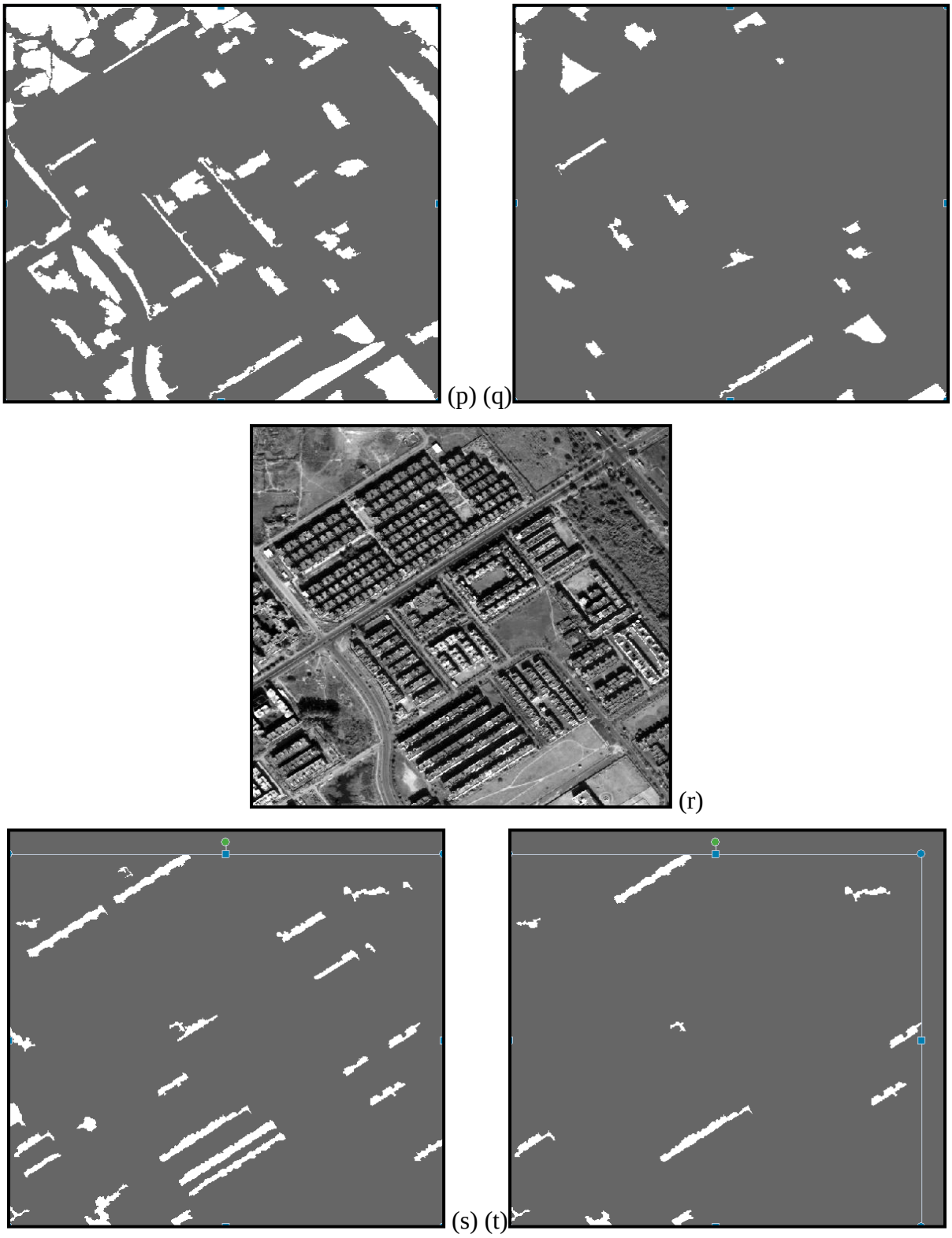

Figure 7.12: Extracted barren land (p) with 17 attributes, (q) with all 43 attributes, (r) original image, and extracted water (s) with 10 attributes and (t) with all 43 attributes.

7.7.2 Object extraction: Study Area-II

Attribute Selection

The segmented LISS-IV multispectral images, as shown in Figure 5.11, have been used for attribute selection. The number of segments used as training samples to extract desired object from the image has been listed in Table 6.18. Segmented image (Seg-L-I) focuses on the linear objects which includes 4 samples of metallic road, 4 of non-metallic road, 3 samples of metro line, 4 samples of canal and remaining 58 samples belong to other objects. To extract compact objects, Seg-L-II image has been considered, from which 10 samples of apartment, 8 samples of house, 4 samples of water catchment, 11 of vegetation, 12 belongs to grassland, 10 of barren land, 6 samples of playground 3 of sand and rest 18 samples belonging to other objects have been selected.

The generated 85 attributes as given in Table 6.19 have been assigned a rank. The rank wise attributes of LISS-IV image for extracting various objects are given in Table 7.7. To extract twelve objects present in the image, 12 decision trees have been generated. These trees have further been reduced by using a selected number of attributes for a particular object. In comparison to Quick-bird Pan-sharpened image, a large number of attributes are required to extract each object. From the attribute selection, it has been noticed that a maximum of 25 attributes are required to extract the object barren land and a minimum of 15 attributes are required to extract the object canal from the image. The number of selected attributes to extract the objects from the image has been highlighted with gray shade in Table 7.7. Class wise ROC curve for selecting attributes to extract different objects from the Panchromatic band Quick-bird image has been drawn in Figure 7.13 (a) to (l).

Table 7.7: Rank wise position of first 25 selected attributes for each class (selected attributes in gray shade) combined from two segmented images.

	Segmented image-I				Segmented image-II							
Rank	Metallic road (1)	Non-metallic road (2)	Metro line (3)	Canal (4)	Apartment (5)	House (6)	Water catchment (7)	Vegetation (8)	Grassland (9)	Barren Land (10)	Play ground (11)	Sand (12)
1	77	5	2	22	12	11	22	81	22	12	17	44
2	41	20	11	2	18	12	2	85	2	19	41	63
3	58	24	21	65	40	19	47	77	1	21	43	64
4	21	34	30	16	49	21	80	83	16	20	31	84
5	30	39	12	20	83	20	20	84	36	30	38	4
6	31	43	18	34	31	30	42	16	20	31	41	16
7	50	53	40	53	32	31	4	35	34	38	44	10
8	68	58	49	58	35	38	42	45	77	41	49	13
9	69	62	83	72	37	41	23	14	17	74	50	41
10	11	72	31	76	38	44	88	16	15	49	57	81
11	81	77	32	78	16	30	81	20	76	38	61	65
12	85	81	35	29	48	12	83	34	52	79	63	35
13	29	11	37	13	19	18	82	53	1	24	87	45
14	35	25	38	3	50	40	85	58	4	42	29	14
15	48	78	16	6	51	49	68	72	54	40	35	16
16	54	1	48	25	54	83	80	76	65	2	48	20
17	67	15	19	44	5	31	33	78	80	4	54	34
18	73	60	50	63	20	32	4	47	24	5	67	53
19	10	8	51	64	24	35	1	13	81	13	73	58
20	70	46	54	84	34	37	15	3	82	43	10	6
21	36	37	34	4	39	38	29	6	6	29	70	25
22	30	18	43	16	43	16	20	25	73	12	2	44
23	34	30	42	10	53	48	72	44	74	81	3	53
24	38	38	25	13	58	19	77	63	3	29	23	4
25	33	36	29	41	62	50	17	64	4	3	28	7

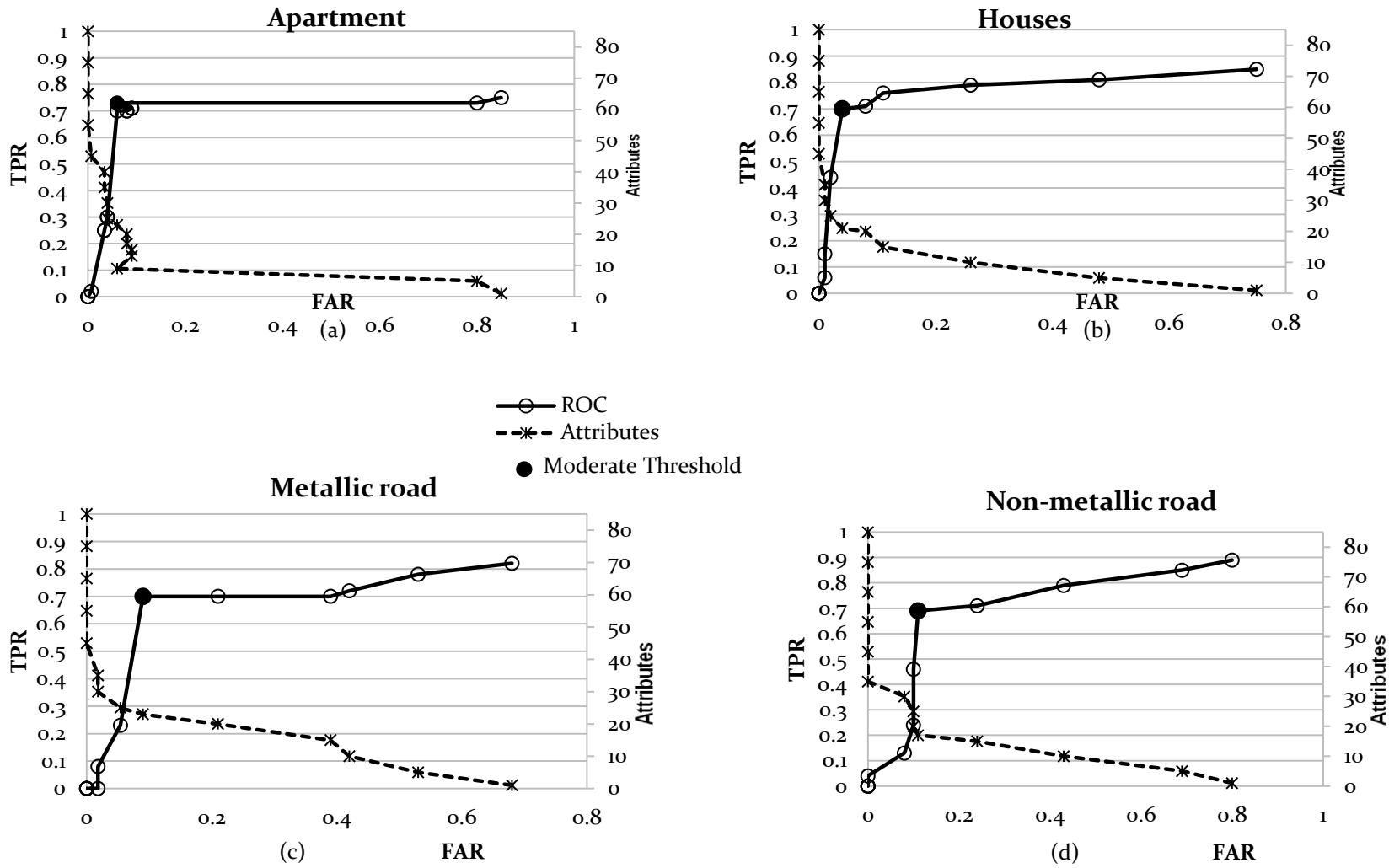

Figure 7.13: ROC curve and attribute selection curve for moderate threshold selection from Multi spectral image LISS-IV for; (a) Apartments, (b) Houses, (c) Metallic road, (d) Non-metallic road.

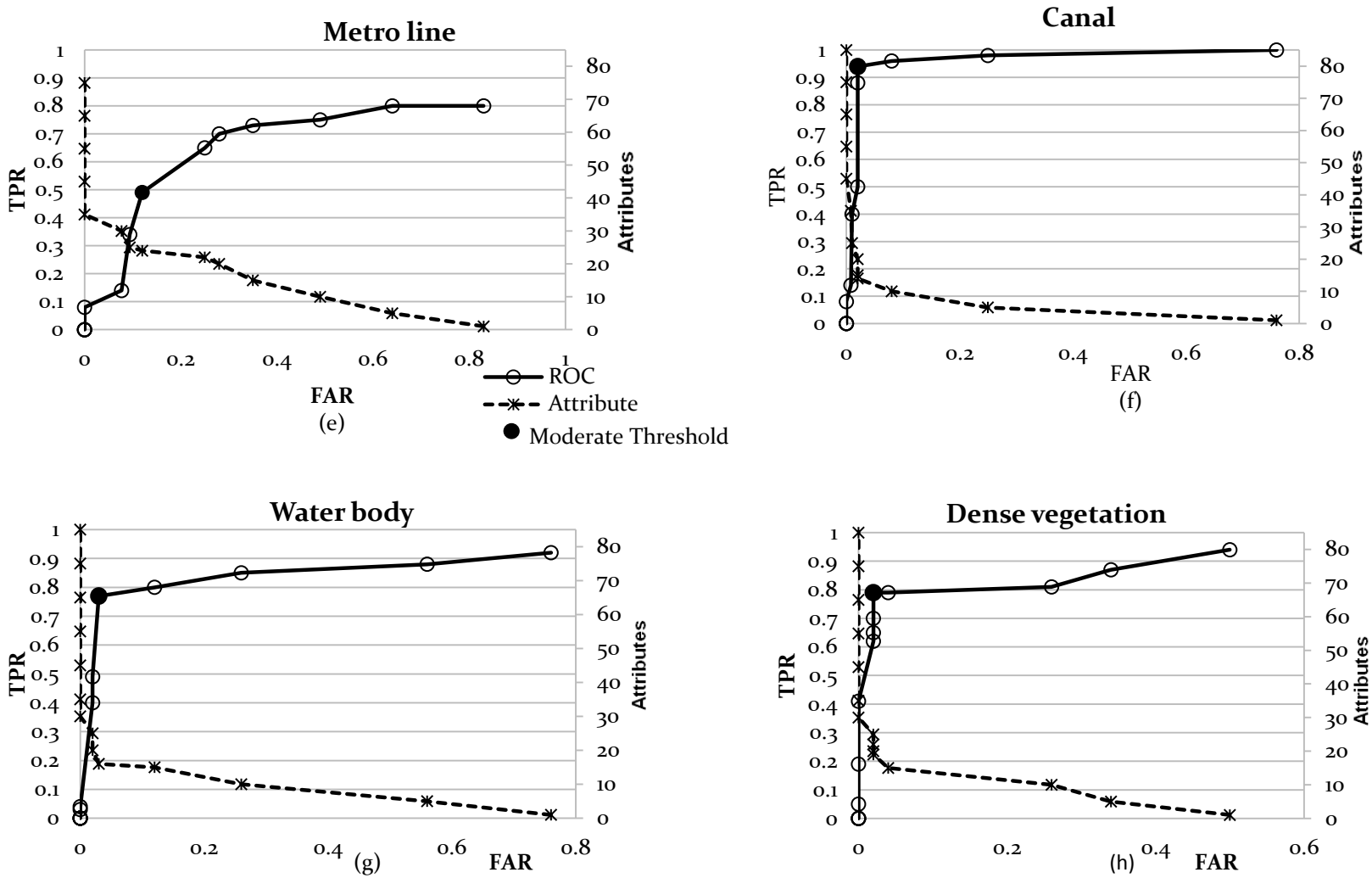

Figure 7.13: ROC curve and attribute selection curve for moderate threshold selection from Multi spectral LISS-IV image for; (e) Metro line, (f) Canal, (g) Water body, (h) Vegetation.

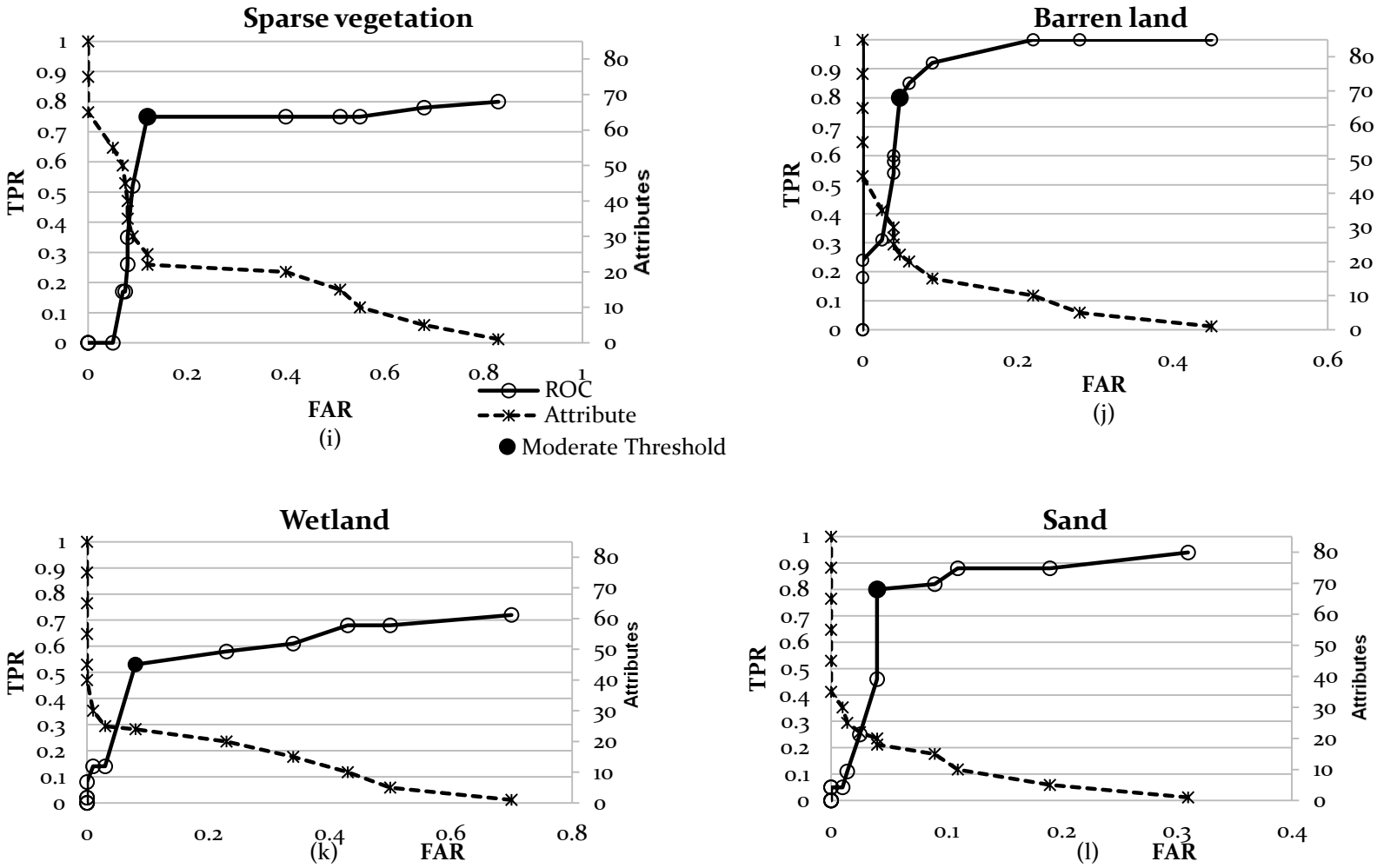

Figure 7.13: ROC curve and attribute selection curve for moderate threshold selection from Multi spectral LISS-IV image for; (i) Grassland, (j) Barren land, (k) Playground and (l) Sand.

Image Object Extraction

To extract all twelve objects present in the LISS-IV multispectral image, the C4.5 algorithm has been applied to the segmented image. Twelve different trees have been generated from the extraction of the desired object with ranked attributes. The number of selected attributes to extract all twelve objects is shown as a bar chart (Figure 7.14). The object extraction has been performed using both selected attributes and all attributes.

The bar chart shows the variation in the required number of attributes for extracting various objects. It has been observed that more number of attributes in comparison of high-resolution image are required to extract an object from the medium resolution LISS-IV image. This is due to the reason that the medium resolution image has less variation in attribute values and these attribute values in turn represent the characteristics of the object.

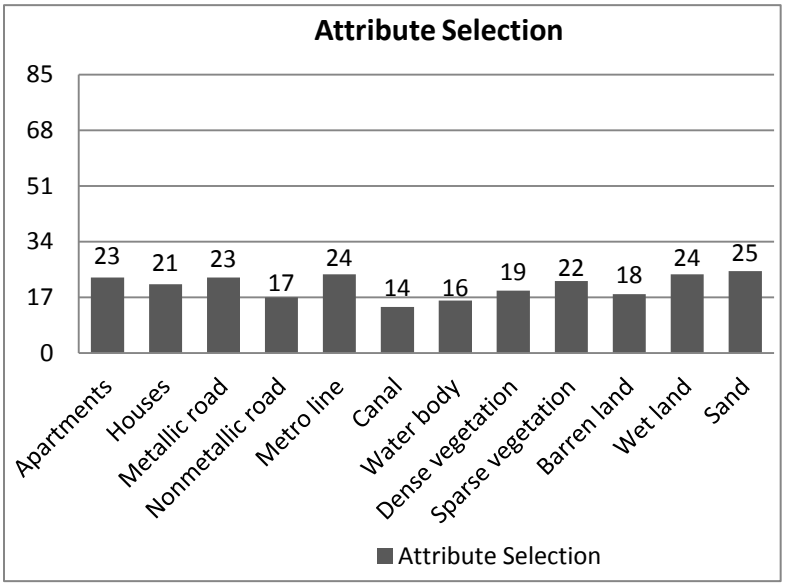

Figure 7.14: Bar chart of class wise selected attributes.

Assessment of Object Extraction Quality

Segmented images Seg-L-I and Seg-L-II have been used for extracting linear and compact objects from the image respectively. A testing data with reference file for medium resolution LISS-IV image has been generated. The reference file includes 127 and 137 samples for all 12 classes from Seg-L-I and Seg-L-II, respectively (as given in Table 7.8), has been used to assess the quality.

The ROC curve for training data has been generated at the time of attribute selection and the number of attributes, which provide high value of TPR at low FAR, has been selected. The object is extracted using the selected number of attributes and the value of TPR and FAR has been calculated using the testing data to find the potential of the generated tree. The object has also been extracted using all attributes. The results have been compared.

Table 7.8: Object wise testing samples of LISS-IV Multispectral image.

Desired object	Seg-L-I image	Seg-L-II image
Apartments	12	11
Houses	10	11
Metallic road	8	10
Nonmetallic road	4	5
Metro line	4	4
Canal	4	4
Water catchment	4	4
Dense vegetation	26	30
Sparse vegetation	20	22
Barren land	22	22
Wetland	10	10
Sand	3	4

The TPR and FAR values of the extracted object at a selected number of attributes is calculated and listed in Table 7.9. From the analysis of the results, it is observed that there is slight variation in the values of TPR and FAR for each extracted object, in comparison to that observed in case of

training datasets. The canal, water body, both types of vegetation and sand emerge with high extraction quality while metro line and wet land has the lowest extraction accuracy.

The desired objects from the segmented images are again extracted by using all attributes. The generated tree with all attributes has been used for the extraction of an object. The TPR and FAR values for these extracted image objects are listed in Table 7.9. The results show that, the TPR value goes down for all objects, when they are extracted using all attributes.

Table 7.9: Quality comparison of extracted object with selected and with all attributes.

Object	**No. of selected attributes**	**Training sample with selected attributes**		**Testing sample with selected attributes**		**Testing sample with 'All (85)' attributes**	
		TPR	**FAR**	**TPR**	**FAR**	**TPR**	**FAR**
Apartments	23	0.70	0.06	0.67	0.07	0.18	0.07
Houses	21	0.72	0.01	0.70	0.05	0.19	0.06
Metallic road	23	0.70	0.09	0.50	0.12	0.14	0.08
Nonmetallic road	17	0.69	0.18	0.65	0.18	0.14	0.05
Metro line	24	0.49	0.12	0.44	0.16	0.02	0.10
Canal	14	0.96	0.01	0.94	0.02	0.27	0.05
Water body	16	0.77	0.03	0.76	0.03	0.13	0.05
Dense vegetation	19	0.79	0.02	0.78	0.04	0.14	0.08
Sparse vegetation	22	0.75	0.12	0.70	0.12	0.11	0.07
Barren land	18	0.60	0.04	0.57	0.07	0.09	0.06
Wet land	24	0.51	0.18	0.49	0.20	0.04	0.08
Sand	25	0.80	0.04	0.75	0.04	0.10	0.06

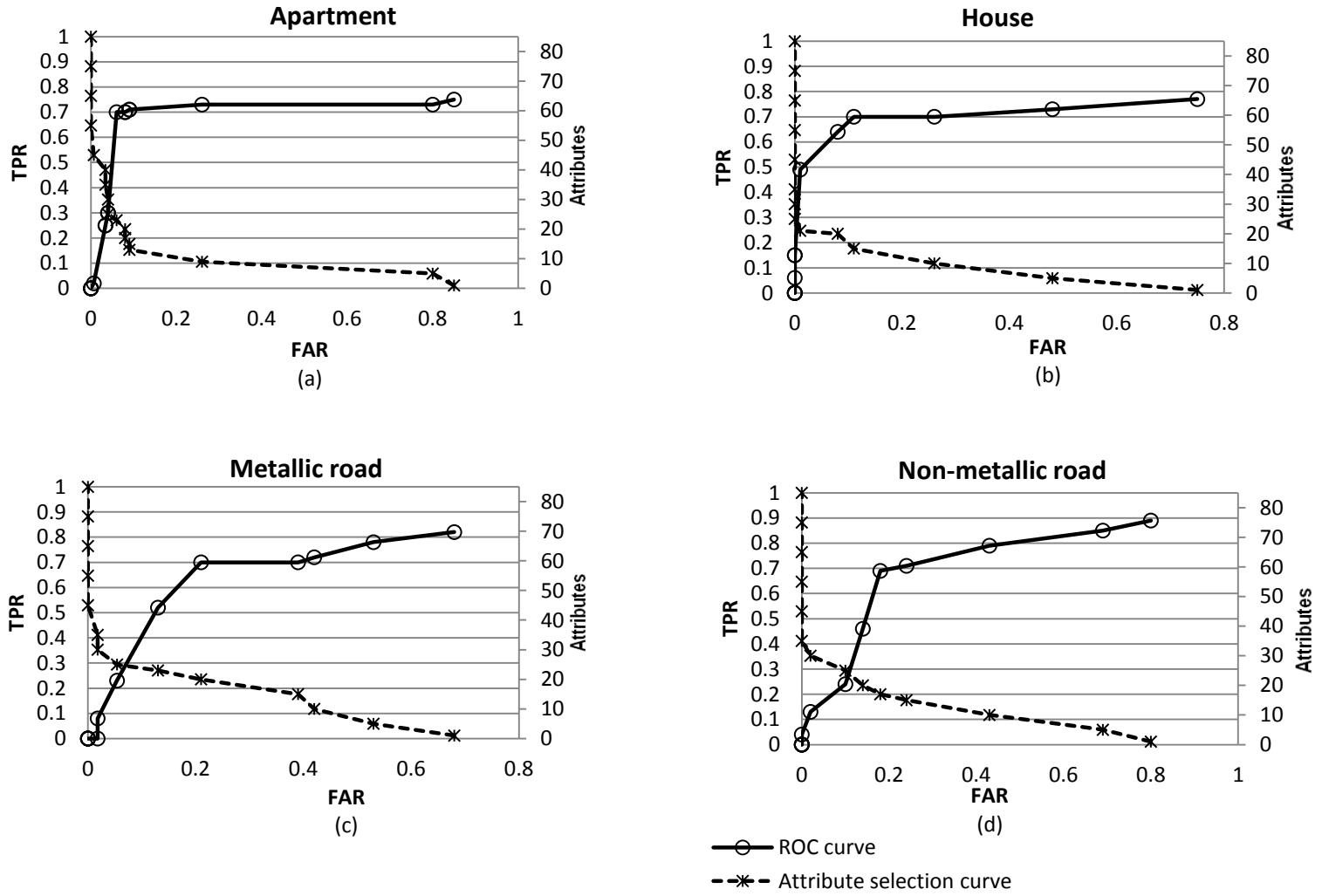

Figure 7.15: ROC curve and attribute selection curve of Multi spectral image LISS-IV for; (a) Apartments, (b) Houses, (c) Metallic road, (d) Non-metallic road.

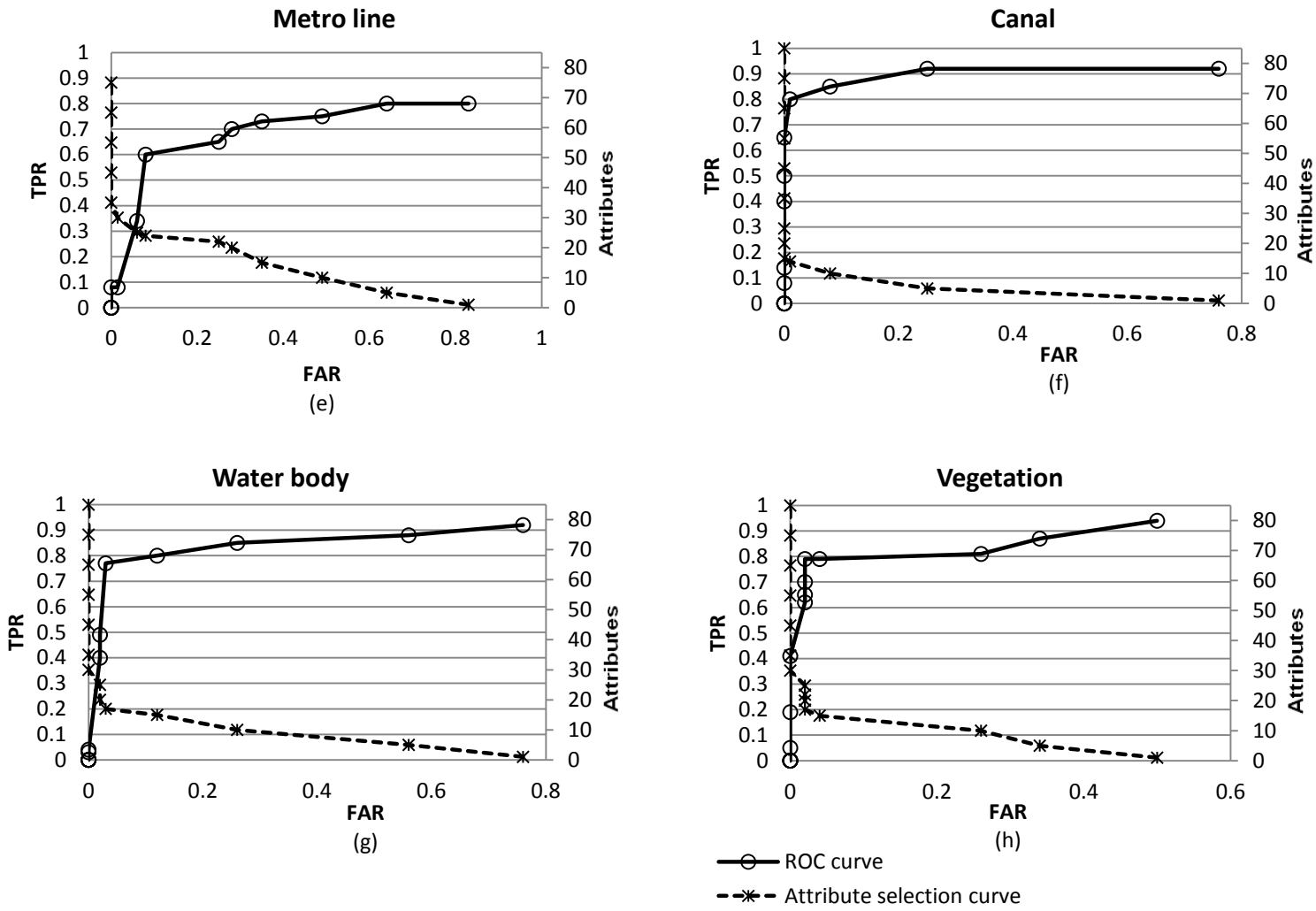

Figure 7.15: ROC curve and attribute selection curve of Multi spectral LISS-IV image for; (e) Metro line, (f) Canal, (g) Water body, (h) Vegetation.

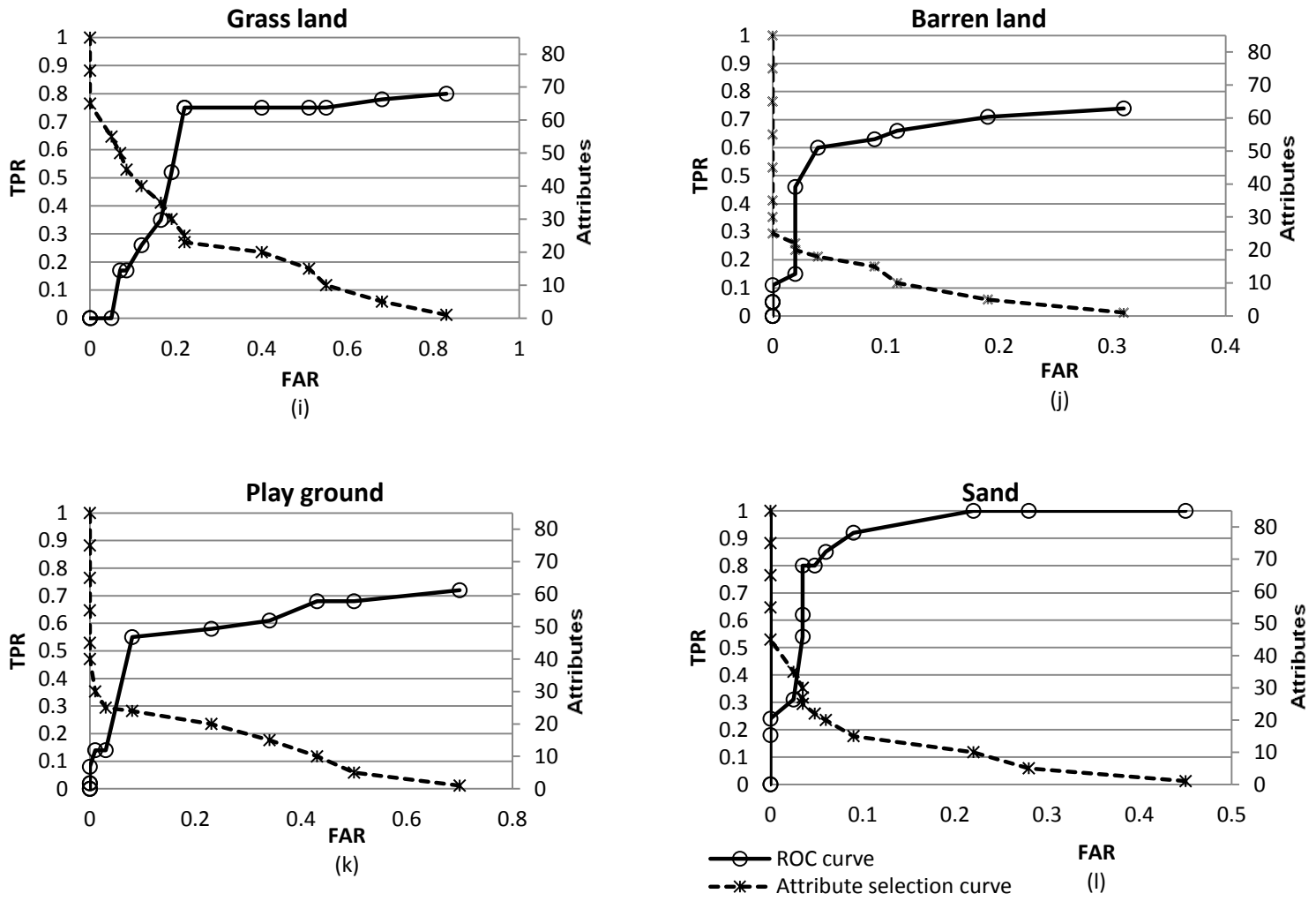

Figure 7.15: ROC curve and attribute selection curve of Multi spectral LISS-IV image for; (i) Grassland, (j) Barren land, (k) Playground and (l) Sand.

Values of TPR and FAR have been calculated for all the extracted objects, by varying the number of attributes and the ROC curves have been drawn (Figure 7.15). The ROC curves follow the similar shape as obtained in Quick-bird image. From the Table 7.9, it is observed that the extraction quality of the canal is the highest due to its unique shape and large variation in its DN value. Wet land has been extracted with the lowest accuracy.

The binary image for object extraction using selected number of attributes and using all attributes has been shown in Figure 7.16. From these binary images, it can be seen that the canal, water body, dense vegetation and sand objects have been extracted with high accuracy while metallic road, metro line, barren land and wet land have low extraction accuracy, when using selected number of attributes. However, the extraction quality of all objects degraded to very low value due to more degradation in the value of the TPR when object extraction has been performed using all attributes. The reason of the fall in the value of TPR is that the characteristics of the lower ranked attributes may match with more than one object hence they misclassified the segments.

Additionally, by comparing the extraction quality of the LISS-IV MS image with Quick-bird Pan image, it is observed that extraction quality of the object extraction from Quick-bird Pan image is low in comparison to that of the LISS-IV image, the reason is that quick-bird Pan image has only one band thus confusion occurs among the classes. However, objects are extracted with high extraction quality from the Quick-bird Pan-sharpened image, it is because of its fine spatial resolution multi spectral in nature with sharpened boundaries.

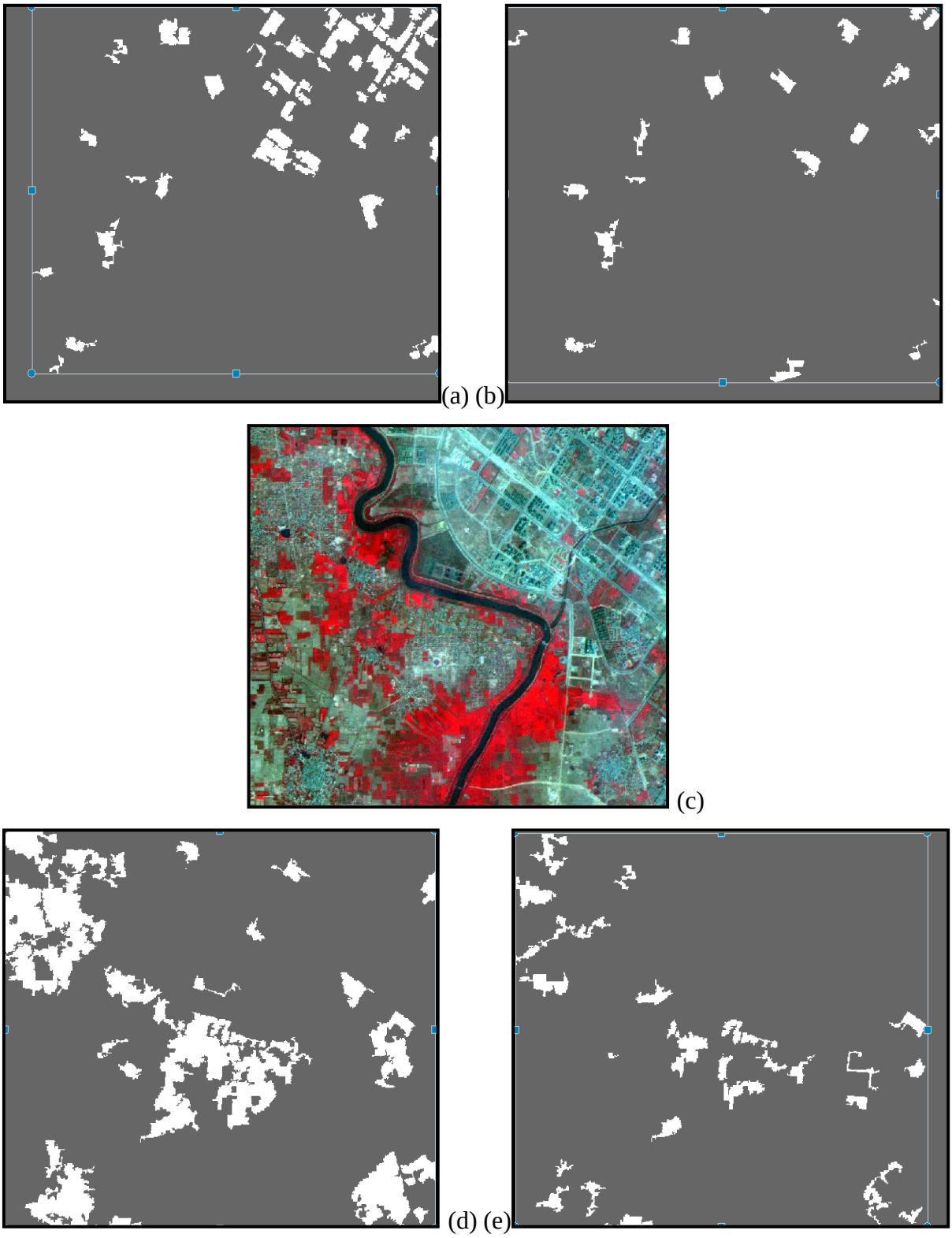

(a) (b) (c) (d) (e)

Figure 7.16: Extracted apartment (a) with 23 attributes, (b) with all 85 attributes, (c) original image, and extracted houses (d) with 21 attributes and (e) with all 85 attributes.

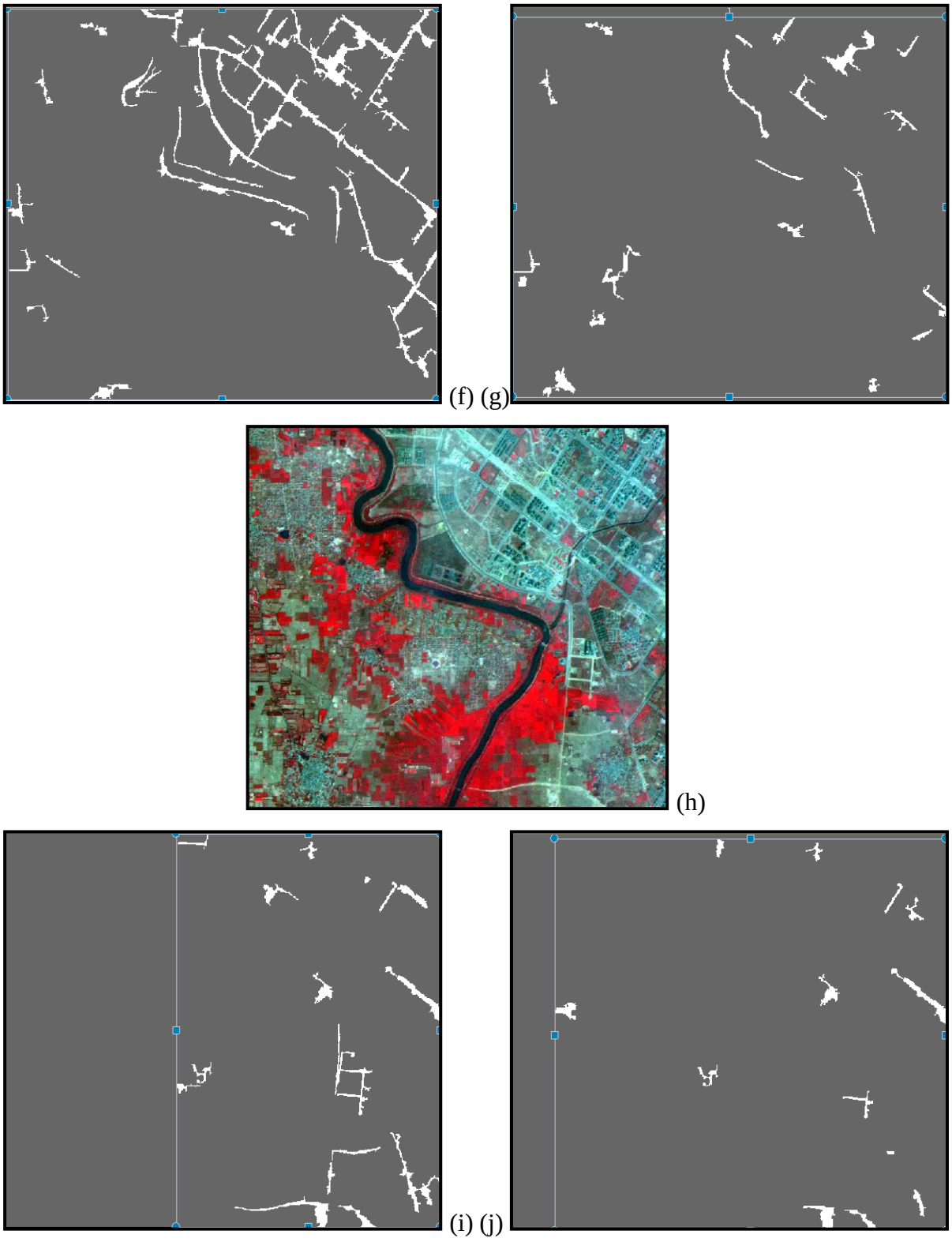

Figure 7.16: Extracted metallic road (f) with 23 attributes, (g) with all 85 attributes, (h) original image, and extracted nonmetallic road (i) with 17 attributes and (j) with all 85 attributes.

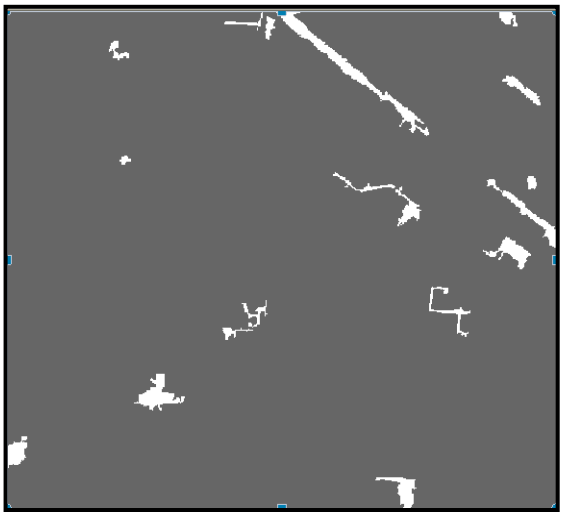

(k)

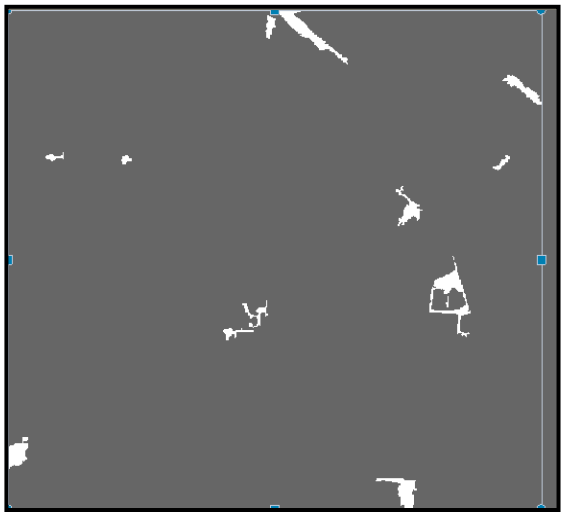

(l)

(m)

(n)

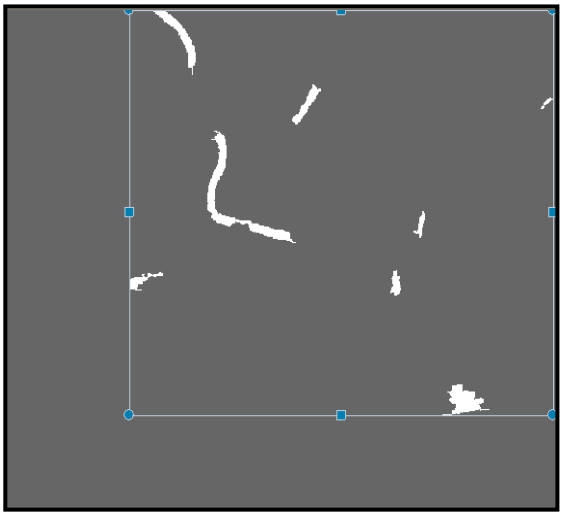

(o)

Figure 7.16: Extracted metro line (k) with 24 attributes, (l) with all 85 attributes, (m) original image, and extracted canal (n) with 14 attributes and (o) with all 85 attributes.

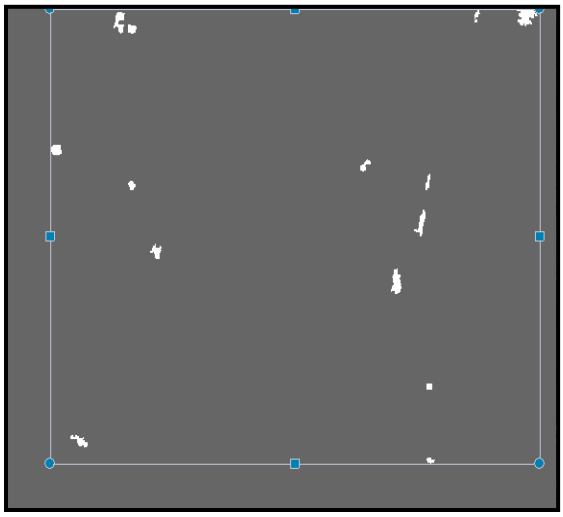
(p)
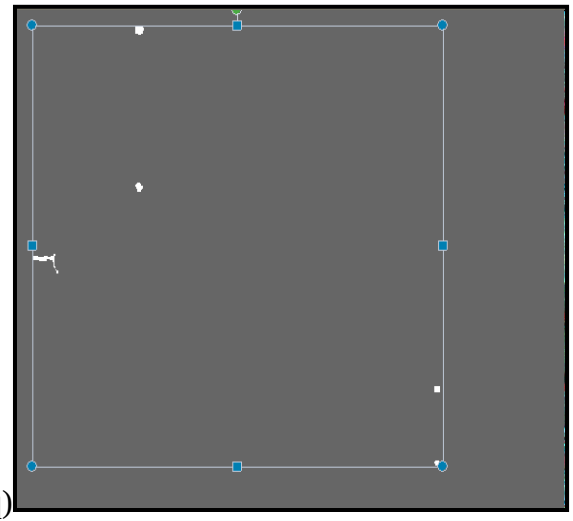
(q)


(r)

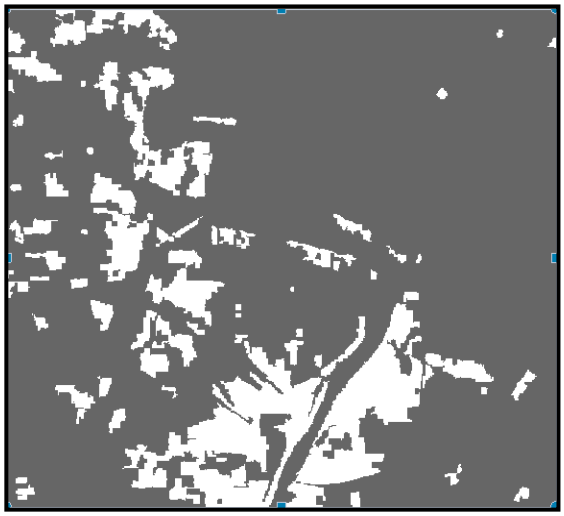
(s)
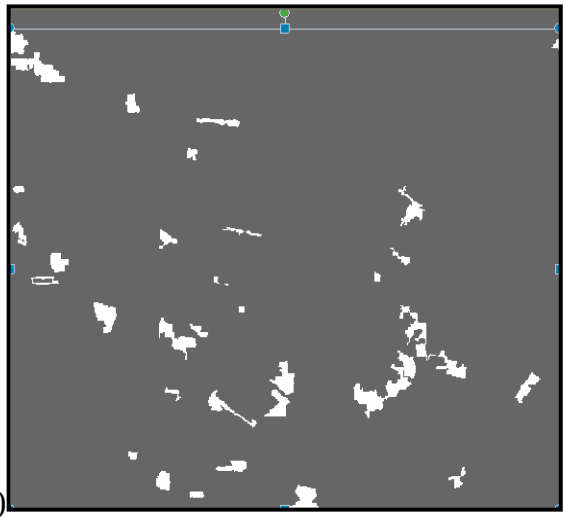
(t)

Figure 7.16: Extracted water (p) with 16 attributes, (q) with all 85 attributes, (r) original image, and extracted dense vegetation (s) with 19 attributes and (t) with all 85 attributes.

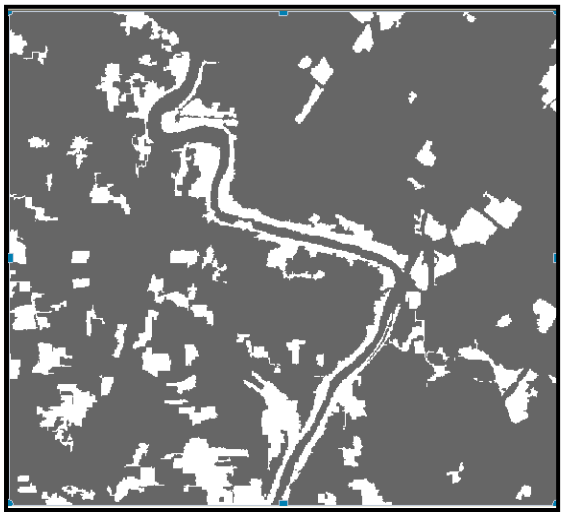

(u)

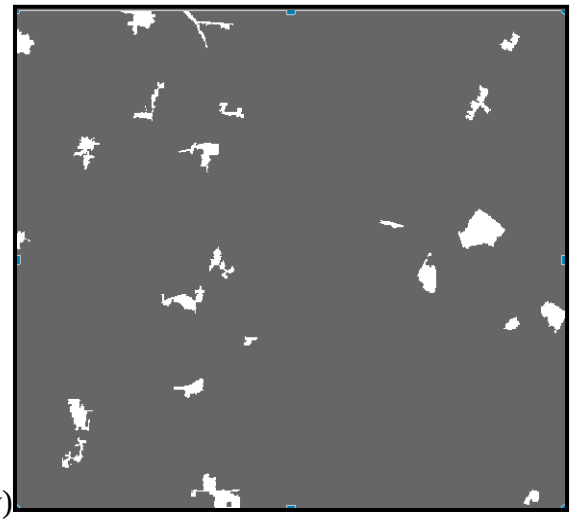

(v)

(w)

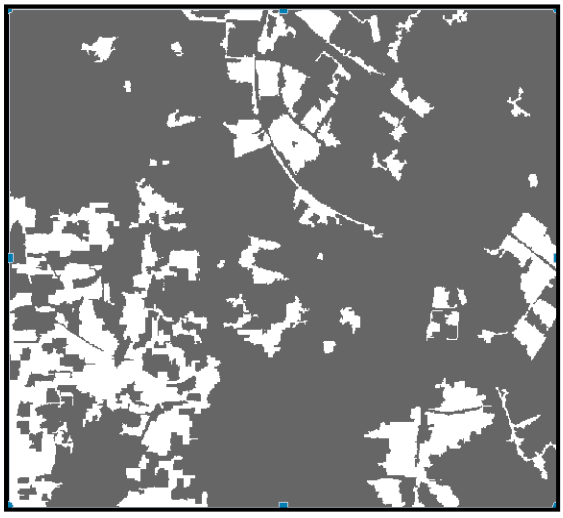

(x)

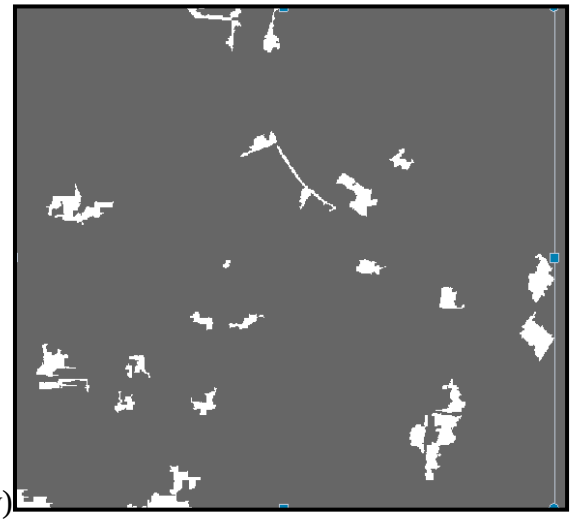

(y)

Figure 7.16: Extracted sparse vegetation (u) with 22 attributes, (v) with all 85 attributes, (w) original image, and extracted barren land (x) with 18 attributes and (y) with all 85 attributes.

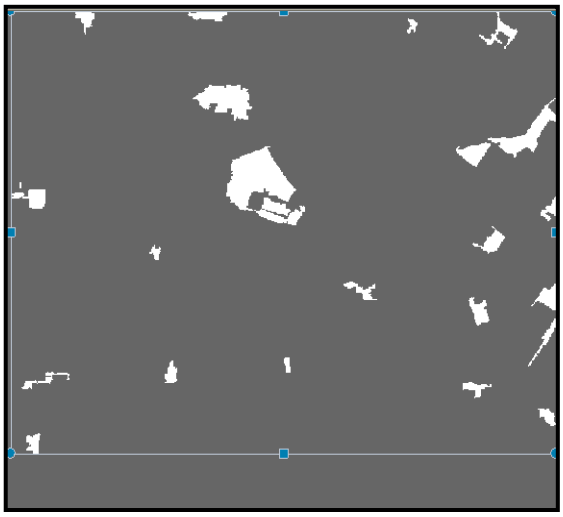
(z)
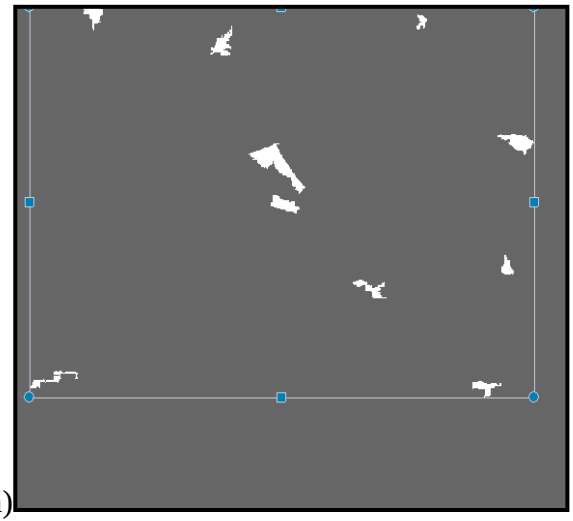
(aa)


(ab)

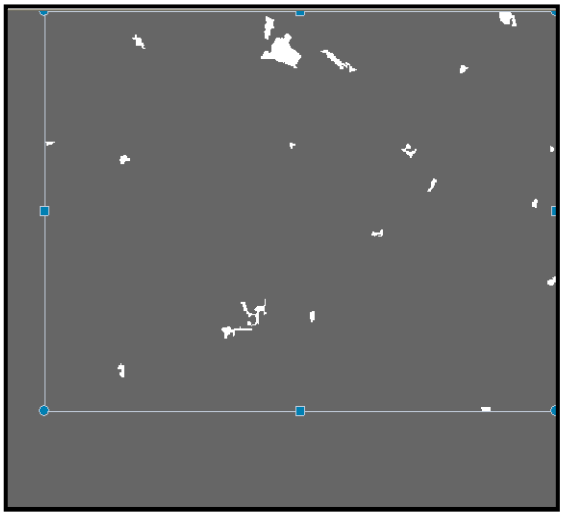
(ac)
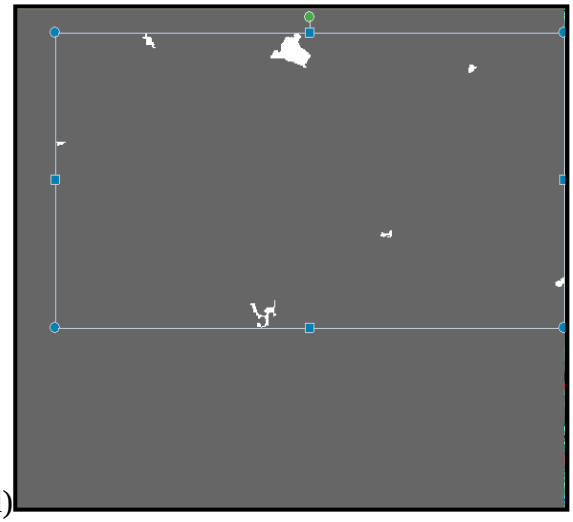
(ad)

Figure 7.16: Extracted coarse wetland (z) with 24 attributes, (aa) with all 85 attributes, (ab) original image, and extracted sand (ac) with 25 attributes, and (ad) with all 85 attributes.

7.8 Summary

The aim of this chapter was to propose an approach for extraction of objects from high spatial resolution remote sensing data. The C4.5 decision tree algorithm was used for object extraction. Attribute selection, object extraction and the assessment of extraction accuracy using ROC curve was performed on three data sets namely; Quick-bird Pan-sharpened image, Quick-bird Pan image and LISS-IV multispectral image. The results may be summarized as,

i). Too many attributes reduce the efficiency of the object extraction algorithm and also affect the extraction quality. A new approach for attribute selection, named as combined decision tree-ROC curve approach was proposed. In this approach, the decision tree is used for attribute ranking. The ROC is used for selecting the number of attributes, which gives highest accuracy.

ii). The number of attributes have been reduced from 100 to a range of 4 to 20 (depending upon the object extracted) for Pan-sharpened image, , from 43 attributes to between 10 and 24 for Panchromatic image, and from 85 to between 14 and 25 in case of LISS-IV image.

iii). Object extraction has been performed using both selected number of attributes as well as using all attributes. It has been observed that the highest extraction quality has been obtained using selected numbers of attributes and it is the worst when using all attributes.

iv). Object extraction for three types of objects namely; linear shape object, regular shape compact object and the irregular shape compact object have been performed.

v). The ROC curve has been used for assessing the extraction accuracy. From Quick-bird Pan-sharpened image, among all the eight objects, the object water has emerged with the highest extraction quality (TPR of 1 and FAR of 0.03) whereas the barren land has the worst extraction (TPR of 0.38 and FAR of 0.08). The object non-metallic road has been extracted with high quality (TPR is 0.65 and FAR is 0.04) and the object trees has been extracted with very low extraction quality (TPR is 0.35 and FAR is 0.34) from the Quick-bird Pan image. The extraction quality of the object canal is the highest and it is the lowest

for the object metro line, among all twelve objects present in the LISS-IV multispectral image. The value of TPR is 0.94 and FAR is 0.021 for object canal while these values are 0.44 and 0.16 respectively for the object metro line.

Chapter 8:

CONCLUSION AND FUTURE RESEARCH

8.1 Introduction

In case of high-resolution images, pixels are smaller than the object under consideration, spectral information within an image is spatially heterogeneous. The object under consideration is composed of several pixels, thus within class spectral variation increases. The pixel-based image classification is affected by 'salt and pepper' noise and produces relatively low classification accuracy (Yan *et al.*, 2006).

In recent years, OBIA has become an advanced research topic in the field of remote sensing by developing the processes for extraction of information from high to very high spatial resolution remote sensing data.

The present research was devoted to develop approaches for selection of segmentation parameters values, assessment of the quality of the formed segments and selection of attributes. A non-parametric decision tree based approach was proposed for attribute selection as well as image classification and individual object extraction.

8.2 Summary of the Study

Segmentation parameter selection and the segmentation quality evaluation techniques are not available in any of the commercial software for OBIA, including eCognition, which has been mostly used for research throughout the world. In the existing software, the segmentation parameter selection process is largely based on trial and error, which is very subjective. The assessment of the segmentation quality is also usually represented visually, as human perception is the best judgment but lacks a quantitative evaluation in the form of a suitable quality measure.

Further, the segmented image is used for image classification, in which numbers of attributes generated in the segmentation process are used. In most of the OBIA techniques, the image is classified using all attributes, however some attributes may be redundant and may therefore reduce the quality, if used. Additionally, the classification algorithm is also limited for object-based image classification.

To accomplish the objectives of the research, an in-house software has been developed on Matlab platform. In the developed software, various modules, namely; segmentation parameters values fixation, segmentation quality evaluation, attribute selection, image classification, object extraction and their quality assessment have been incorporated. The experimental investigations carried out in this research have led to a number of conclusions that are enumerated in the next section.

8.3 Conclusion

From the analysis of results obtained in object-based image analysis on various datasets, following conclusions have been drawn,

i. In this research, a Matlab based software has been developed which can be used alongside existing software for fixation of parameters values, segmentation quality assessment, attribute selection, image classification and object extraction.

ii. The efficacy of all the algorithms implemented has been tested successfully for linear, compact-regular and compact-irregular features on three types of data sets, the Quick-bird image Pan-sharpened, Quick-bird image Pan image and the LISS-IV MS image.

iii. Semiautomatic fitness functions for calculating scale, shape and compactness parameter's values based on their internal variation during merging of sub-segments have been proposed.

iv. The use of fitness functions has assisted in fixing the values of scale, shape and compactness parameters for image segmentation in a multi-segmentation process. This reduces the user’s effort in fixing the values by trial and error.

v. The SFI and ΔSI indices for segmentation quality assessment have been proposed and the quality of Quick-bird Pan-sharpened, Quick-bird Pan and the LISS-IV MS segmented images has been assessed. The results obtained from the proposed index have also been compared with that of existing segmentation quality evaluation index.

vi. The proposed SFI and ΔSI indices produce more realistic values of segmentation quality as these appropriately takes into account errors of commission and omission in their computations.

vii. The proposed indices have shown its robustness in assessing the quality of segmentation for both compact shape as well as linear shape features.

viii. Attributes ranking has been performed using C4.5 decision tree algorithm. These ranked attributes have been further used for image classification and object extraction.

ix. The pessimistic error pruning (PEP) has been applied to the decision tree to prune the decision tree for image classification.It has been observed that images classified using pruned tree produces better accuracy in comparison to when they are classified using an unpruned tree.

x. Highest classification accuracy is achieved for the Quick-bird Pan-sharpened image, due to its high spatial resolution and multi-band nature. Quick-bird Pan image produces low classification accuracy as compared to other datasets, as it is single band data. The LISS-IV multispectral image produced better results in comparison to Quick-bird Pan image due to multi band data, and poor result in comparison to Pan-sharpened image, because of its low spatial resolution.

xi. For assessing classification quality, various accuracy measures such as overall accuracy, individual class accuracies and Kappa coefficient, have been calculated. For Quick-bird Pan-sharpened image, Quick-bird Pan image and LISS-IV image; highest OA and Kappa have been obtained as 91.03%, 0.893, 62.5%, 0.572 and 78.91%, 0.76 respectively.

xii. A quantitative combined decision tree-ROC curve based approach has been proposed to select the important attributes for individual object extraction.

xiii. The attribute set gets reduced between 4 and 20 from 100 for Pan-sharpened image, from 43 to 10 and 24 for Pan image, and from 85 attributes to 14 and 25 in case of LISS-IV image.

xiv. The ROC curve has also been used for assessing the extraction accuracy. The highest extraction quality has been obtained using selected numbers of attributes while extraction quality is worst when using all attributes.

xv. From Quick-bird Pan-sharpened image, among all the eight objects, the object water has emerged with the highest extraction quality, while the barren land has a worst extraction. The object non-metallic road has been extracted with high quality and the object trees has been extracted with very low extraction quality from the Quick-bird Pan image. The extraction quality of the object canal is the highest and it is the lowest for the object metro line, among all twelve objects present in the LISS-IV multispectral image.

xvi. The highest extraction quality has been achieved (TPR of 1 and FAR of 0.03) for Quick-bird Pan-sharpened image. The corresponding values TPR and FAR for Quick-bird PAN image are 0.65 and 0.04 respectively and for LISS-IV multispectral image, a value of TPR is 0.94 and FAR is 0.021.

8.4 Major Research Contributions

The major research contributions of this research can be listed as,

i). New fitness functions have been proposed for fixation of values of segmentation parameters.

ii). A set of quality indices that take into account errors of omission and commission have been proposed to assess the quality of segmentation.

iii). A quantitative method of attribute selection has been suggested. The use of selected attributes has resulted in an increase in the accuracy for extraction of information derived from high resolution remote sensing data.

8.5 Future Research

The work presented in the thesis can be envisaged as a contribution in the area of OBIA in urban scenarios. This research has focused on the segmentation parameter selection, its quality assessment, image classification and individual object extraction with selected attributes. Some issues, which may require further attention, have been identified and may be enumerated as;

i). Image segmentation has been performed using bottom up multi-resolution image segmentation available in the commercial eCognition software. A new segmentation technique needs may be developed and implemented.

ii). Proper segmentation of the image is the basic requirement. Selection of the parameter values for segmenting the image is very tough. Although, some fitness functions have been generated for this, but improvement in these fitness functions may be possible.

iii). Image classification and object extraction have been performed on very high-resolution images. The inclusion of height information from sensors such as LiDAR, to perform an OBIA in an image fusion environment, to minimize the misclassifications between the classes may also be worth exploring.

CONTENTS